



HAL
open science

Synthesis and photophysical study of cation-responsive and photoactive supramolecules based on “Click” triazole and azacrown moieties

Yibin Ruan

► **To cite this version:**

Yibin Ruan. Synthesis and photophysical study of cation-responsive and photoactive supramolecules based on “Click” triazole and azacrown moieties. Other. École normale supérieure de Cachan - ENS Cachan, 2012. English. NNT : 2012DENS0089 . tel-00907278

HAL Id: tel-00907278

<https://theses.hal.science/tel-00907278>

Submitted on 21 Nov 2013

HAL is a multi-disciplinary open access archive for the deposit and dissemination of scientific research documents, whether they are published or not. The documents may come from teaching and research institutions in France or abroad, or from public or private research centers.

L'archive ouverte pluridisciplinaire **HAL**, est destinée au dépôt et à la diffusion de documents scientifiques de niveau recherche, publiés ou non, émanant des établissements d'enseignement et de recherche français ou étrangers, des laboratoires publics ou privés.

**THESE DE DOCTORAT
DE L'ECOLE NORMALE SUPERIEURE DE CACHAN**

Présentée par

Yibin RUAN

**pour obtenir le grade de
DOCTEUR DE L'ECOLE NORMALE SUPERIEURE DE CACHAN**

Domaine :
CHIMIE

Sujet de la thèse :

**Synthesis and Photophysical Study of Cation-responsive and
Photoactive Supramolecules Based on "Click" Triazole and Azacrown
Moieties**

Thèse présentée et soutenue à Cachan le 20 Décembre 2012 devant le jury
composé de :

Clotilde Policar	Professeur des Universités	Présidente
Jérôme Chauvin	Maître de conférences	Rapporteur
Frédéric Fages	Professeur des Universités	Rapporteur
Stéphane Aloïse	Maître de conférences	Examineur
Joanne Xie	Professeur des Universités	Co-Directrice de thèse
Isabelle Leray	Directrice de Recherche	Directrice de thèse

**Laboratoire de photophysique et photochimie
supramoléculaires et macromoléculaires**
PPSM-UMR 8531
Ecole Normale Supérieure de CACHAN
61, avenue du Président Wilson, 94235 CACHAN CEDEX

Acknowledgement

This dissertation is accomplished under many people's help. I owe my gratitude to all those people who have made this dissertation possible. This invaluable experience is the one I will cherish forever.

Foremost, I would like to thank my advisor Dr. Isabelle Leray for the opportunity to work in ENS Cachan and for her intelligent guidance in this dissertation. I am grateful for the thoughtful comments and the training that she has provided for me. Her insightful scientific knowledge and hard working spirit always inspire me to focus on my project. I really appreciate her unconditional understanding, encouragement and patient during my hard time in organic synthesis.

I would like to express my heartfelt thanks to my co-advisor Prof. Joanne Xie for her guidance in my thesis. "Click" would become much more difficult for me without her intelligent decision on my research project. I am very impressive by her high efficiency in the work. I am also indebted to her great help in my life from my settling down. I can not imagine the life without her help. Also thank for inviting me to enjoy dinner in her house for several times.

Special thanks go to Prof. Yunbao Jiang in Xiamen University. He is my science mentor. His insightful knowledge, confident prediction and unselfish supporting always inspire me move on in my work during these years. Things I learned from him will benefit me in the whole life. I would like to thank Prof. Xianzhi Huang, who always supported me in the life during my stay in Xiamen University and he is my example in my life.

I would like to thank Dr. Stéphane Aloïse for his useful discussion, patience and inspiration. I would like to extend my gratitude to my committee: Prof. Clotilde Policar, Dr. Jérôme Chauvin, Prof. Frédéric Fages and Dr. Stéphane Aloïse for taking the time to read my dissertation and useful discussion.

I really appreciate Stéphane Maisonneuve to help me get familiar with the lab, for his help in organic synthesis, data processing and NMR spectra. He is always warmhearted to help me out of the difficulty. I would like to thank Chun Li for leaving me a series of fluorescent molecular for spectroscopic investigations. I am grateful to Jean-Pierre Lefèvre for his patient training in microfluid. I would like to give great thanks to Arnaud Brosseau for his kind help in transient spectroscopy. I acknowledge Jérémy Bell for teaching me mechanism calculation and his kind asking about thesis in the morning. I appreciate Alexis Depauw for the help in organic synthesis and funny dancing in the lab. I am indebted to Yanhua Yu for her instructive

organic synthesis assistance and great friendship.

I would like to thank Prof. Keitaro Nakatani, Prof. Jacques Delaire, Nicolas Bogliotti, Rémi Métivier, Prof. Pierre Audebert, Prof. Robert Pansu, Gilles Clavier, Rachel Méallet-Renault, Valérie Alain-Rizzo, Clémence Allain, Fabien Miomandre for their help in my work; to Jacky Fromont for handling my computer problems; to Andrée Husson and Christian Jean-Baptiste for their administrative help.

I owe thanks to Qing Zhou for assisting me every aspect of life in last three years. I acknowledge Cong Lv for the great friendship and her nice gifts. I thank Yuheng Yang for his helpful discussion.

I appreciate the help from the members of PPSM: Djibril Faye, Laura Jonusauskaite, Haitao Zhang, Issa Samb, Olivier Noël, Sandrine Peyrat, Ni Ha Nguyen, Karima Ouhenia, Jia Su, Yang Si, Yuan Li, Jonathan Piard, Chloé Gazon, Eva Jullien, Jérémy Malinge, Cassandre Quinton, Johan Saba. Thanks for the nice study environment in these three years.

I wish to convey my thanks to Min Zhang and Haibin Zhao for picking me up and wonderful dinner at my first night in France; to Yao Wang, Xiao Wu, Yuanyuan Liao, Zhenzhen Yi, Jiayi Gao, Zongwei Tang to celebrate my birthday together, to Xiaoju Ni, Gele Qing, Fan Yang, Zhe Sun, Feifei Shi, Xiaoqian Xu, Yingying Chen, Fangzhou Zhang, He Huang for their help in my daily life.

I would like to take this chance to extend my thanks to my labmates in Xiamen University. I want to express my gratitude to Prof. Yibing Zhao, Prof. Qiuquan Wang, Prof. Shunhua Li, Prof. Hong Zheng for their great help in my study during my stay in Xiamen University. Thank Aifang Li, Jinsong Zhao and Jiangshan Shen. Words just can not express my great gratitude to them for their tremendous help in my study and in my life. Thank Qianqian Jiang and Mingbo Zhang for their invaluable friendship. Thank Jinhe Wang, Donghua Li, Qiuju Jiang, Han Zhang, Daiping Guo, Tao Yu, Rong Zhou, Suying Xu, Fang Wang, Zhao Li, Wenxia Liu, Lin Guo, Rui Yang, Qinxian Liao, Lifeng Han, Yufeng Gao, Qiangli Wang, Jie Han, Hui He, Yanjun Huang, Zhan Chen, Tao Jiang, Qian Wang, Fu Cai, Wenbin He, Wenjuan Ouyang, Na Chen, Ying Zhan. Four years' life in ROOM 536 will definitely be the most precious memory in my life. I will never forget the beautiful memories and the difficulty that we shared together.

Lastly but certainly not least, I would give my greatest appreciation to my family and girl friend for their constant love and supporting, making me bravely face the difficulty and go through those tough days.

Yibin RUAN
ENS CACHAN

Abbreviations

μM	Micromolar
Ag NPs	Silver nanoparticles
AIE	Aggregation induced emission
Au NPs	Gold nanoparticles
Boc	<i>t</i> -Butyloxy carbonyl
BODIPY	Boron-dipyrromethene
BPO	Benzoyl peroxide
CyD	Cyclodextrin
Dansyl	5-(Dimethylamino)naphthalene-1-sulfonyl
DCM	Dichloromethane
DMAP	4-Dimethylaminopyridine
DMF	Dimethylformamide
DMSO	Dimethyl sulfoxide
EDTA	Ethylenediaminetetraacetic acid
em	Emission
Equiv	Equivalent
ESI	Electrospray Ionisation
Et	Ethyl
Ex	Excitation
FAB-MS	Fast Atom Bombardment Mass Spectroscopy
FC	Franck Condon
FRET	Förster resonance energy transfer
FTIR	Fourier Transform Infrared Spectroscopy
HEPES	<i>N</i> -2-Hydroxyethylpiperazine- <i>N'</i> -2-ethanesulfonic Acid
HOMO	Highest occupied molecular orbital
Hz	Hertz
IC	Internal conversion
ICD	Induced circular dichroism
ILCT	Intraligand charge-transfer
ISC	Intersystem crossing
LLCT	Ligand-to-ligand charge-transfer
LUMO	Lowest unoccupied molecular orbital
mM	Milli molar
Me	Methyl
MeCN	Acetonitrile
MLCT	Metal-to-ligand charge-transfer
NBD	7-Nitrobenzo-2-oxa-1,2-diazole
NBS	<i>N</i> -Bromosuccinimide
nM	Nano molar
NMR	Nuclear magnetic resonance

PB	Phosphate buffer
PCT	Photoinduced charge transfer
PET	Photoinduced electron transfer
ppb	Parts per billion
RT	Room temperature
Terpy	Terpyridine
THF	Tetrahydrofuran
Ts	Tosyl
UV	Ultra-violet
WHO	World health organization

Table of Contents

General introduction	- 3 -
Chapter 1. Introduction of Molecular Fluorescence and Fluorescent Chemosensors Design	- 5 -
1.1. Introduction of molecular fluorescence	- 7 -
1.1.1. Light absorption	- 7 -
1.1.2. Molecular fluorescence	- 8 -
1.2. Fluorescent chemosensor design	- 10 -
1.2.1. Photoinduced electron transfer	- 12 -
1.2.2. Photoinduced charge transfer	- 14 -
1.2.3. Energy transfer	- 16 -
1.2.4. Formation of excimers.....	- 18 -
1.2.5. Chemodosimeters	- 19 -
1.3. Applications of fluorescent chemosensors	- 20 -
1.4. Objectives	- 21 -
References	- 24 -
Chapter 2. Clickable Fluorescent Chemosensors for Detection of Heavy Metal Ions: Triazole as a Linker	- 27 -
2.1. Introduction of “Click” reaction	- 29 -
2.1.1. Cu(I)-catalyzed Huisgen 1,3-dipolar cycloaddition of azides and terminal alkynes (CuAAC)	- 30 -
2.1.2. Mechanism of the CuAAC	- 31 -
2.1.3. Catalyst of the CuAAC.....	- 33 -
2.1.4. Applications of the CuAAC reaction.....	- 34 -
2.1.4.1. Triazole as a linker	- 35 -
2.1.4.2. Triazole as the single binding site for metal ions	- 36 -
2.1.4.3. Triazole as the co-binding site for metal ions.....	- 37 -
2.1.5. Related works in Xie’s group	- 44 -
2.2. Fluorescein-Triazole derivatives for selective detection of Hg²⁺	- 47 -
2.2.1. Introduction	- 47 -
2.2.2. Synthesis of Fluorescein-triazole derivatives	- 47 -
2.2.3. Photophysical properties of Flu-1	- 48 -
2.2.4. Complexation properties of Flu-1	- 49 -
2.2.5. Conclusion.....	- 58 -
2.3. Fluorescein-Triazole derivatives for selective detection of Cu²⁺/ Cu⁺	- 59 -
2.3.1. Introduction	- 59 -
2.3.2. Synthesis of Fluorescein-triazole derivatives	- 60 -
2.3.3. Photophysical properties of Flu-3	- 61 -
2.3.4. Complexation properties of Flu-3	- 62 -
2.3.5. Conclusion.....	- 69 -
References	- 70 -

Chapter 3. Clickable Fluorescent Chemosensors for Detection of Heavy Metal Ions: Triazoles as Binding Sites	- 79 -
3.1. Introduction of click triazole as ionophores	- 81 -
3.2. NBD-Triazole based Hg²⁺ chemosensor	- 82 -
3.2.1. Introduction	- 82 -
3.2.2. Synthesis of NBD-1 and NBD-2	- 83 -
3.2.3. Photophysical properties of NBD-1	- 83 -
3.2.4. Complexation properties of NBD-1	- 84 -
3.2.5. Binding mode of NBD-1 to Hg ²⁺	- 91 -
3.2.6. Conclusion.....	- 95 -
3.3. Rhodamine-Triazole based Hg²⁺ chemosensor	- 96 -
3.3.1. Introduction	- 96 -
3.3.2. Synthesis of Rho-1 and Rho-2	- 96 -
3.3.3. Photophysical properties of Rho-1 and Rho-2	- 97 -
3.3.4. Complexation properties of Rho-1 and Rho-2	- 97 -
3.3.5. Sensing mechanism of Hg ²⁺ based on Rho-1	- 103 -
3.3.6. Conclusion.....	- 107 -
3.4. Pyrene-Triazole based Hg²⁺ chemosensor	- 108 -
3.4.1. Introduction	- 108 -
3.4.2. Synthesis of CDPy	- 109 -
3.4.3. Photophysical properties of CDPy	- 109 -
3.4.4. Structural conformation of CDPy	- 111 -
3.4.5. Complexation properties of CDPy	- 114 -
3.4.6. Conclusion.....	- 122 -
3.5. Benzothiadiazolyl-Triazole based chemosensors	- 123 -
3.5.1. Introduction	- 123 -
3.5.2. Synthesis of Benzo-x derivatives	- 123 -
3.5.3. Photophysical properties of Benzo-x series	- 124 -
3.5.4. Complexation properties of Benzo-x series	- 127 -
3.5.4.1. Selectivity of Benzo-x series to metal ions	- 127 -
3.5.4.2. Spectral titration of Benzo-x series with Cu ²⁺ , Hg ²⁺ and Ni ²⁺	- 130 -
3.5.5. Conclusion.....	- 143 -
References	- 145 -
Chapter 4. Fluorescent Calix[4]bisazacrown Based Chemosensors	- 149 -
4.1 Fluorescent Calix[4]bisazacrown for selective recognition of potassium	- 151 -
4.1.1. Introduction of selective fluoroionophores of potassium	- 151 -
4.1.1.1. Crown ethers.....	- 151 -
4.1.1.2. Cryptand	- 153 -
4.1.1.3. Calixarene.....	- 154 -
4.1.2. Synthesis of Calix-Dansyl	- 164 -
4.1.3. Photophysical properties of Calix-Dansyl	- 166 -
4.1.4. Complexation properties of Calix-Dansyl in organic solvents	- 166 -

4.1.5. Conclusion.....	- 176 -
4.2. Sulfonated Fluorescent Calix[4]bisazacrown for Selective Detection of Aluminum(III)	- 177 -
4.2.1. Introduction of selective fluoroionophores of aluminum(III)	- 177 -
4.2.2. Synthesis of SulfCalix-Dansyl	- 183 -
4.2.3. Photophysical properties of Calix-Dansyl	- 183 -
4.2.4. Photophysical properties of SulfCalix-Dansyl	- 184 -
4.2.5. Complexation of SulfCalix-Dansyl in buffer solutions.....	- 186 -
4.2.6. Conclusion.....	- 195 -
References	- 197 -
Chapter 5. Preliminary Investigation on Modulation of Cation Binding in the Excited State	- 203 -
5.1. Preliminary investigation on cation photoejection based on a fullerene-azacrown dyad.....	- 205 -
5.1.1. Introduction	- 205 -
5.1.2. Synthesis of Full-aza	- 211 -
5.1.3. Photophysical properties of Full-aza	- 212 -
5.1.4. Complexation properties of Full-aza	- 214 -
5.1.5. Conclusion.....	- 219 -
5.2. Preliminary investigation on metal ions translocation based on betaine pyridinium-azacrown dyad	
.....	- 220 -
5.2.1. Introduction	- 220 -
5.2.2. Synthesis of Bet-aza and Bet-DiMe	- 221 -
5.2.3. Photophysical properties of Bet-aza	- 222 -
5.2.4. Complexation properties of Bet-aza	- 227 -
5.2.5. Conclusion.....	- 235 -
Reference	- 237 -
General conclusion	- 243 -
Chapter 6. Experimental Section	- 247 -
6.1. General procedures	- 249 -
6.2. Synthesis and characterization	- 250 -
6.3. Spectroscopic measurement	- 264 -
6.3.1. Instrumentation.....	- 264 -
6.3.2. Time-resolved spectroscopy	- 264 -
6.3.3. Transient absorption spectroscopy	- 266 -
6.4. Reagents and solvents	- 266 -
6.5. Experimental protocols	- 267 -
6.5.1. Determination of fluorescence quantum yield.....	- 267 -
6.5.2. Measurement of stability constants	- 267 -
Reference	- 268 -

General introduction

General introduction

Public health problems such as Alzheimer, Menkes and Wilson's diseases caused by environmental contaminants are growing worldwide concerns. Researches led by chemists and biologists have discovered that various metal ions are very closely related to life processes. For example, accumulation of excessive heavy metal ions such as Hg^{2+} , Cd^{2+} , Cu^{2+} and Pb^{2+} in human body leads to various deleterious effects on health problems due to their high toxicity, while some of the other metal ions such as K^+ and Ca^{2+} are necessary for the functions of living cells. In order to understand the relationships between the metal ions and human health, determining and trafficking trace amount of metal ions *in vitro* and *vivo* have become the key issue for both the chemists and biologists. Fluorescence imaging is definitely one of the most powerful tools. To meet this demand, design and synthesis of versatile fluorescent probes with high sensitivity and high selectivity for the target analytes thus becomes the most attractive research field in chemistry and biology. Moreover, development of fluorescent chemosensors promotes the on-site and real-time detection which is quite important for the environmental monitoring.

In the first chapter, we introduce the concept of fluoroionophore as selective chemosensors and review the basic principles that have been widely used in molecular recognition. Selective chemosensors for Hg^{2+} and Cu^{2+} were utilized as examples to elucidate the applications of these principles.

The second and third chapter describe design, synthesis, photophysical and complexation study of fluorescent chemosensors based on 1,2,3-triazole moiety. Click reaction, mainly referring to Cu(I)-catalyzed Huisgen 1,3-dipolar cycloaddition of azides and alkynes, has provided us with great convenience in organic synthesis. The resultant 1,4-disubstituted 1,2,3-triazole group has been demonstrated to be a very flexible moiety in fluorescent chemosensor. The roles of triazole can be concluded as following: (i) acts as part of the conjugated fluorophores; (ii) provides binding site for target analytes; (iii) contributes as a linker. In order to have a better understanding of 1,2,3-triazole group, it was conjugated with a series of fluorophores, such as fluorescein, NBD, rhodamine, pyrene, and benzothiadiazole. The second and third chapter are then organized by the functions of triazole in these fluorophores: (1) when the triazole was coupled with fluorescein, new fluorophores with

triazole group as the linker were constructed; (2) for NBD- and rhodamine triazole derivatives, triazole group acted as the most important binding site; (3) in pyrene derivative, seven triazole units were assembled on the β -cyclodextrin and complexation properties of the resultant ensemble was investigated; (4) when triazole was conjugated with benzothiadiazole as part of the fluorophore, the effects of the number of triazole, the substituent position and the terminal amino acid group were examined and the metallo-responsive properties of the different benzothiadiazole-triazole fluorophores were studied and here triazole group functions as the co-binding sites. Through our study, the functions of the triazole group in fluorescent chemosensors have been clearly elucidated.

The fourth chapter deals with the design and synthesis of fluorophores consisting of calix[4]arene framework functionalized with dansyl fluorophore. Previous work in our lab, an A-D (acceptor-donor(donor as binding site)) type fluorophore containing BODIPY was used to selectively detect potassium in EtOH/H₂O mixed solution. By retaining the binding motif, we designed and synthesized a new ligand with D-A (donor-acceptor (acceptor as binding site)) type fluorophore with dansyl instead of BODIPY to study its photophysical and complexation properties. Sulfonation of its calix[4]arene moiety gave a water soluble fluorophore. At the beginning, we intended to investigate the influence of additional sulfonate groups on the binding response to K⁺; however, unfortunately this ligand showed no response to K⁺ in pure water. Anyhow, this new ligand with four sulfonate groups exhibited strong binding affinity to Al³⁺ under weak acidic conditions through the formation of colloid particles Al(OH)₃. Detailed spectral investigations were carried out to illustrate the binding process.

The fifth chapter is our preliminary investigation on modulation of cation binding in the excited state. The first part is based on the fullerene moiety attached with an aza-15-crown-5. Fullerene moiety has been widely reported to be an excellent electron acceptor due to its small organization energy and when incorporated with various donors long-live charge separated species were detected. Based on these phenomena, a new ligand composing of fullerene and aza-15-crown-5 was synthesized and used for studying photointerruption of cation binding through the formation of charge separated state. The second part of this chapter summarizes the preliminary investigation of a dyad consisting of betaine pyridinium and aza-15-crown-5. Dipole moment inversion after laser excitation is thought to promote the translocation of cation from benzimidazole moiety to aza-15-crown-5 moiety.

Chapter 1. Introduction of Molecular Fluorescence and Fluorescent Chemosensors Design

1.1. Introduction of molecular fluorescence^{1,2}

When light interacts with matter, the photons can be absorbed, scattered or will not interact with the material and pass straightly through it, depending on the properties of the composition of the object and the wavelength of the light. Before introducing the basic concepts of absorption and fluorescence spectra, different types of electronic transitions are presented by the example of formaldehyde, as presented in Figure 1-1. An electronic transition takes place when an electron from an orbital of the molecule in the ground state is excited to an unoccupied orbital with higher energy level. The energy level of these electronic transitions generally follows the order: $n \rightarrow \pi^* < \pi \rightarrow \pi^* < n \rightarrow \sigma^* < \sigma \rightarrow \sigma^*$. With respect to absorption and fluorescence spectroscopy, two important type of orbital are considered: the Highest Occupied Molecular Orbital (HOMO) and Lowest Unoccupied Molecular Orbital (LUMO). Both refer to the ground state of the molecules and the greater the extent of the π electron system, the lower energy of the low-lying $\pi \rightarrow \pi^*$ transition and consequently the larger the wavelength of the corresponding absorption band.

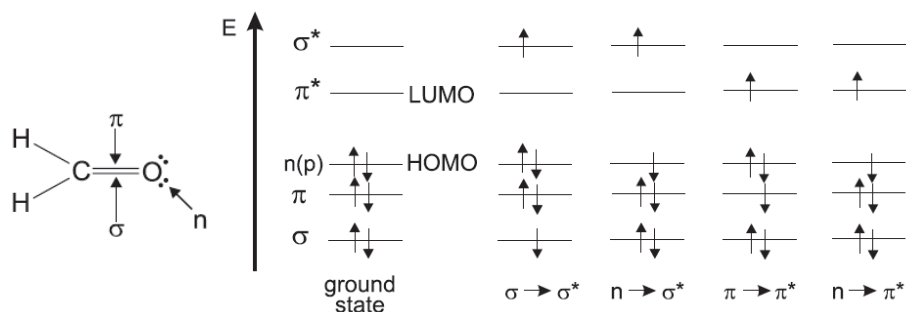


Figure 1-1. Energy level of molecular orbital in formaldehyde and possible electronic transitions.

The Perrin-Jablonski diagram (Figure 1-2) displays all the possible photophysical processes in a molecular system: photon absorption, internal conversion, fluorescence, intersystem crossing, phosphorescence. The singlet electronic states are denoted as S_0, S_1, S_2, \dots and triplet states, T_1, T_2, \dots

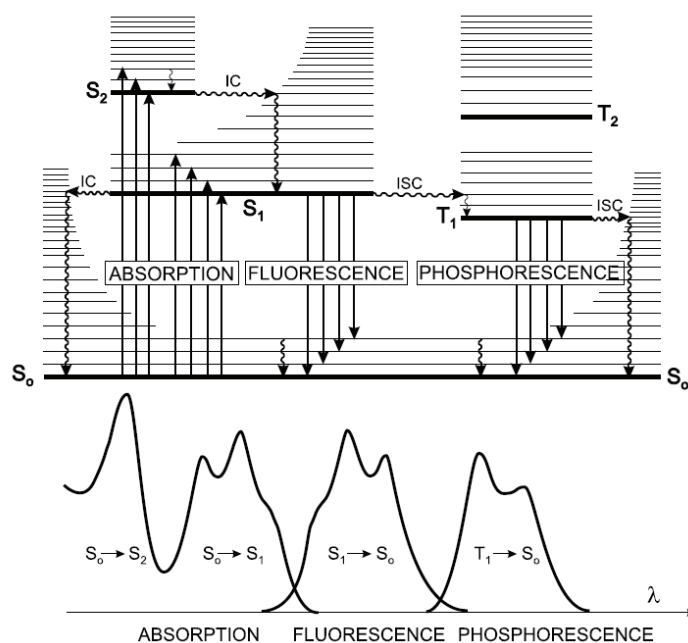
1.1.1. Light absorption

Absorption is known as a process by which the energy of a photon is taken up. It's a very fast process (10^{-15} s) with respect to all the other processes in Figure 1-2, so that there is no concomitant displacement of the nuclei according to Franck-Condon principle. Experimentally, the efficiency of light absorption at a wavelength by an absorbing medium is characterized by the absorbance $A(\lambda)$ or the transmittance $T(\lambda)$. In many cases, the absorbance

of a sample follows the Beer-Lambert law, as presented in eq. 1-1:

$$A(\lambda) = \log \frac{I_{\lambda}^0}{I_{\lambda}} = \varepsilon(\lambda)lc \quad (\text{eq. 1-1})$$

Where I_{λ}^0 and I_{λ} are the light intensities of the beam entering and leaving the absorbing medium, respectively; $\varepsilon(\lambda)$ represents the molar absorption coefficient (usually expressed in $\text{L mol}^{-1} \text{cm}^{-1}$), c is the concentration of (in mol L^{-1}) of chromophore and l is the absorption path length (in cm).



Characteristic times

Absorption: 10^{-15} s

Vibrational relaxation: $10^{-15} - 10^{-10}$ s

Fluorescence : $10^{-9} - 10^{-7}$ s

Intersystem crossing: $10^{-10} - 10^{-8}$ s

Internal conversion: $10^{-15} - 10^{-10}$ s

Phosphorescence: $10^{-6} - 1$ s

Figure 1-2. Perrin-Jablonski diagram and illustration of the relative positions of absorption, fluorescence and phosphorescence spectra.

1.1.2. Molecular fluorescence

Upon absorbing a photon, electron of a molecule in the ground state is excited to an orbital with higher energy level followed by the vibrational relaxation to the 0 vibrational level of S_1 singlet state within a time scale of 10^{-13} - 10^{-11} s. Emission of the photons accompanying the $S_1 \rightarrow S_0$ relaxation is called fluorescence and often its characteristics do not depend on the excitation wavelength. It should be noted that the fluorescence spectrum locates in the higher wavelength region when compared with its absorption spectrum due to

the energy loss in the interconversion process, as shown in Figure 1-2. The variation of wavenumbers between the maximum of the first absorption band and the maximum fluorescence is called the *Stokes shift*, which is related to the solvents used for investigation. In highly diluted solution, the fluorescence intensity is proportional to the concentration of fluorophore:

$$I_F = kI_0(\lambda_{exc})\Phi_F\varepsilon(\lambda_{exc})lC \quad (\text{eq. 1-2})$$

where k is the proportionality factor, $I_0(\lambda_{exc})$ is the light intensity at the excitation wavelength; $\varepsilon(\lambda_{exc})$ is the molar absorption coefficient of the fluorophore at the excitation wavelength, l the optical path in the sample and C the concentration of the fluorophore; Φ_F is fluorescence quantum yield.

After light excitation, the electrons in the excited state can be deactivated by different pathways: internal conversion, fluorescence emission, intersystem crossing, and probably electron transfer, and energy transfer. Lifetime as another important characteristic of fluorescence represents the average time of the molecules in the S_1 excited state. According to the classical chemical kinetics, the deactivation rate of the excited molecules is expressed as the following differential equation (eq. 1-3) in the case of one component:

$$-\frac{d[{}^1A^*]}{dt} = (k_r^S + k_{nr}^S)[{}^1A^*] \quad (\text{eq. 1-3})$$

where $[{}^1A^*]$ represents the concentration of the excited molecules at S_1 state, k_r^S and k_{nr}^S are the rate constants for radiative deactivation $S_1 \rightarrow S_0$ with fluorescence emission and non-radiative process such as internal conversion and intersystem crossing, respectively. Integration of eq. 1-3 yields the time evolution of the concentration of excited molecules $[{}^1A^*]$, as shown in eq. 1-4. $[{}^1A^*]_0$ is the concentration of excited molecules at time 0 after pulse light excitation.

$$[{}^1A^*] = [{}^1A^*]_0 \exp\left(-\frac{t}{\tau_s}\right) \quad (\text{eq. 1-4}) \quad \text{With } \tau_s = \frac{1}{k_r^S + k_{nr}^S} \quad (\text{eq. 1-5})$$

The fluorescence quantum yield Φ_F is the ratio of the number of the emitted photons to the number of absorbed photons, that is the fraction of the excited molecules that deactivate to ground state S_0 with emission of fluorescence photons, expressed as eq. 1-6. The fluorescence quantum yield is usually determined by comparison with a fluorescence standard, as depicted

in Chapter 6 (Experimental section).

$$\Phi_F = \frac{k_r^s}{k_r^s + k_{nr}^s} = k_r^s \tau_s \quad (\text{eq. 1-6})$$

When a population of fluorophores is illuminated by a linearly polarized incident light, those whose transition moments are oriented in a direction close to the electric vector of the incident beam are preferentially excited. Fluorescence anisotropy is caused by the anisotropic distribution of the excited fluorophores. The changes in the direction of the transition moment during the lifetime of excited state will cause decrease of anisotropy. Several reasons are proposed for depolarization, such as Brownian motion, torsional vibrations and energy transfer to another molecule with different orientation. Therefore, fluorescence polarization measurements can provide useful information on the molecular mobility, size, shape, and flexibility of molecules, fluidity of a medium and order parameters. As presented in Figure 1-3, the components of fluorescence intensity that are parallel and perpendicular to the electric vector of the incident light are denoted as I_{\parallel} and I_{\perp} , respectively. The polarization state of fluorescence is characterized either by polarization ratio p (eq. 1-7) or emission anisotropy r (eq. 1-8). Their relationship is shown in eq. 1-9.

$$p = \frac{I_{\parallel} - I_{\perp}}{I_{\parallel} + I_{\perp}} \quad (\text{eq. 1-7}) \quad r = \frac{I_{\parallel} - I_{\perp}}{I_{\parallel} + 2I_{\perp}} \quad (\text{eq. 1-8})$$

$$r = \frac{2p}{3 - p} \quad (\text{eq. 1-9})$$

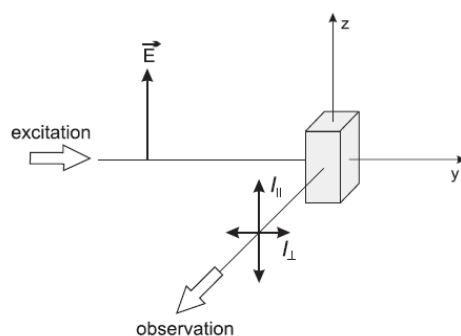


Figure 1-3. Usual configuration for measuring fluorescence polarization.

1.2. Fluorescent chemosensor design

Detection of biologically and environmentally important metal ions has attracted much attention of chemists and biologists. The fluctuations of metal ions in the blood fluid are closely related to the functions and diseases.^{3,4} With the advance of the analytical techniques,

various approaches such as flame photometry, atomic absorption spectrometry, ion sensitive electrodes, electron microprobe analysis are now available for the detection of metal ions.⁵ However, many of them require complicated sample pretreatment, high cost and sophisticated instruments. Moreover, many of them are not able to work in living samples.

In the context, fluorescent chemical sensors display several advantages in terms of sensitivity, selectivity, response time and fluorescence imaging.^{6,7,8,9} Its great simplicity also brings us the possibility of on-site and real-time detection. Therefore, great efforts have been devoted to the development of fluorescent chemosensors for detection of metal ions. As shown in Figure 1-4, a fluorescent chemosensor comprises of a fluorophore and an ionophore linked with/without spacer.⁷ The fluorophore acts as the signal transducer, which convert the recognition event into the photophysical changes, such as spectra, fluorescence quantum yield and lifetime. These changes are due to the perturbation of photoinduced processes such as electron transfer, charge transfer, energy transfer, and formation of excimer. With respect to ionophore, it is the recognition moiety that mainly determines the binding selectivity and sensitivity. The specific interactions between ionophore and guests are often based on the noncovalent bonding, such as hydrogen bonding, metal complexation, π - π stacking, hydrophobic forces and electrostatic interactions.¹⁰ It is affected by the characteristic of cation, solvent environment, pH, and ionic strength. Regarding the integrated fluoroionophore, some atoms from the fluorophore may participate to the binding processes. Therefore, sensing selectivity and sensitivity are dependent on the whole structure of fluoroionophore. Following we will present how different principles can be utilized in fluorescent chemosensors design according to the literatures.

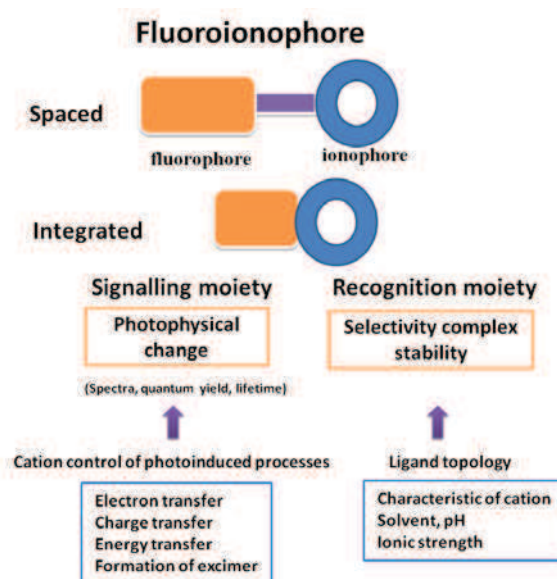


Figure 1-4. Illustration of fluoroionophore.

1.2.1. Photoinduced electron transfer

A series of fluorescent sensors for cations and anions has been developed based on this principle. Figure 1-5 depicts the electronic transitions before and after complexation with cations. Upon excitation of the fluorophore, an electron in HOMO goes to LUMO. Under this condition, if there is an orbital from another part of this fluorophore with energy level between HOMO and LUMO of the fluorophore, a PET from this full orbital to the HOMO of the fluorophore can take place, and a further electron transfer from the LUMO of the fluorophore to the external orbital retrieves the stable ground state. As a result, the excited electron deactivates by non-radiative pathway and results in fluorescence quenching. Upon complexation with cation, the energy level of external orbital is reduced to lower than that of HOMO of the fluorophore and consequently the electron transition from full external orbital to HOMO of the fluorophore is suppressed and cause fluorescence enhancement. Typically, the cation receptor involves aliphatic or aromatic amines as quenchers, in which the PET can take place from amino group to fluorophore and quench its fluorescence intensity.

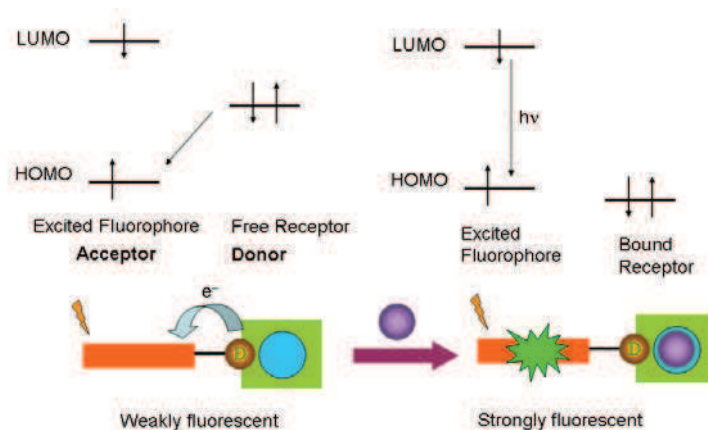


Figure 1-5. Cation recognition based on fluorescent PET sensors (reductive electron transfer).

The thermodynamic feasibility of the excited singlet state electron transfer reaction can be calculated by employing Rehm-Weller equation (eq. 1-10). If the ΔG^0 is negative, then the electron transfer is thermodynamically possible.

$$\Delta G^0 = E_{D^{*+}/D}^0 - E_{A/A^{\bullet-}}^0 - \Delta E_{00}(A) - \Delta H_{solv} - \frac{e^2}{4\pi\epsilon r} \quad (\text{eq. 1-10})$$

Where ΔG^0 represents variations of the standard free enthalpy of the electron transfer, $E_{D^{*+}/D}^0$ and $E_{A/A^{\bullet-}}^0$ are standard electrode potential of donor (D) and acceptor (A), respectively;

$\Delta E_{00}(A)$ is singlet excited energy of the fluorophore, ΔH_{solv} is enthalpy of solvation effect, e is the electron charge, ϵ is the dielectric constant of the solvent, and r is the distance between two ions.

In the other case, PET process can take place in the bound complex when the energy level of LUMO of the transition cation is between HOMO and LUMO of the fluorophore. As show in Figure 1-6, in this case fluorophore acts as electron donor. Upon excitation of the fluorophore in the complex, the excited electron can deactivate through an electron transfer to LUMO of transition metal ions. As a result of this non-radiative pathway, the emission of the fluorophores is quenched. The thermodynamic feasibility can also described by Rehm-Weller equation as follow (eq. 1-11):

$$\Delta G^0 = E_{D^{+}/D}^0 - E_{A/A^{\bullet-}}^0 - \Delta E_{00}(D) - \Delta H_{solv} - \frac{e^2}{4\pi\epsilon r} \quad (\text{eq. 1-11})$$

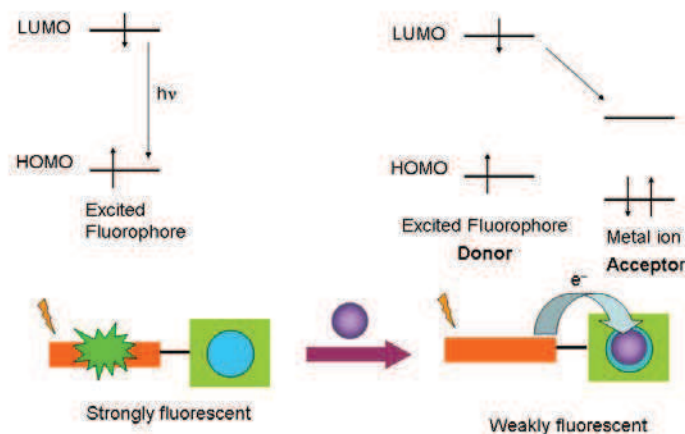


Figure 1-6. Cation recognition based on fluorescent PET sensors (oxidative electron transfer).

Spectral properties of fluorescein derivatives have been extensively studied by using PET mechanism. For **PET-1**, in the excited state electron transfer from aromatic amino group to xanthene moiety leads to its low fluorescence quantum yield.¹¹ Upon complexation with Hg^{2+} , the PET process is suppressed, accompanied with strong fluorescence enhancement. As we depict in Figure 1-7, an OFF-ON type of Hg^{2+} selective fluorescent chemosensor was developed. In contrast, ligand **PET-2** exhibited strong fluorescence quenching upon complexation with Hg^{2+} , which was attributed to electron transfer from dansyl fluorophore to Hg^{2+} in the complex.¹² An ON-OFF type chemosensor based on different PET mechanism was constructed. According to this principle, large numbers of fluoroionophores have been developed by changing the fluorophore and/or changing the binding motif.^{13,14,15,16,17} It should

be noted that generally the absorption spectrum of the fluorophore does not change after complexation with metal ions when the sensing mechanism is based on PET process.

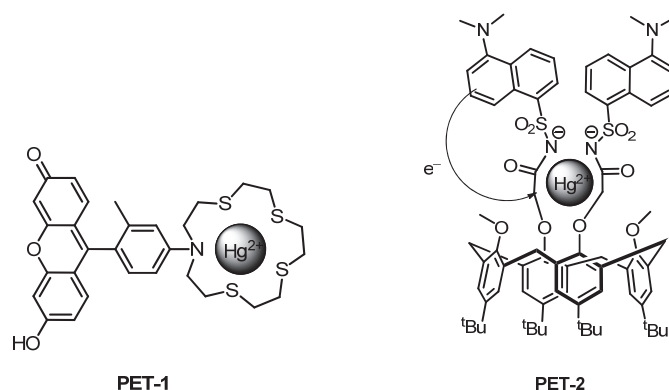


Figure 1-7. PET type OFF-ON (**PET-1**) and ON-OFF (**PET-2**) Hg^{2+} chemosensors.

1.2.2. Photoinduced charge transfer

The photoinduced charge transfer is a phenomenon when an electron-donating group ($-\text{NH}_2$, $-\text{NMe}_2$, $-\text{CH}_3\text{O}$) is conjugated with an electron-withdrawing group ($>\text{C}=\text{O}$, $-\text{CN}$), upon excitation of a fluorophore, an electron will move from one orbital to the other, accompanied with by an instantaneous change in the dipole moment of the fluorophore. The higher the polarity of the solvent, the lower energy of the relaxed state and the larger red shift of the emission spectrum, which is called as the positive solvatochromism.

Based on the close relationship between the microenvironment and spectral properties of the ICT type fluorophore, it can thus be anticipated that cation interaction with the donor or acceptor moiety will also change the photophysical properties of fluorophore by affecting the charge transfer efficiency. Utilization of the PCT type fluorophores in cation sensing then have two different manners: for the first case cations interact with acceptor group and for the other case the cations complex with donor group. These two different binding modes can give distinguished spectral changes.

In the case of cation interacting with the acceptor group, complexation enhances the electron withdrawing character of the acceptor, resulting in red shift of the absorption spectrum and increased molar absorption coefficient. The fluorescence spectrum in principle shifts in the same direction as that of absorption spectrum. The other emission parameters are accordingly changed. The red shift of spectra generally is explained by the cation-stabilized excited state of the fluorophore. As shown in Figure 1-8, in the free ligand **PCT-1**, intramolecular charge transfer in coumarin moiety from amino group to carbonyl group occurs upon excitation.¹⁸ Complexation between cation and carbonyl group causes

enhancement of intramolecular charge transfer and consequently both the absorption and fluorescence spectra show remarkable red shift. This principle is widely used in colorimetric and fluorescent detection of metal ions.¹⁹

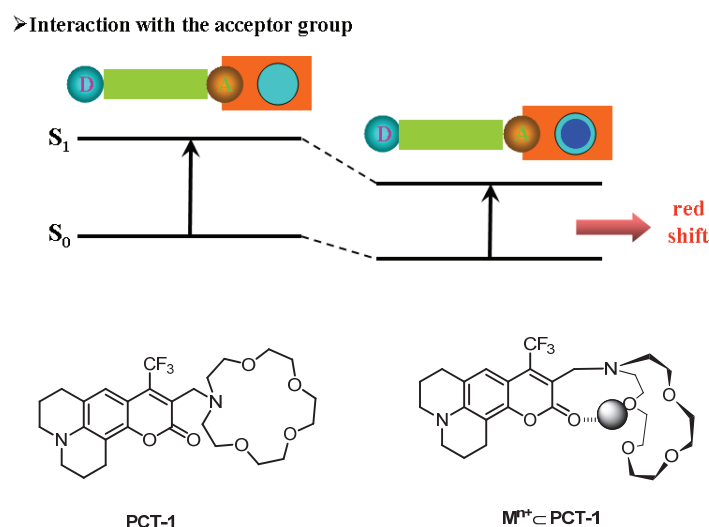


Figure 1-8. Cation recognition based on fluorescent ICT sensors (interact with acceptor group).

In contrast, when the cation binds to the donor group of fluoroionophore, it reduces its electron-donating character and meanwhile decreases the conjugation of the π system, which is expected to result in blue shift of the absorption spectrum and decreased absorption extinction coefficient. However, the fluorescence spectrum often undergoes with a much slighter blue shift when compared with that of the absorption spectrum. This phenomenon can be attributed to the photodisruption between cation and donor group.²⁰ Upon excitation, charge transfer from the donor group to the acceptor produces partially positive character of donor group and thus decreases its binding ability with cations. The emissive species may actually come from the loose complex or the free ligand, which has been evidenced by transient absorption technique. For instance, when azacrown are conjugated with strongly electron-withdrawing merocyanine to construct **PCT-2** (Figure 1-9), intramolecular charge transfer from the amino group to dicyanomethylene group is reduced upon complexation with cations.²¹ Large blue shift was observed in the presence of cation, meanwhile slight blue shift of the fluorescence took place. Such kind of chemosensors has been constructed for selective detection of metal ions.^{22,23}

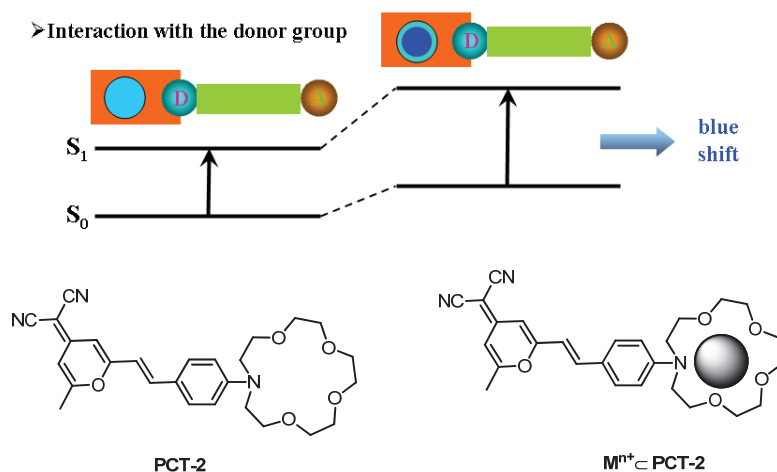


Figure 1-9. Cation recognition based on fluorescent ICT sensors (interact with donor group).

1.2.3. Energy transfer

Energy transfer from an excited fluorophore (donor) to another fluorophore (acceptor) is possible when the emission of the donor partially overlaps with the absorption of the acceptor, as shown in Figure 1-10. Two different pathways are available for the occurrence of energy transfer. Radiative transfer refers to the photons emitted by donor absorbed by an acceptor. The transfer efficiency depends on the spectral overlap and the concentrations. In the diluted solution, this approach is not important. For the second pathway, non-radiative transfer results from short- or long-range interaction between fluorophores. It requires interaction between a donor fluorophore and acceptor fluorophore beside the spectral overlap, which is also called resonance energy transfer (RET) or excitation energy transfer (EET). Non radiative energy transfer can result from different interaction mechanisms. Förster type is based on long-rang dipole-dipole Coulombic interaction, in which the initially excited electron on the donor return to the ground state orbital on donor and simultaneously an electron on the acceptor is promoted to the excited state; while Dexter's type based on electron exchange between donor and acceptor is only available in short range due to the requirement of orbital coupling, as shown in Figure 1-11.

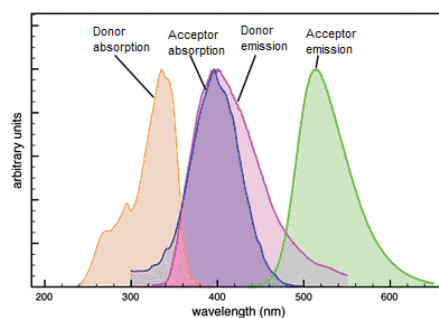


Figure 1-10. Spectral overlap between donor emission and acceptor absorption.

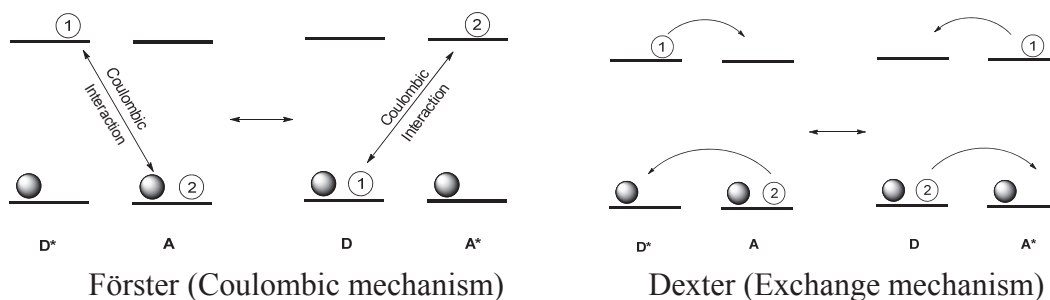


Figure 1-11. Mechanism of energy transfer, Förster and Dexter type.

According to the Förster theory, the energy transfer rate can be calculated by eq. 1-12 and 1-13:

$$k_t = \frac{1}{\tau_D^0} \left[\frac{R_0}{r} \right]^6 \quad (\text{eq. 1-12})$$

$$R_0^6 = \frac{9000(\ln 10)\kappa^2\Phi_D^0}{128\pi^5 N_A n^4} \int_0^\infty I_D(\lambda)\varepsilon(\lambda)\lambda^4 d\lambda \quad (\text{eq. 1-13})$$

where k_t represents the energy transfer rate constant, τ_D^0 is lifetime of donor in the absence of transfer, R_0 is Förster radius, r is the distance between donor and acceptor, κ^2 is the orientation factor, Φ_D^0 is the fluorescence quantum yield of the donor in the absence of transfer, N_A is Avogadro number, n is average refractive index of the medium in the wavelength range where spectral overlap is significant, $I_D(\lambda)$ is the fluorescence spectrum of the donor normalized, $\varepsilon(\lambda)$ is the molar absorption coefficient of the acceptor.

The transfer efficiency is given by eq. 1-14:

$$\Phi_T = \frac{k_T}{1/\tau_D^0 + k_T} = \frac{1}{1 + (r/R_0)^6} \quad (\text{eq. 1-14})$$

The resonance energy transfer is sixth power dependence on the distance, which is quite useful as a ruler in biological processes.

From the above introduction of RET processes, modulation of factors such as spectral overlap, orientation of the fluorophore pair, distance between the donor and acceptor, can significantly affect the energy transfer efficiency and realize the ratiometric detection of metal ions.^{24,25,26} As shown in Figure 1-12, the addition of Cu^{2+} selectively induces the ring-opening

of rhodamine fluorophore, leading to the spectral overlap between coumarine and ring-opening form of rhodamine.²⁵ Subsequently energy transfer occurred, evidenced by fluorescence quenching of coumarine and fluorescence enhancement of rhodamine.

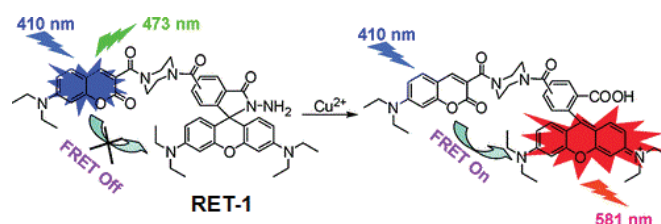


Figure 1-12. Ratiometric detection of Cu^{2+} based on RET mechanism.

1.2.4. Formation of excimers

Excimers are defined as the dimer formed by collision between an excited fluorophore and an identical fluorophore in the ground state. Excitation energy is delocalized over the two fluorophores, which leads to a new structureless emission located at longer wavelength than that of the monomer. Formation of excimer is diffusion-controlled process and is affected by temperature, viscosity and molecular structural conformation. For intermolecular formation of excimers, generally high concentration of the fluorophores is required to get sufficient collision during the lifetime of monomer. In contrast, intramolecular formation of excimers is independent of concentration but related to the molecular structural conformation. The fluorescence intensity ratio of the excimer and monomer is used to characterize the efficiency of formation of excimer. As shown in Figure 1-13, **EXC-1** exhibits strong monomer emission due to the extended conformation of two pyrene fluorophore.²⁷ Upon complexation with metal ions, conformation change of the carbohydrate ring forces two pyrenyl group into 1,3-diaxial orientation, which facilitate the formation of excimer complex. The fluorescence intensity ratio of the excimer and monomer was then used to indicate the concentration of metal ions in solutions. Ratiometric detection shows great advantage to detect metal ions with a built-in correction for environmental effects.^{28,29,30,31}

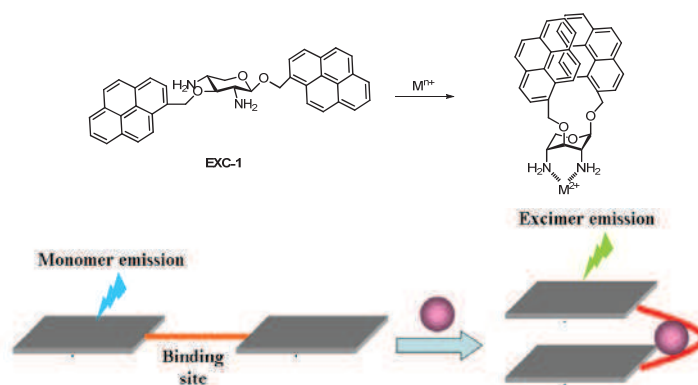


Figure 1-13. Cation recognition based on formation of excimer.

1.2.5. Chemodosimeters

Chemodosimeters represent a new approach for the detection of analytes by chemical processes.^{32,33,34,35} They show great advantages in terms of selectivity and sensitivity when compared with coordination-based sensors, but also display disadvantages in relatively long response time, irreversibility and the possible release of toxic species. For example, a number of chemodosimeters have been reported for the selective detection of Hg^{2+} by using mild reactions. As shown in Figure 1-14, phosphorus-selenium moiety in **CDM-1** showed strong binding affinity to Hg^{2+} . The Hg^{2+} addition promoted transformation of phosphorus-selenium into phosphane oxide, which resulted in fluorescence enhancement. By changing the components of fluorophore, such a turn-on fluorescent approach gave a detection limit of Hg^{2+} at 0.18 ppb in $\text{CH}_3\text{CN}/\text{H}_2\text{O}$ (80:20) at pH 7.³²

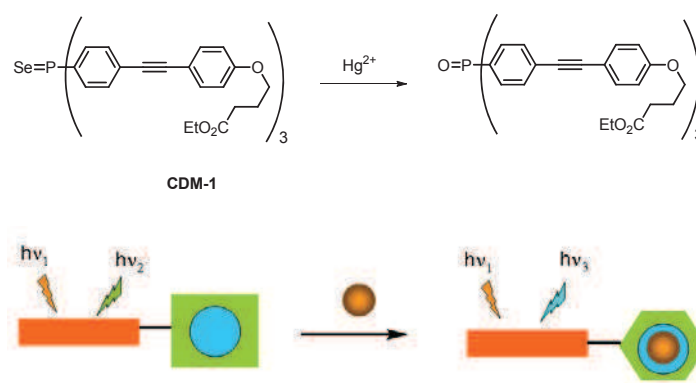


Figure 1-14. Chemodosimeters based on modification of fluorophore component.

The other approach is based on analyte-induced elimination of ionophores.³⁵ As shown in Figure 1-15, addition of Hg^{2+} to the solution of **CMD-2** led to the deprotection of vinyl ether group, which turned on the green emission of the fluorescein. This probe worked efficiently at the ppb level of Hg^{2+} in pure water.

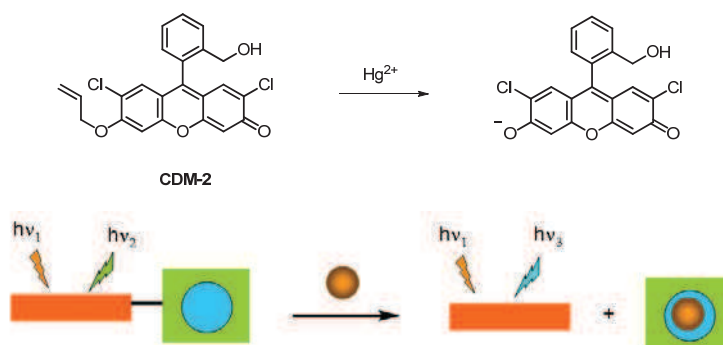


Figure 1-15. Chemodosimeters based on analyte-induced elimination of ionophore.

It should be pointed out that among the reported chemodosimeters, ring-opening of rhodamine lactam is the most commonly used.^{36,37} As shown in Figure 1-16, **CDM-3** with a rhodamine spirolactam attached with carbohydrazone unit showed highly selective response to Hg^{2+} in an aqueous DMF (v/v=1:1) with a detection limit of 2 ppb. The structure of **CDM-3** and complex **CDM-3- Hg^{2+}** were fully characterized by X-ray crystallography, clearly demonstrating the ring-opening structure in the complex.³⁸

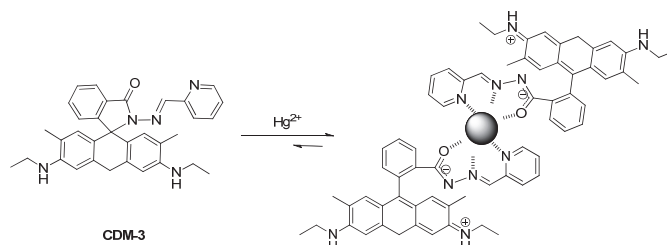


Figure 1-16. Chemodosimeters based on ring-opening of rhodamine spirolactam.

1.3. Applications of fluorescent chemosensors

The applications of fluorescent chemosensors can be mainly categorized into two important fields: detection of environmentally important pollutants such as heavy metal ions and as the probes for fluorescence imaging to monitor biologically important species.³⁹ In former, by incorporation into microfluidic devices, very efficient methods have been developed for the detection of Pb^{2+} with the detection limit meeting with the requirement of WHO.⁴⁰ The latter application attracts much more interest for its great advantage in visualization of biologic events in a spatio-temporal manner, providing more information for the early disease diagnosis and therapy. Considering the practical manipulations and limitations of technique, most researches have used zebrafish as a model animal to study the uptake and distribution of target analytes in live animal, as presented in Figure 1-17.⁴¹ For example, a selenolactone rhodamine based sensor **IMA-1** was successively applied in fluorescence imaging of mercury species in cells and zebrafish through a deselenation reaction.⁴²

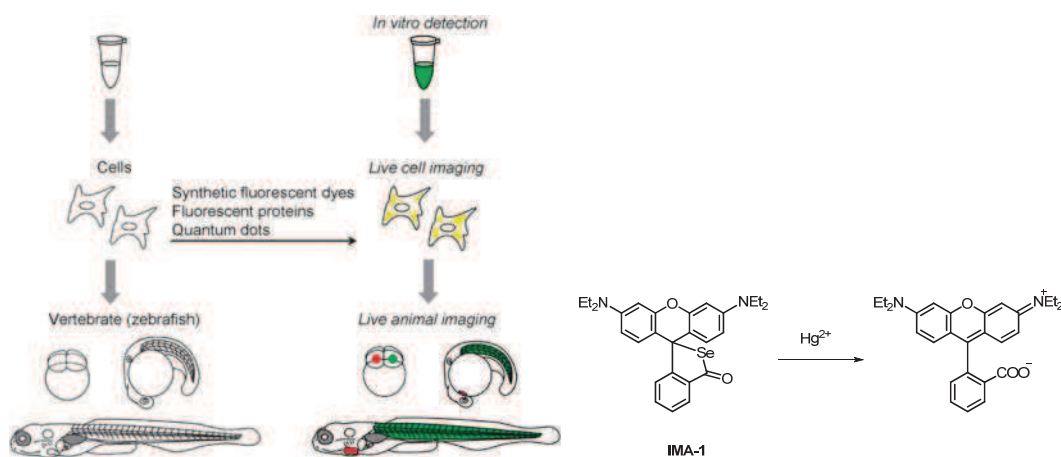


Figure 1-17. Schematic illustration of fluorescence imaging based fluorescent probes.

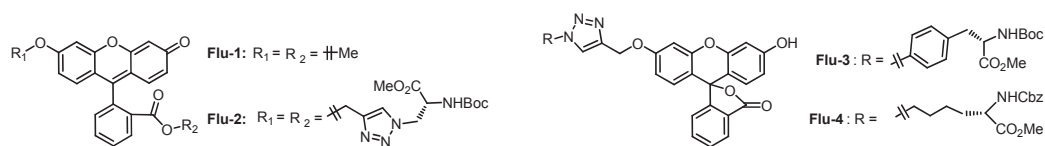
1.4. Objectives

A series of new easily accessible fluoroionophores has been synthesized through Cu(I)-catalyzed 1,3-dipolar Huisgen alkyne-azide cycloaddition reaction in the Xie's group, as presented in Scheme 1-1. In this dissertation, we intend to make a systematic investigation on their spectroscopic and metallo-responsive properties to clearly elucidate the roles of 1,4-disubstituted 1,2,3-triazolyl group in fluorescent chemosensors and finally establish a useful guideline for our future work on designing new probes. These works will be presented in Chapter 2 and 3. We believe this will be meaningful due to the wide applications of “click” reaction and highly flexible coordination chemistry of triazole group.

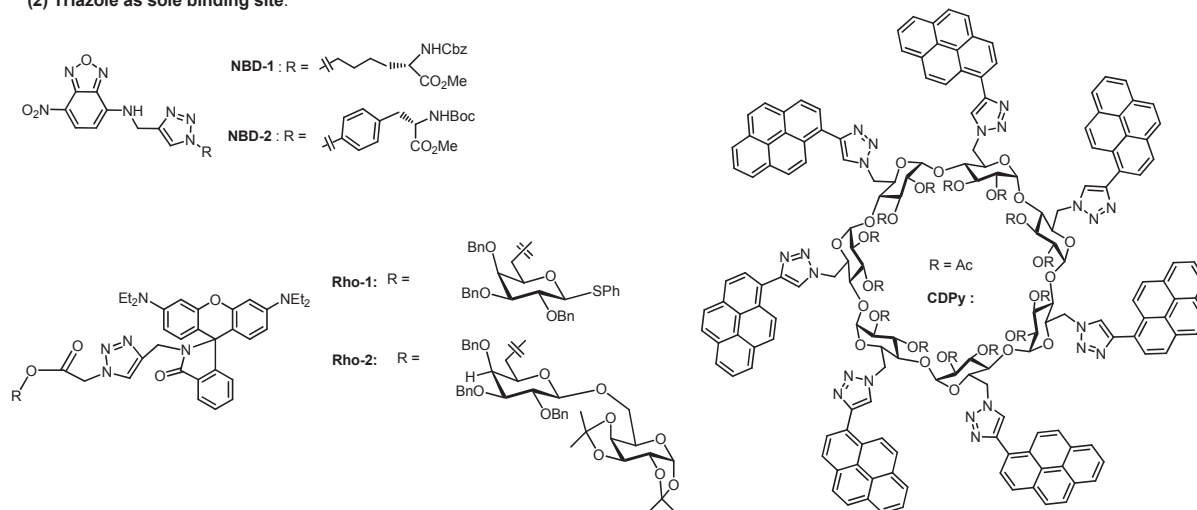
Moreover, two new fluoroionophores (Scheme 1-2) bearing calix[4]bisazacrown will be created to understand the effect of structural modifications on the binding selectivity and sensitivity of calix[4]bisazacrown moiety to metal ions (Chapter 4).

According to literatures that C_{60} is a good electron acceptor and long-live charge separated state could be created, a new fluoroionophore (Scheme 1-3) consisting of C_{60} and aza-15-crown-5 can be synthesized to investigate the photoejection phenomenon in the excited state. Finally, dipole moment inversion in betaine pyridinium incorporated with 15-crown-5 as the binding motif (Scheme 1-3) will be used to study the photoinduced cation translocation in the excited state. These related works will be discussed in Chapter 5.

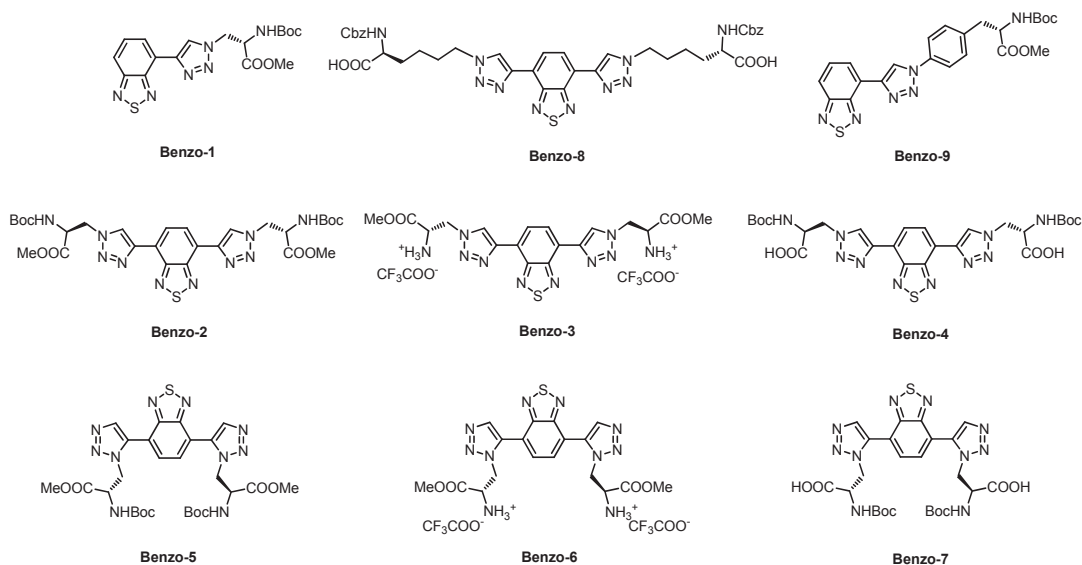
(1) Triazole as linker:



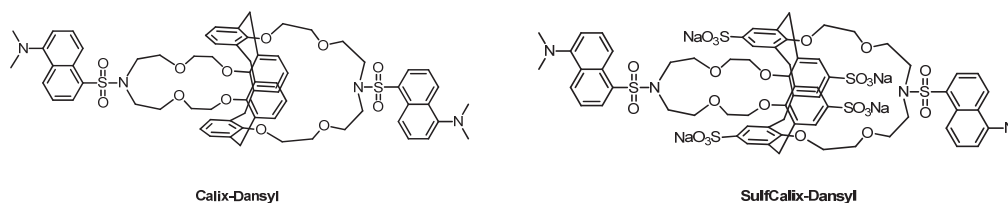
(2) Triazole as sole binding site:



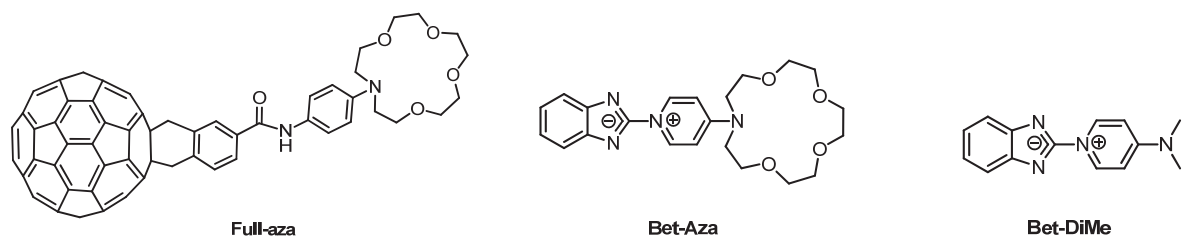
(3) Triazole as co-binding site:



Scheme 1-1. New fluoroionophores based on triazole.



Scheme 1-2. New fluoroionophores based on calix[4]bisazacrown.



Scheme 1-3. New fluoroionophores based on fullerene and betaine pyridinium.

References

- [1] Valeur, B. "*Molecular Fluorescence: Principles and Applications*" Wiley-VCH Verlag GmbH, **2001**.
- [2] Lakowicz, J. R. "*Principles of Fluorescence Spectroscopy 3rd edition*" Springer, **2006**.
- [3] "*Metals in chemical biology.*" Nature Chemical Biology **2008**, *4*, 143-143.
- [4] Drago, D.; Bolognin, S.; Zatta, P. "*Role of Metal Ions in the A beta Oligomerization in Alzheimer's Disease and in Other Neurological Disorders.*" Current Alzheimer Research **2008**, *5*, 500-507.
- [5] Harvey, D. "*Modern Analytical Chemistry*" McGraw-Hill Science, **1999**.
- [6] de Silva, A. P.; Gunaratne, H. Q. N.; Gunnlaugsson, T.; Huxley, A. J. M.; McCoy, C. P.; Rademacher, J. T.; Rice, T. E. "*Signaling recognition events with fluorescent sensors and switches.*" Chemical Reviews **1997**, *97*, 1515-1566.
- [7] Valeur, B.; Leray, I. "*Design principles of fluorescent molecular sensors for cation recognition.*" Coordination Chemistry Reviews **2000**, *205*, 3-40.
- [8] Prodi, L.; Bolletta, F.; Montalti, M.; Zaccheroni, N. "*Luminescent chemosensors for transition metal ions.*" Coordination Chemistry Reviews **2000**, *205*, 59-83.
- [9] Callan, J. F.; de Silva, A. P.; Magri, D. C. "*Luminescent sensors and switches in the early 21st century.*" Tetrahedron **2005**, *61*, 8551-8588.
- [10] Gellman, S. H. "*Introduction: Molecular recognition.*" Chemical Reviews **1997**, *97*, 1231-1232.
- [11] Yoon, S.; Miller, E. W.; He, Q.; Do, P. H.; Chang, C. J. "*A bright and specific fluorescent sensor for mercury in water, cells, and tissue.*" Angewandte Chemie-International Edition **2007**, *46*, 6658-6661.
- [12] Metivier, R.; Leray, I.; Valeur, B. "*Lead and mercury sensing by calixarene-based fluoroionophores bearing two or four dansyl fluorophores.*" Chemistry-a European Journal **2004**, *10*, 4480-4490.
- [13] Domaille, D. W.; Que, E. L.; Chang, C. J. "*Synthetic fluorescent sensors for studying the cell biology of metals.*" Nature Chemical Biology **2008**, *4*, 168-175.
- [14] Lim, C. S.; Kang, D. W.; Tian, Y. S.; Han, J. H.; Hwang, H. L.; Cho, B. R. "*Detection of mercury in fish organs with a two-photon fluorescent probe.*" Chemical Communications **2010**, *46*, 2388-2390.
- [15] Chen, T.; Zhu, W. P.; Xu, Y. F.; Zhang, S. Y.; Zhang, X. J.; Qian, X. H. "*A thioether-rich crown-based highly selective fluorescent sensor for Hg(2+) and Ag(+) in aqueous solution.*" Dalton Transactions **2010**, *39*, 1316-1320.
- [16] Jeong, H. J.; Li, Y.; Hyun, M. H. "*A Fluorescent Chemosensor Based on 7-Nitrobenz-2-oxa-1,3-diazole (NBD) for the Selective Detection of Hg(II).*" Bulletin of the Korean Chemical Society **2011**, *32*, 2809-2812.
- [17] Liu, X. Q.; Shu, X.; Zhou, X.; Zhang, X.; Zhu, J. "*Ultra-Sensitive Fluorescent Sensor for Hg²⁺ Based on a Donor-Acceptor-Donor Framework.*" Journal of Physical Chemistry A **2010**, *114*, 13370-13375.
- [18] Bourson, J.; Pouget, J.; Valeur, B. "*Ion-Responsive Fluorescent Compounds .4. Effect of*

Cation Binding on the Photophysical Properties of a Coumarin Linked to Monoaza-Crown and Diaza-Crown Ethers. Journal of Physical Chemistry **1993**, *97*, 4552-4557.

[19]Ahamed, B. N.; Ghosh, P. "Selective colorimetric and fluorometric sensing of Cu(II) by iminocoumarin derivative in aqueous buffer." Dalton Transactions **2011**, *40*, 6411-6419.

[20]Ley, C.; Lacomat, F.; Plaza, P.; Martin, M. M.; Leray, I.; Valeur, B. "Femtosecond to Subnanosecond Multistep Calcium Photoejection from a Crown Ether-Linked Merocyanine." Chemphyschem **2009**, *10*, 276-281.

[21]Bourson, J.; Valeur, B. "Ion-Responsive Fluorescent Compounds .2. Cation-Steered Intramolecular Charge-Transfer in a Crowned Merocyanine." Journal of Physical Chemistry **1989**, *93*, 3871-3876.

[22]Wagner, S.; Brodner, K.; Coombs, B. A.; Bunz, U. H. F. "Pyridine-Substituted BODIPY as Fluorescent Probe for Hg²⁺." European Journal of Organic Chemistry **2012**, 2237-2242.

[23]Yuan, M. J.; Li, Y. L.; Li, J. B.; Li, C. H.; Liu, X. F.; Lv, J.; Xu, J. L.; Liu, H. B.; Wang, S.; Zhu, D. "A colorimetric and fluorometric dual-modal assay for mercury ion by a molecule." Organic Letters **2007**, *9*, 2313-2316.

[24]Liu, Y. L.; Lv, X.; Zhao, Y.; Chen, M. L.; Liu, J.; Wang, P.; Guo, W. "A naphthalimide-rhodamine ratiometric fluorescent probe for Hg²⁺ based on fluorescence resonance energy transfer." Dyes and Pigments **2012**, *92*, 909-915.

[25]Yuan, L.; Lin, W. Y.; Chen, B.; Xie, Y. A. "Development of FRET-Based Ratiometric Fluorescent Cu²⁺ Chemodosimeters and the Applications for Living Cell Imaging." Organic Letters **2012**, *14*, 432-435.

[26]Chen, Y. T.; Wan, L.; Yu, X.; Li, W. J.; Bian, Y. Z.; Jiang, J. Z. "Rational Design and Synthesis for Versatile FRET Ratiometric Sensor for Hg²⁺ and Fe²⁺: A Flexible 8-Hydroxyquinoline Benzoate Linked Bodipy-Porphyrin Dyad." Organic Letters **2011**, *13*, 5774-5777.

[27]Yuasa, H.; Miyagawa, N.; Izumi, T.; Nakatani, M.; Izumi, M.; Hashimoto, H. "Hinge sugar as a movable component of an excimer fluorescence sensor." Organic Letters **2004**, *6*, 1489-1492.

[28]Kim, H. J.; Hong, J.; Hong, A.; Ham, S.; Lee, J. H.; Kim, J. S. "Cu(2+)-induced intermolecular static excimer formation of pyrenealkylamine." Organic Letters **2008**, *10*, 1963-1966.

[29]Zhou, Y.; Zhu, C. Y.; Gao, X. S.; You, X. Y.; Yao, C. "Hg²⁺-Selective Ratiometric and "Off-On" Chemosensor Based on the Azadiene-Pyrene Derivative." Organic Letters **2010**, *12*, 2566-2569.

[30]Karuppanan, S.; Chambron, J. C. "Supramolecular Chemical Sensors Based on Pyrene Monomer-Excimer Dual Luminescence." Chemistry-an Asian Journal **2011**, *6*, 964-984.

[31]Manandhar, E.; Wallace, K. J. "Host-guest chemistry of pyrene-based molecular receptors." Inorganica Chimica Acta **2012**, *381*, 15-43.

[32]Samb, I.; Bell, J.; Toullec, P. Y.; Michelet, V.; Leray, I. "Fluorescent Phosphane Selenide As Efficient Mercury Chemodosimeter." Organic Letters **2011**, *13*, 1182-1185.

[33]Du, J. J.; Hu, M. M.; Fan, J. L.; Peng, X. J. "Fluorescent chemodosimeters using "mild" chemical events for the detection of small anions and cations in biological and environmental media." Chemical Society Reviews **2012**, *41*, 4511-4535.

[34]Duong, T. Q.; Kim, J. S. "Fluoro- and Chromogenic Chemodosimeters for Heavy Metal

- Ion Detection in Solution and Biospecimens.*" Chemical Reviews **2010**, *110*, 6280-6301.
- [35]Ando, S.; Koide, K. "*Development and Applications of Fluorogenic Probes for Mercury(II) Based on Vinyl Ether Oxymercuration.*" Journal of the American Chemical Society **2011**, *133*, 2556-2566.
- [36]Chen, X. Q.; Pradhan, T.; Wang, F.; Kim, J. S.; Yoon, J. "*Fluorescent Chemosensors Based on Spiroring-Opening of Xanthenes and Related Derivatives.*" Chemical Reviews **2012**, *112*, 1910-1956.
- [37]Kim, H. N.; Lee, M. H.; Kim, H. J.; Kim, J. S.; Yoon, J. "*A new trend in rhodamine-based chemosensors: application of spirolactam ring-opening to sensing ions.*" Chemical Society Reviews **2008**, *37*, 1465-1472.
- [38]Wu, D. Y.; Huang, W.; Duan, C. Y.; Lin, Z. H.; Meng, Q. J. "*Highly sensitive fluorescent probe for selective detection of Hg²⁺ in DMF aqueous media.*" Inorganic Chemistry **2007**, *46*, 1538-1540.
- [39]Nolan, E. M.; Lippard, S. J. "*Tools and tactics for the optical detection of mercuric ion.*" Chemical Reviews **2008**, *108*, 3443-3480.
- [40]Zhao, L. Y.; Wu, T.; Lefevre, J. P.; Leray, I.; Delaire, J. A. "*Fluorimetric lead detection in a microfluidic device.*" Lab on a Chip **2009**, *9*, 2818-2823.
- [41]Ko, S. K.; Chen, X.; Yoon, J.; Shin, I. "*Zebrafish as a good vertebrate model for molecular imaging using fluorescent probes.*" Chemical Society Reviews **2011**, *40*, 2120-2130.
- [42]Chen, X. Q.; Baek, K. H.; Kim, Y.; Kim, S. J.; Shin, I.; Yoon, J. "*A selenolactone-based fluorescent chemodosimeter to monitor mercury/methylmercury species in vitro and in vivo.*" Tetrahedron **2010**, *66*, 4016-4021.

**Chapter 2. Clickable Fluorescent Chemosensors for Detection of
Heavy Metal Ions: Triazole as a Linker**

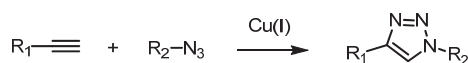


2.1. Introduction of “Click” reaction

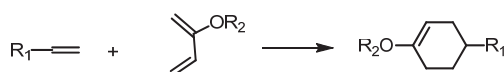
Due to the increasing demand of pharmaceuticals, considerable efforts have been devoted to the natural product syntheses. Though imitation strategy of the nature’s carbonyl chemistry by the formation of carbon-carbon bond has been well developed, it brings in a lot of problems such as difficulty in global protection and deprotection of functional groups, large-scale production. Also it takes usually long time to an analogue series. According to a theoretical investigation, the number of reasonable drug candidates (≤ 30 non-hydrogen atoms; ≤ 500 daltons; consisting of only H, C, N, O, P, S, F, Cl, and Br; likely to be stable at ambient temperature in the presence of water and oxygen) was estimated to between 10^{62} and 10^{63} molecules.¹ For this consideration, avoiding the tedious and sophisticated construction of contiguous carbon-carbon bonds is crucial in rapid screening of the molecules and promoting drug discovery. Furthermore, it should be noted that not only the natural products have the biological effects, molecules with same active sites but different linkers can exert the same useful influence. By paying more attention to the properties than structures, if a more modular and faster style of synthesis were proved effective, the pharmaceuticals would benefit enormously. Following this idea, the concept of “click” chemistry was initially introduced by Sharpless et al to promote a new approach to the development of drug discovery.² They proposed a set of stringent criteria for this so-call “click” reaction as following: the reaction must be modular, wide in scope, give very high yields, generate only inoffensive byproducts that can be removed by nonchromatographic methods and be stereospecific (but not necessarily enantioselective); the required process characteristics include simple reaction conditions (ideally, the process should be insensitive to oxygen and water), readily available starting materials and reagents, the use of no solvent or a solvent that is benign (such as water) or easily removed and simple product isolation.

Based on the these requirements, to date several types of chemical transformation can be classified as “click” reactions.² The most common examples are as following:

(1) Cycloaddition of unsaturated species, mainly referring to both 1,3-dipolar cycloaddition reactions and Diels-Alder cycloaddition.

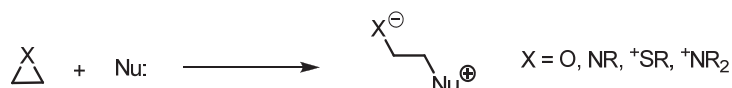


1,3-Dipolar Huisgen Cycloaddition



Diels-Alder Cycloaddition

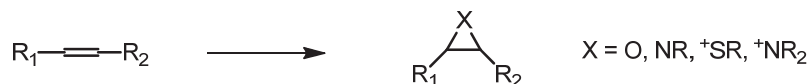
(2) Nucleophilic substitution, particularly ring-opening reactions of strained heterocyclic electrophiles such as epoxides, aziridines and episulfonium ions.



(3) Carbonyl chemistry of the “non-aldol” type, including formation of ureas, thioureas, aromatic heterocycles, oxime ethers, hydrazones and amide.



(4) Addition to carbon-carbon multiple bonds, such as epoxidation, dihydroxylation, aziridination and sulfenyl halide addition and Michael additions of Nu-H reactants.

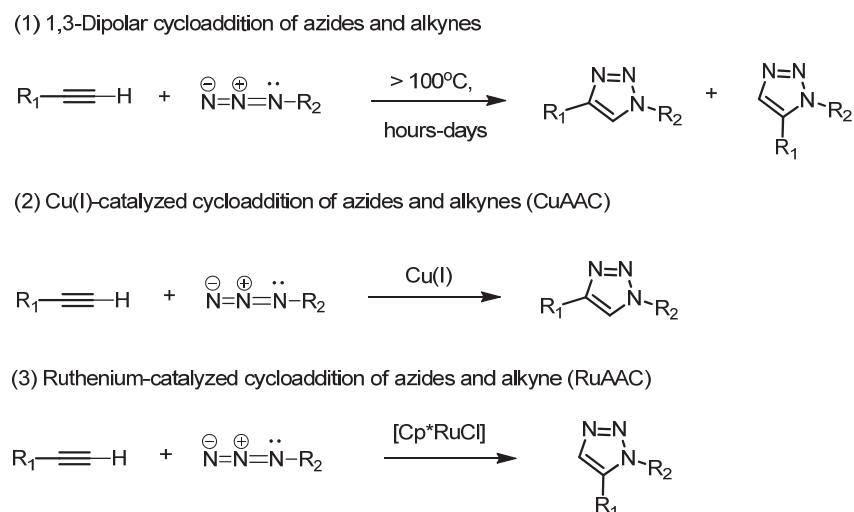


Besides these reactions, the sequential combination of any two of the above “click” reactions has been termed as a “double click” reaction.

2.1.1. Cu(I)-catalyzed Huisgen 1,3-dipolar cycloaddition of azides and terminal alkynes (CuAAC)

Of all the aforementioned reactions that meet with the criteria of “click” reaction, Cu(I)-catalyzed Huisgen 1,3-dipolar cycloaddition of azides and alkynes (CuAAC) to form regioselectively 1,4-substituted 1,2,3-triazole has become the most widely used, not only organic chemistry but also in material science,³ biological conjugation^{4,5} and drug discovery⁶ etc. In fact, thermal reactions of terminal or internal alkynes with organic azides had been investigated thoroughly by Huisgen and coworkers in 1950s-70s.⁷ The cycloaddition was usually operated at elevated temperature due to the large energy barrier and moreover the similar magnitude of differences in HOMO-LUMO energy level for both azides and alkynes, leading to the formation of a mixture of regioisomeric 1,2,3-triazole products with asymmetrical alkynes, as shown in Scheme 2-1 (1). Fortunately, these problems were solved

under the catalysis of Cu(I), independently reported by Sharpless and Meldal in 2001, to afford selectively 1,4-substituted 1,2,3-triazole (Scheme 2-1 (2)).^{8,9} The rate of this cycloaddition under catalysis of Cu(I) was increased 10^7 times, making the reaction proceed very fast even at room temperature.^{10,11} Further detailed investigations show that this reaction is not significantly dependent on the electronic and steric effect of azides and alkynes and it's not very sensitive to solvents and not affected by the existence of most organic and inorganic functional groups.¹² The exclusive formation of 1,4-disubstituted 1,2,3-triazole makes it fully meet with the criteria of “click” reactions. To date, most reported “click” reaction are referring to CuAAC. Later in 2005 it was found that ruthenium complex could catalyze organic azides reacting with terminal alkynes to give regioselectively 1,5-substituted triazole product (Scheme 2-1 (3)).^{13,14} However, this reaction is more sensitive to solvents and the steric demands of the azide substitutes than CuAAC.



Scheme 2-1. Cycloaddition of 1,3-dipolar cycloaddition of azides and terminal alkynes under different conditions, (1) thermal cycloaddition; (2) with Cu(I) catalyst; and (3) with ruthenium complex catalyst.

2.1.2. Mechanism of the CuAAC

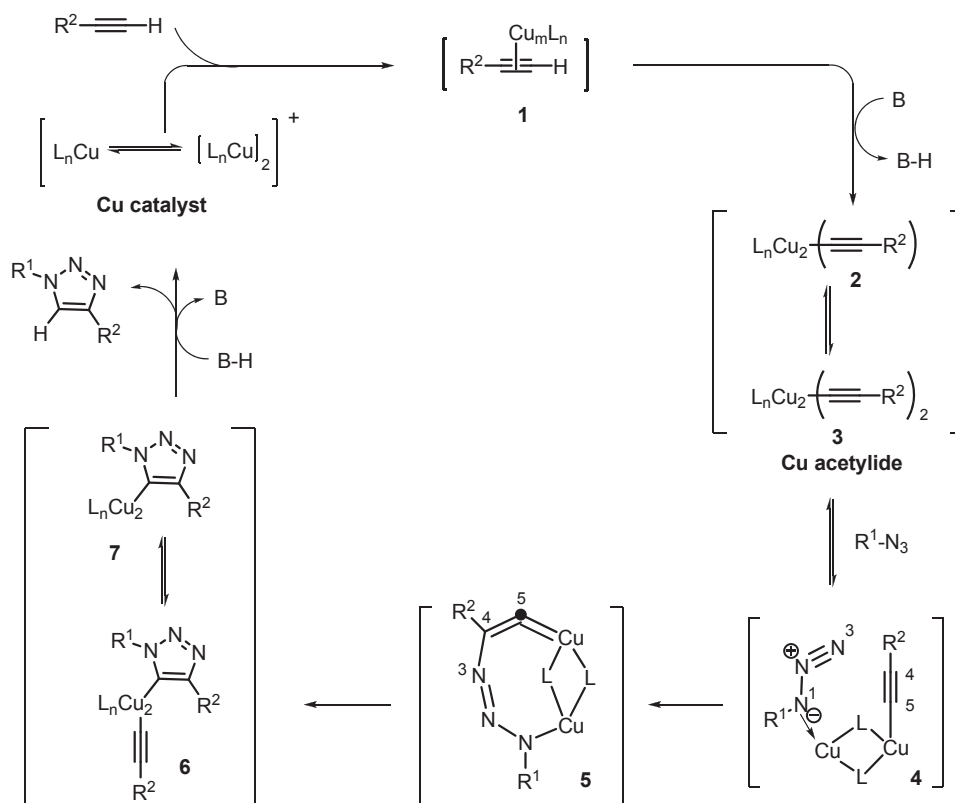
The unique character of CuAAC transformation that it proceeds smoothly in aqueous or/and organic solution, performs within a wide range of pH (4-12) and temperature (0-160 °C) and tolerates a series of functional groups attracts much attention on the study of its reaction mechanism.^{12,15,16} It has been recognized that the thermal dipolar cycloaddition of alkynes and azides occurs through concerted mechanism. Based on this fact, the most direct reaction pathway of CuAAC can be supposed to be the concerted cycloaddition of Cu-alkynes complex and azides. However, the results of DFT calculation demonstrate that its activation barrier for this process is even higher than that of the uncatalyzed process. Therefore this

mechanism is unable to explain the extreme acceleration of the reaction rate in the presence of Cu(I).

At present the generally accepted explanation is stepwise cycloaddition catalyzed by a monomeric Cu(I) species, as shown in Scheme 2-2, proposed by Script group based on their kinetics investigation and DFT calculations.¹⁶ This stepwise catalytic cycle begins with the formation of copper acetylide via the π complex. Mechanical calculation demonstrates that the formation of copper complex is exothermic by 11.7 kcal/mol, which can explain the reaction rate acceleration of CuAAC in aqueous solutions. Meanwhile the DFT calculations also indicate that copper coordination dramatically lower pK_a of the proton of terminal alkyne by as much as 9.8 pH units, promoting the deprotonation of alkyne in aqueous solution even in the absence of additional base. Kinetics study shows that the reaction is found to be second order in copper; however, with increasing copper concentrations, reactivity is reduced due to the formation of metal aggregates.¹⁶ It has to be pointed out that the second order rate law in the catalyst during the initial stage of reaction does not definitely mean the involvement of two copper in the catalytic cycle. Anyway, this finding could be simply interpreted as the activation of azide and alkyne by two different metal centers. However, multinuclear Cu-acetylide species are common in solution and perhaps the second metal center is coordinating to the alkyne by π -complexation, which can change the reactivity of acetylide. The catalytic active species of copper acetylide complex is not well understood yet. In the presence of excess copper, CuAAC reaction was found to be first order with respect to azide and between first and second order for alkyne. The latter finding comes up with two possible explanations. On the one hand, it's proposed two separate pathways to triazoles involving one and two alkynes; on the other hand, the preferred catalytic mechanism involves two alkynes but is inhibited by the excess of alkyne, giving the intermediate rate constant between the first and second order. In the latter case, the excess of alkyne may coordinatively saturate copper and suppress the activation of azide. The commercial available copper acetylides, which are presumably saturated with alkyne, show no catalytic activity, indicating the importance of ligand dissociation for the catalysis. According to the current evidences, the active copper acetylide species require two metal centers, one or two alkyne and other liable ligands that allow for competitive binding of azide.

Following the formation of active copper acetylide, competitive binding of azide followed by nucleophilic attack of acetylide forms a metallocyclic intermediate **5** (Scheme 2-2). It adjusts the bound azide properly for the subsequent contraction by a transannular association of the N(1) lone pair with C(5)-Cu π^* orbital to form triazole copper derivative **7**. It's

supposed that this process is likely very fast due to no or very low energy barrier. Protonation of **7** then finally gives the products and regenerate the catalyst. However, there remains a lot to learn about the exact mechanism of the reactions, such as the active copper acetylide species.



Scheme 2-2. Mechanism of 1,3-dipolar cycloaddition of azide and terminal alkyne under the catalysis of Cu(I).^{11,16}

2.1.3. Catalyst of the CuAAC

Although the exact mechanism of CuAAC reaction is not very well understood and the active copper acetylide is quite difficult to identify, the source of catalytically active copper for CuAAC is remarkably flexible.¹² The copper(I) species can be obtained from the commercially available copper(I) salts, but it can also be generated by reduction of copper(II) in combination with an appropriate reductant or even the solid copper. The choice of the catalyst is dependent on the conditions under which the reactions are conducted, as recently summarized by Meldal and Tornøe.¹⁷ The most widely used approach in aqueous solutions is to generate the constant source of Cu(I) by the combination of copper sulfate pentahydrate or copper acetate with sodium ascorbate. Ascorbate here is essential for both the reduction of oxygen in solution to decrease the side oxidation products and the reduction of copper(II) to the catalytically active copper(I) oxidation state. Water appears to be the ideal choice since it can support copper(I) acetylide in their reactive state by reducing formation of aggregated

copper acetylides. Therefore this approach generally furnishes the triazole product with almost quantitative yield with purity greater than 90% without addition of external base and protection of the reaction mixture from oxygen.

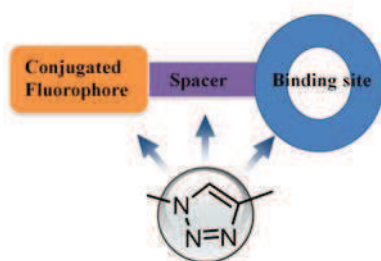
The commercial available copper(I) salts (bromide, chloride, acetate) have been commonly employed when the click reactions are performed in organic solvents (typically THF, MeCN, or DMF) under inert atmosphere since the copper(I) is sensitive to oxygen. It's not recommended to use copper(I) iodide due to the ability of iodide to form bridged bond to promote the formation of polynuclear copper acetylide and then reduce its catalytic activity. Formation of copper(I) acetylide is not energy favorably in organic solvent, external organic bases usually improve the reaction rate. The additional base like 2,6-lutidine and diisopropylethyl amine can help the deprotonation of alkyne and also are considered to be a ligand to stabilize copper(I), keeping the catalytically active sites in solutions.

Even the solid metal copper, in the forms of copper wire or turnings, has been also proved to be catalytically active in CuAAC reactions. The great advantage of this approach is that it's very easy to remove copper from the reaction mixture and it's suitable for the reaction where it's not allowed the presence of reductant.

2.1.4. Applications of the CuAAC reaction

As we have described above, the great advantages including the simplicity, high reaction yield, mild reaction conditions, and inert to other functional groups lead to the very wide applications of the CuAAC reactions, such as organic synthesis, drug discovery, material science, and biological conjugation. However, it would be impossible for us to make complete overview of these numerous applications in the context of this thesis. Herein, we focus on the applications of CuAAC reaction as a tool for the synthesis of new fluorophores and how the resulting triazole group can be utilized in chemosensors for the detection of various biologically and environmentally important metal species.¹⁸ In addition to the synthetic simplicity and modular nature of this reactions, the resulting 1,2,3-triazole group plays several important roles in molecular sensing, mainly summarized in Scheme 2-3: (1) acts as a linker/spacer; (2) conjugates with the fluorophores to create new fluorophores; (3) contributes to the binding of target analytes through the nitrogen atoms in the fused triazole ring.¹⁸ Upon binding to the target analytes, spectral changes can occur by different sensing mechanisms, such as photoinduced electron transfer, charge transfer, and aggregate formation. The following review of chemosensors containing triazole will be categorized based on the different binding motifs. However, it also has to be pointed out that in some cases the binding

mechanisms are not well understood and the function of triazole must be postulated.



Scheme 2-3. Roles of 1,4-disubstituted 1,2,3-triazole in chemosensors.

2.1.4.1. Triazole as a linker

A Hg^{2+} selective fluoroionophore was grafted onto the mesoporous SBA-15 by click chemistry to construct a fluorescent surface sensor **8** (Figure 2-1).¹⁹ Its complexation properties were investigated in ethanol buffered aqueous solutions and the results demonstrated that it showed highly selective response to Hg^{2+} with significant fluorescence enhancement even in the presence of competing ions. An improved analytical performance characteristic toward Hg^{2+} in terms of sensitivity and selectivity was observed when compared with the free alkynyl dye precursor. Triazole group here was thought to be a linker rather than a binding site to Hg^{2+} .

A series of Zn^{2+} selective fluorescent sensors **9-11** based on calix[4]arene-salicylaldimine has been developed by Rao's group (Figure 2-1).^{20,21,22} These molecules share the same structural features with the terminal salicylaldimine derivatives all linked by triazole moiety to the lower rim of calix[4]arene framework. Compound **9** was found to show selective response to Zn^{2+} over a range of metal ions including Cd^{2+} , resulting in a 65-fold fluorescence enhancement in methanol. It's postulated from a model molecule which possesses only the triazole group without schiff base binding site that the triazole moiety acts as a linker rather than binding site for Zn^{2+} . In their continuous work on ligand **10**, quite similar spectral behavior was observed for Zn^{2+} . The 1:1 complex of **10**- Zn^{2+} was verified by solid evidences such as ^1H NMR and crystallography. Further modification on the terminal group by incorporation of thiophene shows that the complex **11**- Zn^{2+} can be utilized as a secondary sensing platform for the detection of -SH containing analytes. Triazole moiety in **11** is still demonstrated to be a linker by DFT calculations.

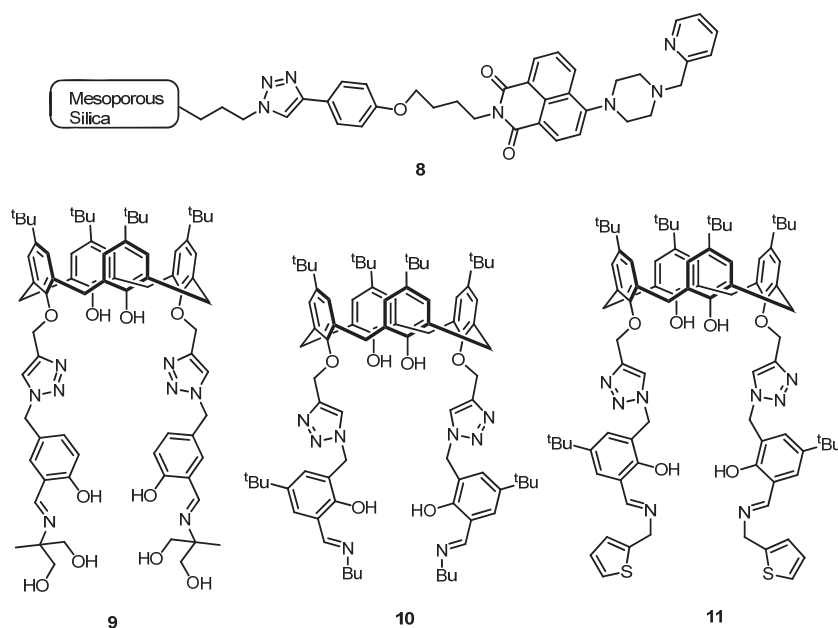


Figure 2-1. Triazole as linkers.

2.1.4.2. Triazole as the single binding site for metal ions

1,2,3-Triazole containing three contiguous nitrogen atoms with two of them in the form of sp^2 hybridization is found to be a good binding site to metal ions. Although not so many examples have been reported up to now, by incorporating 1,2,3-triazole into appropriate fluorophores or polymers, results moderate selectivity to metal ions.

Fluorescent conjugated polymers have been well known for their capability of signal amplification due to the highly efficient exciton transfer along the conjugated main chain.²³ 1,2,3-Triazole was incorporated into the main chain to obtain polymer **12** by “click” reaction (Figure 2-2).²⁴ About 86% fluorescence quenching was observed in the presence of excessive amounts of Hg^{2+} in MeOH/ H_2O (v/v = 1:1) solution. The K_{sv} (Stern-Volmer constant) value was calculated to be as high as $1.58 \times 10^5 M^{-1}$, indicating the moderate sensitivity to Hg^{2+} . The fluorescence quenching was attributed to a PET process as well as heavy metal ion effects. The selectivity to Hg^{2+} was ascribed to several factors, such as the structural rigidity of triazole unit, the soft acid property and large radius of Hg^{2+} , and specific strong Hg-N binding. However, polymer **12** suffered from the interference from Ag^+ , which quenched about 34% fluorescence intensity at its saturated state. Along similar lines by using the binding ability of triazole and conjugated polymers as signal transduction platform, polymer **13** was also synthesized with a shorter conjugated chain (Figure 2-2).²⁵ Investigation on polymer **13** showed quite similar results as polymer **12**, with profound fluorescence quenching by Hg^{2+} and Ag^+ in CH_3CN . These two pieces of works may indicate that triazole

triazole groups, resulting in two potential binding sites: between the triazoles below the calixarene and in the crown ether above the ring. It was found that in MeCN/CHCl₃ the fluorescence of **15** was strongly quenched in the presence of Hg²⁺, Cu²⁺, Cr³⁺ and Pb²⁺ but enhanced by K⁺, Ba²⁺ and Zn²⁺. The control experiment with monotriazole derivative and ¹H NMR titration indicated that K⁺ binds to the crown ether while Pb²⁺ to the triazoles pocket. Additionally, the addition of K⁺ to strongly quenched Pb²⁺-**15** complex restored the fluorescence intensity, which realized a switchable fluorescent chemosensors. The revival of fluorescence was explained by the electrostatic repulsion and allosteric effect.

By clicking two pyrene fluorophores to the framework of calix[4]arene, a new chemosensor **16** was synthesized (Figure 2-3).³⁴ The addition of Cd²⁺ and Zn²⁺ resulted in the ratiometric change of **16** in MeCN, with increased pyrene monomer emission and quenching pyrene excimer emission. By examining the effect of competing metal ions, only Cu²⁺ and Hg²⁺ were found to quench completely the fluorescence, suggesting the moderate selectivity of **16** to Cd²⁺ and Zn²⁺ over the other tested cations. Comparison of the ¹H NMR spectra of **16** and its complexes demonstrates that the initial π - π interaction of two neighborhood pyrenes subunits was interrupted after complexation with Cd²⁺ and Zn²⁺. Metal induced conformational change led to the separation of two pyrene units and the increasing monomer emission. The 1:1 binding mode was further confirmed by FAB-MS spectra, where the peaks of **16**-Cd²⁺ and **16**-Zn²⁺ could be observed.

Another chemosensor **17** (Figure 2-3) containing bis-triazole binding motif and 8-hydroxyquinoline fluorophore appended onto the calix[4]arene shows selective response to Hg²⁺ in aqueous MeCN solution.³⁵ Other metal ions except Fe³⁺ showed almost no influence. ¹H NMR studies indicated the involvement of both hydroxyquinoline and triazole in the metal binding.

Modification on ligand **15** by changing the crown ether into bis-enaminone groups created a new chemosensor **18** (Figure 2-3).³⁶ Its fluorescence intensity was selectively enhanced in the presence of Ag⁺ in MeOH/CHCl₃. Even in the presence of competing metal ions, compound **18** retained the high selectivity to Ag⁺. Moreover, it was found that the subsequent binding constant K_{21} is larger than K_{11} , indicating a positive allosteric effect in the binding process. ¹H NMR studies revealed that two distal bis-enaminone and bis-triazole groups cooperatively bound to Ag⁺. Additional cation- π interaction between phenoxy rings and Ag⁺ was supposed to help increase the binding ability to Ag⁺. ESI-MS spectra further confirmed the formation of complex with stoichiometry of ligand and metal to be 1:2.

When the pyrene moieties are appended to homooxacalix[3]arene by triazoles groups, a new type of fluorescent chemosensor **19** is developed (Figure 2-3).³⁷ With the addition of Pb^{2+} , the initial π - π interaction between the adjacent pyrene subunits was attenuated, concomitantly with the enhanced monomer emission of pyrene and quenching emission of excimer. Investigation on the effect of coexisting metal ions showed that no significant interference was observed and high selectivity was retained. The binding mode was studied by ^1H NMR titration, which showed only the nitrogen atom in triazole participated to the complexation with Pb^{2+} . In their later work, Yamato et al further utilized the interference from Zn^{2+} to construct a ratiometric detection platform for both Zn^{2+} and H_2PO_4^- in $\text{MeCN}/\text{CH}_2\text{Cl}_2$. The addition of Zn^{2+} to the solution of **19** causes similar ratiometric pattern as that of Pb^{2+} , however to a lesser extent. The subsequent addition of H_2PO_4^- to Zn^{2+} -**19** complex partially restored the spectra, with no interference from other tested anions.³⁸ ^1H NMR studies demonstrated that upon complexation with Zn^{2+} , ligand **19** was adjusted to make a more suitable cavity for the binding of H_2PO_4^- through the electrostatic interaction and multiple hydrogen bonding interactions.

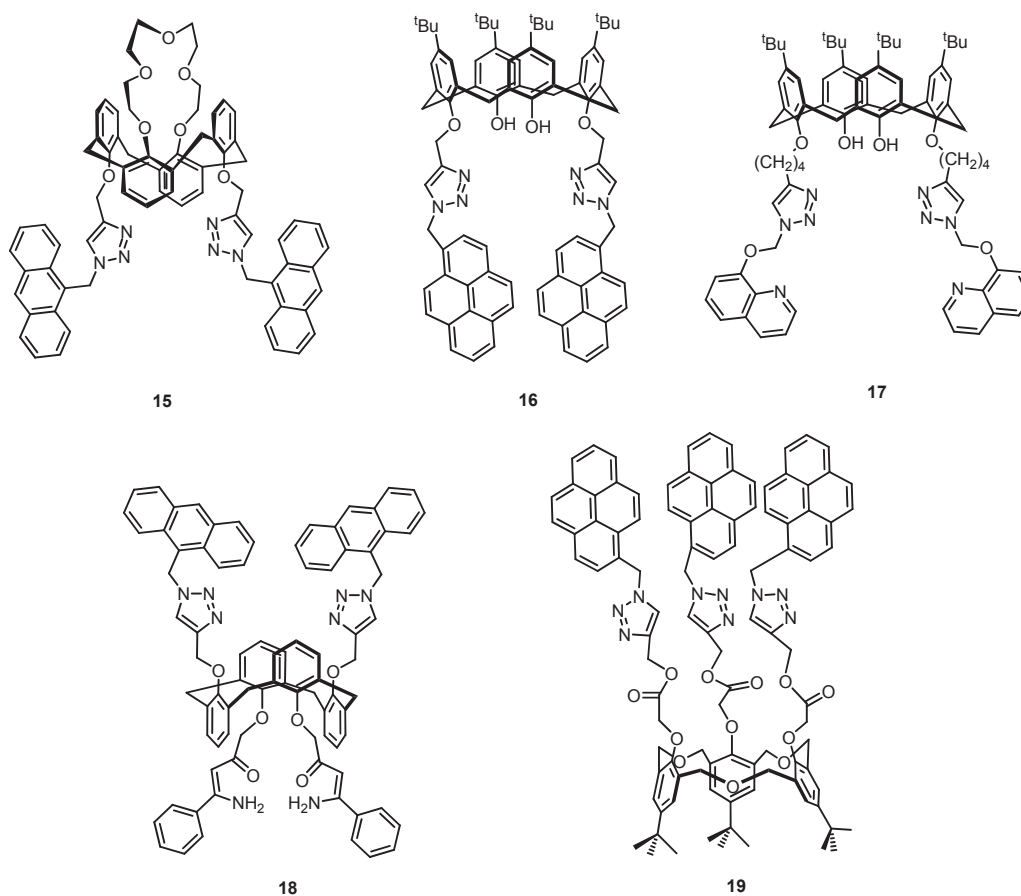


Figure 2-3. Calixarene-triazole sensors.

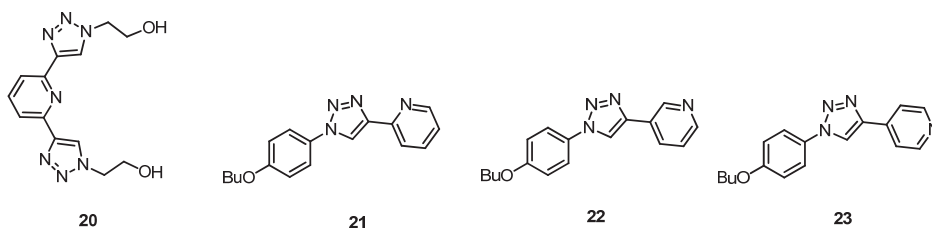
Triazole-pyridine based sensors

The triazole group was merged with adjacent pyridyl building blocks to form a terdentate ligand **20** (Figure 2-4), resembling a terpy motif.³⁹ Optical and electrochemical investigations on its coordination chemistry properties demonstrated that distinctive favorable differences were observed due to the less steric hindrance resulting from triazole moiety when compared with terpy. This preliminary study explores a new binding motif for the coordination chemistry and the construction of supramolecular structure.

When triazole group was incorporated into pyridine at different positions (**21**, **22**, **23**), new structural motifs were constructed (Figure 2-4). Spectral investigations demonstrated that upon addition of metal ions induces turn-on fluorescence.⁴⁰ Although these molecules were all metallochromic, the authors emphasized that structural motif of **21** was most attractive since it represented a modification of bipyridine units and possessed wide potential applications in coordination chemistry.

Two epimeric glycoligands **24** and **25** consisting of triazole-pyridine and isopropylidene furanose were reported by Policar's group (Figure 2-4).⁴¹ These two ligands displayed very interesting solvatochromism, with a strong excimer emission promoted by hydrophobic interaction in water-containing medium. Study of the metal selectivity illustrated that they showed strong binding affinity to Cu^{2+} , which was independent on the configuration of sugar ring. Stepwise replacement of pyridine by benzothiadiazole gave **26** and **27** (Figure 2-4).⁴² Metal complexation study on these two ligands demonstrated that the metal selectivity depended on the nature of fluoroionophore moiety. For **27**, it exhibited stronger binding ability to Ni^{2+} than Cu^{2+} in MeCN.

Recently, a new binding motif was created by conjugation of triazole with bipyridyl unit. When connected to some appropriate fluorophores, the ensemble shows highly selective response to Al^{3+} in MeCN. Detailed results (ligands: **84** - **86**) will be described in Chapter 4.



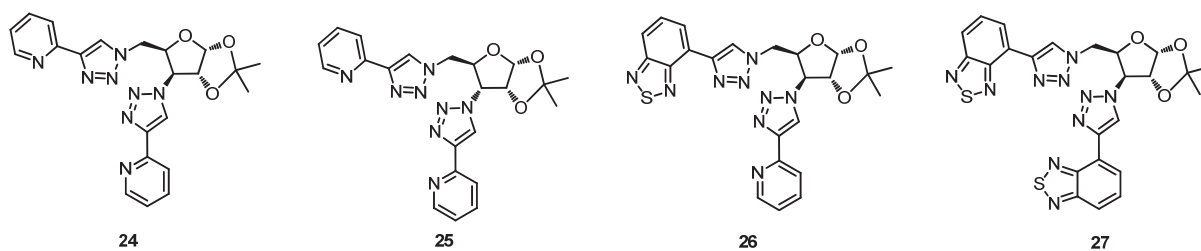


Figure 2-4. Pyridine-triazole sensors.

Triazole-macrocycle based sensors

Macrocylic binding motifs are the most commonly used building blocks in supramolecular chemistry. Coupled with the fluorophores, many of them have been reported to be selective chemosensors for analytes. The incorporation of clickable triazole into cyclam has been recently developed by Todd's group for selective binding to transition metal ions.^{18,43,44,45} A water soluble Zn^{2+} selective sensor **28** (Figure 2-5) was synthesized by appending a naphthalimide fluorophore to cyclen by CuAAC.⁴³ It showed selective response to Zn^{2+} with a significant fluorescence enhancement over a wide pH range. The binding mode was verified by X-ray crystallography which demonstrated that the fluorescence enhancement was due to the coordination of Zn^{2+} to the cyclam ring and pendant triazole. Still ligand **28** suffered from the interference of Cu^{2+} and Hg^{2+} , and complete fluorescence quenching was observed in the competition assays. Later, **29**, a variant of **28** by appending two naphthalimides to the same cyclen, was designed to improve the sensing performance (Figure 2-5).⁴⁴ However, it was still unable to reduce severe interference from Cu^{2+} and Hg^{2+} . More recently, sensor **30** was synthesized to modify the fluorescent response to metal ion by changing the fluorophore (Figure 2-5).⁴⁵ The sensor **30** was highly responsive to Hg^{2+} and Cu^{2+} with large fluorescence quenching in buffer solutions, which can be distinguished by subsequent addition of anions ($I^-/S_2O_3^{2-}$) who can restored the fluorescence quenched by Hg^{2+} but not for Cu^{2+} . Crystal of the complex **30**- Hg^{2+} demonstrated that formation of a metallocycle involving triazole nitrogen atom and the size match between Hg^{2+} and cyclam contributed to its selectivity to Hg^{2+} and Cu^{2+} instead of Zn^{2+} .

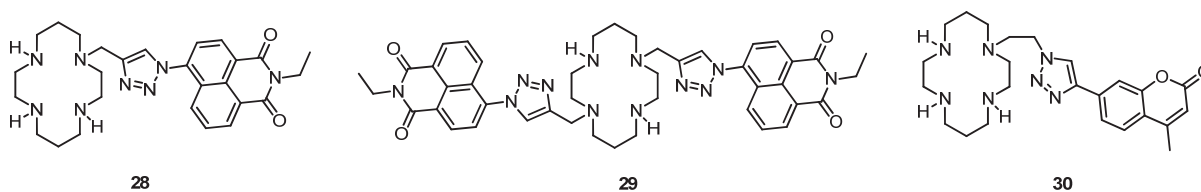


Figure 2-5. Macrocycle-triazole sensors.

Other triazole based sensors

An alkyne pyridine was attached to Ag NPs, which were subsequently subjected to click reaction with ester azide to obtain modified Ag NPs **31** (Figure 2-6).⁴⁶ With the addition of various metal ions, only Cd^{2+} could lead to the aggregation of Ag NPs and induced a distinct color change from yellow to red. This phenomenon was assigned that the triazole and ester groups from different Ag NPs could form hybrid assemblies after complexation with Cd^{2+} and consequently induce the aggregation and colorimetric change. Later, **32** was further developed by using bifunctionalized Ag NPs for selective detection of Co^{2+} (Figure 2-6).⁴⁷ Stabilized simultaneously by thioacetic acid and triazole-pyridine, the Ag NPs formed aggregates only in the presence of Co^{2+} , concomitantly with solution color change from yellow to red. While the Ag NPs functionalized only with thioacetic acid resulted in non-specific aggregation and Ag NPs functionalized only with triazole-pyridine exhibited no response. The cooperative complexation of triazole and carboxyl group was proved to be crucial to the sensing selectivity and sensitivity. Au NPs bearing podand triazole **33** (Figure 2-6) was prepared *via* an *in situ* click reaction and showed selective response to Pb^{2+} .⁴⁸ The aggregation of Au NPs only occurred in the presence of Pb^{2+} , resulting from intermolecular association.

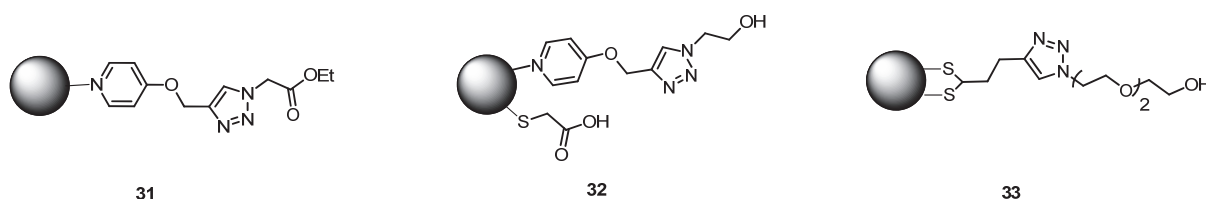


Figure 2-6. Nanoparticles-triazole sensors.

Enclosed binding pockets were constructed by clicking pyrene fluorophores to both ends of alkyl and polyoxoethylene chain with varying lengths.^{49,50} Formation of excimer emission band might indicate the bent binding pocket form through π - π interaction. Alkyl linked bistriazole ligand **34** (Figure 2-7) exhibited non-specific fluorescence quenching to Ni^{2+} , Pb^{2+} , Cu^{2+} , Hg^{2+} , and Cr^{3+} ; however, it showed a ratiometric response to Cd^{2+} and Zn^{2+} with enhanced monomer and quenched excimer. Based on the ^1H NMR studies, it was postulated two different binding modes contributed to the different spectral change: (1) Ni^{2+} and Pb^{2+} bound to triazole and oxygen which distorted the original conformation; (2) Zn^{2+} and Cd^{2+} coordinated only to triazole which caused the separation of two pyrene fluorophores. Alkyl chain was then replaced by polyoxoethylene to increase the solubility and enhance the binding ability. However, they did not show improved selectivity when the spectral investigation was performed in MeCN. It should be pointed out that solvent selection plays a crucial role to determine the selectivity. In aqueous methanol, compound **35** (Figure 2-7) with varying chain lengths shows consistently selective response to Hg^{2+} and Ag^+ in a fluorescence

turn-off manner.

A new rhodamine triazole-based ligand **36** (Figure 2-7) was recently synthesized by clicking a propargyl group to rhodamine 6G hydroxamate, exhibiting selective response to platinum in aqueous solutions.⁵¹ Preorganization of triazole and rhodamine hydroxamate was demonstrated to be very important for metal binding. Only in the presence of platinum, ring-opening of rhodamine spirolactam occurred and subsequently induced fluorescence enhancement and solution color change from colorless to pink red. However, there was no discussion about the binding mode in this work. A similar binding motif with longer linker was incorporated into rhodamine B to create a new rhodamine-based sensor **37** (Figure 2-7).⁵² Only Hg^{2+} here could induced ring-opening of spirolactam in MeCN but still no binding mode was proposed for this process.

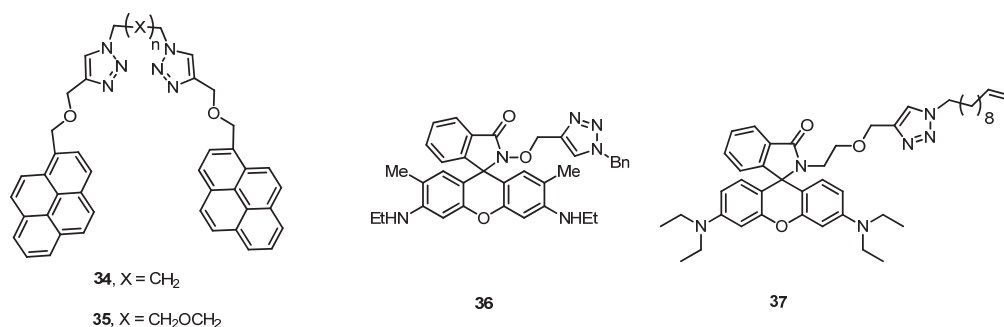


Figure 2-7. Alkyl/polyoxoethanene/rhodamine-triazole sensors.

Pyrene fluorophores were attached to 2,2'-binaphthol by click chemistry to create a new sensor **38** (Figure 2-8).⁵³ After screening a series of metal ions, ligand **38** showed a ratiometric response to Ag^+ with enhanced monomer emission and quenched excimer emission, while its fluorescence was completely quenched by Hg^{2+} and no spectral changes were observed for other metal ions. The detailed ¹H NMR titrations indicated that upon complexation with Ag^+ through triazole groups, the pyrene subunits were separated from each other which resulted in the ratiometric spectral change. However, for its complexation with Hg^{2+} involving both triazole group and oxygen atoms, a possible conformation change from folded to open-winged occurred, causing the on-off type signaling behavior. By installation of bis-triazolyl binding motif on the sugar scaffold, a new sensor **39** (Figure 2-8) was developed for selective detection Ag^+ in water.⁵⁴ It's worthy of notice that the common drawback of insolubility in water of other “click” chemosensors is solved here by utilization of sugar framework. The following investigation on its photophysical properties to metal ions was also carried out in water. Only the addition of Ag^+ induced remarkable fluorescence quenching, which was ascribed to the heavy metal effect and the size match between ligand and Ag^+ .

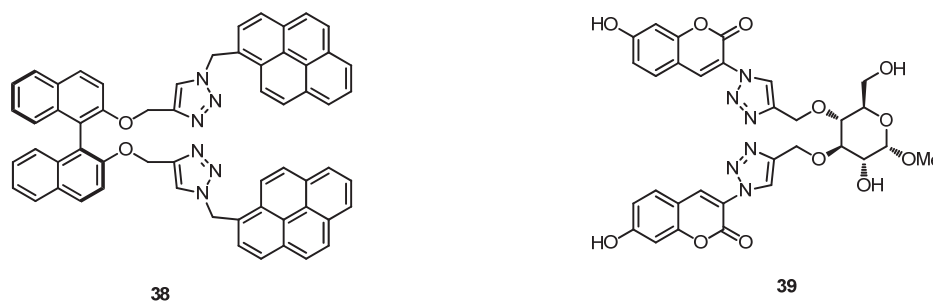


Figure 2-8. Binaphthol/sugar bis-triazoles sensors.

2.1.5. Related works in Xie's group

Xie's group first reported the generation of new fluorophores by installation of triazole group to pyridyl moiety.⁵⁵ The fact that 2-pyridyl triazole substituted sugar derivative **40a** (Figure 2-9) exhibits emission at around 320 nm while no emission bands are observed when the pyridyl moiety was replaced with phenyl or hydroxymethyl group, strongly demonstrated that emission was exclusively originated from the conjugated triazole-pyridine system. Moreover, when such fluorophores were assembled on a β -cyclodextrin (β -CyD) scaffold (ligand **41**), it exhibited varied spectral responses to metal ions in MeOH, with the most significant fluorescence enhancement in the presence of Zn^{2+} . Comparison of association constants of **40a**- Zn^{2+} and **41**- Zn^{2+} indicated that multiple binding sites oriented by β -CyD can dramatically increase the binding ability of pyridyl-triazolyl motif.

As a continuing program on exploring the applications of clickable triazole moiety in fluorescent chemosensors, the attached seven pyridine units in **41** are replaced by benzothiadiazole and appended to β -CyD scaffold to create a new multichromophoric sensor **42** (Figure 2-9).⁵⁶ Red shift for both the absorption and fluorescence spectra of **42** are observed when compared with those of TMS-ethynyl benzothiadiazole due to the increasing conjugation between triazole and benzothiadiazole. Spectral investigation of **42** to metal ions was performed in MeCN, demonstrating that Ni^{2+} quenched its fluorescence most efficiently followed by Cu^{2+} , Co^{2+} and Hg^{2+} . Fluorescence titration gave a very high stability constant of complex Ni^{2+} -**42** up to seven orders of magnitude. A model compound of sugar derivative **40b** showed the same selectivity; however, it gave a much lower binding constant to Ni^{2+} when compared with that of complex Ni^{2+} -**42**, which can be explained by the loss of cooperativity.

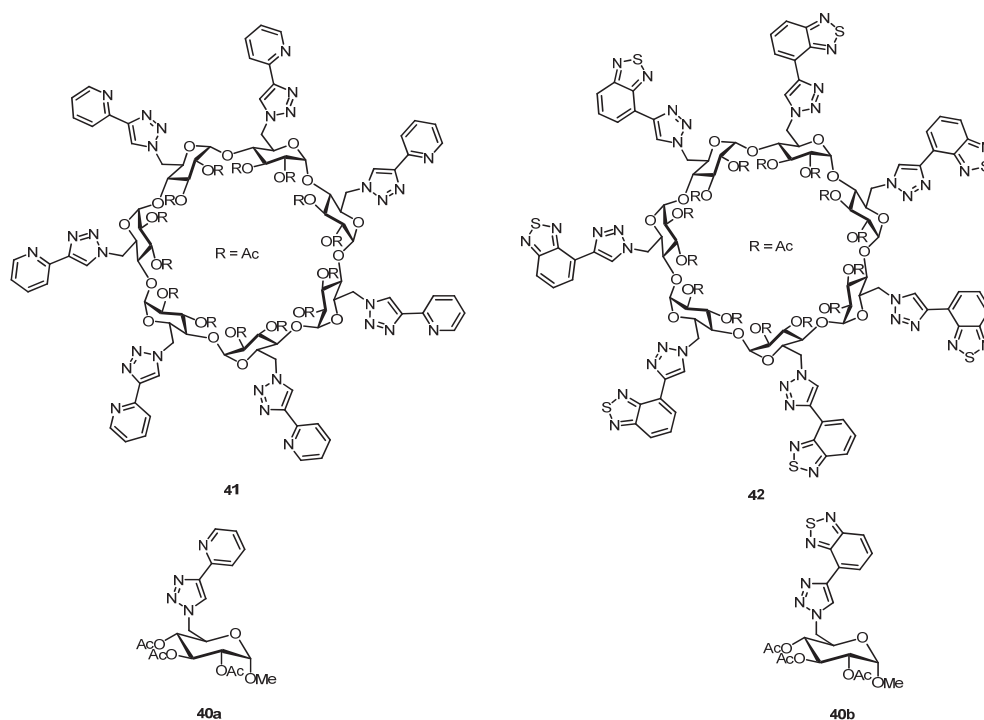
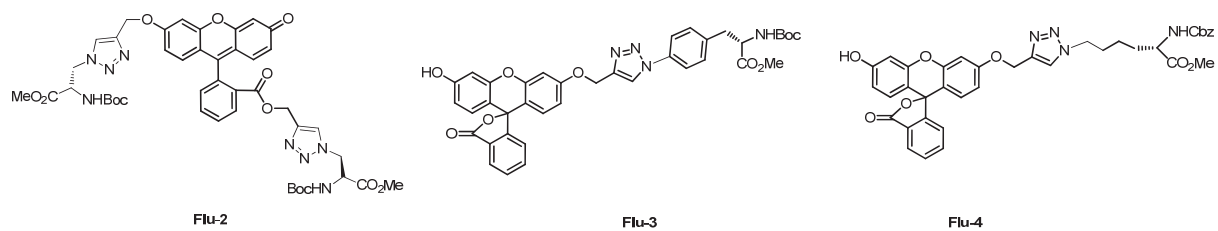


Figure 2-9. Triazole-based sensors in Xie's group.

By combination of the supramolecular structure of CyD with the flexible coordination chemistry of triazole, the exciting results from the above two sensors (**41** and **42**) and the boosting applications of triazole in sensing molecules inspire us to make a deep investigation of the functions of triazole in fluorescent chemosensors, which would be quite meaningful as a guideline for the further development of “click” sensors. Furthermore, with great efforts dedicated to the development of fluorescent sugar/amino acids derivatives based on click reaction, up to now we have already successfully made a series of triazole-based fluorescent molecules, providing a possibility for a detailed study of relationship between structure and functions. The selected fluorophores are categorized by the functions of triazole: (1) triazole as a linker with fluorescein derivatives as the fluorophores; (2) triazole as a sole binding site for metal ions with NBD and rhodamine derivatives as the fluorophores; (3) multiple triazole assemble as binding sites for metal ions with pyrene as the signal reporting sites; (4) triazole as a co-binding site assisted by the benzothiadiazole with the conjugation of both moieties as the fluorophores. This chapter is mainly concerned with the triazole as a linker/spacer through designing fluorescein-based sensors **Flu-2**, **Flu-3**, and **Flu-4**, as shown in Scheme 2-4. The other roles of triazole will be discussed in Chapter 3.



Scheme 2-4. Molecular structures of fluorescein-triazole derivatives.

2.2. Fluorescein-Triazole derivatives for selective detection of Hg²⁺

2.2.1. Introduction

Fluorescein derivatives have been extensively utilized in biological applications due to their excellent photophysical properties.⁵⁷ Appropriate modification of fluorescein either on xanthene moiety or phenyl moiety can result in plenty of interesting properties for the further applications.⁵⁸ Many of them have been used as fluorescent chemosensors for monitoring pH,⁵⁹ metal ions,^{60,61,62,63,64,65,66,67} anion^{68,69} and other biologically important targets.⁷⁰ At present there are mainly three approaches proposed for the sensory mechanisms: (a) spirolactone ring opening; (b) photoinduced electron transfer (PET); (c) modulation on hydroxyl/carbonyl group.^{67,71,72} Lippard's group has pioneered in the field of developing NO, Zn²⁺ and Hg²⁺ "turn-on" fluorescent chemosensors through suppressing the PET process from electron donating nitrogen atom to various fluorescein fluorophores. Herein we turn our attention to modulation of hydroxyl/carbonyl group of xanthene moiety for sensory applications as its photophysical properties can be easily manipulated by changing chemical environment based on covalent and/or non-covalent interactions. For example, alkylation of hydroxyl group will significantly reduce the fluorescence efficiency.^{71,72} In addition, fluorescein derivatives display quite different spectral behavior in solutions with different hydrogen bonding ability and/or polarity.⁷³ Based on the cleavage of C-O ether bond, many "turn-on" fluorescent chemosensors for different analytes have been developed.^{74,75,76,77,78,79,80,81} To date, however little attention has been paid to metal coordination interaction with carbonyl group of xanthene moiety, which is stronger than hydrogen bond while weaker than covalent bond. According to the literatures, hydrogen bonding interaction usually increases fluorescence quantum yield of fluorescein derivatives;⁷³ however, formation of C-O ether bond usually induces fluorescence quenching.⁷² When the carbonyl group in xanthene moiety is a binding site for metal ions, how metal coordination interaction will affect spectral properties of the xanthene moiety attracts our interest. Therefore we used a model compound **Flu-1** to investigate metal coordination effect on spectral properties of xanthene fluorophores; while **Flu-2** readily synthesized from click chemistry is used to investigate the influence of triazolyl amino ester on metal complexing property of fluorescein derivative.

2.2.2. Synthesis of Fluorescein-triazole derivatives

Preparation of **Flu-1** and **Flu-2** is shown in Scheme 2-5. Fluorescein was first reacted with

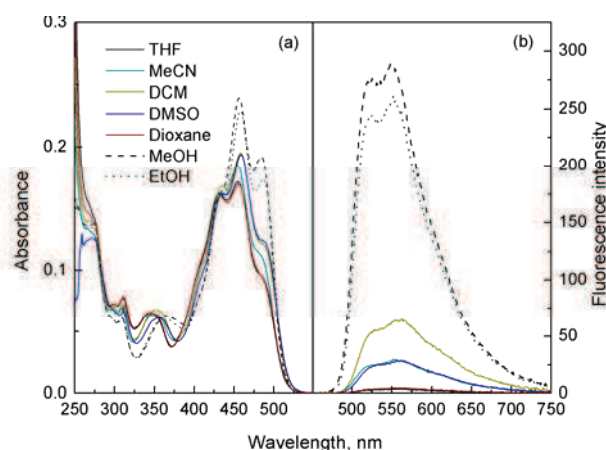


Figure 2-10. Absorption (a) and fluorescence (b) spectra of **Flu-1** in various solvents; excitation wavelengths corresponding to the maximum absorption band, [**Flu-1**] = 10 μM .

Compounds	Solvents	$\lambda_{\text{max}}^{\text{A}}$	ϵ_{00}	$\lambda_{\text{max}}^{\text{F}}$	$\Phi_{\text{F}}^{\text{a}}$
		[nm]		[$10^4 \text{ L}\cdot\text{mol}^{-1}\cdot\text{cm}^{-1}$]	
Flu-1	Dioxane	432, 456, 487	1.7, 1.8, 1.0	518, 562	0.6
	DMSO	433, 458, 488	1.7, 2.1, 1.3	527, 562	4.0
	CH_2Cl_2	434, 458, 488	1.8, 2.1, 1.3	529, 561	8.5
	MeCN	432, 454, 485	1.7, 1.9, 1.2	520, 553	3.6
	THF	431, 455, 486	1.7, 1.8, 1.0	518, 562	0.5
	EtOH	433, 458, 487	1.7, 2.5, 1.9	523, 549	27.3
	MeOH	432, 456, 484	1.7, 2.5, 2.0	523, 549	27.2
Flu-2	Dioxane	433, 456, 488	1.8, 2.2, 1.4	526, 565	1.8
	DMSO	438, 460, 489	1.9, 2.2, 1.4	524, 559	4.2
	CH_2Cl_2	434, 458, 490	1.9, 2.2, 1.3	528, 561	8.1
	MeCN	432, 456, 486	1.8, 2.1, 1.3	522, 557	4.6
	THF	433, 456, 488	1.8, 1.9, 1.1	526, 565	1.1
	EtOH	434, 459, 489	1.8, 2.5, 1.9	523, 553	24.1
	MeOH	433, 457, 486	1.8, 2.6, 2.0	523, 553	24.8

Table 2-1. Photophysical parameters of **Flu-1** and **Flu-2** in different organic solvents, ^a Coumarin 153 in EtOH was used as the standard.⁸⁴

2.2.4. Complexation properties of Flu-1

Considering the lower background of **Flu-1** in THF when compared with other tested solvents, THF was used as the solvent medium at first to investigate metal binding ability of **Flu-1** and effect of metal coordination interaction on its photophysical properties. We tested spectral response of **Flu-1** to various metal ions such as Hg^{2+} (40 μM), Li^+ , Na^+ , K^+ , Ag^+ , Ba^{2+} ,

Cd^{2+} , Co^{2+} , Cu^{2+} , Fe^{2+} , Mg^{2+} , Mn^{2+} , Ni^{2+} , Pb^{2+} and Zn^{2+} at $80 \mu\text{M}$ in THF. To our surprise, only the addition of Hg^{2+} resulted in blue shift of the absorption and emission bands, concomitantly with remarkable fluorescence enhancement (Figure 2-11). Other tested metal ions showed almost no influence. The selectivity of **Flu-1** to Hg^{2+} was further confirmed in the presence of interfering metal ions. As shown in Figure 2-12, except Ag^+ , the coexisting metal ions (1 equiv with respect to Hg^{2+}) produced no influence on the spectral response of **Flu-1** to Hg^{2+} in THF. These results demonstrated that **Flu-1**, containing carbonyl group as the single binding site, exhibits selective response to Hg^{2+} in THF.

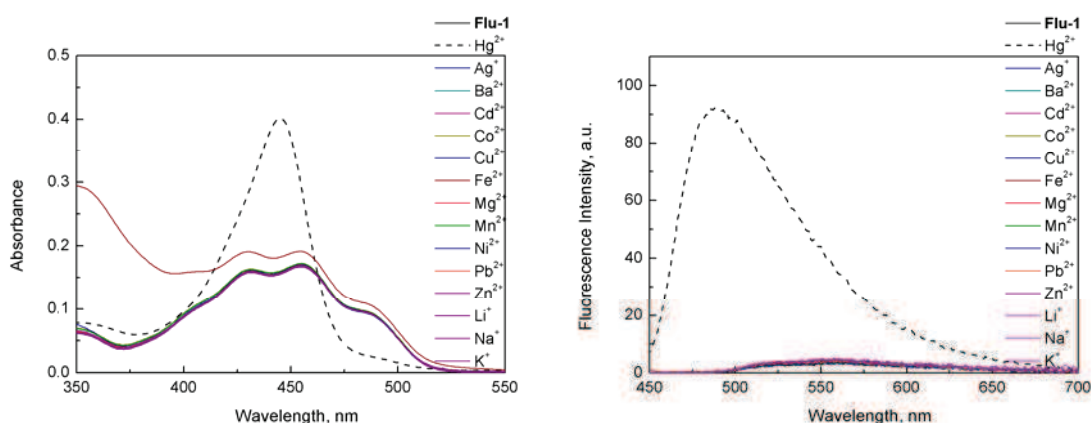


Figure 2-11. Absorption (left) and fluorescence (right) spectra of **Flu-1** in the presence of various metal ions in THF; $[\text{M}^{n+}] = 80 \mu\text{M}$, $[\text{Hg}^{2+}] = 40 \mu\text{M}$, $[\text{Flu-1}] = 10 \mu\text{M}$, $\lambda_{\text{ex}} = 445 \text{ nm}$.

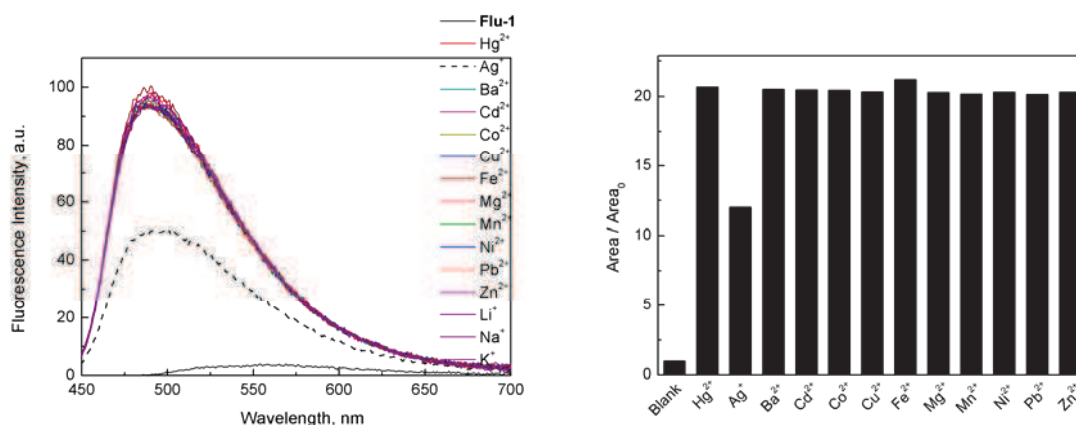


Figure 2-12. Fluorescence spectra of **Flu-1** in the coexistence of various metal ions and Hg^{2+} in THF; $[\text{M}^{n+}] = 40 \mu\text{M}$, $[\text{Hg}^{2+}] = 40 \mu\text{M}$, $[\text{Flu-1}] = 10 \mu\text{M}$, $\lambda_{\text{ex}} = 446 \text{ nm}$.

Spectral titrations were carried out to get insight into the binding process of **Flu-1** to Hg^{2+} in THF. As shown in Figure 2-13 (left), upon addition of increasing $[\text{Hg}^{2+}]$, absorption band of **Flu-1** at 490 nm decreases, concomitantly with appearance of a new narrow band at 445 nm .

Well-defined isosbestic points were observed at 462 and 403 nm, indicating equilibrium of the complexation process. Job's plot which shows the maximum at 0.5 of the fraction demonstrates that the binding stoichiometry between **Flu-1** and Hg^{2+} is 1:1 (Figure 2-14). The binding constant in the ground state was determined to be $3.55 \times 10^5 \text{ M}^{-1}$ by using nonlinear regression analysis based on 1:1 binding ratio (Figure 2-13 (left)). Meanwhile, addition of Hg^{2+} induced a blue shift of the emission band from 560 to 489 nm, with remarkably enhanced fluorescence intensity (ca. 13 folds) (Figure 2-13 (right)) and solution color changing from dark to cyan under UV irradiation at 365 nm. The association constant in the excited state was determined to be $3.14 \times 10^5 \text{ M}^{-1}$. The binding constant of a carbonyl- Hg^{2+} interaction in aqueous or acetone solution has been reported to be 10^4 - 10^5 M^{-1} by Avirah et al.^{85,86} The detection limit was calculated according to the following equation:

$$s = \sqrt{\frac{\sum (x_i - \bar{x})^2}{n-1}}, \quad c_{\text{limit}} = \frac{3s}{k}$$

Where s is standard deviation of **Flu-1** solution without addition of Hg^{2+} , c_{limit} the limit of detection and k is the slope of the working curve. A detection limit of 39 nM could be obtained for analyzing Hg^{2+} under the above conditions. However, when the titrations were performed in water-THF mixed solution (v/v = 5:95), quite little influence was observed on the spectral properties of **Flu-1** even in the presence of 4.0 equiv Hg^{2+} , which could be attributed to strong hydration of Hg^{2+} inhibiting its complexation with the carbonyl group (Figure 2-15).

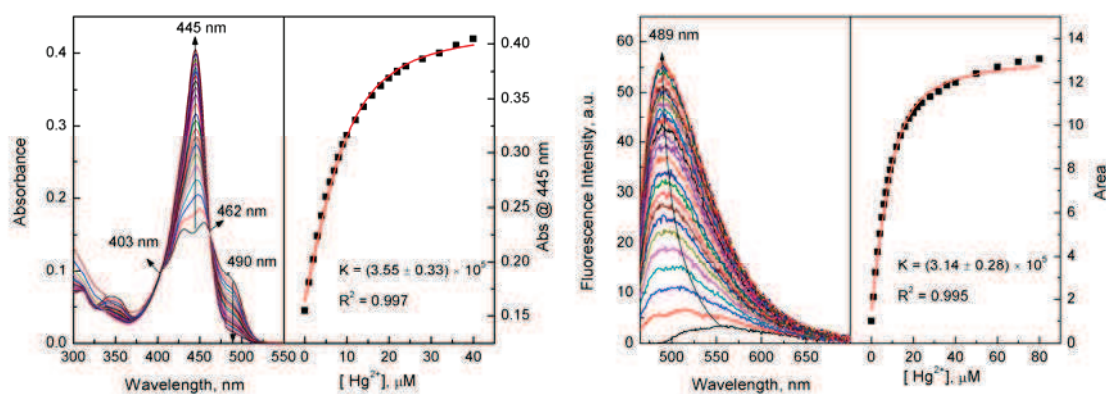


Figure 2-13. Absorption (left) and fluorescence (right) spectra of **Flu-1** in the presence of varying $[\text{Hg}^{2+}]$ in THF; $[\text{Flu-1}] = 10 \mu\text{M}$, $\lambda_{\text{ex}} = 460 \text{ nm}$.

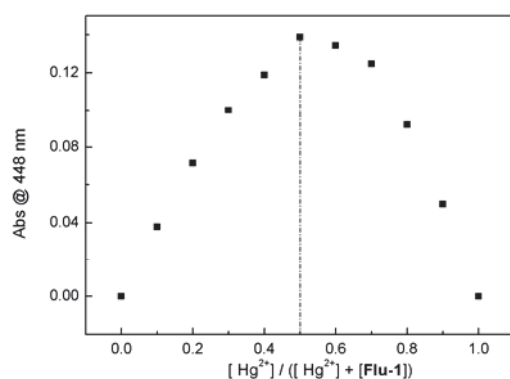


Figure 2-14. Job's plot for **Flu-1**-Hg²⁺ in THF. The total concentration of [Hg²⁺] and [Flu-1] is 20 μM.

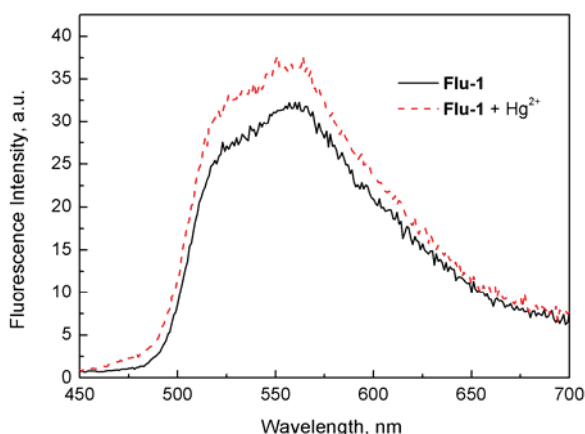


Figure 2-15. Fluorescence spectra of **Flu-1** in the presence of 4 equiv Hg²⁺ in THF/H₂O (v:v = 95:5), [Flu-1] = 10 μM, [Hg²⁺] = 40 μM, λ_{ex} = 446 nm.

Intermolecular hydrogen bonding-induced fluorescence enhancement of **Flu-1** with quite slight wavelength shift (Figure 2-10) and Hg²⁺ specific chelation-promoted fluorescence enhancement with remarkable blue shift (Figure 2-11) led us to explore the possibility of ratiometric detection of Hg²⁺ by changing solvent medium. We then performed the spectral titration in CH₂Cl₂/MeOH (v/v = 9:1). As shown in Figure 2-16 (left), the absorption spectra exhibit almost the same behavior as in THF. With increasing [Hg²⁺], absorbance of **Flu-1** at 489 nm decreases and a new sharp band at 446 nm appears. It reaches an equilibrium more quickly at 2.0 equiv level and the association constant ($4.49 \times 10^6 \text{ M}^{-1}$) is enhanced about one order of magnitude when compared with that in THF. However, the fluorescence change was quite different. With increasing [Hg²⁺], fluorescence intensity at 559 nm decreases, meanwhile a new band at 478 nm enhances progressively (Figure 2-16 (right)) and solution

color changed from yellow to cyan under irradiation at 365 nm. An isoemissive point was observed at 524 nm. The ratio of the fluorescence intensity at 559 and 478 nm increases linearly as a function of $[\text{Hg}^{2+}]$ (0-1 equiv). The higher association constant ($8.76 \times 10^5 \text{ M}^{-1}$) indicates that **Flu-1** has a stronger binding ability to Hg^{2+} in $\text{CH}_2\text{Cl}_2/\text{MeOH}$ (v/v = 9:1).

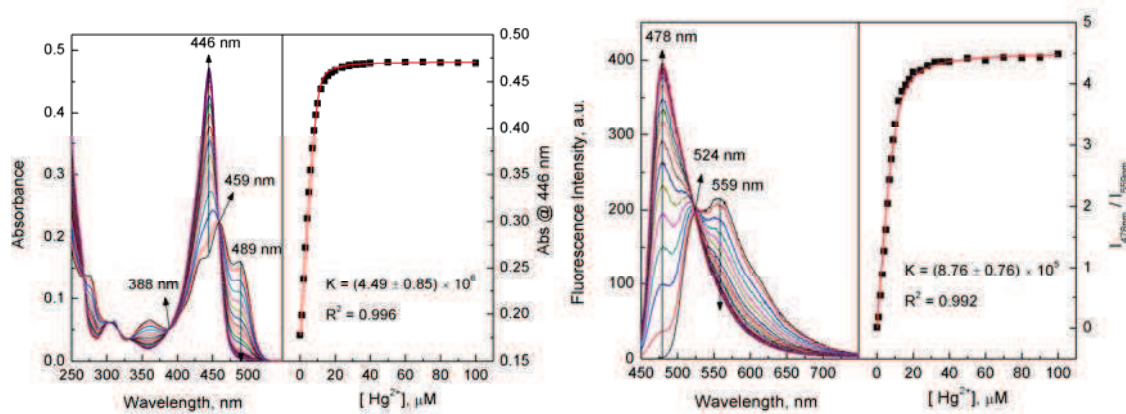


Figure 2-16. Absorption (left) and fluorescence (right) spectra of **Flu-1** in the presence of varying $[\text{Hg}^{2+}]$ in $\text{CH}_2\text{Cl}_2/\text{MeOH}$ (v/v = 9:1); $[\text{Flu-1}] = 10 \mu\text{M}$, $\lambda_{\text{ex}} = 446 \text{ nm}$.

Reversibility of **Flu-1** to Hg^{2+} was examined by addition of 2 equiv of Br^-/Cl^- to the complex solution in THF (Figure 2-17 (a)). Immediate fluorescence quenching and solution color change from cyan to dark indicated decomplexation of **Flu-1**- Hg^{2+} . The same reversibility was observed in $\text{CH}_2\text{Cl}_2/\text{MeOH}$ (v/v = 9:1) (Figure 2-17 (b)) where recovery of the fluorescence spectra and solution color were observed after the addition of 2 equiv I^- .

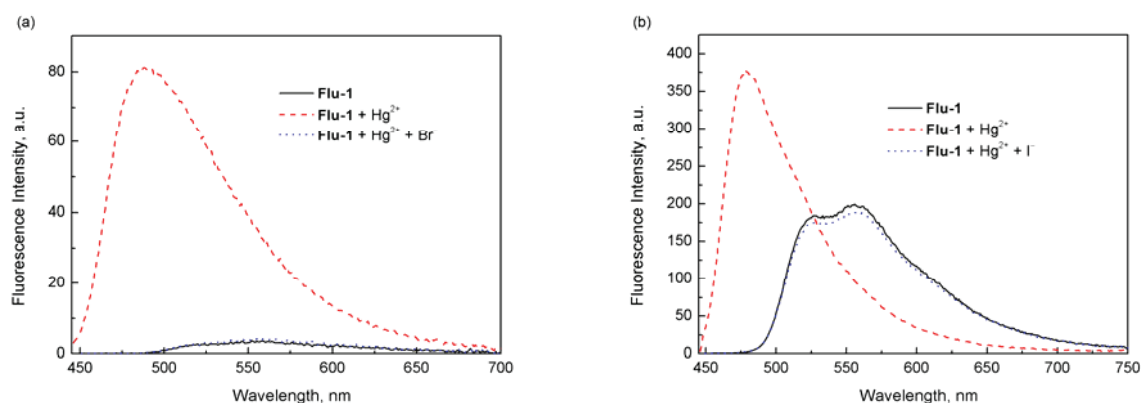


Figure 2-17. Fluorescence spectra of **Flu-1** in the presence of Hg^{2+} , Hg^{2+} and Br^- in THF (left) or in the presence of Hg^{2+} , Hg^{2+} and I^- in $\text{CH}_2\text{Cl}_2/\text{MeOH}$ (v/v = 9:1) (right). $[\text{Flu-1}] = 10 \mu\text{M}$, $[\text{Hg}^{2+}] = 40 \mu\text{M}$, $[\text{Br}^-] = [\text{I}^-] = 80 \mu\text{M}$, $\lambda_{\text{ex}} = 446 \text{ nm}$.

^1H NMR titration in CD_3CN was carried out to examine the binding sites of **Flu-1** to Hg^{2+} .

By comparing the NMR spectra of **Flu-1** with a known fluorescein methyl ester derivative **Flu-Ref** (Figure 2-18),⁷¹ we could assign the signal at 3.6 ppm to methyl group of benzoic moiety while the one at 3.9 ppm to methyl group of xanthene moiety, as further confirmed by 2D NMR (HMQC). The chemical shifts of protons of the xanthene ring ranged from 6.3 to 7.0 ppm while protons of the benzoic acid moiety located in the range of 7.3 to 8.2 ppm. As shown in Figure 2-18, upon complexation with Hg^{2+} , all the protons of xanthene moiety shifted downfield dramatically (*ca.* 0.6-1.0 ppm) while protons of benzoic acid moiety shifted downfield slightly (less than 0.1 ppm), suggesting that the complexation should probably occur on the xanthene moiety rather than on the benzoic unit. Meanwhile, protons of methyl ether at 3.9 ppm also shifted downfield by 0.2 ppm and split into two groups while protons of methyl ester at 3.6 ppm were almost not shifted. This fact further supported our assumption that xanthene moiety participated in the complexation process. By analysis of molecular structure of **Flu-1**, it's quite obvious that carbonyl group is the binding site for Hg^{2+} , which was further confirmed by investigation of IR spectra of **Flu-1** in the presence and absence of Hg^{2+} (Figure 2-19). Characteristic carbonyl stretching frequency of the xanthene moiety appeared at 1723 cm^{-1} and bending vibration at 1212 cm^{-1} . In **Flu-1-Hg}^{2+}** complex, they both downshifted to 1653 and 1184 cm^{-1} , respectively. Binding kinetics was also examined, which showed that the recognition process reached equilibrium immediately after complete mixing (Figure 2-20), indicating a fast complexation process. Our results therefore demonstrated that chelation of carbonyl group to Hg^{2+} reduced the electronic density on the xanthene moiety and consequently caused remarkable blue shift of both absorption and fluorescence spectra. Similar to hydrogen bonding interaction, coordination of Hg^{2+} to carbonyl group of xanthene fluorophore might reduce radiationless deactivation of the excited states in organic medium, resulting in enhanced fluorescence efficiency.

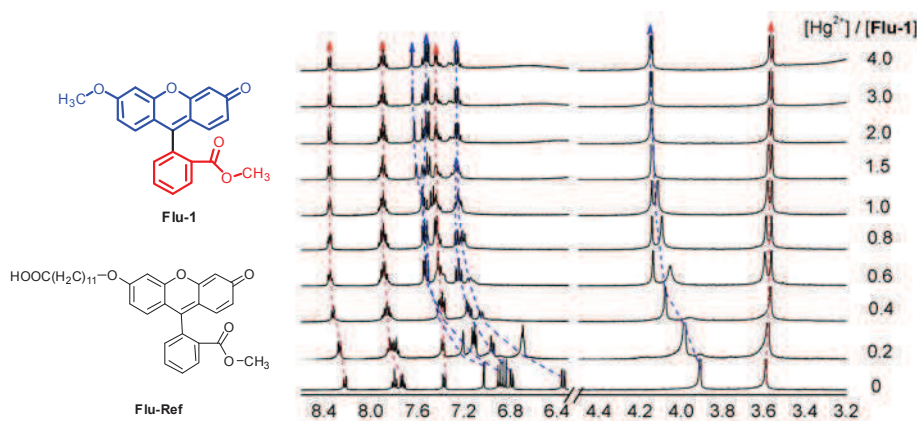


Figure 2-18. Partial ^1H NMR spectra of **Flu-1** in the presence of varying concentrations of Hg^{2+} in CD_3CN .

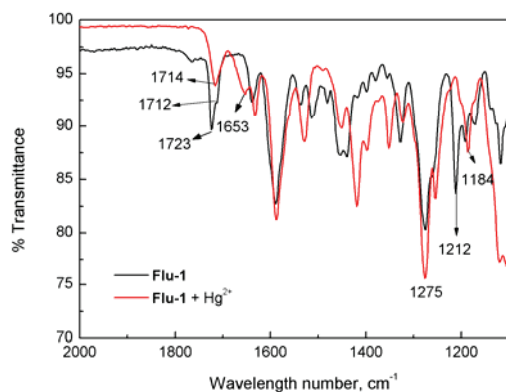


Figure 2-19. Partial FTIR of **Flu-1** and **Flu-1** + Hg²⁺; solid complex was prepared by mixing **Flu-1** and 1 equiv. Hg(ClO₄)₂ in MeCN and then solvent was removed under vacuum.

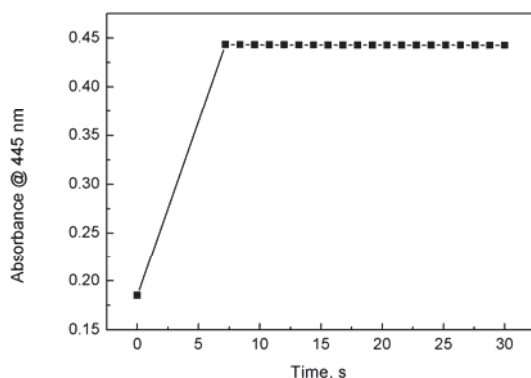


Figure 2-20. Time-dependent absorbance of **Flu-1** at 445 nm in the presence of 2 equiv of Hg²⁺ in THF.

Flu-2, where the two methyl groups were replaced by two triazolyl amino esters, was used to investigate how substituents on the xanthene ring affected the binding process of carbonyl to metal ions. **Flu-2** shows almost the same photophysical properties as those of **Flu-1**, including solvatochromism, spectral wavelength and fluorescence quantum yields (Figure 2-21, Table 2-1). This indicates that triazolyl moiety produces no electronic effects on the fluorescent core. Further investigations of its metal ion binding properties showed that introduction of triazolyl group did not affect the selective binding interaction between carbonyl group and Hg²⁺ in THF (Figure 2-22 and Figure 2-23). Interestingly, spectral titrations of **Flu-2** to Hg²⁺ in THF and CH₂Cl₂/MeOH (v/v = 9:1) exhibited the very similar spectral behavior as that of **Flu-1**, such as association constants ($2.94 \times 10^5 \text{ M}^{-1}$ in THF (Figure 2-24) and $2.26 \times 10^6 \text{ M}^{-1}$ in CH₂Cl₂/MeOH (v/v = 9:1) (Figure 2-25), binding stoichiometry and reversibility (Figures 2-26 and 2-27). These results together demonstrate that carbonyl group of the xanthenic moiety actually could be a selective binding site for Hg²⁺ and triazolyl moiety acts only as a linker. However, easy accessibility of click reaction might

facilitate versatile functionalization on the triazolyl moiety to investigate other sensing approaches, such as FRET.

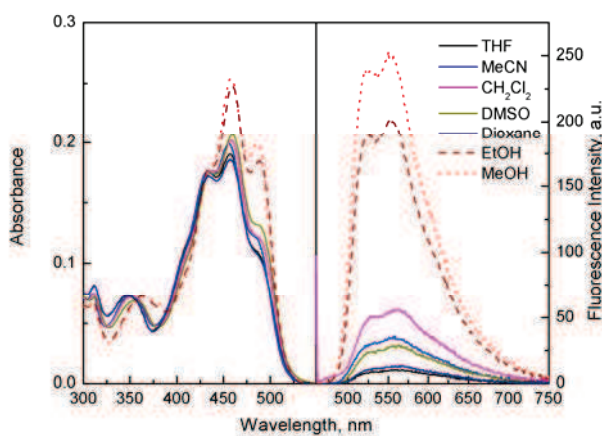


Figure 2-21. Absorption (left) and fluorescence (right) spectra of **Flu-2** in various solvents; excitation wavelengths correspond to the peaks of absorption band in different solvents, $[\text{Flu-2}] = 10 \mu\text{M}$.

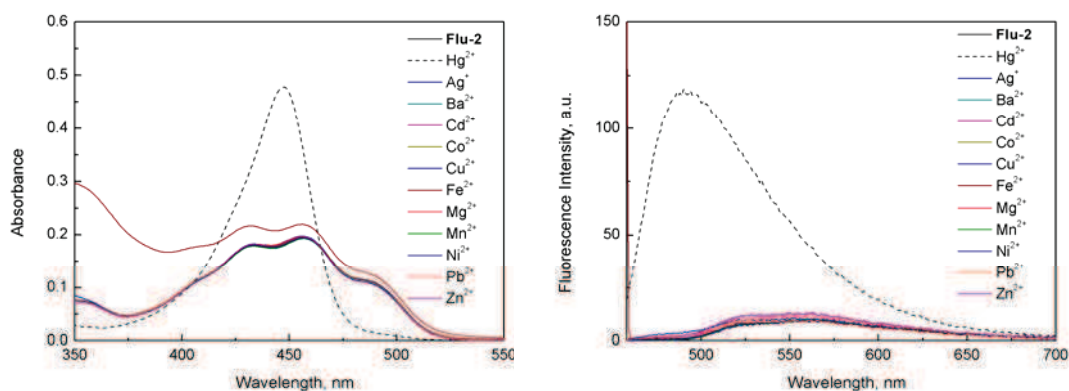


Figure 2-22. Absorption (left) and fluorescence (right) spectra of **Flu-2** in the presence of various metal ions in THF; $[\text{M}^{n+}] = 80 \mu\text{M}$, $[\text{Hg}^{2+}] = 40 \mu\text{M}$, $[\text{Flu-2}] = 10 \mu\text{M}$, $\lambda_{\text{ex}} = 456 \text{ nm}$.

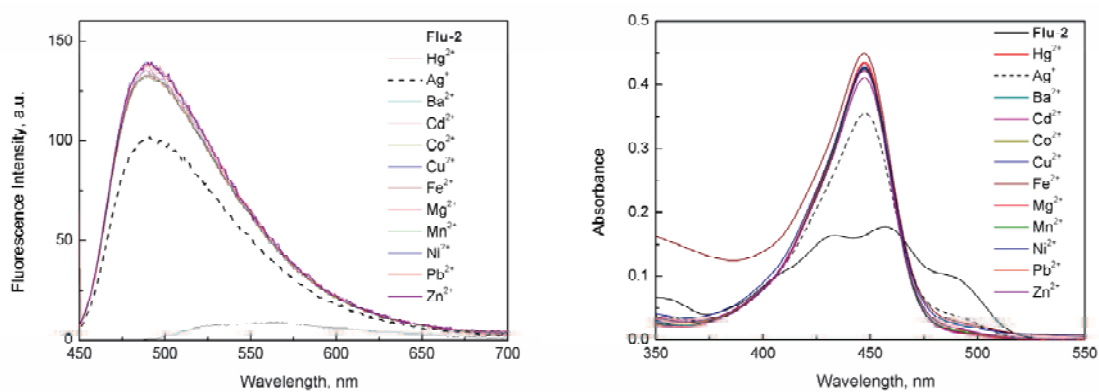


Figure 2-23. Absorption (left) and fluorescence (right) spectra of **Flu-2** in the coexistence of various metal ions and Hg^{2+} in THF; $[\text{M}^{n+}] = 40 \mu\text{M}$, $[\text{Hg}^{2+}] = 40 \mu\text{M}$, $[\text{Flu-2}] = 10 \mu\text{M}$, $\lambda_{\text{ex}} = 448 \text{ nm}$.

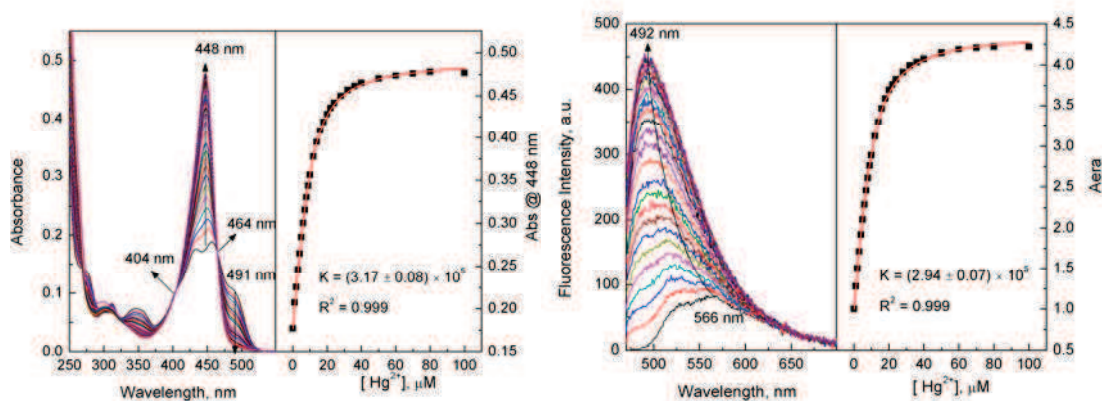


Figure 2-24. Absorption (left) and fluorescence (right) spectra of **Flu-2** in the presence of varying concentrations of Hg^{2+} in THF, $[\text{Flu-2}] = 10 \mu\text{M}$, $\lambda_{\text{ex}} = 468 \text{ nm}$.

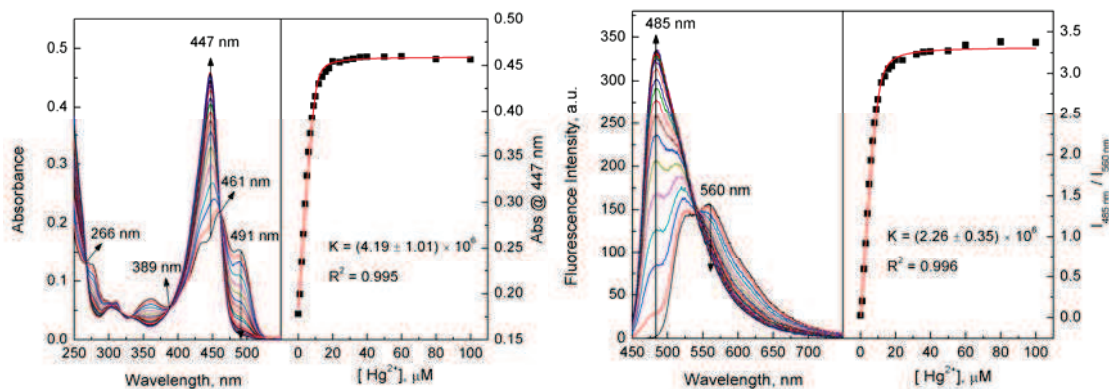


Figure 2-25. Absorption (left) and fluorescence (right) spectra of **Flu-2** in the presence of varying concentrations of Hg^{2+} in $\text{CH}_2\text{Cl}_2/\text{MeOH}$ ($v/v = 9:1$), $[\text{Flu-2}] = 10 \mu\text{M}$, $\lambda_{\text{ex}} = 447 \text{ nm}$.

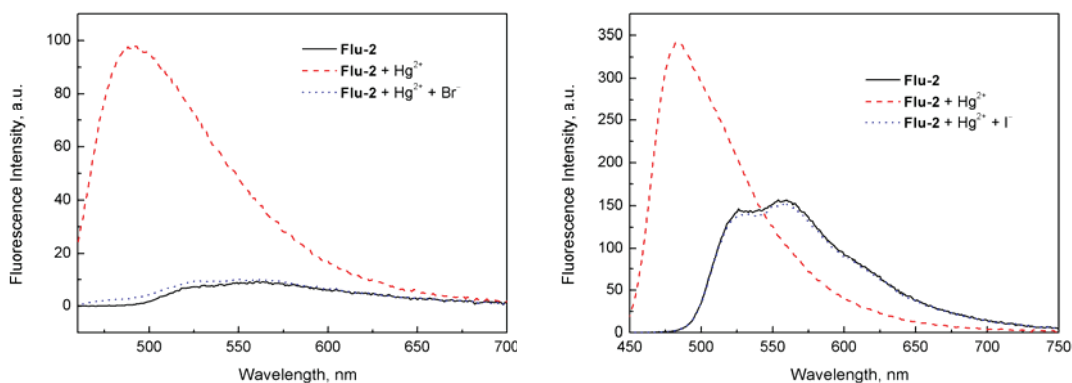


Figure 2-26. Fluorescence spectra of **Flu-2** in the presence of Hg^{2+} and then addition of Br^-/I^- in THF (left) and DCM/MeOH ($v/v = 9:1$) (right), $[\text{Flu-2}] = 10 \mu\text{M}$, $[\text{Hg}^{2+}] = 40 \mu\text{M}$, $[\text{Br}^-] = [\text{I}^-] = 80 \mu\text{M}$, $\lambda_{\text{ex}} = 457$ (left), 447 (right) nm.

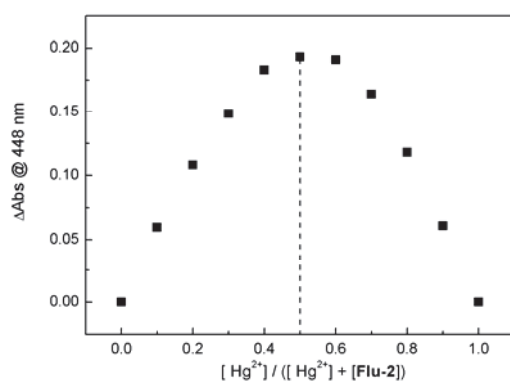
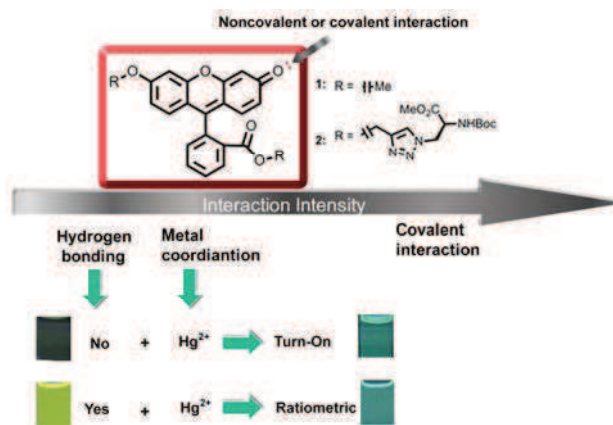


Figure 2-27. Job plot for **Flu-2**-Hg²⁺. The total concentration of [Hg²⁺] and [**Flu-2**] is 20 μM.

2.2.5. Conclusion

In summary, we have found that easily synthesized fluorescein derivatives **Flu-1** and **Flu-2** could be used as highly selective chemosensors for Hg²⁺ over a range of metal ions in THF. In the absence and presence of intermolecular hydrogen bonding interaction, we have developed “turn-on” fluorescence response to Hg²⁺ in THF and ratiometric detection of Hg²⁺ in CH₂Cl₂/MeOH (v/v = 9:1), respectively. ¹H NMR titration and IR spectra suggested that specific spectral behavior was due to the complexation between carbonyl group of xanthene moiety and Hg²⁺. We thus demonstrates how metal coordination, one of most important non-covalent interactions, affects the spectral properties of xanthene fluorophore through direct interaction with its carbonyl group, as shown in Scheme 2-6. Furthermore, combination of different non-covalent and/or covalent interactions with carbonyl group may further promote the extensive applications of xanthene dyes in biological and environmental systems. Comparison of **Flu-1** and **Flu-2** shows that introduction of triazolyl amino ester moiety in fluorescein does not influence the binding selectivity of fluorescein core structure and triazolyl acts thus only as a linker.⁸⁷



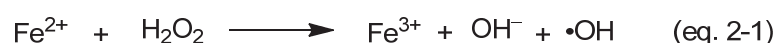
Scheme 2-6. Schematic illustration of interaction between fluorescein derivatives and metal ions.

2.3. Fluorescein-Triazole derivatives for selective detection of Cu^{2+} / Cu^+

2.3.1. Introduction

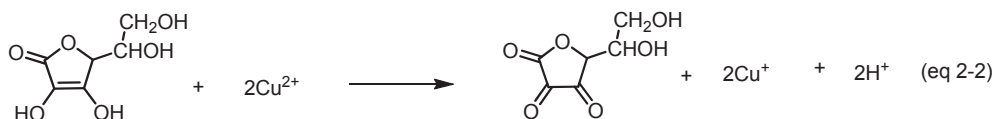
Copper as one of the most important trace essential elements is involved in electron transfer processes of a number of biological reactions.^{88,89} Its intracellular level is directly associated with functions of proteins and various neurodegenerative diseases such as Alzheimer, Menkes and Wilson's diseases.⁹⁰ Owing to its importance, using optical techniques to monitor the trafficking and location of Cu^{2+} in living cells has attracted much attention and resulted in fruitful works in recent years. Among the reported methods, fluorescent chemosensors show distinct advantages in sensitivity and biological imaging. However, for the intrinsic paramagnetic property of Cu^{2+} , many probes show a "turn-off" response *via* electron/energy transfer process.^{91,92,93,94,95,96,97} "Turn-on" fluorescent probes reported for Cu^{2+} are mainly based on chelation-enhanced fluorescence^{98,99,100,101} or chemodosimeters.^{102,103,104,105,106,107} Transformation of rhodamine-B derivatives from non-fluorescent spirolactam to fluorescent ring-opened amide form usually displays color change and fluorescence enhancement, making it as a charming sensory platform.^{108,109} Colorimetric method has also been extensively utilized due to its extreme simplicity that it could be read out by naked eyes without the aid of sophisticated instruments, facilitating the realization of point-of-use application.^{110,111,112} Jiang et al reported visual detection of Cu^{2+} by azide- and terminal alkyne-functionalized gold nanoparticles (Au NPs) using click chemistry.¹¹⁰ However, up to now most probes available for naked-eye detection of Cu^{2+} still suffer from limited sensitivity and/or interference from other metal ions. To overcome the limitations, new elements such as catalysis and conjugated polymers could be incorporated to amplify the sensing processes.

Fenton reaction, as recognized in 1894 classically refers to the reaction between H_2O_2 and Fe^{2+} under acidic conditions.¹¹³ The generally accepted mechanism of Fenton process is initiated by the formation of hydroxyl radical, as shown in equation (eq. 2-1) and this reaction takes place in acidic medium.



Due to its capability to generate highly reactive hydroxyl radical ($\cdot\text{OH}$), Fenton reaction has been recognized to be sources of aging process and a variety of diseases. Nevertheless it's also successfully applied in food chemistry and environmental engineering to remove many

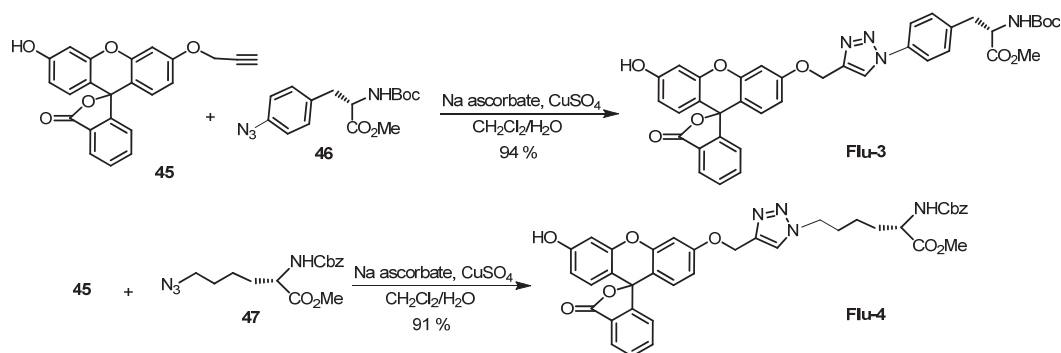
hazardous organic pollutants from water.^{114,113,115} Copper ions have been found to actively form hydroxyl radicals under aerobic conditions in the presence of ascorbate acid, which can lead to DNA or RNA strand scission. Under the conditions of excessive ascorbate acid, Cu^{2+} is continually reduced to Cu^+ (eq 2-2) which converted the dissolved oxygen into hydrogen peroxide (eq 2-2 to eq 2-4). The resulting Cu^+ and hydrogen peroxide can undergo Fenton reaction to produce hydroxyl radical and hydroxide anion, as shown in eq. 2-5.^{116,117}



In spite of its great importance, Fenton reaction is still rarely used in sensory processes.^{118,119} Yang et al found that DNAzyme could be cleaved into ssDNA in the presence of ascorbic acid and Cu^{2+} , which enhanced stabilization of Au NPs against salt-induced aggregation. They successfully utilized this protocol for colorimetric detection of Cu^{2+} .¹¹⁹ However, their system suffered from low sensitivity and blurry color change. So far most reports on Fenton reactions have paid much more attention to free radical species; however, here we envision that the pH change induced by Fenton reaction could be another novel approach for highly sensitive naked-eye and “turn-on” fluorescent detection of Cu^{2+} when fluorescein lactone derivatives are used as indicators.

2.3.2. Synthesis of Fluorescein-triazole derivatives (Synthesized by Chun Li)

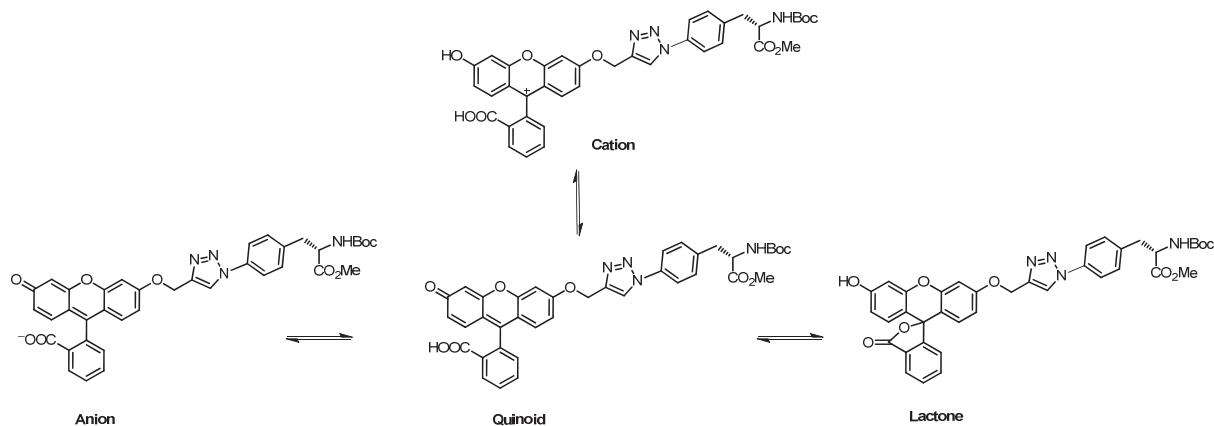
Flu-3 and **Flu-4** were easily synthesized by click reaction of fluorescein alkyne **45** with azide **46** or **47** in a mixture of CH_2Cl_2 and water (Scheme 2-7).¹²⁰



Scheme 2-7. Synthesis of fluorescein derivatives **Flu-3** and **Flu-4**.

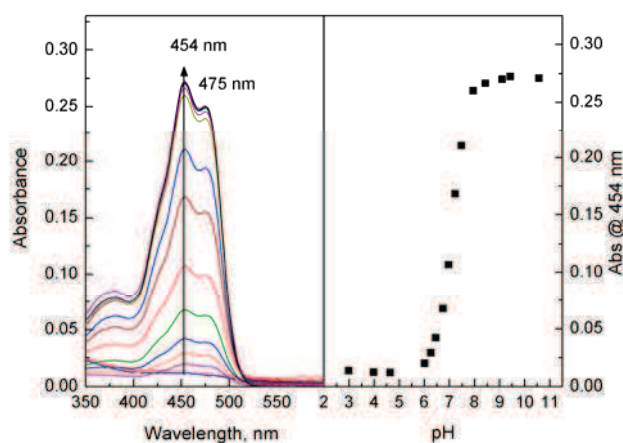
2.3.3. Photophysical properties of Flu-3

Forms of fluorescein derivatives existing in solution depend closely on pH, hydrogen-bonding interaction and polarity of their environment.¹²¹ **Flu-3** may exist in four different forms including lactone, quinoid, cation and monoanion, as shown in Scheme 2-8. Its photophysical properties are then strongly associated with the changes of environment.



Scheme 2-8. Possible existing forms of **Flu-3**.

We first investigated spectral properties of **Flu-3** under different pH conditions. As shown in Figure 2-28, **Flu-3** shows weak absorption or emission bands in the visible region when the pH is below 6.0. With increasing pH, it exhibits absorption band centered at 454 nm and emission band at 517 nm, respectively. Meanwhile color change from colorless to yellow was observed, indicating the transformation of **Flu-3** from lactone to monoanion/quinoid form. Both absorption and emission reach plateaus when the pH is above 8.0. Therefore the observed pK_a of **Flu-3** in the ground and excited states are both ca. 7.0. As the pH of Milli-Q water used in our work is ca. 5.5, existing form of **Flu-3** in pure water should be lactone which could be a potentially “turn-on” fluorescent chemosensor.



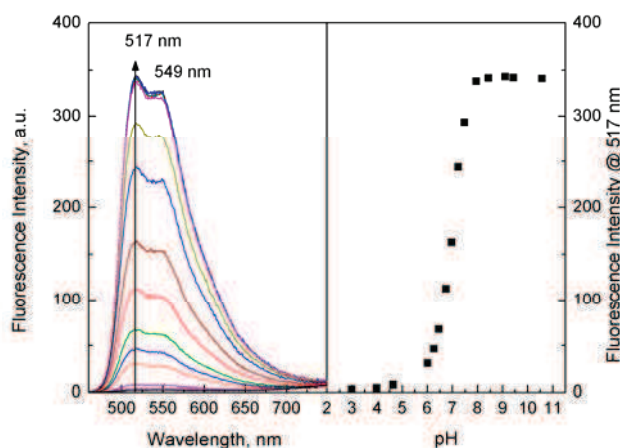
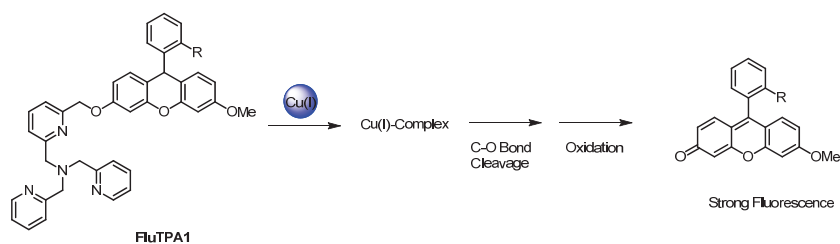


Figure 2-28. Absorption (top) and fluorescence (bottom) spectra of compound **Flu-3** in 10 mM HEPES solution under different pH conditions. [**Flu-3**] = 10.0 μM , λ_{ex} = 454 nm.

2.3.4. Complexation properties of Flu-3

For the sake of high sensitivity, several signal amplification approaches such as fluorescent conjugated polymers, Au NPs, DNAzyme and metal ions catalyzed reactions have been incorporated into metal ions sensing processes.^{23,122,123} Hydrolysis of non-fluorescent probes catalyzed by Cu^{2+} shows amplified fluorescence signal transduction.^{124,104} Taki et al developed a highly sensitive fluorescein derivatives (**FluTPA1**) for the detection of intracellular cuprous based on the cleavage of C-O bond of benzyl ether through a copper-active intermediate, as shown in Scheme 2-9.⁷⁷ Since **Flu-3** has a similar binding site to **FluTPA1** comprised of 1,2,3-triazole and oxygen atom, we intend to investigate the spectral response of **Flu-3** to Cu^+ . Cu^+ was generated *in situ* by reduction of Cu^{2+} with sodium ascorbate (AsCH^-). Introduction of 1 mM AsCH^- could slightly induce ring-opening of **Flu-3**, probably because of slight increase of pH (Figure 2-29). Surprisingly, further addition of 0.5 μM Cu^{2+} led to color change from colorless to light yellow and dramatically enhanced emission (Figure 2-29). Figure 2-30 shows the kinetics profiles of **Flu-3** in the presence of varying concentrations of Cu^{2+} . When [Cu^{2+}] is 500 nM, it reaches equilibrium in 5 min and keeps constant in the next further 10 min. With decreasing concentration of Cu^{2+} , the reaction time prolongs. When [Cu^{2+}] is reduced to 200 nM, the equilibrium is obtained in 25 min with ca. 6-fold fluorescence enhancement (ca. 52% hydrolysis of **Flu-3**, estimated from the fluorescence intensity) (Figure 2-31). Consequently, under this condition one copper ion can catalyzed 25 equiv **Flu-3** into ring-opening form, demonstrating the efficient catalysis assisted signal amplification for the detection of Cu^{2+} . However, when [Cu^{2+}] is lowered down to 100 nM, just very slight incremental of fluorescence intensity could be observed in 20 min and prolonging the reaction time did not produce any obvious enhanced fluorescence.



Scheme 2-9. Cu(I) chemodosimeter based on **FluTPA1**.

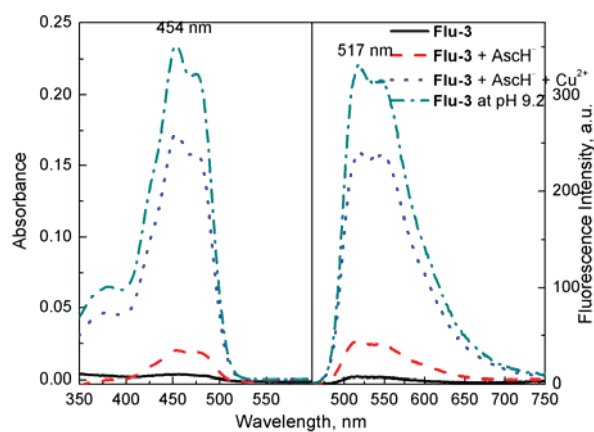


Figure 2-29. Absorption (left) and fluorescence (right) spectra of **Flu-3**, **Flu-3** in the absence and presence of Cu^{2+} in H_2O or **Flu-3** at pH 9.2. $[\text{Flu-3}] = 10.0 \mu\text{M}$, $[\text{Cu}^{2+}] = 0.5 \mu\text{M}$, $[\text{AscH}^-] = 1.0 \text{mM}$, $\lambda_{\text{ex}} = 454 \text{nm}$, reaction time 7 min.

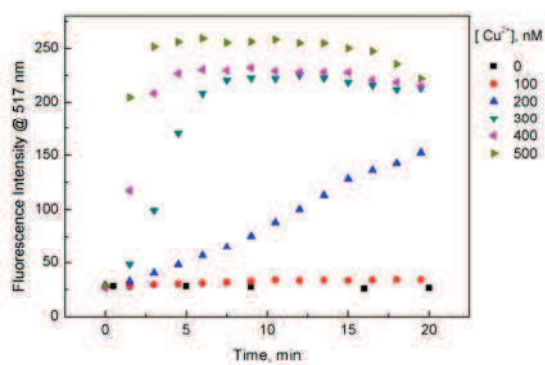


Figure 2-30. Kinetics profiles of **Flu-3** in the presence of different concentrations of Cu^{2+} in H_2O . $[\text{Flu-3}] = 10.0 \mu\text{M}$, $[\text{AscH}^-] = 1.0 \text{mM}$, $\lambda_{\text{ex}} = 454 \text{nm}$.

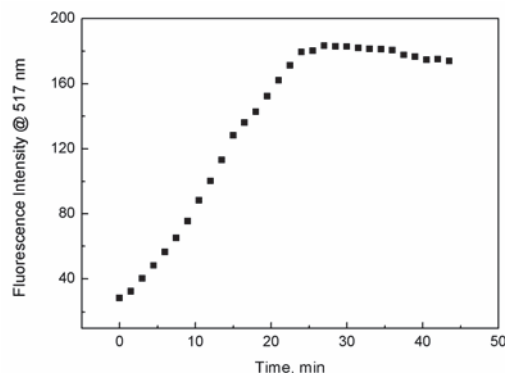


Figure 2-31. Kinetics profiles of **Flu-3** in the presence of 200 nM Cu^{2+} in H_2O . [**Flu-3**] = 10.0 μM , [AscH^-] = 1.0 mM, λ_{ex} = 454 nm.

Selectivity of this protocol was evaluated by screening a series of metal ions such as Co^{2+} , Fe^{2+} , Pb^{2+} , Hg^{2+} , Cd^{2+} , Ni^{2+} , Ag^+ , Mn^{2+} , Zn^{2+} , Ba^{2+} , Ca^{2+} and Mg^{2+} at 40 μM level. As displayed in Figure 2-32, only Cu^{2+} and Cu^+ induce fluorescence enhancement of **Flu-3**. Pb^{2+} , Hg^{2+} and Ag^+ show a slight quenching effect while others produce almost no changes. Figure 2-33 displays that except Cu^{2+} and Cu^+ , other metal ions cause no detectable color changes, demonstrating its high selectivity for visual detection of copper ions. Its selectivity was further confirmed by competition experiments, as shown in Figure 2-34. Even in the presence of 8-fold concentration excess compared to [Cu^{2+}], most ions produce almost no effect on detection of Cu^{2+} except Pb^{2+} and Hg^{2+} . Moreover, the interference may be probably attributed to acidic species contained in the sources metal ions or hydrolysis reaction.

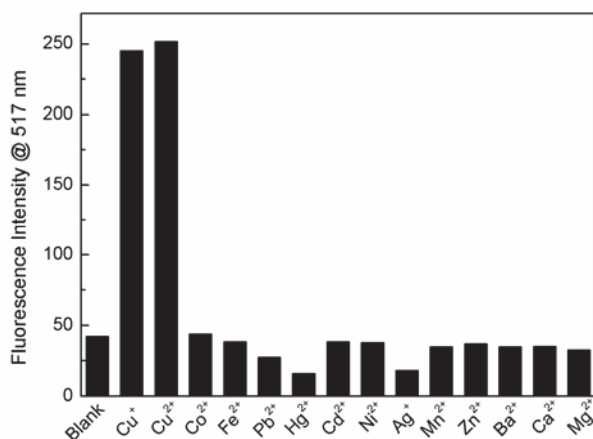


Figure 2-32. Fluorescence intensity at 517 nm of **Flu-3** in the presence of various metal ions in H_2O . [**Flu-3**] = 10.0 μM , [Cu^+] = [Cu^{2+}] = 0.5 μM and other metal ions 40 μM , [AscH^-] = 1.0 mM, reaction time 7 min.

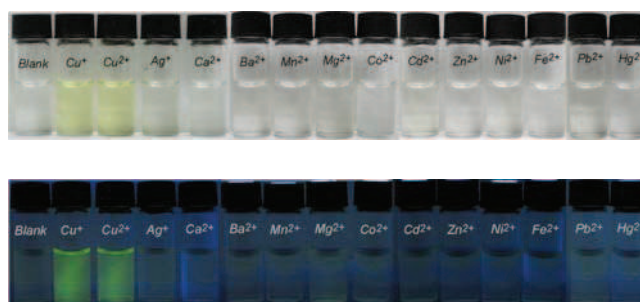


Figure 2-33. Change in color (top) and fluorescence (bottom) of **Flu-3** in the presence of various metal ions in H₂O. [**Flu-3**] = 10.0 μM, [Cu⁺] = [Cu²⁺] = 0.5 μM and other metal ions 40 μM, [AsCH⁻] = 1.0 mM, illuminated under 365 nm, reaction time 7 min.

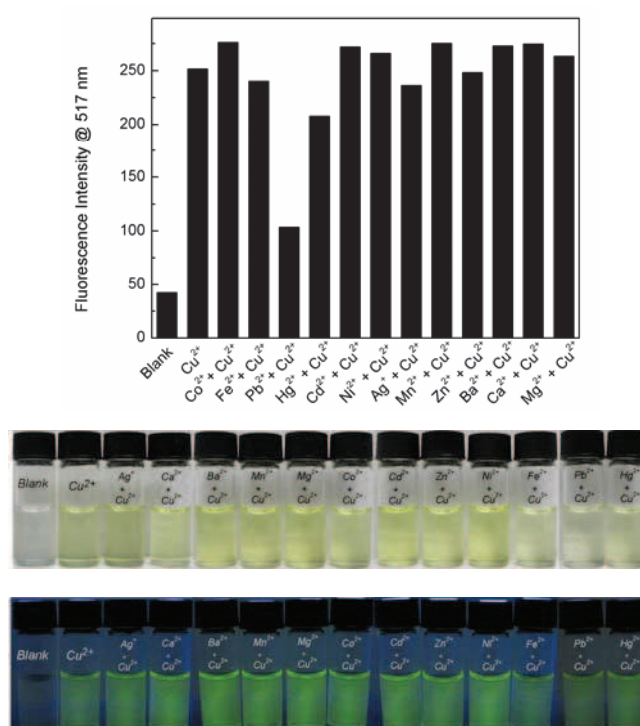


Figure 2-34. Fluorescence intensity at 517 nm (top), color (middle) and fluorescence (bottom) change of **Flu-3** in the presence of various metal ions and then further addition of Cu²⁺ in H₂O. [**Flu-3**] = 10.0 μM, [Cu²⁺] = 5.0 μM and other metal ions 40 μM, [AsCH⁻] = 1.0 mM, illuminated under 365 nm, reaction time 5 min.

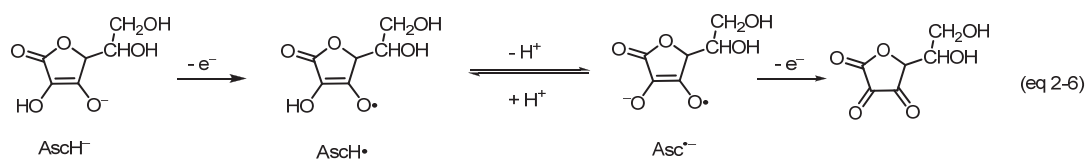
Fast and sensitive visual detection of Cu²⁺ in water may facilitate the on-site application. Figure 2-35 shows the color and fluorescence change of **Flu-3** in the presence of different [Cu²⁺]. It is found that no color change could be observed when [Cu²⁺] is 100 nM. However, with increasing [Cu²⁺], the solution color changes from colorless to light yellow. Surprisingly, 200 nM Cu²⁺ could already be clearly read out by naked eyes, that is, the naked-eye detection limit of our protocol for Cu²⁺ could be down low to 200 nM just in 10 min response time. This

result shows great advantages in the response time, sensitivity, simplicity and cost when compared with other reported colorimetric methods.



Figure 2-35. Change in color (left) and fluorescence (right) of **Flu-3** in the presence of varying concentrations of Cu^{2+} in H_2O . [**Flu-3**] = $10.0 \mu\text{M}$, [Cu^{2+}] = 0, 100, 200, 300, 400, 500 nM, [AscH^-] = 1.0 mM, illuminated under 365 nm, reaction time 10 min.

To get insight into the sensing mechanism, several control experiments were carried out. In our assay we found that in the absence of AscH^- , addition of Cu^+ couldn't cause any change of the spectral properties of **Flu-3** (Figure 2-36). Therefore AscH^- and Cu^+ both together contribute to the change of spectra. As we have mentioned above that coexistence of AscH^- and Cu^+ can undergo Fenton reaction to yield $\cdot\text{OH}$ and hydroxide under aerobic condition (eq 2-2 to eq 2-5). We assume that spectral change of lactone **Flu-3** in the presence of AscH^- and Cu^{2+} might come from the pH change of solution induced by Fenton reaction. Figure 2-37 shows the pH profile of AscH^- solution after addition of Cu^{2+} which is consistent with the production of hydroxide by the Fenton reaction, causing the increase of pH, followed by the neutralisation with H^+ produced from deprotonation of ascorbate radical ($\text{AscH}\cdot$) (eq 2-6), leading to the decrease of the pH. In the presence of **Flu-3**, pH change matches perfectly with that of AscH^- and Cu^{2+} . Further experiments in buffered solutions at pH 7.2 (HEPES) and 6.0 (HEPES and PB) demonstrates that fluorescence enhancement were inhibited in the presence of Cu^{2+} (Figure 2-38). So here we have verified that it's the pH increase induced by Fenton reaction that causes the spectral change of **Flu-3** and reactive hydroxyl radical couldn't promote the C-O ether bond cleavage in our case. Actually, hydroxyl radical could be reduced into H_2O in the presence of large excess of AscH^- . Since it is a pH-dependent sensing process, ligand **Flu-4** should also show a similar behavior upon addition of Cu^{2+} under the same condition. The kinetic profile of **Flu-4** (Figure 2-39) confirmed this behavior.



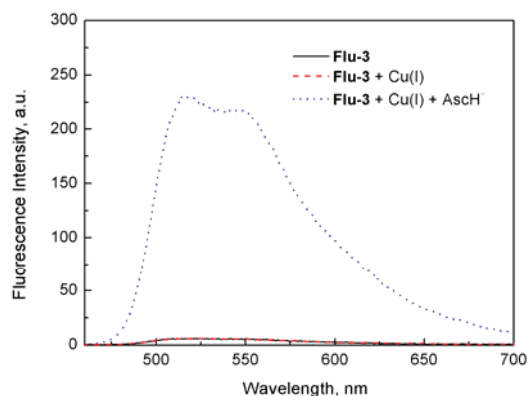


Figure 2-36. Fluorescence spectra of **Flu-3**, **Flu-3** + Cu^+ in the absence and presence of AscH^- in H_2O . $[\text{Flu-3}] = 10.0 \mu\text{M}$, $[\text{Cu}^+] = 0.5 \mu\text{M}$, $[\text{AscH}^-] = 1.0 \text{mM}$, $\lambda_{\text{ex}} = 454 \text{nm}$.

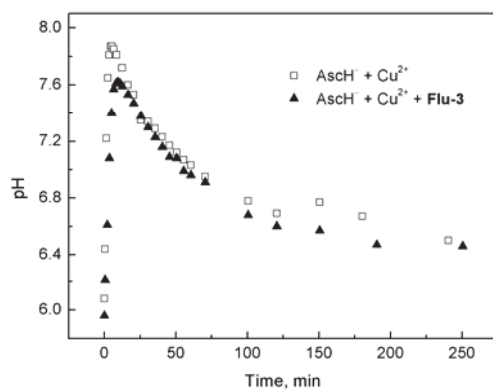


Figure 2-37. Kinetics profiles of pH change of $\text{AscH}^- + \text{Cu}^{2+}$ in the absence and presence of **Flu-3** in H_2O . $[\text{Flu-3}] = 10.0 \mu\text{M}$, $[\text{Cu}^{2+}] = 0.5 \mu\text{M}$, $[\text{AscH}^-] = 1.0 \text{mM}$

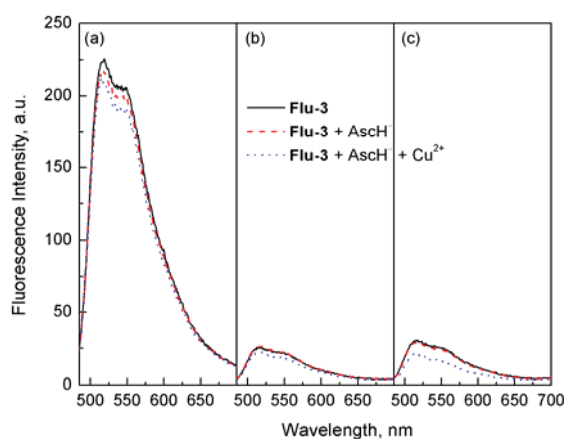


Figure 2-38. Fluorescence spectra of **Flu-3** in the absence and presence of Cu^{2+} in buffered solution. (a) 10 mM HEPES at pH 7.2; (b) 10 mM HEPES at pH 6.0; (c) 10 mM $\text{NaHPO}_4\text{-NaH}_2\text{PO}_4$ at pH 6.0. $[\text{Flu-3}] = 10.0 \mu\text{M}$, $[\text{Cu}^{2+}] = 0.5 \mu\text{M}$, $[\text{AscH}^-] = 1.0 \text{mM}$, $\lambda_{\text{ex}} = 480 \text{nm}$, reaction time 8 min.

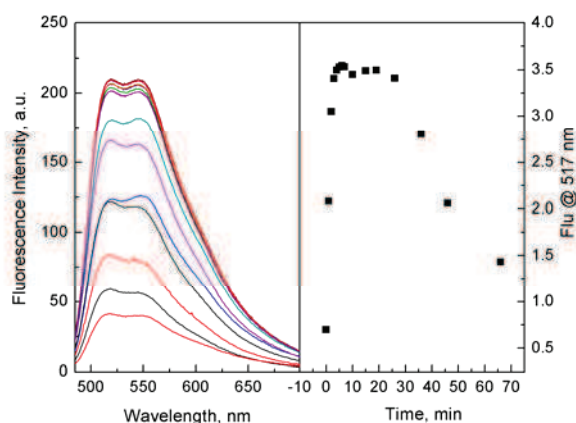


Figure 2-39. Kinetics profiles of **Flu-4** in the presence of Cu^{2+} in H_2O . $[\text{Flu-4}] = 10.0 \mu\text{M}$, $[\text{Cu}^{2+}] = 0.5 \mu\text{M}$, $[\text{AscH}^-] = 1.0 \text{ mM}$, $\lambda_{\text{ex}} = 454 \text{ nm}$.

Introduction of other stronger binding ligands like EDTA is usually necessary for the reversibility of a chemosensor. However, in our sensing system it seemed to heal up by itself. As shown in Figure 2-40, fluorescence intensity of **Flu-3** decreases to the initial level when the reaction time prolongs to 80 min. It's attributed that self-recovery is due to neutralisation of the hydroxide by H^+ yielded from deprotonation of ascorbate radical (AscH^\cdot), as shown in eq 2-6. Moreover, the auto-reversibility of the fluorescence spectra demonstrated that hydroxyl radical didn't react with **Flu-3**.

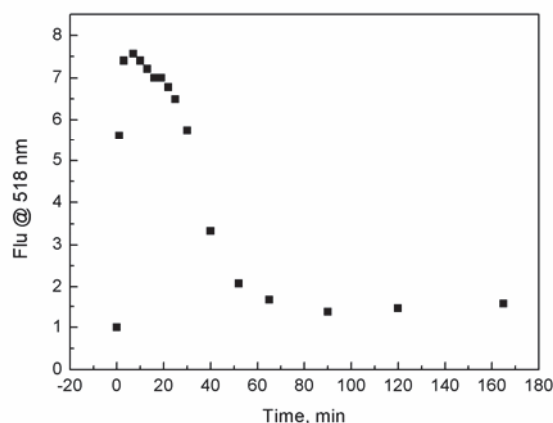
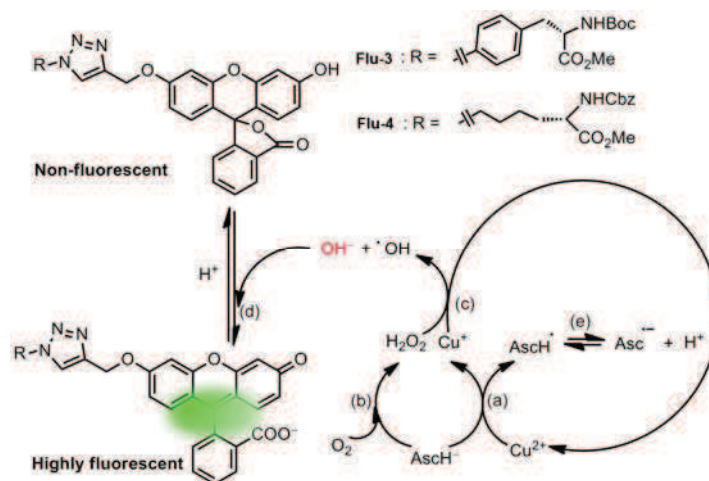


Figure 2-40. Kinetics profiles of **Flu-3** in the presence of Cu^{2+} in H_2O . $[\text{Flu-3}] = 10.0 \mu\text{M}$, $[\text{Cu}^{2+}] = 0.5 \mu\text{M}$, $[\text{AscH}^-] = 1.0 \text{ mM}$, $\lambda_{\text{ex}} = 454 \text{ nm}$.

Based on the above investigations, the sensing mechanism is depicted in Scheme 2-10. Under aerobic condition, ascorbate (AscH^-) not only involves in the reduction of Cu^{2+} (a), but also reacts with O_2 to produce H_2O_2 (b). Hydroxide and $\cdot\text{OH}$ are then yielded in the following

Fenton reaction between Cu^{2+} and H_2O_2 (c). Increase of pH by hydroxide promotes the ring-opening of **Flu-3** (d), which results in fluorescence enhancement and remarkable color change. It's noteworthy that recycle of Cu^{2+} (c) may dramatically amplify signal transduction. Neutralisation of the hydroxide by H^+ yielded from deprotonation of ascorbate radical ($\text{AscH}\cdot$) (e) induces the ring closing of the lactone and make the system reversible.



Scheme 2-10. Proposed mechanism for detection of Cu^{2+} based on Fenton reaction.

2.3.5. Conclusion

In summary, using Cu^{2+} -catalyzed Fenton reaction, we have developed a novel approach for highly sensitive naked-eye and fluorescence “turn-on” detection of Cu^{2+} . In our assay Cu^{2+} could selectively participate in Fenton reaction to yield hydroxide which promoted hydrolysis of **Flu-3** and consequently resulted in the color change and fluorescence enhancement. And the naked-eye detection limit of this protocol could be as low as 200 nM, which is better than other reported systems. In view of its simplicity, short response time, low cost, high selectivity and ultralow naked-eye detection, our system gives hints on design of chemosensors based on mimicking efficient catalytic biological reactions.¹²⁵

References

- [1] Bohacek, R. S.; McMartin, C.; Guida, W. C. "The art and practice of structure-based drug design: A molecular modeling perspective." Medicinal Research Reviews **1996**, *16*, 3-50.
- [2] Kolb, H. C.; Finn, M. G.; Sharpless, K. B. "Click chemistry: Diverse chemical function from a few good reactions." Angewandte Chemie-International Edition **2001**, *40*, 2004-2021.
- [3] Golas, P. L.; Matyjaszewski, K. "Marrying click chemistry with polymerization: expanding the scope of polymeric materials." Chemical Society Reviews **2010**, *39*, 1338-1354.
- [4] Amblard, F.; Cho, J. H.; Schinazi, R. F. "Cu(I)-Catalyzed Huisgen Azide-Alkyne 1,3-Dipolar Cycloaddition Reaction in Nucleoside, Nucleotide, and Oligonucleotide Chemistry." Chemical Reviews **2009**, *109*, 4207-4220.
- [5] Mamidyala, S. K.; Finn, M. G. "In situ click chemistry: probing the binding landscapes of biological molecules." Chemical Society Reviews **2010**, *39*, 1252-1261.
- [6] Hein, C. D.; Liu, X. M.; Wang, D. "Click chemistry, a powerful tool for pharmaceutical sciences." Pharmaceutical Research **2008**, *25*, 2216-2230.
- [7] Padwa, A. "1,3-dipolar cycloaddition chemistry" Wiley, **1984**.
- [8] Rostovtsev, V. V.; Green, L. G.; Fokin, V. V.; Sharpless, K. B. "A stepwise Huisgen cycloaddition process: Copper(I)-catalyzed regioselective "ligation" of azides and terminal alkynes." Angewandte Chemie-International Edition **2002**, *41*, 2596-2599.
- [9] Tornøe, C. W.; Christensen, C.; Meldal, M. "Peptidotriazoles on solid phase: [1,2,3]-triazoles by regioselective copper(I)-catalyzed 1,3-dipolar cycloadditions of terminal alkynes to azides." Journal of Organic Chemistry **2002**, *67*, 3057-3064.
- [10] Appukkuttan, P.; Dehaen, W.; Fokin, V. V.; Van der Eycken, E. "A microwave-assisted click chemistry synthesis of 1,4-disubstituted 1,2,3-triazoles via a copper(I)-catalyzed three-component reaction." Organic Letters **2004**, *6*, 4223-4225.
- [11] Himo, F.; Lovell, T.; Hilgraf, R.; Rostovtsev, V. V.; Noodleman, L.; Sharpless, K. B.; Fokin, V. V. "Copper(I)-catalyzed synthesis of azoles. DFT study predicts unprecedented reactivity and intermediates." Journal of the American Chemical Society **2005**, *127*, 210-216.
- [12] Hein, J. E.; Fokin, V. V. "Copper-catalyzed azide-alkyne cycloaddition (CuAAC) and beyond: new reactivity of copper(I) acetylides." Chemical Society Reviews **2010**, *39*, 1302-1315.
- [13] Zhang, L.; Chen, X. G.; Xue, P.; Sun, H. H. Y.; Williams, I. D.; Sharpless, K. B.; Fokin, V. V.; Jia, G. C. "Ruthenium-catalyzed cycloaddition of alkynes and organic azides." Journal of the American Chemical Society **2005**, *127*, 15998-15999.
- [14] Boren, B. C.; Narayan, S.; Rasmussen, L. K.; Zhang, L.; Zhao, H. T.; Lin, Z. Y.; Jia, G. C.; Fokin, V. V. "Ruthenium-catalyzed azide-alkyne cycloaddition: Scope and mechanism." Journal of the American Chemical Society **2008**, *130*, 8923-8930.
- [15] Bock, V. D.; Hiemstra, H.; van Maarseveen, J. H. "Cu-I-catalyzed alkyne-azide "click" cycloadditions from a mechanistic and synthetic perspective." European Journal of Organic Chemistry **2006**, 51-68.
- [16] Rodionov, V. O.; Fokin, V. V.; Finn, M. G. "Mechanism of the ligand-free Cu-I-catalyzed azide-alkyne cycloaddition reaction." Angewandte Chemie-International Edition **2005**, *44*,

2210-2215.

[17] Meldal, M.; Todd, M. H. "Cu-Catalyzed Azide-Alkyne Cycloaddition." Chemical Reviews **2008**, *108*, 2952-3015.

[18] Lau, Y. H.; Rutledge, P. J.; Watkinson, M.; Todd, M. H. "Chemical sensors that incorporate click-derived triazoles." Chemical Society Reviews **2011**, *40*, 2848-2866.

[19] Jin, Z.; Zhang, X. B.; Xie, D. X.; Gong, Y. J.; Zhang, J.; Chen, X.; Shen, G. L.; Yu, R. Q. "Clicking Fluoroionophores onto Mesoporous Silicas: A Universal Strategy toward Efficient Fluorescent Surface Sensors for Metal Ions." Analytical Chemistry **2010**, *82*, 6343-6346.

[20] Pathak, R. K.; Ibrahim, S. M.; Rao, C. P. "Selective recognition of Zn²⁺ by salicylaldimine appended triazole-linked di-derivatives of calix[4]arene by enhanced fluorescence emission in aqueous-organic solutions: role of terminal -CH₂OH moieties in conjunction with the imine in recognition." Tetrahedron Letters **2009**, *50*, 2730-2734.

[21] Pathak, R. K.; Dikundwar, A. G.; Row, T. N. G.; Rao, C. P. "A lower rim triazole linked calix[4]arene conjugate as a fluorescence switch on sensor for Zn²⁺ in blood serum milieu." Chemical Communications **2010**, *46*, 4345-4347.

[22] Pathak, R. K.; Hinge, V. K.; Mondal, M.; Rao, C. P. "Triazole-Linked-Thiophene Conjugate of Calix[4]arene: Its Selective Recognition of Zn²⁺ and as Biomimetic Model in Supporting the Events of the Metal Detoxification and Oxidative Stress Involving Metallothionein." Journal of Organic Chemistry **2011**, *76*, 10039-10049.

[23] Thomas, S. W.; Joly, G. D.; Swager, T. M. "Chemical sensors based on amplifying fluorescent conjugated polymers." Chemical Reviews **2007**, *107*, 1339-1386.

[24] Wu, Y. Z.; Dong, Y.; Li, J. F.; Huang, X. B.; Cheng, Y. X.; Zhu, C. J. "A Highly Selective and Sensitive Polymer-based Fluorescence Sensor for Hg²⁺-Ion Detection via Click Reaction." Chemistry-an Asian Journal **2011**, *6*, 2725-2729.

[25] Huang, X. B.; Meng, J.; Dong, Y.; Cheng, Y. X.; Zhu, C. J. "Polymer-based fluorescence sensor incorporating triazole moieties for Hg²⁺ detection via click reaction." Polymer **2010**, *51*, 3064-3067.

[26] Nguyen, D. M.; Frazer, A.; Rodriguez, L.; Belfield, K. D. "Selective Fluorescence Sensing of Zinc and Mercury Ions with Hydrophilic 1,2,3-Triazolyl Fluorene Probes." Chemistry of Materials **2010**, *22*, 3472-3481.

[27] Kim, J. S.; Quang, D. T. "Calixarene-derived fluorescent probes." Chemical Reviews **2007**, *107*, 3780-3799.

[28] Chang, K. C.; Su, I. H.; Lee, G. H.; Chung, W. S. "Triazole- and azo-coupled calix[4]arene as a highly sensitive chromogenic sensor for Ca²⁺ and Pb²⁺ ions." Tetrahedron Letters **2007**, *48*, 7274-7278.

[29] Ni, X. L.; Zeng, X.; Redshaw, C.; Yamato, T. "Synthesis and evaluation of a novel pyrenyl-appended triazole-based thiacalix[4]arene as a fluorescent sensor for Ag⁺ ion." Tetrahedron **2011**, *67*, 3248-3253.

[30] Souchon, V.; Maisonneuve, S.; David, O.; Leray, I.; Xie, J.; Valeur, B. "Photophysics of cyclic multichromophoric systems based on beta-cyclodextrin and calix[4]arene with appended pyridin-2'-yl-1,2,3-triazole groups." Photochemical & Photobiological Sciences **2008**, *7*, 1323-1331.

[31] Colasson, B.; Save, M.; Milko, P.; Roithova, J.; Schroder, D.; Reinaud, O. "A ditopic calix[6]arene ligand with N-methylimidazole and 1,2,3-triazole substituents: Synthesis and

- coordination with Zn(II) cations." *Organic Letters* **2007**, *9*, 4987-4990.
- [32] Zhan, J. Y.; Tian, D. M.; Li, H. B. "Synthesis of calix[4]crowns containing soft and hard ion binding sites via click chemistry." *New Journal of Chemistry* **2009**, *33*, 725-728.
- [33] Chang, K. C.; Su, I. H.; Senthilvelan, A.; Chung, W. S. "Triazole-modified calix[4]crown as a novel fluorescent on-off switchable chemosensor." *Organic Letters* **2007**, *9*, 3363-3366.
- [34] Park, S. Y.; Yoon, J. H.; Hong, C. S.; Souane, R.; Kim, J. S.; Matthews, S. E.; Vicens, J. "A Pyrenyl-Appended Triazole-Based Calix[4]arene as a Fluorescent Sensor for Cd²⁺ and Zn²⁺." *Journal of Organic Chemistry* **2008**, *73*, 8212-8218.
- [35] Tian, D. M.; Yan, H. J.; Li, H. B. "A selective fluorescent probe of Hg²⁺ based on triazole-linked 8-oxyquinoline calix[4]arene by click chemistry." *Supramolecular Chemistry* **2010**, *22*, 249-255.
- [36] Ho, I. T.; Haung, K. C.; Chung, W. S. "1,3-Alternate Calix[4]arene as a Homobinuclear Ditopic Fluorescent Chemosensor for Ag⁺ Ions." *Chemistry-an Asian Journal* **2011**, *6*, 2738-2746.
- [37] Ni, X. L.; Wang, S.; Zeng, X.; Tao, Z.; Yamato, T. "Pyrene-Linked Triazole-Modified Homooxacalix[3]arene: A Unique C-3 Symmetry Ratiometric Fluorescent Chemosensor for Pb²⁺." *Organic Letters* **2011**, *13*, 552-555.
- [38] Ni, X. L.; Zeng, X.; Redshaw, C.; Yamato, T. "Ratiometric Fluorescent Receptors for Both Zn²⁺ and H₂PO₄⁻ Ions Based on a Pyrenyl-Linked Triazole-Modified Homooxacalix[3]arene: A Potential Molecular Traffic Signal with an R-S Latch Logic Circuit." *Journal of Organic Chemistry* **2011**, *76*, 5696-5702.
- [39] Li, Y. J.; Huffman, J. C.; Flood, A. H. "Can terdentate 2,6-bis(1,2,3-triazol-4-yl) pyridines form stable coordination compounds?" *Chemical Communications* **2007**, 2692-2694.
- [40] Schweinfurth, D.; Hardcastle, K. I.; Bunz, U. H. F. "1,3-Dipolar cycloaddition of alkynes to azides. Construction of operationally functional metal responsive fluorophores." *Chemical Communications* **2008**, 2203-2205.
- [41] Garcia, L.; Maisonneuve, S.; Xie, J. A.; Guillot, R.; Dorlet, P.; Riviere, E.; Desmadril, M.; Lambert, F.; Policar, C. "Sugars to Control Ligand Shape in Metal Complexes: Conformationally Constrained Glycoligands with a Predetermination of Stereochemistry and a Structural Control." *Inorganic Chemistry* **2010**, *49*, 7282-7288.
- [42] Garcia, L.; Maisonneuve, S.; Marcu, J. O. S.; Guillot, R.; Lambert, F.; Xie, J.; Policar, C. "Intrinsically Fluorescent Glycoligands To Study Metal Selectivity." *Inorganic Chemistry* **2011**, *50*, 11353-11362.
- [43] Tamanini, E.; Katewa, A.; Sedger, L. M.; Todd, M. H.; Watkinson, M. "A Synthetically Simple, Click-Generated Cyclam-Based Zinc(II) Sensor." *Inorganic Chemistry* **2009**, *48*, 319-324.
- [44] Tamanini, E.; Flavin, K.; Motevalli, M.; Piperno, S.; Gheber, L. A.; Todd, M. H.; Watkinson, M. "Cyclam-Based "Clickates": Homogeneous and Heterogeneous Fluorescent Sensors for Zn(II)." *Inorganic Chemistry* **2010**, *49*, 3789-3800.
- [45] Lau, Y. H.; Price, J. R.; Todd, M. H.; Rutledge, P. J. "A Click Fluorophore Sensor that Can Distinguish Cu-II and Hg-II via Selective Anion-Induced Demetallation." *Chemistry-a European Journal* **2011**, *17*, 2850-2858.
- [46] Li, H. B.; Yao, Y.; Han, C. P.; Zhan, J. Y. "Triazole-ester modified silver nanoparticles:

- click synthesis and Cd²⁺ colorimetric sensing.* Chemical Communications **2009**, 4812-4814.
- [47] Yao, Y.; Tian, D. M.; Li, H. B. "Cooperative Binding of Bifunctionalized and Click-Synthesized Silver Nanoparticles for Colorimetric Co²⁺ Sensing." Acs Applied Materials & Interfaces **2010**, 2, 684-690.
- [48] Li, H. B.; Zheng, Q. L.; Han, C. P. "Click synthesis of podand triazole-linked gold nanoparticles as highly selective and sensitive colorimetric probes for lead(II) ions." Analyst **2010**, 135, 1360-1364.
- [49] Hung, H. C.; Cheng, C. W.; Wang, Y. Y.; Chen, Y. J.; Chung, W. S. "Highly Selective Fluorescent Sensors for Hg²⁺ and Ag⁺ Based on Bis-triazole-Coupled Polyoxyethylenes in MeOH Solution." European Journal of Organic Chemistry **2009**, 6360-6366.
- [50] Hung, H. C.; Cheng, C. W.; Ho, I. T.; Chung, W. S. "Dual-mode recognition of transition metal ions by bis-triazoles chained pyrenes." Tetrahedron Letters **2009**, 50, 302-305.
- [51] Kim, H.; Lee, S.; Lee, J.; Tae, J. "Rhodamine Triazole-Based Fluorescent Probe for the Detection of Pt²⁺." Organic Letters **2010**, 12, 5342-5345.
- [52] Lu, H.; Qi, S. L.; Mack, J.; Li, Z. F.; Lei, J. P.; Kobayashi, N.; Shen, Z. "Facile Hg²⁺ detection in water using fluorescent self-assembled monolayers of a rhodamine-based turn-on chemodosimeter formed via a "click" reaction." Journal of Materials Chemistry **2011**, 21, 10878-10882.
- [53] Liu, X. C.; Yang, X.; Fu, Y.; Zhu, C. J.; Cheng, Y. X. "Novel fluorescent sensor for Ag⁺ and Hg²⁺ based on the BINOL-pyrene derivative via click reaction." Tetrahedron **2011**, 67, 3181-3186.
- [54] He, X. P.; Song, Z.; Wang, Z. Z.; Shi, X. X.; Chen, K. X.; Chen, G. R. "Creation of 3,4-bis-triazolocoumarin-sugar conjugates via fluorescent dual click chemistry and their quenching specificity with silver(I) in aqueous media." Tetrahedron **2011**, 67, 3343-3347.
- [55] David, O.; Maisonneuve, S.; Xie, J. "Generation of new fluorophore by Click chemistry: synthesis and properties of beta-cyclodextrin substituted by 2-pyridyl triazole." Tetrahedron Letters **2007**, 48, 6527-6530.
- [56] Maisonneuve, S.; Fang, Q.; Xie, J. "Benzothiadiazoyl-triazoyl cyclodextrin: a selective fluoroionophore for Ni(II)." Tetrahedron **2008**, 64, 8716-8720.
- [57] Sameiro, M.; Goncalves, T. "Fluorescent Labeling of Biomolecules with Organic Probes." Chemical Reviews **2009**, 109, 190-212.
- [58] Duan, Y. S.; Liu, M.; Sun, W.; Wang, M.; Liu, S. Z.; Li, Q. X. "Recent Progress on Synthesis of Fluorescein Probes." Mini-Reviews in Organic Chemistry **2009**, 6, 35-43.
- [59] Margulies, D.; Melman, G.; Shanzer, A. "A molecular full-adder and full-subtractor, an additional step toward a moleculator." Journal of the American Chemical Society **2006**, 128, 4865-4871.
- [60] Nolan, E. M.; Lippard, S. J. "Small-Molecule Fluorescent Sensors for Investigating Zinc Metalloneurochemistry." Accounts of Chemical Research **2009**, 42, 193-203.
- [61] Nolan, E. M.; Lippard, S. J. "A "Turn-On" fluorescent sensor for the selective detection of mercuric ion in aqueous media." Journal of the American Chemical Society **2003**, 125, 14270-14271.
- [62] Nolan, E. M.; Lippard, S. J. "MS4, a seminaphthofluorescein-based chemosensor for the ratiometric detection of Hg(II)." Journal of Materials Chemistry **2005**, 15, 2778-2783.
- [63] Nolan, E. M.; Racine, M. E.; Lippard, S. J. "Selective Hg(II) detection in aqueous

- solution with thiol derivatized fluoresceins.* Inorganic Chemistry **2006**, *45*, 2742-2749.
- [64] Nolan, E. M.; Lippard, S. J. "Turn-on and ratiometric mercury sensing in water with a red-emitting probe." Journal of the American Chemical Society **2007**, *129*, 5910-5918.
- [65] Yoon, S.; Albers, A. E.; Wong, A. P.; Chang, C. J. "Screening mercury levels in fish with a selective fluorescent chemosensor." Journal of the American Chemical Society **2005**, *127*, 16030-16031.
- [66] Yoon, S.; Miller, E. W.; He, Q.; Do, P. H.; Chang, C. J. "A bright and specific fluorescent sensor for mercury in water, cells, and tissue." Angewandte Chemie-International Edition **2007**, *46*, 6658-6661.
- [67] Swamy, K. M. K.; Kim, H. N.; Soh, J. H.; Kim, Y.; Kim, S. J.; Yoon, J. "Manipulation of fluorescent and colorimetric changes of fluorescein derivatives and applications for sensing silver ions." Chemical Communications **2009**, 1234-1236.
- [68] Jang, Y. J.; Jun, E. J.; Lee, Y. J.; Kim, Y. S.; Kim, J. S.; Yoon, J. "Highly effective fluorescent and colorimetric sensors for pyrophosphate over $H_2PO_4^-$ in 100% aqueous solution." Journal of Organic Chemistry **2005**, *70*, 9603-9606.
- [69] Swamy, K. M. K.; Lee, Y. J.; Lee, H. N.; Chun, J.; Kim, Y.; Kim, S. J.; Yoon, J. "A new fluorescein derivative bearing a boronic acid group as a fluorescent chemosensor for fluoride ion." Journal of Organic Chemistry **2006**, *71*, 8626-8628.
- [70] McQuade, L. E.; Ma, J.; Lowe, G.; Ghatpande, A.; Gelperin, A.; Lippard, S. J. "Visualization of nitric oxide production in the mouse main olfactory bulb by a cell-trappable copper(II) fluorescent probe." Proceedings of the National Academy of Sciences of the United States of America **2010**, *107*, 8525-8530.
- [71] Guarin, S. A. P.; Tsang, D.; Skene, W. G. "Spectroscopic studies of a fluorescent fluoresceinophane formed via a practical synthetic route." New Journal of Chemistry **2007**, *31*, 210-217.
- [72] Zhang, X. F.; Liu, Q.; Wang, H. B.; Fu, Z.; Zhang, F. S. "Photophysical behavior of lipophilic xanthene dyes without the involvement of photoinduced electron transfer mechanism." Journal of Photochemistry and Photobiology a-Chemistry **2008**, *200*, 307-313.
- [73] Martin, M. M. "Hydrogen bond effects on radiationless electronic transitions in xanthene dyes." Chemical Physics Letters **1975**, *105*, 105-111.
- [74] Santra, M.; Ryu, D.; Chatterjee, A.; Ko, S. K.; Shin, I.; Ahn, K. H. "A chemodosimeter approach to fluorescent sensing and imaging of inorganic and methylmercury species." Chemical Communications **2009**, 7599-7599.
- [75] Santra, M.; Ko, S. K.; Shin, I.; Ahn, K. H. "Fluorescent detection of palladium species with an O-propargylated fluorescein." Chemical Communications **2010**, *46*, 3964-3966.
- [76] Chen, X.; Ko, S. K.; Kim, M. J.; Shin, I.; Yoon, J. "A thiol-specific fluorescent probe and its application for bioimaging." Chemical Communications **2010**, *46*, 2751-2753.
- [77] Taki, M.; Iyoshi, S.; Ojida, A.; Hamachi, I.; Yamamoto, Y. "Development of Highly Sensitive Fluorescent Probes for Detection of Intracellular Copper(I) in Living Systems." Journal of the American Chemical Society **2010**, *132*, 5938-5939.
- [78] Garner, A. L.; St Croix, C. M.; Pitt, B. R.; Leikauf, G. D.; Ando, S.; Koide, K. "Specific fluorogenic probes for ozone in biological and atmospheric samples." Nature Chemistry **2009**, *1*, 316-321.
- [79] Garner, A. L.; Koide, K. "Oxidation State-Specific Fluorescent Method for Palladium(II)

and Platinum(IV) Based on the Catalyzed Aromatic Claisen Rearrangement." Journal of the American Chemical Society **2008**, *130*, 16472-16473.

[80] Garner, A. L.; Song, F. L.; Koide, K. "Enhancement of a Catalysis-Based Fluorometric Detection Method for Palladium through Rational Fine-Tuning of the Palladium Species." Journal of the American Chemical Society **2009**, *131*, 5163-5171.

[81] Song, F. L.; Watanabe, S.; Floreancig, P. E.; Koide, K. "Oxidation-Resistant Fluorogenic Probe for Mercury Based on Alkyne Oxymercuration." Journal of the American Chemical Society **2008**, *130*, 16460-16461.

[82] Miura, T.; Urano, Y.; Tanaka, K.; Nagano, T.; Ohkubo, K.; Fukuzumi, S. "Rational design principle for modulating fluorescence properties of fluorescein-based probes by photoinduced electron transfer." Journal of the American Chemical Society **2003**, *125*, 8666-8671.

[83] Li, C.; Tang, J.; Xie, J. "Synthesis of crosslinking amino acids by click chemistry." Tetrahedron **2009**, *65*, 7935-7941.

[84] Grabolle, M.; Spieles, M.; Lesnyak, V.; Gaponik, N.; Eychemuller, A.; Resch-Genger, U. "Determination of the Fluorescence Quantum Yield of Quantum Dots: Suitable Procedures and Achievable Uncertainties." Analytical Chemistry **2009**, *81*, 6285-6294.

[85] Avirah, R. R.; Jyothish, K.; Ramaiah, D. "Dual-mode semisquaraine-based sensor for selective detection of Hg^{2+} in a micellar medium." Organic Letters **2007**, *9*, 121-124.

[86] Avirah, R. R. "Synthesis and Study of Photophysical And Metal Ion Binding Properties of a Few Novel Semisquaraine and Croconaine Dyes." Cochin University of Science and Technology, **2010**.

[87] Ruan, Y. B.; Xie, J. "Unexpected highly selective fluorescence 'turn-on' and ratiometric detection of Hg^{2+} based on fluorescein platform." Tetrahedron **2011**, *67*, 8717-8723.

[88] Kuo, Y. M.; Zhou, B.; Cosco, D.; Gitschier, J. "The copper transporter *CTR1* provides an essential function in mammalian embryonic development." Proceedings of the National Academy of Sciences of the United States of America **2001**, *98*, 6836-6841.

[89] Que, E. L.; Domaille, D. W.; Chang, C. J. "Metals in neurobiology: Probing their chemistry and biology with molecular imaging." Chemical Reviews **2008**, *108*, 4328-4328.

[90] Drago, D.; Bolognin, S.; Zatta, P. "Role of Metal Ions in the A beta Oligomerization in Alzheimer's Disease and in Other Neurological Disorders." Current Alzheimer Research **2008**, *5*, 500-507.

[91] Torrado, A.; Walkup, G. K.; Imperiali, B. "Exploiting polypeptide motifs for the design of selective Cu(II) ion chemosensors." Journal of the American Chemical Society **1998**, *120*, 609-610.

[92] Zheng, Y. J.; Gattas-Asfura, K. M.; Konka, V.; Leblanc, R. M. "A dansylated peptide for the selective detection of copper ions." Chemical Communications **2002**, 2350-2351.

[93] Boiocchi, M.; Fabbrizzi, L.; Licchelli, M.; Sacchi, D.; Vazquez, M.; Zampa, C. "A two-channel molecular dosimeter for the optical detection of copper(II)." Chemical Communications **2003**, 1812-1813.

[94] Tang, B.; Niu, J. Y.; Yu, C. G.; Zhuo, L. H.; Ge, J. C. "Highly luminescent water-soluble CdTe nanowires as fluorescent probe to detect copper(II)." Chemical Communications **2005**, 4184-4186.

[95] Xie, J.; Menand, M.; Maisonneuve, P.; Metivier, R. "Synthesis of bispyrenyl sugar-aza-crown ethers as new fluorescent molecular sensors for Cu(II)." Journal of Organic

Chemistry **2007**, *72*, 5980-5985.

[96]Zheng, Y. J.; Huo, Q.; Kele, P.; Andreopoulos, F. M.; Pham, S. M.; Leblanc, R. M. "A new fluorescent chemosensor for copper ions based on tripeptide glycyl-histidyl-lysine (GHK)." *Organic Letters* **2001**, *3*, 3277-3280.

[97]Jung, H. S.; Kwon, P. S.; Lee, J. W.; Kim, J. I.; Hong, C. S.; Kim, J. W.; Yan, S. H.; Lee, J. Y.; Lee, J. H.; Joo, T.; Kim, J. S. "Coumarin-Derived Cu^{2+} -Selective Fluorescence Sensor: Synthesis, Mechanisms, and Applications in Living Cells." *Journal of the American Chemical Society* **2009**, *131*, 2008-2012.

[98]Xu, Z. C.; Yoon, J.; Spring, D. R. "A selective and ratiometric Cu^{2+} fluorescent probe based on naphthalimide excimer-monomer switching." *Chemical Communications* **2010**, *46*, 2563-2565.

[99]Lu, H.; Xue, Z. L.; Mack, J.; Shen, Z.; You, X. Z.; Kobayashi, N. "Specific Cu^{2+} -induced J-aggregation and Hg^{2+} -induced fluorescence enhancement based on BODIPY." *Chemical Communications* **2010**, *46*, 3565-3567.

[100] Martinez, R.; Zapata, F.; Caballero, A.; Espinosa, A.; Tarraga, A.; Molina, P. "2-aza-1,3-butadiene derivatives featuring an anthracene or pyrene unit: Highly selective colorimetric and fluorescent signaling of Cu^{2+} cation." *Organic Letters* **2006**, *8*, 3235-3238.

[101] Kim, H. J.; Park, S. Y.; Yoon, S.; Kim, J. S. "FRET-derived ratiometric fluorescence sensor for Cu^{2+} ." *Tetrahedron* **2008**, *64*, 1294-1300.

[102] Kovacs, J.; Rodler, T.; Mokhir, A. "Chemodosimeter for Cu-II detection based on cyclic peptide nucleic acids." *Angewandte Chemie-International Edition* **2006**, *45*, 7815-7817.

[103]Qi, X.; Jun, E. J.; Xu, L.; Kim, S. J.; Hong, J. S. J.; Yoon, Y. J.; Yoon, J. Y. "New BODIPY derivatives as OFF-ON fluorescent chemosensor and fluorescent chemodosimeter for Cu^{2+} : Cooperative selectivity enhancement toward Cu^{2+} ." *Journal of Organic Chemistry* **2006**, *71*, 2881-2884.

[104]Kim, M. H.; Jang, H. H.; Yi, S.; Chang, S. K.; Han, M. S. "Coumarin-derivative-based off-on catalytic chemodosimeter for Cu^{2+} ions." *Chemical Communications* **2009**, 4838-4840.

[105]Li, N.; Xiang, Y.; Tong, A. J. "Highly sensitive and selective "turn-on" fluorescent chemodosimeter for Cu^{2+} in water via Cu^{2+} -promoted hydrolysis of lactone moiety in coumarin." *Chemical Communications* **2010**, *46*, 3363-3365.

[106]Lin, W. Y.; Yuan, L.; Tan, W.; Feng, J. B.; Long, L. L. "Construction of Fluorescent Probes Via Protection/Deprotection of Functional Groups: A Ratiometric Fluorescent Probe for Cu^{2+} ." *Chemistry-a European Journal* **2009**, *15*, 1030-1035.

[107]Li, A. F.; He, H.; Ruan, Y. B.; Wen, Z. C.; Zhao, J. S.; Jiang, Q. J.; Jiang, Y. B. "Oxidative cyclization of N-acylhydrazones. Development of highly selective turn-on fluorescent chemodosimeters for Cu^{2+} ." *Organic & Biomolecular Chemistry* **2009**, *7*, 193-200.

[108]Duong, T. Q.; Kim, J. S. "Fluoro- and Chromogenic Chemodosimeters for Heavy Metal Ion Detection in Solution and Biospecimens." *Chemical Reviews* **2010**, *110*, 6280-6301.

[109]Kim, H. N.; Lee, M. H.; Kim, H. J.; Kim, J. S.; Yoon, J. "A new trend in rhodamine-based chemosensors: application of spirolactam ring-opening to sensing ions." *Chemical Society Reviews* **2008**, *37*, 1465-1472.

[110]Zhou, Y.; Wang, S. X.; Zhang, K.; Jiang, X. Y. "Visual detection of copper(II) by azide-

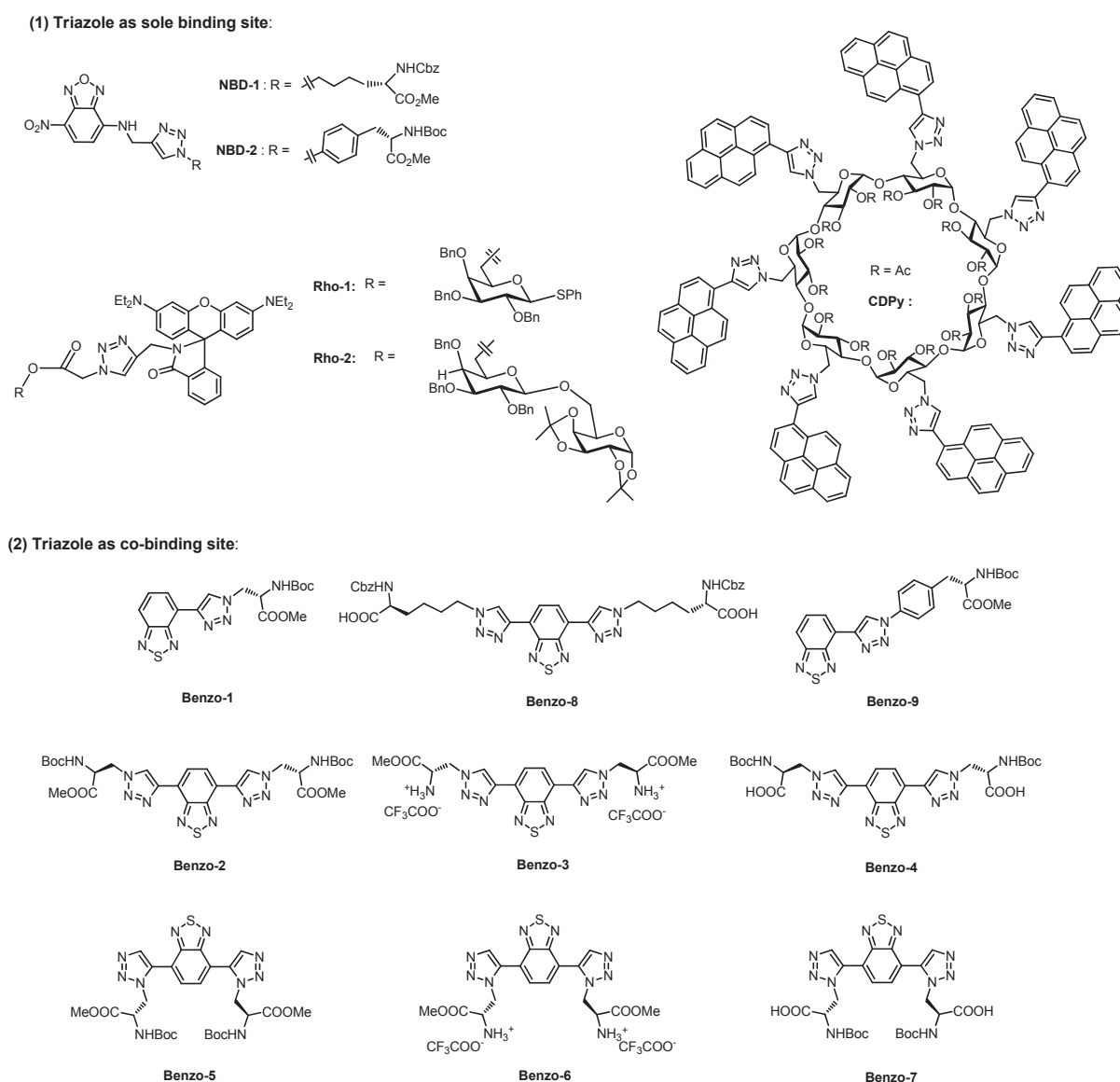
- and alkyne-functionalized gold nanoparticles using click chemistry.*" Angewandte Chemie-International Edition **2008**, *47*, 7454-7456.
- [111]Liu, J.; Lu, Y. "Colorimetric Cu^{2+} detection with a ligation DNzyme and nanoparticles." Chemical Communications **2007**, 4872-4874.
- [112]Xu, X. Y.; Daniel, W. L.; Wei, W.; Mirkin, C. A. "Colorimetric Cu^{2+} Detection Using DNA-Modified Gold-Nanoparticle Aggregates as Probes and Click Chemistry." Small **2010**, *6*, 623-626.
- [113]Brillas, E.; Sires, I.; Oturan, M. A. "Electro-Fenton Process and Related Electrochemical Technologies Based on Fenton's Reaction Chemistry." Chemical Reviews **2009**, *109*, 6570-6631.
- [114]Rivas, F. J.; Beltran, F. J.; Gimeno, O.; Frades, J. "Treatment of olive oil mill wastewater by Fenton's reagent." Journal of Agricultural and Food Chemistry **2001**, *49*, 1873-1880.
- [115]Valko, M.; Morris, H.; Cronin, M. T. D. "Metals, toxicity and oxidative stress." Current Medicinal Chemistry **2005**, *12*, 1161-1208.
- [116]Shinar, E.; Navok, T.; Chevion, M. "The Analogous Mechanisms of Enzymatic Inactivation Induced by Ascorbate and Superoxide in the Presence of Copper." Journal of Biological Chemistry **1983**, *258*, 4778-4783.
- [117]Tang, S. S.; Lin, C. C.; Chang, G. G. "Metal-catalyzed oxidation and cleavage of octopus glutathione transferase by the Cu(II)-ascorbate system." Free Radical Biology and Medicine **1996**, *21*, 955-964.
- [118]Sang, Y.; Zhang, L.; Li, Y. F.; Chen, L. Q.; Xu, J. L.; Huang, C. Z. "A visual detection of hydrogen peroxide on the basis of Fenton reaction with gold nanoparticles." Analytica Chimica Acta **2010**, *659*, 224-228.
- [119]Wang, Y.; Yang, F.; Yang, X. R. "Label-free colorimetric biosensing of copper(II) ions with unimolecular self-cleaving deoxyribozymes and unmodified gold nanoparticle probes." Nanotechnology **2010**, *21*, 205502.
- [120]Li, C.; Henry, E.; Mani, N. K.; Tang, J.; Brochon, J. C.; Deprez, E.; Xie, J. "Click Chemistry to Fluorescent Amino Esters: Synthesis and Spectroscopic Studies." European Journal of Organic Chemistry **2010**, 2395-2405.
- [121]Song, A. M.; Zhang, J. H.; Zhang, M. H.; Shen, T.; Tang, J. A. "Spectral properties and structure of fluorescein and its alkyl derivatives in micelles." Colloids and Surfaces a-Physicochemical and Engineering Aspects **2000**, *167*, 253-262.
- [122]Liu, J.; Lu, Y. "Rational design of "Turn-On" allosteric DNzyme catalytic beacons for aqueous mercury ions with ultrahigh sensitivity and selectivity." Angewandte Chemie-International Edition **2007**, *46*, 7587-7590.
- [123]Huang, C. C.; Chang, H. T. "Selective gold-nanoparticle-based "turn-on" fluorescent sensors for detection of mercury(II) in aqueous solution." Analytical Chemistry **2006**, *78*, 8332-8338.
- [124]Wang, Q. L.; Zhang, H.; Jiang, Y. B. "A highly selective and sensitive turn-on catalytic chemodosimeter for Cu^{2+} in aqueous solution." Tetrahedron Letters **2009**, *50*, 29-31.
- [125]Ruan, Y. B.; Li, C.; Tang, J.; Xie, J. "Highly sensitive naked-eye and fluorescence "turn-on" detection of Cu^{2+} using Fenton reaction assisted signal amplification." Chemical Communications **2010**, *46*, 9220-9222.

Chapter 3. Clickable Fluorescent Chemosensors for Detection of Heavy Metal Ions: Triazoles as Binding Sites



3.1. Introduction of click triazole as ionophores

In the second chapter, we have developed fluorescent chemosensors for selective detection of Hg^{2+} and $\text{Cu}^{2+}/\text{Cu}^+$ by using triazole moiety as a linker. As presented in the introduction of Chapter 2, flexible coordination chemistry of triazole moiety makes it become a common binding site in fluorescent chemosensors. In this chapter, we intend to elucidate the roles of triazole as the binding sites through a series of click fluorophores, as shown in Scheme 3-1.



Scheme 3-1. Triazole-based new fluoroionophores studied in this chapter.

3.2. NBD-Triazole based Hg²⁺ chemosensor

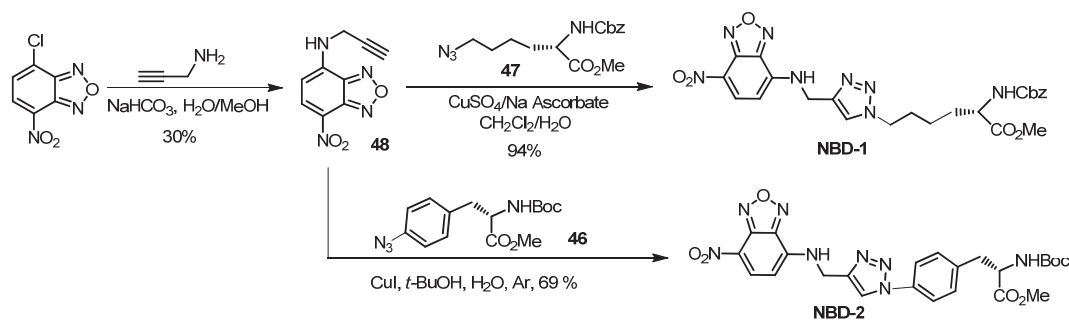
3.2.1. Introduction

Contamination of mercury is a worldwide concern for decades due to its extreme toxicity, causing adverse effects on human health. Accumulation of mercury in vital organs and tissues may cause serious damages to the central nervous and endocrine systems.¹ Sophisticated techniques such as AAS (atomic absorption spectroscopy), AES (atomic emission spectroscopy), ICP-MS (inductively coupled plasma mass spectroscopy) have been widely used to detect Hg²⁺ in real samples. However, most of them require complicated sample preparation processes and expensive instrumentation, making them unsuitable for the real time and on site analysis. Due to the intrinsic characteristics of the fluorescence technique, it shows great advantages in simplification of the instrument, high sensitivity and biological imaging in *vitro* and *vivo* samples. In recent years, considerable efforts have been dedicated to pursuing some excellent chemosensors with high sensitivity and selectivity for detection of Hg²⁺ in real samples.² To date, several approaches mainly based on organic fluorophores,³ DNzyme,^{4,5} nanoparticles,^{6,7} protein^{8,9} and conjugated polymers^{10,11} have been well developed. However, development of facile and practical chemosensors for Hg²⁺ is still a great challenge. Besides considering the performance of the probes in terms of sensitivity and selectivity, the simplicity of the organic synthesis is another important factor in order to realize the applications in real samples. Modular synthesis like click reaction under mild condition, high reaction yields is then highly favorable.

NBD derivatives as one of the most commonly used fluorescent labeling reagents exhibit several great advantages such as their good spectral properties and cell permeability.¹² To date, chemosensors based on NBD have been reported for the detection of various transition metal ions by virtue of ICT (intramolecular charge transfer) and PET (photo-induced electron transfer) processes.^{13,14,15,16,17} On continuing the program of developing chemosensors for metal ions based on triazole, **NBD-1** and **NBD-2** with NBD as signaling reporter and triazole as binding moiety were used as double-channel fluorescent and colorimetric sensors for the detection of Hg²⁺ in EtOH/H₂O mixed solutions. Meanwhile different terminal amino acid groups were integrated to investigate structure-dependent sensitivity.

3.2.2. Synthesis of NBD-1 and NBD-2 (Synthesized by Chun Li)

As shown in Scheme 3-2, NBD-Cl was treated with propargylamine under basic condition to afford propargyl-NBD **48**, followed by click reaction with azido lysine or phenylalanine derivatives **47** and **46** to give the corresponding **NBD-1** and **NBD-2**.¹⁸



Scheme 3-2. Synthesis of **NBD-1** and **NBD-2**.

3.2.3. Photophysical properties of **NBD-1**

All the related photophysical parameters of **NBD-1** in ethanol are collected in Table 3-1. **NBD-1** exhibits a strong absorption band centered at 456 nm with a large extinction coefficient ($\epsilon = 19858 \text{ L} \cdot \text{mol}^{-1} \cdot \text{cm}^{-1}$) and a broad emission band peaked at 534 nm. As shown in Figure 3-1 (a), a continuous red shift of the absorption band is observed with increasing polarity of solvents, from 447 nm in chloroform to 472 nm in DMSO. Fluorescence spectra of **NBD-1** show the similar solvent-dependent behavior, with a red shift from 523 nm in chloroform to 544 nm in DMSO. It's therefore judging from characteristic of solvatochromism that the absorption and emission band of **NBD-1** can be assigned to ICT process from electron-donating amine group to electron-withdrawing nitro group, which is corresponding to the broad structureless feature of the band. Moreover, **NBD-1** shows high quantum yield up to 0.44 in ethanol which is quite different from the reported NBD derivatives with aminoethyl group directly linked to 4-*N* of NBD fluorophore.¹⁴ This can be explained by the transformation of nitrogen hybridization form from sp^3 of amino group into sp^2 in triazole, which reduces the availability of the lone electron pair on nitrogen atom and suppresses the PET process and restore its emissive state. Fluorescence time decay of **NBD-1** was also determined in EtOH. It consists of a long-lived major component (7.37 ns, 90%) and a short-lived minor component (2.9 ns, 10%). This illustrates that emission of **NBD-1** mainly arises from ICT process and short-lived component could be resulted from relatively weak PET from triazole ring to NBD fluorophore.¹⁴ The *stokes shift* of **NBD-1** with 78 nm is appreciated to avoid the overlap between the absorption and emission band and reduce the reabsorption process.

Compound	Solvent	λ_{\max}^A	λ_{\max}^F	$\Delta\lambda_{F-A}$	ϵ_{00}	Φ_F	τ
		[nm]	[nm]	[nm]	[L.mol ⁻¹ .cm ⁻¹]		ns
1	EtOH	456	534	78	1.98×10^4	0.44	7.37, 2.90
2	EtOH	456	534	78	1.85×10^4	0.46	-

Table 3-1. Photophysical data of **NBD-1** and **NBD-2** in EtOH, quantum yields were determined using coumarine 153 as reference.

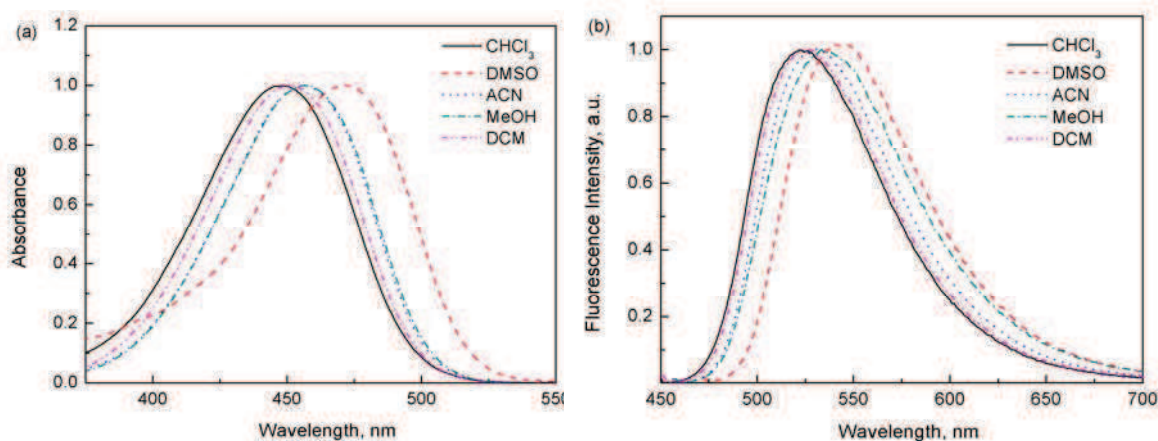


Figure 3-1. Normalized absorption (a) and fluorescence (b) spectra of **NBD-1** in various solvents including CHCl_3 , DMSO, MeCN, MeOH and DCM; excitation wavelengths corresponding to the peaks of absorption band in different solvents, $[\text{NBD-1}] = 10 \mu\text{M}$.

3.2.4. Complexation properties of **NBD-1**

As shown in Scheme 3-2, **NBD-1** contains several nitrogen atoms which are suitable as the binding sites for soft metal ions. Moreover, it's worthy of notice that nitrogen atoms from NBD moiety and triazole ring seem to construct a binding pocket for a specific metal. Considering these factors and the reported flexible coordination chemistry of triazole, an investigation of fluorescence response of **NBD-1** to a series of metal ions such as Ag^+ , Ba^{2+} , Ca^{2+} , Cd^{2+} , Co^{2+} , Cu^{2+} , Fe^{2+} , Hg^{2+} , Mn^{2+} , Mg^{2+} , Ni^{2+} , Pb^{2+} and Zn^{2+} was carried out in ethanol. As shown in Figure 3-2, fluorescence intensity of **NBD-1** is quenched by Ag^+ , Co^{2+} , Ni^{2+} and Hg^{2+} to different extents, following the order $\text{Hg}^{2+} > \text{Ag}^+ > \text{Co}^{2+} > \text{Ni}^{2+}$. Especially for Hg^{2+} , its quenching efficiency was up to 80% and a remarkable red shift by 40 nm was observed. Other metal ions like alkaline earth metals showed almost no influence.

It is reported that selectivity of triazole-containing fluorescent chemosensors sometimes is closely related to solvents medium and meanwhile considering the practical application of chemosensors, the selectivity of **NBD-1** to different metal ions was further examined in

EtOH/HEPES (v/v = 9:1) at pH 7.4. As displayed in Figure 3-3, the selectivity is greatly improved and only Hg^{2+} shows remarkable quenching effect while others exert almost no influence even in large excess. This high selectivity was further confirmed through the following competition experiments. As shown in Figure 3-4, in the presence of 5 equiv of competing metal ions, Fe^{2+} and Pb^{2+} do produce a little interference while other ions show almost no influence on the binding process of **NBD-1** to Hg^{2+} , demonstrating the high selectivity of this approach for the detection of Hg^{2+} . However, sensitivity of **NBD-1** to Hg^{2+} was decreased to some extent due to the hydration of metal ions suppressing the efficient binding process.

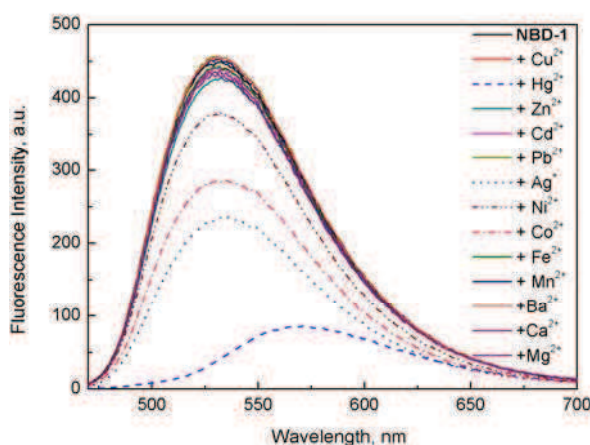


Figure 3-2. Fluorescence spectra of **NBD-1** in the presence of different kinds of metal ions in EtOH. $[\text{NBD-1}] = 10 \mu\text{M}$, $[\text{M}^{n+}] = 200 \mu\text{M}$, $\lambda_{\text{ex}} = 456 \text{ nm}$.

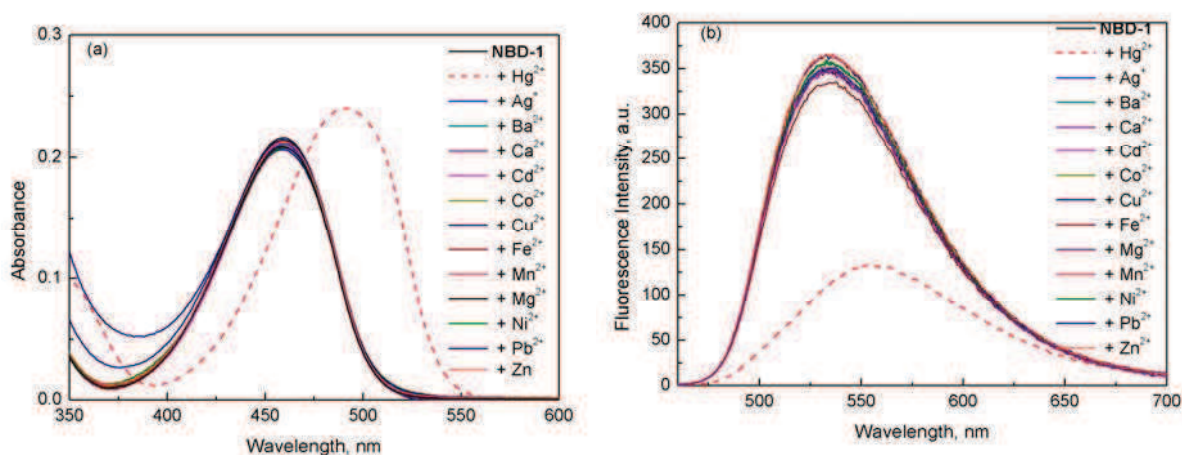


Figure 3-3. Absorption (a) and fluorescence (b) spectra of **NBD-1** in the presence of different metal ions in EtOH/HEPES (v/v = 9:1) at pH 7.4. $[\text{NBD-1}] = 10 \mu\text{M}$, $[\text{Hg}^{2+}] = 40 \mu\text{M}$, $[\text{M}^{n+}] = 200 \mu\text{M}$, $\lambda_{\text{ex}} = 456 \text{ nm}$.

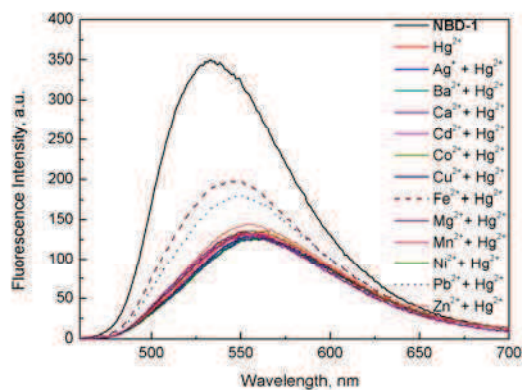


Figure 3-4. Fluorescence spectra of **NBD-1** in the coexistence of different kinds of metal ions and Hg^{2+} in EtOH/HEPES (v/v = 9:1). $[\text{NBD-1}] = 10 \mu\text{M}$, $[\text{M}^{n+}] = 200 \mu\text{M}$, $[\text{Hg}^{2+}] = 40 \mu\text{M}$, $\lambda_{\text{ex}} = 456 \text{ nm}$.

Figure 3-5 shows the gradual evolution of absorption spectra of **NBD-1** upon complexation with Hg^{2+} in ethanol. With increasing $[\text{Hg}^{2+}]$, its absorbance at 455 nm decreases while a new band appears at 493 nm. The red shift of the absorption band from 455 nm to 493 nm led to the solution color changing from light yellow to light orange, facilitating the possibility of naked eyed detection of Hg^{2+} . Three clear isosbestic points are observed at 467, 381 and 329 nm, indicating the interconversion of bound complex and free ligand. Job's plot experiment, also known as the method of continuous variation, was carried out to determine the binding stoichiometry between Hg^{2+} and **NBD-1**. It shows a maximum at 0.5, suggesting resultant complex with 1:1 binding stoichiometry (Figure 3-6). Nonlinear regression analysis of the absorption titration based on the 1:1 binding ratio, giving a large association constant for Hg^{2+} up to $3.23 \times 10^6 \text{ M}^{-1}$ in the ground state.

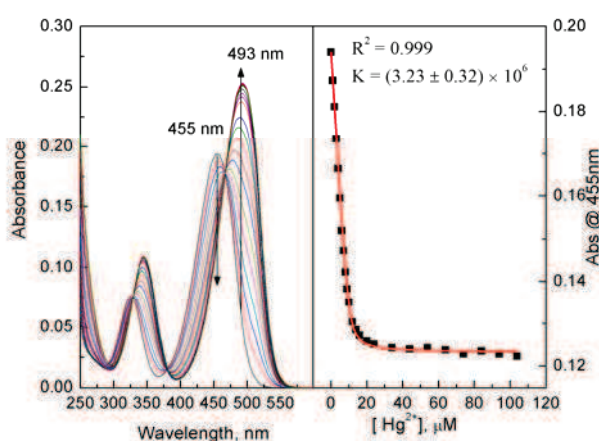


Figure 3-5. Absorption spectra of **NBD-1** in the presence of varying concentrations of Hg^{2+} in ethanol and plot of absorbance of **NBD-1** at 455 nm as the function of $[\text{Hg}^{2+}]$, $[\text{NBD-1}] = 10 \mu\text{M}$.

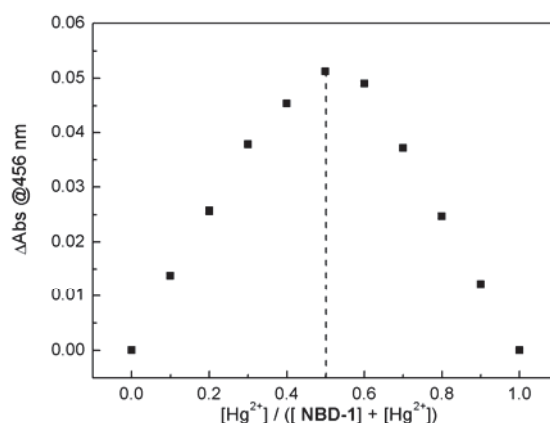


Figure 3-6. Job plot for **NBD-1** - Hg^{2+} . The total concentration of $[\text{Hg}^{2+}]$ and $[\text{NBD-1}]$ is 20 μM .

As shown in Figure 3-7, fluorescence titration was also performed under the identical conditions in ethanol. Fluorescence quenching of **NBD-1** at 533 nm is observed with increasing $[\text{Hg}^{2+}]$, with about 50% quenched in the presence of 10 μM Hg^{2+} and reaches a plateau when $[\text{Hg}^{2+}]$ exceeds 20 μM , concomitantly with a red shift from 531 to 573 nm. Fluorescence titration was also analyzed by nonlinear regression based on 1:1 binding ratio to give us the binding constant in the excited state to be $3.97 \times 10^6 \text{ M}^{-1}$, which is almost the same as that of ground state.

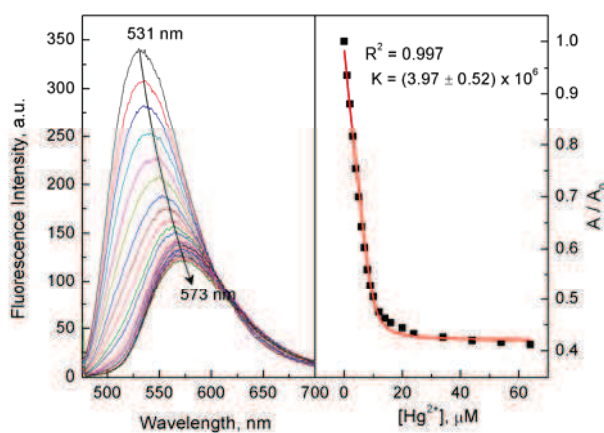


Figure 3-7. Fluorescence spectra of **NBD-1** in the presence of varying concentrations of Hg^{2+} in ethanol and plot of fluorescence integral area of **NBD-1** as the function of $[\text{Hg}^{2+}]$; $[\text{NBD-1}] = 10 \mu\text{M}$, $\lambda_{\text{ex}} = 476 \text{ nm}$.

Before examining the pH effect on the binding process of **NBD-1** to Hg^{2+} , the effect of water content was first tested. As shown in Figure 3-8, with increasing water content, variation of the fluorescence intensity after the addition of Hg^{2+} to **NBD-1** solution decreases dramatically and almost no response is observed when the water content reach 50%. This may be attributed to the strong hydration of Hg^{2+} which suppresses it binding to **NBD-1**. To obtain

an optimal sensing sensitivity, the following investigations were performed in EtOH/H₂O (v/v = 9:1).

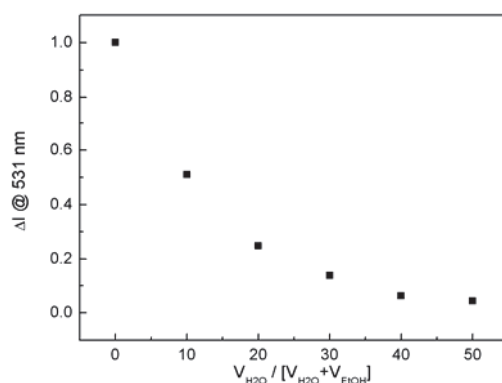


Figure 3-8. Fluorescence variation of **NBD-1** after the addition of Hg^{2+} in EtOH/H₂O mixed solutions, $[\text{NBD-1}] = 10 \mu\text{M}$, $[\text{Hg}^{2+}] = 20 \mu\text{M}$, excited at the absorption maximum wavelength.

The pH effect on the binding process of **NBD-1** to Hg^{2+} was tested in EtOH/HEPES (v/v = 9:1). As presented in Figure 3-9, when the solution pH is lower than 7.4, the variation of fluorescence intensity before and after addition of 4 equiv of Hg^{2+} increases with pH, indicating that decreasing pH suppresses the coordination interaction between **NBD-1** and Hg^{2+} . **NBD-1** works well and shows the maximum fluorescence quenching under neutral or weak basic conditions. In view of the practical application of chemosensors, titration of Hg^{2+} was further carried out in EtOH/HEPES (v/v = 9:1) at physiological pH 7.4. As depicted in Figure 3-10 and Figure 3-11, both absorption and fluorescence titrations show the similar spectral behavior to that in EtOH. Nonlinear regression analysis shows that the stability constants are moderately reduced about one order of magnitude, which may be due to the conformational change and ionic solvation effect. The detection limit of this approach was calculated according to the following equation (eq. 3-1)

$$s = \sqrt{\frac{\sum (x_i - \bar{x})^2}{n-1}}, \quad c_{\text{limit}} = \frac{3s}{k} \quad (\text{eq. 3-1})$$

Where s is standard deviation of **NBD-1** solution without addition of Hg^{2+} , c_{limit} the limit of detection and k is the slope of the working curve. A detection limit of 610 nM could be obtained for analyzing Hg^{2+} under the above conditions.

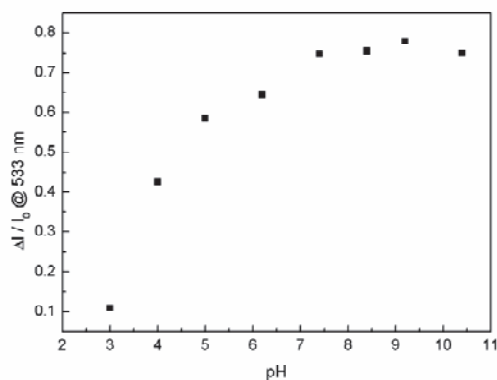


Figure 3-9. Variation of fluorescence intensity of **NBD-1** at 533 nm after the addition of Hg^{2+} in EtOH/HEPES (v/v = 9:1) under different pH conditions. $[\text{NBD-1}] = 10 \mu\text{M}$, $[\text{Hg}^{2+}] = 40 \mu\text{M}$, $\lambda_{\text{ex}} = 459 \text{ nm}$, incubated time: 7 min and I indicate fluorescence intensity at 533 nm.

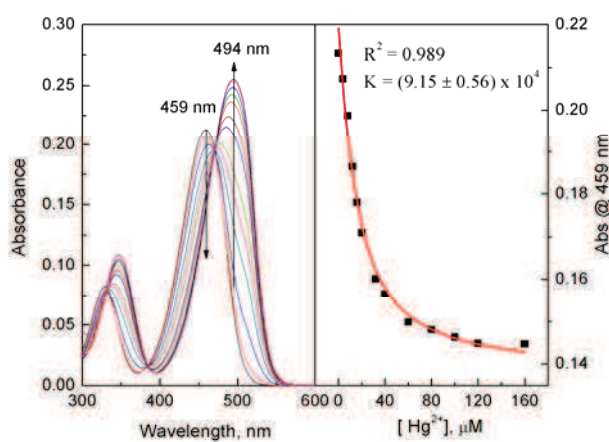


Figure 3-10. Absorption spectra of **NBD-1** in the presence of varying concentrations of Hg^{2+} in EtOH/HEPES (v/v = 9:1) and plot of absorbance of **NBD-1** at 459 nm as the function of $[\text{Hg}^{2+}]$; $[\text{NBD-1}] = 10 \mu\text{M}$.

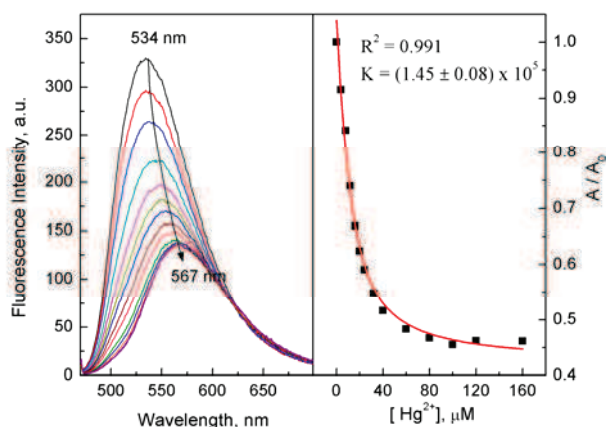


Figure 3-11. Fluorescence spectra of **NBD-1** in the presence of varying concentrations of Hg^{2+} in EtOH/HEPES (v/v = 9:1) and plot of fluorescence integral area of **NBD-1** as the function of $[\text{Hg}^{2+}]$; $[\text{NBD-1}] = 10 \mu\text{M}$, $\lambda_{\text{ex}} = 470 \text{ nm}$.

Reversibility is another important parameter of chemosensors in practical applications. The reversibility of the binding process of **NBD-1** to Hg^{2+} could be easily realized by adding I^- as Hg^{2+} binding agent. As shown in Figure 3-12, addition of I^- results in complete fluorescence recovery. Such reversibility and regeneration are quite important to the fabrication of devices to detect Hg^{2+} .

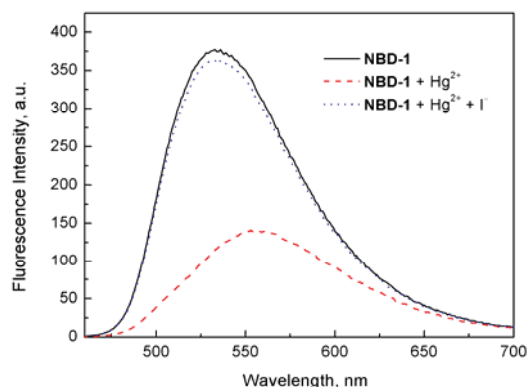


Figure 3-12. Fluorescence spectra of **NBD-1** in the presence of Hg^{2+} and then addition of I^- in EtOH/HEPES (v/v = 9:1), [**NBD-1**] = 10 μM , [Hg^{2+}] = 40 μM , [I^-] = 80 μM , λ_{ex} = 456 nm.

The remarkable wavelength red shift both in the absorption and fluorescence spectra in the presence of Hg^{2+} inspired us to explore the selective naked-eye detection of Hg^{2+} . As shown in Figure 3-13, among the tested metal ions, only Hg^{2+} induces a color change from light yellow to light orange (Figure 3-13a), and when excited under hand-UV lamp at 365 nm, fluorescence of **NBD-1** shows a color change from green to yellow (Figure 3-13b). Furthermore, even in the coexistence of 20 equiv of other metal ions, only small influence has been detected with Fe^{2+} and Pb^{2+} (Figure 3-13c,d). Still, it is very easy to distinguish the color of the solution **NBD-1** in the presence of Hg^{2+} from the other metal ions, demonstrating its great potential in the real and on-site detection.

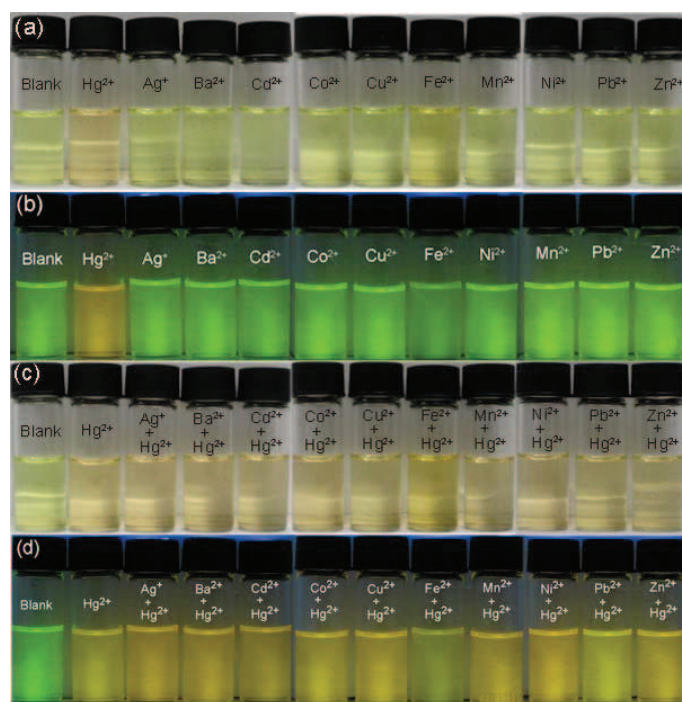


Figure 3-13. Photographs of **NBD-1** in the presence of different metal cations (a) color, (b) fluorescence and coexistence of different kinds of metal ions and Hg²⁺ (c) color, (d) fluorescence in EtOH/HEPES (v/v = 9:1). [NBD-1] = 10 μM, [Hg²⁺] = 40 μM, [Mⁿ⁺] = 200 μM, illuminated under 365 nm.

3.2.5. Binding mode of NBD-1 to Hg²⁺

It's possible that the flexible extended alkyl chain in **NBD-1** may bend back which makes the terminal amino acid moiety participate to the binding process with Hg²⁺. In order to investigate effect of the terminal amino acid group on the binding ability towards Hg²⁺, **NBD-2** with more rigid distal amino acid group to avoid cooperative binding between triazole and amino acid moiety was then examined. As shown in Table 3-1, **NBD-2** displays almost the same photophysical properties as those of **NBD-1**, demonstrating that the terminal amino acid moiety shows no effect on the fluorescent core NBD. To get a detailed binding information, absorption and fluorescence titration **NBD-2** with Hg²⁺ were then carried out in EtOH. Similar spectral behaviors as that of **NBD-1** to Hg²⁺ such as red shift of the spectra and strong fluorescence quenching after complexation were observed (Figures 3-14 and 3-15). Job's plot experiments (Figure 3-16) in EtOH demonstrated 1:1 binding stoichiometry between **NBD-2** and Hg²⁺. However, nonlinear regression analyses of the spectral titrations based on 1:1 binding ratio show that stability constants of **NBD-2**-Hg²⁺ ($\sim 1 \times 10^5 \text{ M}^{-1}$) are about one order of magnitude lower than those of **NBD-1**, which might be explained by the participation of the flexible distal amino acid group of **NBD-1** to the complexation with Hg²⁺.

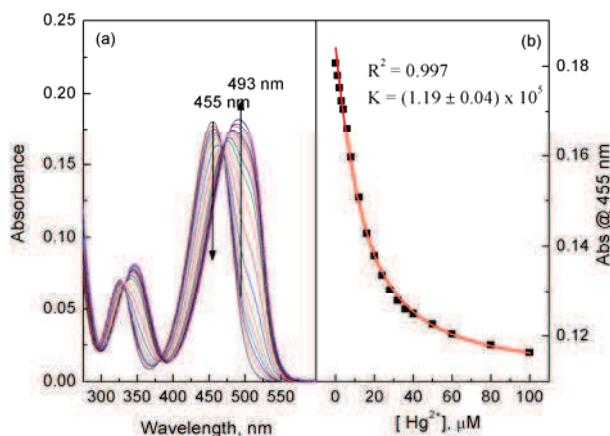


Figure 3-14. (a) Absorption spectra of **NBD-2** in the presence of varying concentrations of Hg^{2+} in ethanol and (b) plot of absorbance of **NBD-2** at 455 nm as a function of $[\text{Hg}^{2+}]$, $[\text{NBD-2}] = 10 \mu\text{M}$.

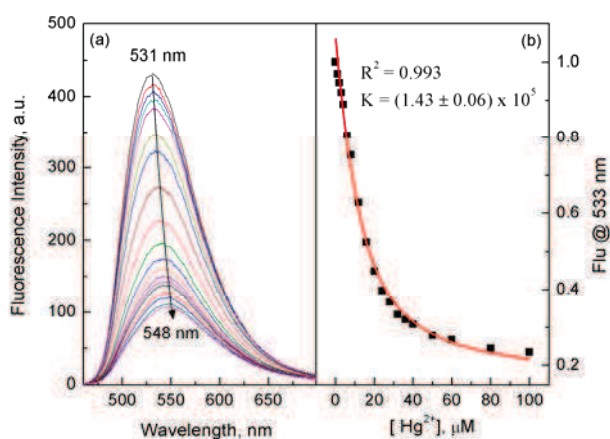


Figure 3-15. (a) Fluorescence spectra of **NBD-2** in the presence of varying concentrations of Hg^{2+} in ethanol and (b) plot of fluorescence intensity of **NBD-2** at 533 nm as the function of $[\text{Hg}^{2+}]$, $[\text{NBD-2}] = 10 \mu\text{M}$, $\lambda_{\text{ex}} = 455 \text{ nm}$.

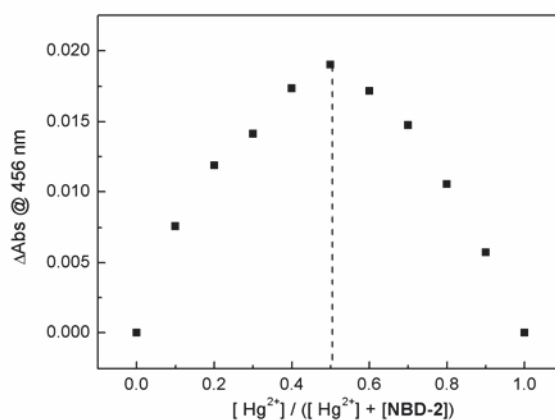


Figure 3-16. Job plot for **NBD-2**- Hg^{2+} . The total concentration of $[\text{Hg}^{2+}]$ and $[\text{NBD-2}]$ is $20 \mu\text{M}$.

To better understand the complexation mode between **NBD-1** and Hg^{2+} , ^1H NMR titration

was carried out in CD₃OD/DMSO-*d*₆ (4:1). As shown in Figure 3-17, with increasing [Hg²⁺], H_a on the triazole ring undergoes a remarkable downfield shift by 0.24 ppm from 8.01 to 8.25. Meanwhile, CH_b and CH_c linked to triazole ring shift downfield slightly. However, no chemical shift is observed for the amino acid moiety. This result demonstrates that triazole group is the main binding site for Hg²⁺. Furthermore, as shown in Figure 3-18, when the assay is performed under acidic condition like pH 3.0, about 20% fluorescence quenching is observed immediately after the addition of 20 μM Hg²⁺ and then the spectra recover partially by itself within 15 min. Since the spectral properties of **NBD-1** show no changes between pH 3.0 and 10.4 (Figure 3-19), it is postulated that NBD fluorophore could not be protonated at pH 3.0. Therefore, the self-recovery of the fluorescence might be attributed to the protonation of triazole moiety which suppresses the complexation of **NBD-1** with Hg²⁺, further confirming that triazole group participates in the complexation with Hg²⁺. However, these conclusions could not explain spectral behavior of **NBD-1** in the presence of Hg²⁺, because generally ICT process could not be affected through a non-conjugated spacer. To make a reasonable explanation on the spectral change, we suppose that the direct complexation of Hg²⁺ to the NBD fluorophore beside triazole group. 4-NH might be a good candidate: if it binds to Hg²⁺ without deprotonation, reduction of the electron density of nitrogen atom would cause blue shift of the spectra; in contrast, if the addition of Hg²⁺ induces deprotonation of 4-NH, it would affect the chemical shift of CH_d and CH_f on NBD ring. However, complexation of **NBD-1** with Hg²⁺ led to a remarkable red shift of the absorption band and no chemical shift of CH_d and CH_f was observed even in the presence of 2.0 equiv of Hg²⁺ (Figure 3-17). These results preclude 4-NH as the binding site of **NBD-1** for Hg²⁺. Samanta et al. have reported spectral response of **NAM** (4-amino-7-nitrobenzo-2-oxa-1,3-diazole) to metal ions and attributed the spectral changes to the binding of metal ions with the NBD fluorophore.¹⁴ Worthy of notice is that no spectral shift was observed for **NAM** after complexation with metal ions. These results indicated that metal coordination of oxadiazole group in NBD could not induce spectral shift. Consequently, the possibility of coordination of NBD fluorophore to Hg²⁺ could be precluded, since binding of Hg²⁺ to **NBD-1** induced spectral shift in our case (Figure 3-5). Finally, there exists another possibility that the binding of triazole moiety to solvated Hg²⁺ might increase local polarity around the NBD fluorophore which results in remarkable red shift and fluorescence quenching. Time decay of both free ligand **NBD-1** and its Hg²⁺ complex were recorded in ethanol. As presented in Figure 3-20, they both display a bi-exponential decay. For free ligand, it contains a major (91%) long lifetime component 7.4 ns and a minor (9%) component 2.9 ns; while the Hg²⁺-complex with a major (84%) component 2.5 ns and a minor (16%) component 4.4 ns. The shorten lifetime in the complex might be attributed to the increasing polarity facilitating some structural

transformation of the charge separated species. Conclusively, the binding mode of complex **NBD-1**- Hg^{2+} is proposed in Scheme 3-3.

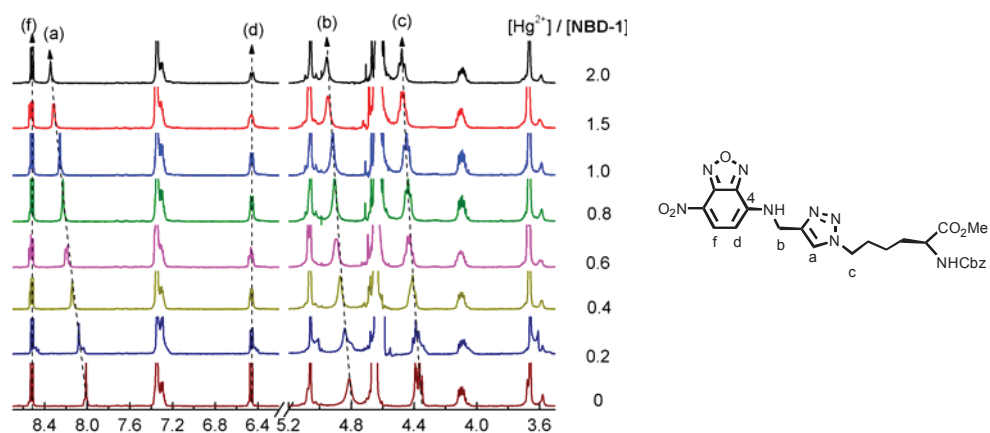


Figure 3-17. Partial ^1H NMR spectra of **NBD-1** in the presence of varying concentrations of Hg^{2+} in $\text{CD}_3\text{OD}/\text{DMSO}-d_6$ (4:1).

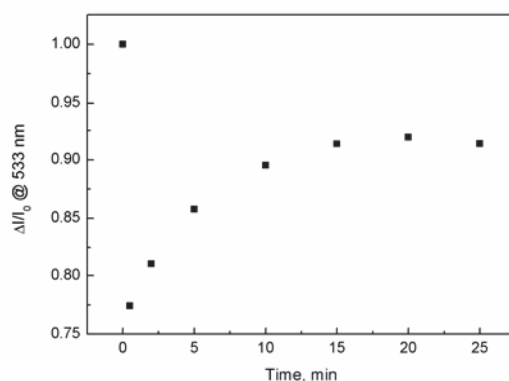


Figure 3-18. Kinetics profiles of fluorescence intensity of **NBD-1** at 533 nm after addition of Hg^{2+} in EtOH/HEPES ($v/v = 9:1$) at pH 3.0; $[\text{NBD-1}] = 10 \mu\text{M}$, $[\text{Hg}^{2+}] = 20 \mu\text{M}$, $\lambda_{\text{ex}} = 459 \text{ nm}$ and I indicate fluorescence intensity at 533 nm.

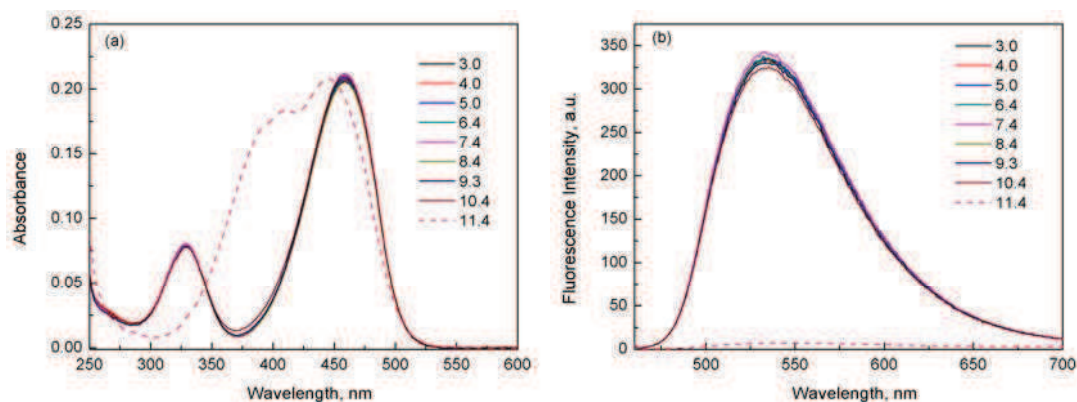


Figure 3-19. Absorption (a) and fluorescence (b) spectra of **NBD-1** in EtOH/HEPES ($v/v = 9:1$) under different pH conditions, $[\text{NBD-1}] = 10 \mu\text{M}$, $\lambda_{\text{ex}} = 459 \text{ nm}$.

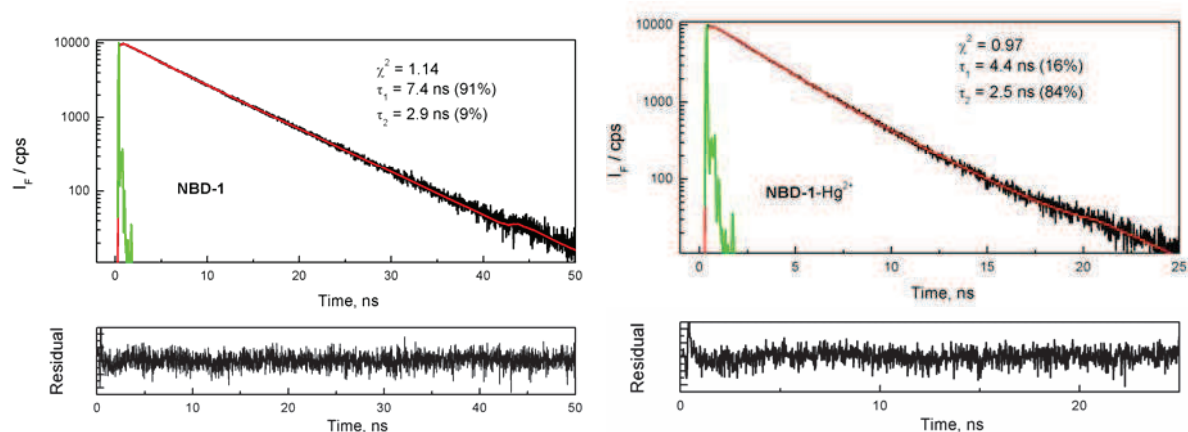
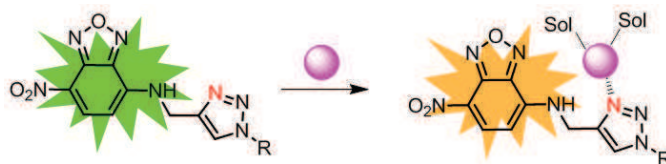


Figure 3-20. Time decay profiles of **NBD-1** and **NBD-1-Hg²⁺** in EtOH, [**NBD-1**] = 10 μ M, [**Hg²⁺**] = 20 μ M, λ_{ex} = 495 nm, λ_{em} = 533 nm for **NBD-1** and 573 nm for **NBD-1-Hg²⁺**.



Scheme 3-3. Schematic illustration of the binding mode between **NBD-1** and **Hg²⁺**.

3.2.6. Conclusion

Compound **NBD-1** with terminal Lys amino acid group linked to NBD fluorophore by triazole was successfully applied in selective recognition of **Hg²⁺** in EtOH/H₂O mixed solution at pH 7.4. After complexation with **Hg²⁺**, remarkable fluorescence quenching of **NBD-1** was observed. Meanwhile a red shift was obtained both in absorption and fluorescence spectra, which was utilized for naked-eye detection of **Hg²⁺**. Other metal ions examined show almost no influence on spectral properties of **NBD-1** in aqueous solution. Control experiments by using **NBD-2** with a more rigid distal amino acid group demonstrated the potential cooperative binding ability of amino acid group in improving the sensitivity of sensing system. Furthermore, ¹H NMR titration was performed to get insight into the complexation mode between **NBD-1** and **Hg²⁺**, which verified the role of triazole group as a binding site. The fluorescence quenching and red shift were postulated to be caused by the increase of the local polarity of the fluorophore.¹⁹

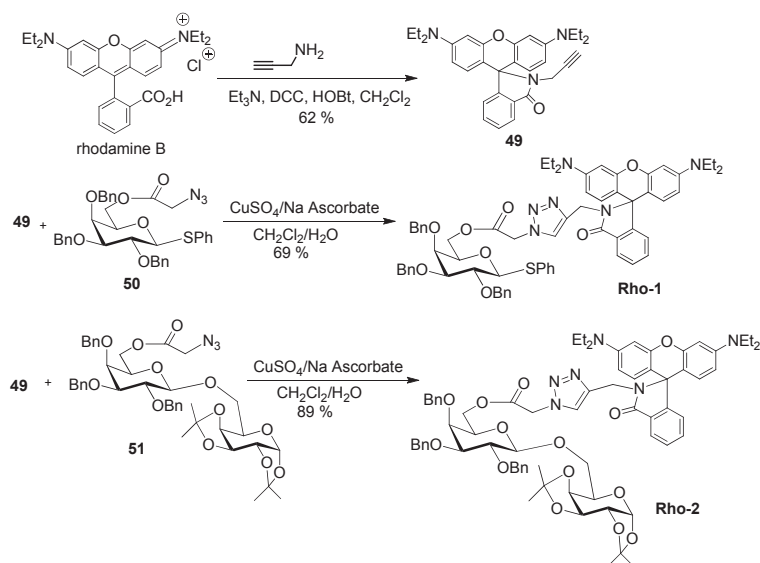
3.3. Rhodamine-Triazole based Hg^{2+} chemosensor

3.3.1. Introduction

Rhodamine derivatives have been extensively explored in detection of metal ions due to their excellent spectral properties.^{3,20} Generally, their spirolactam/spirolactone forms are non-fluorescent and colorless, whereas the corresponding ring-opening forms are strongly fluorescent and pink. Under acidic conditions, ring-opening of rhodamine spirolactone/spirolactams occur by activating the carbonyl group. Metal ions complexation involving the carbonyl group of lactone/lactam ring can induce color change and fluorescence enhancement under the similar mechanism; however, this process is somewhat solvent-dependent. Plenty of structural modifications on rhodamine especially by changing the binding sites linked to the spirolactam moiety have been made to realize the sensing applications for various important analytes. Since its first application in fluorescent chemosensors in 2007, “click” chemistry is rarely used for conjugation with rhodamine fluorophore for this purpose. As we have mentioned above in the chapter 2,^{21,22} up to now only two pieces of works have recently been reported based on the ring-opening of non-fluorescent rhodamine spirolactam for the detection of Pt^{2+} and Hg^{2+} . Further works on combination of these two moieties, with rhodamine as the reporting site and triazole as the binding site, are therefore highly desirable. In the section, we will discuss the application of rhodamine-triazole sugar derivatives for the selective detection of Hg^{2+} in MeCN.

3.3.2. Synthesis of Rho-1 and Rho-2 (synthesized by Hua Yi)

As shown in Scheme 3-4, rhodamine B was treated with propargylamine under basic condition to afford propargyl-rhodamine **49**, which subsequently reacts with sugar-azide derivatives **50** and **51** to give the corresponding **Rho-1** and **Rho-2**.²³

Scheme 3-4. Synthesis of **Rho-1** and **Rho-2**.

3.3.3. Photophysical properties of **Rho-1** and **Rho-2**

Photophysical parameters of both **Rho-1** and **Rho-2** are gathered in Table 3-2.²³ **Rho-1** and **Rho-2** exhibit strong absorption bands at 314 nm and very weak emission bands at 427 and 472 nm, respectively, arising from their spirolactame structures. No other absorption and emission bands are observed in the visible region, which provides a platform for the sensing applications with low background.

	λ_{abs} (nm)	λ_{em} (nm)	$\Delta\nu$ (cm ⁻¹)	Φ_{F}
Rho-1	314	427	8428	0.07
Rho-2	314	472	10560	0.06

Table 3-2. Photophysical data of **Rho-1** and **Rho-2** in CH₂Cl₂, quantum yields were determined using quinine sulfate as reference.

3.3.4. Complexation properties of **Rho-1** and **Rho-2**

The spectral response of **Rho-1** to different metal ions was investigated in MeCN/DMSO (v/v = 99:1). After addition of 4 equiv of metal ions, the mixed solutions were incubated at room temperature for 30 h to reach equilibrium. As shown in Figure 3-21, the presence of 40 μM Hg²⁺ leads to a remarkable absorption band at 555 nm and an emission band at 580 nm, which is consistent with the ring-opening characteristics of rhodamine spirolactam. Beside Hg²⁺, the addition of 40 μM Cu²⁺ also causes a similar spectral change to a lesser extent. While other tested metal ions showed little influence on the spectral properties of **Rho-1**. Be reminiscent of the binding mode of **NBD-1**, it's postulated that selective binding of triazole to

Hg^{2+} assisted by carbonyl group of spirolactam causes the ring-opening of **Rho-1**. More detailed investigation on the binding mode will be discussed in next section.

It's well known that the ring-opening of rhodamine spirolactone/spirolactam always displays a visible color and fluorescence change. In our assays, as shown in Figure 3-22, the presence of Hg^{2+} can result in solution color changing from colorless to pink under room light and fluorescence from dark to yellow under UV light at 365 nm. Corresponding to the spectral change, Cu^{2+} can also be detected by naked eyes though with much weak color while other solutions keep colorless, demonstrating the possibility of selective naked-eye detection of Hg^{2+} .

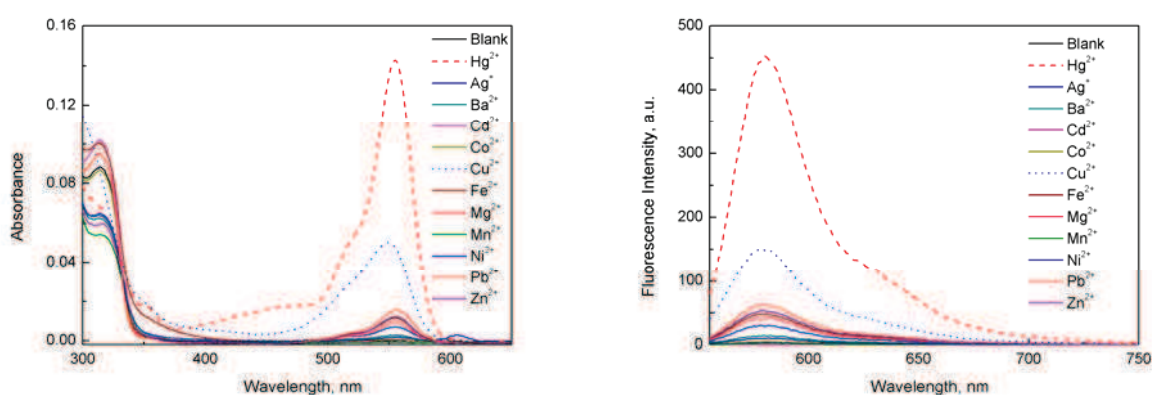


Figure 3-21. Absorption (left) and fluorescence (right) spectra of **Rho-1** in the presence of various metal ions in MeCN/DMSO (v:v = 99:1); [**Rho-1**] = 10 μM , [$\text{M}^{\text{n}+}$] = 40 μM , λ_{ex} = 555 nm and the mixtures were incubated for 30 h at *ca.* 18 $^{\circ}\text{C}$ before recording the spectra.



Figure 3-22. Color (up) and fluorescence (bottom) changes of **Rho-1** in the presence of various metal ions in MeCN/DMSO (v:v = 99:1); [**Rho-1**] = 10 μM , [$\text{M}^{\text{n}+}$] = 40 μM , λ_{ex} = 365 nm. The mixtures were incubated for 30 h at *ca.* 18 $^{\circ}\text{C}$.

Figure 3-23 depicts the kinetics profile of **Rho-1** to Hg^{2+} in MeCN/DMSO (v:v=99:1) at room temperature (*ca.* 18 $^{\circ}\text{C}$). It took about 26 h to reach the equilibrium with 10 μM **Rho-1** and 40 μM Hg^{2+} in the system. The extremely long response time is unfavourable as a

chemosensor. In order to reduce the response time of **Rho-1** to Hg^{2+} , appropriate stimulus such as light and heat can be utilized to accelerate the ring-opening reaction. Single molecule fluorescence photoswitching has been well developed during the last two decades due to their ability to address the problems in various fields.²⁴ Among the reported photochromic molecules, rhodamine derivatives are found to show photoswitching activity.^{25,26,27} Irradiated by UV light, ring-opening of spirolactam occurred and it was reversed under thermal conditions. Considering that the coordination of metal ions to carbonyl group of spirolactam ring might affect photochromic performance, we here attempt to reduce the response time by adding a UV light stimulus. Quite surprisingly, as shown in Figure 3-24, when irradiated with UV lamp at 313 nm where spirolactam **Rho-1** exhibits its maximum absorption, response time of Hg^{2+} -induced ring-opening of **Rho-1** can be dramatically reduced to 2 min. Control experiment in the absence of Hg^{2+} only showed slight increase of the fluorescence intensity at 580 nm, illustrating that UV irradiation could induce the ring-opening of rhodamine lactam and complexation with Hg^{2+} promoted this process more efficiently. It should be noted that ring-opening form of **Rho-1** in the presence of Hg^{2+} was stable in MeCN at room temperature and no reversible process could be observed even after keeping the solution of ring-opening form in the dark for hours.

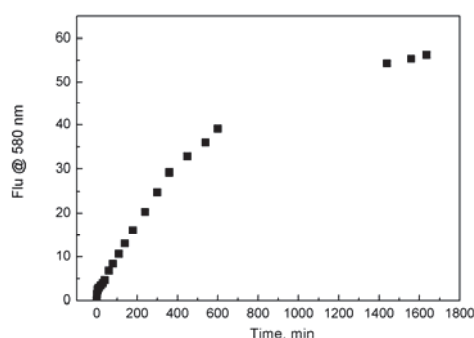


Figure 3-23. Kinetics profile of **Rho-1** in the presence of Hg^{2+} in MeCN/DMSO (v:v = 99:1) without irradiation at *ca.* 18 °C; [**Rho-1**] = 10 μM , [Hg^{2+}] = 40 μM .

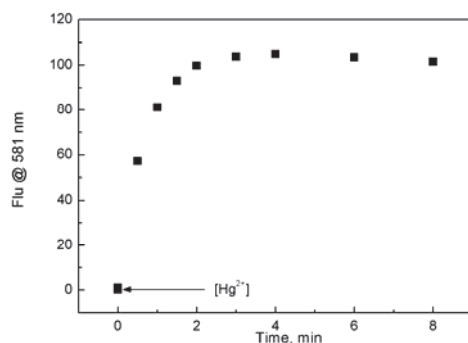


Figure 3-24. Kinetics profile of **Rho-1** in the presence of Hg^{2+} in MeCN/DMSO (v:v = 99:1) under irradiation with 313 nm light (irradiation power 33.0 mW) at *ca.* 18 °C; [**Rho-1**] = 10 μM , [Hg^{2+}] = 40 μM and λ_{ex} = 555 nm.

Selectivity of **Rho-1** to Hg^{2+} under irradiation was evaluated by screening a series of metal ions, such as Ag^+ , Ba^{2+} , Cd^{2+} , Co^{2+} , Cu^{2+} , Fe^{2+} , Mg^{2+} , Mn^{2+} , Ni^{2+} , Pb^{2+} and Zn^{2+} . As shown in Figure 3-25, in accordance with the results in the absence of irradiation, Hg^{2+} results in significant fluorescence enhancement and a new absorption band in visible region, and Cu^{2+} to a much lesser extent. **Rho-1** was still optically silent to other metal ions under this condition. Therefore, the external light stimulus did not change the binding selectivity of **Rho-1** but dramatically reduced response time of **Rho-1** to Hg^{2+} .

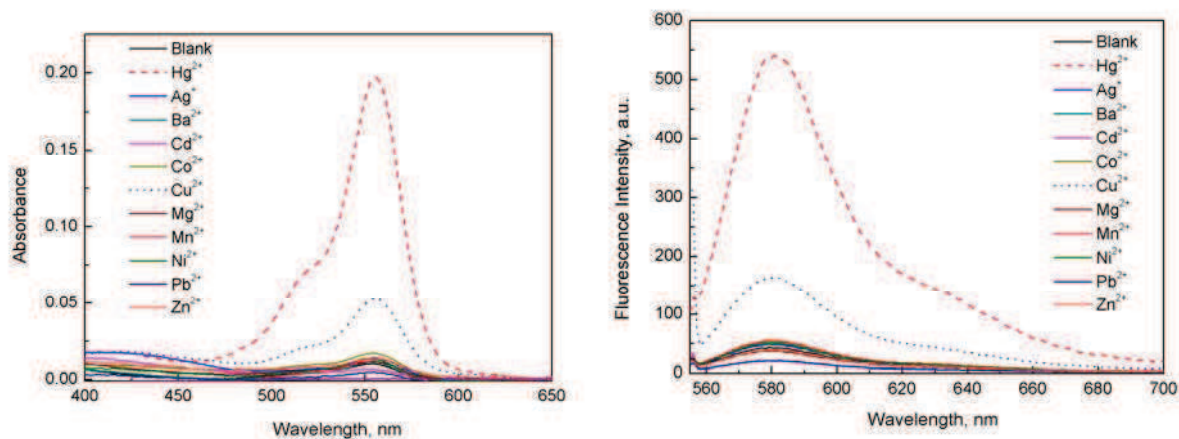


Figure 3-25. Absorption (left) and fluorescence (right) spectra of **Rho-1** in the presence of various metal ions in MeCN/DMSO (v:v = 99:1) under irradiation with 313 nm light for 2 min (irradiation power 33.0 mW) at *ca.* 18 °C; [**Rho-1**] = 10 μM , [M^{n+}] = 40 μM , λ_{ex} = 555 nm.

Fluorescence titration of **Rho-1** with Hg^{2+} under irradiation of UV light at 313 nm was performed in MeCN/DMSO (v:v=99:1). As shown in Figure 3-26, even in the absence of Hg^{2+} , **Rho-1** is already slightly transformed into ring opening amide, resulting in a weak emission at 581 nm. With increasing [Hg^{2+}], a progressive enhancement of fluorescence

intensity is clearly observed. Meanwhile the solution color changes from colorless to pink. When $[\text{Hg}^{2+}]$ exceeds $20 \mu\text{M}$, the spectra reach a plateau.

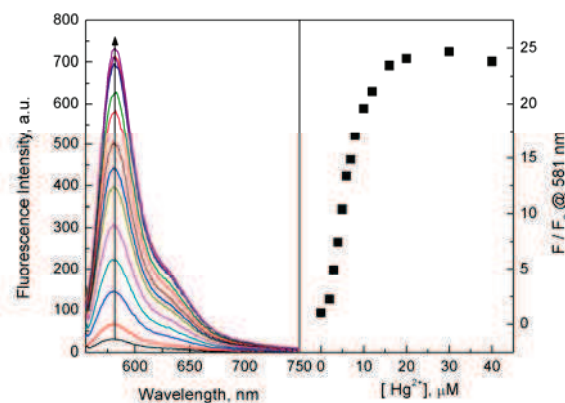


Figure 3-26. Fluorescence spectra of **Rho-1** in the presence of various concentrations of Hg^{2+} in MeCN/DMSO (v:v = 99:1) under irradiation with 313 nm light for 2 min (irradiation power 33.0 mW) at *ca.* 18 °C; $[\text{Rho-1}] = 10 \mu\text{M}$, $\lambda_{\text{ex}} = 555 \text{ nm}$.

In order to evaluate the effect of sugar moiety on the binding ability of **Rho-1** to Hg^{2+} , we further examined the spectral response of **Rho-2** to metal ions under the identical conditions. As can be seen from Table 3-2, modification on the sugar part by incorporating one more sugar unit produces little influence on the spectral properties of rhodamine spirolactam and **Rho-2** still exhibits no absorption or fluorescence bands in visible region. Under identical conditions, selectivity of **Rho-2** to metal ions under irradiation at 313 nm was examined in MeCN/DMSO (v:v = 99:1). As shown in Figure 3-27, only the addition of Hg^{2+} causes a remarkable fluorescence enhancement accompanied by solution color change from colorless to pink. Interference from Cu^{2+} still existed but to a much lesser extent and other metal ions just produced little influence. These results demonstrated that selectivity of **Rho-1** was dependent on the triazole and spirolactam moiety and almost unrelated to the sugar moiety which was far away from the binding sites. Kinetic study of **Rho-2** to Hg^{2+} under irradiation was also conducted in MeCN/DMSO (v:v = 99:1) (Figure 3-28). It reaches the equilibrium within 4 min, which is a bit slower than that of **Rho-1**. This probably can be attributed to larger steric effect of the sugar moiety in **Rho-2** than that of **Rho-1**. Fluorescence titration of **Rho-2** with Hg^{2+} was also carried out in MeCN/DMSO (v:v = 99:1). As presented in Figure 3-29, initial addition of $2 \mu\text{M}$ Hg^{2+} just results in slightly enhanced fluorescence at 580 nm. However, dramatic increment of fluorescence intensity can be observed with concentrations of Hg^{2+} ranging from 2.0 to $10.0 \mu\text{M}$ and it reaches a plateau when $[\text{Hg}^{2+}]$ exceeds $10 \mu\text{M}$. From the comparison of metallo-responsive properties of **Rho-1** and **Rho-2**, we can demonstrate that triazole group and carbonyl group play crucial roles as binding sites to Hg^{2+} ,

whereas the sugar moiety just makes a minor contribution.

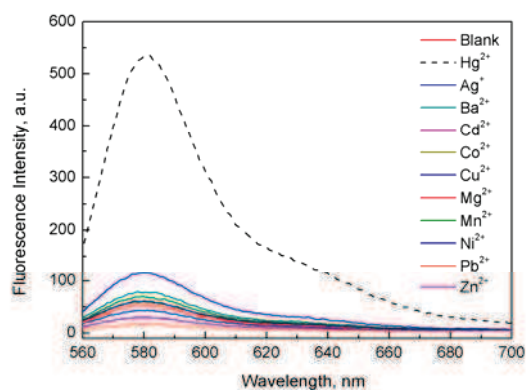


Figure 3-27. Fluorescence spectra of **Rho-2** in the presence of various metal ions in MeCN/DMSO (v:v = 99:1) under irradiation with 313 nm light for 3 min (irradiation power 33.6 mW) at *ca.* 18 °C; [**Rho-2**] = 10 μM , [Hg^{2+}] = 20 μM , [M^{n+}] = 40 μM and λ_{ex} = 555 nm.

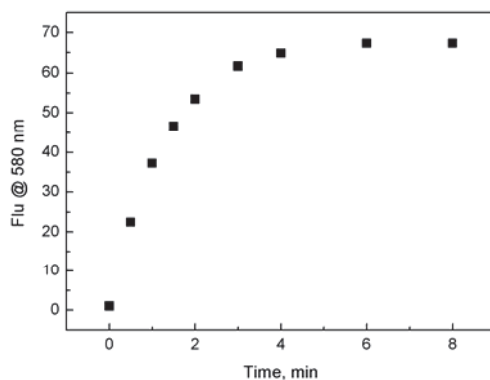


Figure 3-28. Kinetics profile of **Rho-2** in the presence of Hg^{2+} in MeCN/DMSO (v:v = 99:1) under irradiation with 313 nm light (irradiation power 33.6 mW) at *ca.* 18 °C; [**Rho-2**] = 10 μM , [Hg^{2+}] = 40 μM and λ_{ex} = 555 nm.

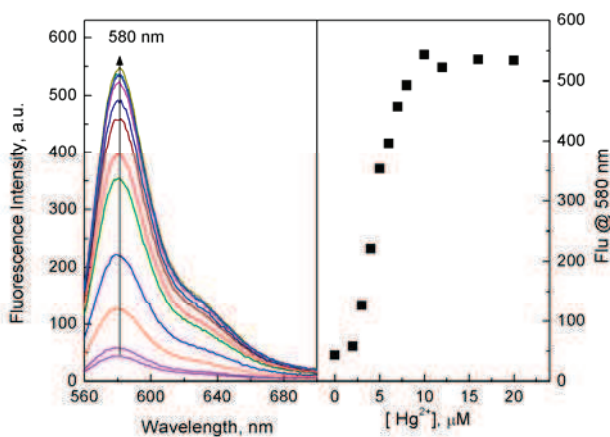


Figure 3-29. Fluorescence spectra of **Rho-2** in the presence of various concentrations of Hg^{2+} in MeCN/DMSO (v:v = 99:1) under irradiation with 313 nm light for 3 min (irradiation power 33.6 mW) at *ca.* 18 °C; [**Rho-2**] = 10 μM and λ_{ex} = 555 nm.

3.3.5. Sensing mechanism of Hg^{2+} based on **Rho-1**

Based on the above spectral investigations, we postulate that triazole and carbonyl group in the spiro lactam ring are the binding sites for Hg^{2+} . Upon complexation with Hg^{2+} , it promotes the ring-opening of spiro lactam under UV irradiation. However, the exact sensing mechanism is much more complicated than we have expected. Figure 3-30 shows the assay of **Rho-1** to Hg^{2+} in pure MeCN without any DMSO. Upon addition of Hg^{2+} but before irradiation with UV lamp, very weak emission (absorbance at 555 nm lower than 0.01) at 580 nm appears due to the very slow metal-induced transformation of spiro lactam to opening forms. It's quite strange to find that after irradiation at 311 nm for 2 min, a remarkable fluorescence quenching rather than fluorescence enhancement was observed, inconsistent with the previous results when there was small percentage of DMSO. The decreased fluorescence intensity may be attributed to the photobleaching of rhodamine fluorophore. Anyhow, this result clearly illustrates that the small amount of DMSO in the system is crucial to photochromism. To get insight into the binding interaction, stepwise addition of DMSO and Hg^{2+} to the solution of **Rho-1** was carried out. As shown in Figure 3-31, introduction of 10 μL DMSO to 2.5 mL MeCN solution of **Rho-1** causes no change, indicating no solute-solvent interaction in the ground state. Subsequent addition of Hg^{2+} induces obvious absorption change (Figure 3-34), demonstrating the complexation between **Rho-1** and Hg^{2+} . However, very slight fluorescence enhancement at 580 nm is observed, indicating Hg^{2+} -induced ring-opening process proceeds very slowly. Dramatic increment of fluorescence is attained after irradiation for 0.5 min, demonstrating that DMSO interacts with **Rho-1**- Hg^{2+} complex in the excited state. We have observed that Hg^{2+} is unable to efficiently induce ring-opening of **Rho-1** in pure MeCN even under irradiation; whereas further addition of 25 μL DMSO to the solution containing **Rho-1**- Hg^{2+} complex induces great fluorescence enhancement after irradiation for 2 min (Figure 3-32), further confirming the important role of DMSO for this photochromism. Selectivity examination shown in Figure 3-25 illustrates that interaction with Hg^{2+} is also a prerequisite for the subsequent photochromism. Therefore it can be concluded that the coexistence of both DMSO and Hg^{2+} is necessary for the photochromism of **Rho-1** and DMSO is thought to interact with **Rho-1**- Hg^{2+} complex in the excited state.

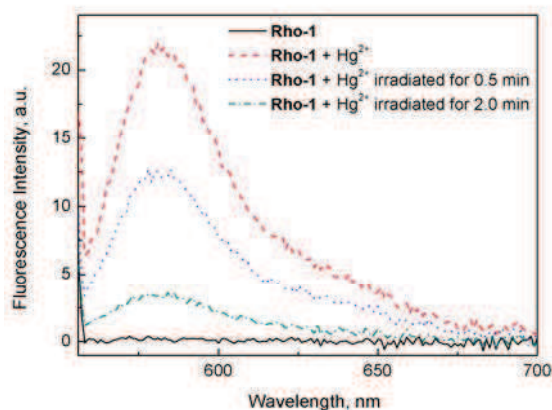


Figure 3-30. Fluorescence spectra of **Rho-1** at ca. 20°C in pure MeCN, in the presence of Hg^{2+} and under irradiation with 313 nm (excitation power 34.0 mW); $[\text{Rho-1}] = 10 \mu\text{M}$, $[\text{Hg}^{2+}] = 40 \mu\text{M}$, fluorescence spectra excited at $\lambda_{\text{ex}} = 555 \text{ nm}$.

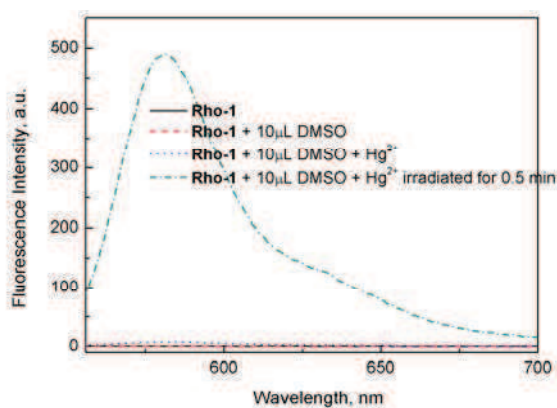


Figure 3-31. Fluorescence spectra of **Rho-1** at ca. 20 °C in MeCN (2.5 mL), in the presence of DMSO, after addition of Hg^{2+} and under irradiation with 313 nm for 0.5 min (excitation power 30 mW); $[\text{Rho-1}] = 10 \mu\text{M}$, $[\text{Hg}^{2+}] = 40 \mu\text{M}$, fluorescence spectra excited at $\lambda_{\text{ex}} = 555 \text{ nm}$.

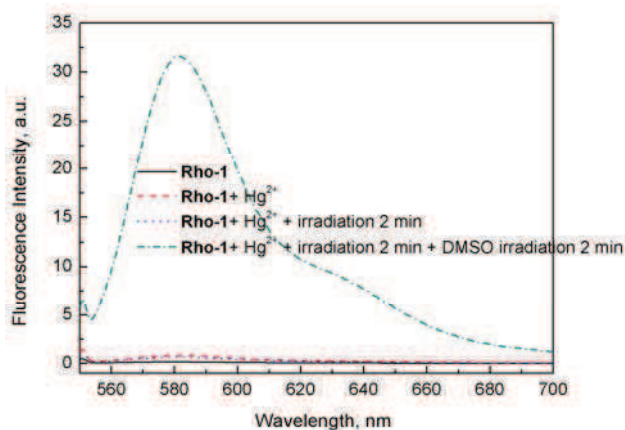


Figure 3-32. Influence of fluorescence spectra of **Rho-1** at ca. 20°C in 2.5 mL MeCN, in the presence of Hg^{2+} under irradiation with 313 nm (excitation power 30 mW, 2 min), with or without DMSO (25 μL); $[\text{Rho-1}] = 10 \mu\text{M}$, $[\text{Hg}^{2+}] = 40 \mu\text{M}$, fluorescence spectra excited at $\lambda_{\text{ex}} = 555 \text{ nm}$.

So how DMSO functions in the photochromic process? As shown in Figure 3-33, addition of CF_3COOH to the solution of **Rho-1** can efficiently promote the photochromic transformation in pure MeCN under illumination. It has been reported that DMSO can react with reactive oxygen species such as H_2O_2 and hydroxyl radical to produce some acidic species.^{28,29} All the assays above are performed under aerobic condition. It's possible that the oxygen contained in the solution can be transferred into reactive oxygen species under UV irradiation. Herein, we compare the photochromic transformation of **Rho-1**- Hg^{2+} under Ar and aerobic conditions. As shown in Figure 3-34, bubbled with Ar for 3 min, the photochromic process becomes more efficient than that under aerobic conditions, excluding the possibility that degradation of DMSO by reactive oxygen species results in acidic compounds and induces the photochromic transformation. The other evidence comes from the selectivity of **Rho-1** to Hg^{2+} . Assuming that acidic species from the degradation of DMSO is the only reason for promoting photochromic reaction, then all the tested metal ions would equally have the same effect on the photochromic process. Furthermore, it should be noted that sometimes a certain amount of acidic species are contained in $\text{Hg}(\text{ClO}_4)_2$, so is it possible that the photochromic reaction is promoted by these acidic species rather than the complexation of Hg^{2+} ? As we can see from the Figure 3-30, no photochromic process was observed in pure MeCN, illustrating that the complexation is the reason promoting photochromic process. Nevertheless, the highly polar DMSO could complex with Hg^{2+} which might facilitate the lactame ring-opening. Together, we here conclude the possible sensing mechanism, as depicted in Scheme 3-5. Upon complexation with Hg^{2+} , ring-opening of the resultant **Rho-1**- Hg^{2+} complex proceeds very slowly at room temperature in MeCN/DMSO (99:1), taking about 26 hours to attain the equilibrium. However, after irradiation at 311 nm, **Rho-1**- Hg^{2+} is transferred into excited state, followed by interaction with DMSO and subsequently caused the fast cleavage of the C-N bond in the spirolactam ring.

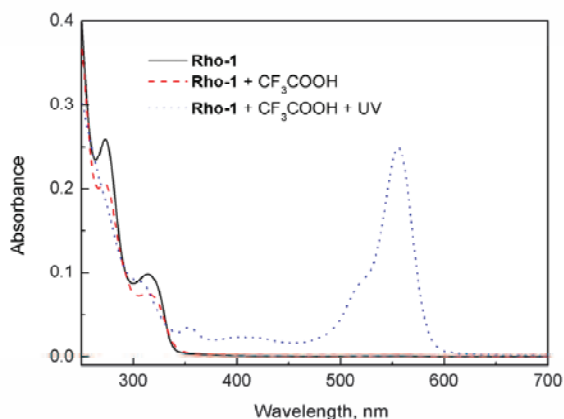


Figure 3-33. Absorption spectra of **Rho-1**, in the presence of CF_3COOH and under irradiation with 313 nm (excitation power 30 mW, 2 min) at ca.20°C; $[\text{Rho-1}] = 10 \mu\text{M}$, $[\text{CF}_3\text{COOH}] = 0.1 \text{ mM}$, fluorescence spectra excited at $\lambda_{\text{ex}} = 555 \text{ nm}$.

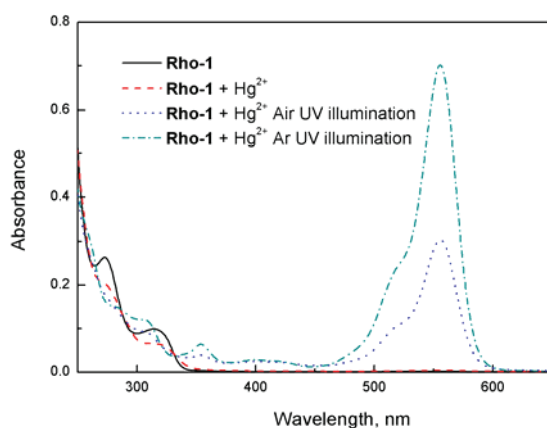
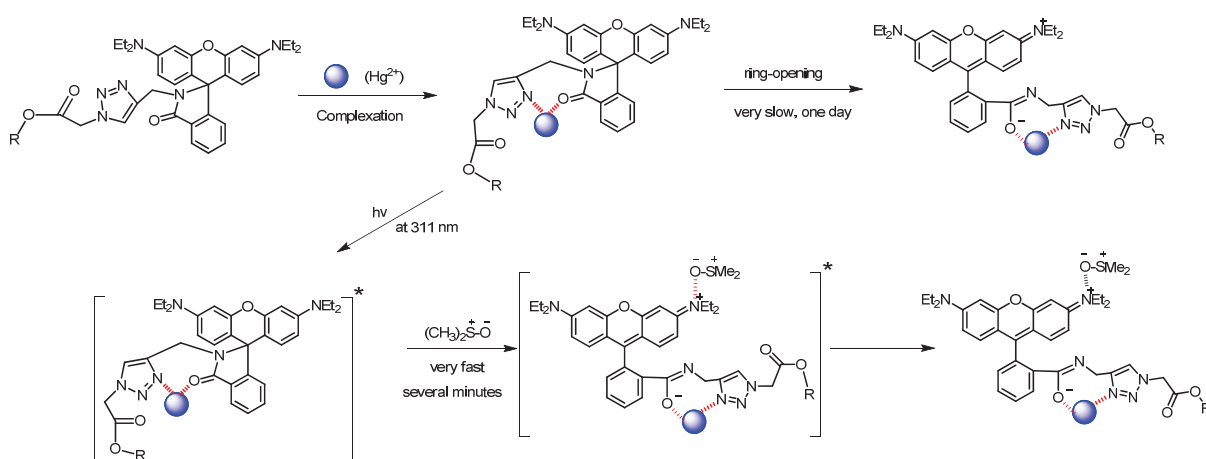


Figure 3-34. Absorption spectra of **Rho-1-Hg²⁺** in MeCN/DMSO (99:1), under aerobic and Ar condition after irradiation with 313 nm (excitation power 30 mW, 2 min) at ca.20°C; $[\text{Rho-1}] = 10 \mu\text{M}$, $[\text{Hg}^{2+}] = 40 \mu\text{M}$, fluorescence spectra excited at $\lambda_{\text{ex}} = 555 \text{ nm}$.



Scheme 3-5. Schematic illustration of the proposed sensing mechanism.

Considering the important role of DMSO in the photochromic transformation, we also examined the photochromic behavior of **Rho-1**-Hg²⁺ in MeCN/DMSO (1:99), as shown in Figure 3-35. Very weak absorption band at 560 nm was observed after irradiation at 311 nm for 2 min. When compared with the results in MeCN/DMSO (99:1), it is found that the photochromic conversion efficiency is greatly decreased. This may be related to the different thermal stability of ring-opening form of **Rho-1** in MeCN and DMSO, as we can always see that the color of the stock solution in DMSO is colorless (spirolactam) while it's pinkish (partially ring-opening) in MeCN.

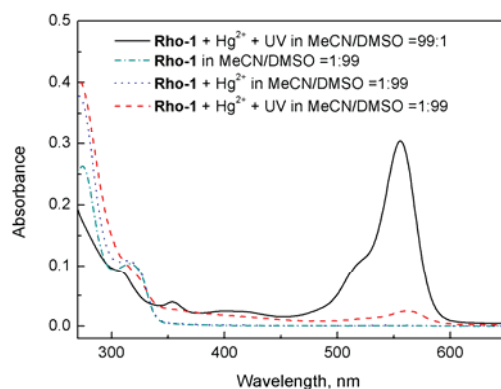


Figure 3-35. Absorption spectra of **Rho-1** at ca. 20°C in MeCN/DMSO (1:99), in the presence of Hg²⁺, with and without irradiation at 313 nm (excitation power 30 mW) for 2 min; [**Rho-1**] = 10 μM, [Hg²⁺] = 40 μM.

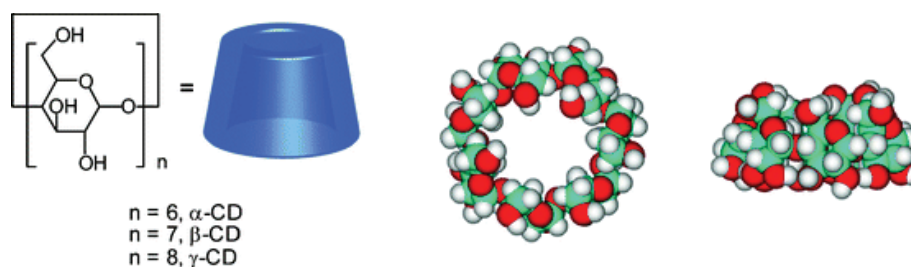
3.3.6. Conclusion

The galactosyl rhodamine derivatives **Rho-1** and **Rho-2** synthesized by click chemistry were explored to study their sensing applications. It was found that Hg²⁺ was capable to induce the ring-opening of **Rho-1**, with the appearance of strong absorption band at 555 nm and emission band at 580 nm after 26 h incubation at room temperature. In order to reduce the response time, photochromic approach was utilized. The results demonstrated that the spirolactam ring opening was dramatically accelerated by irradiation at 313 nm in the presence of Hg²⁺, reducing the response time to 2 min in MeCN/DMSO (99:1). Selectivity of **Rho-1** and **Rho-2** towards Hg²⁺ has also been demonstrated, except Cu²⁺ other metal ions showed almost no influence on the photochromic process. Detailed investigation on its sensing mechanism indicates that small amount of DMSO plays an important role during the photochromic transformation. It's thought to react with excited **Rho-1**-Hg²⁺ and accelerate the ring-opening of spirolactam. To the best of our knowledge, this is the first example of Hg²⁺-promoted photochromism of rhodamine derivatives.

3.4. Pyrene-Triazole based Hg²⁺ chemosensor

3.4.1. Introduction

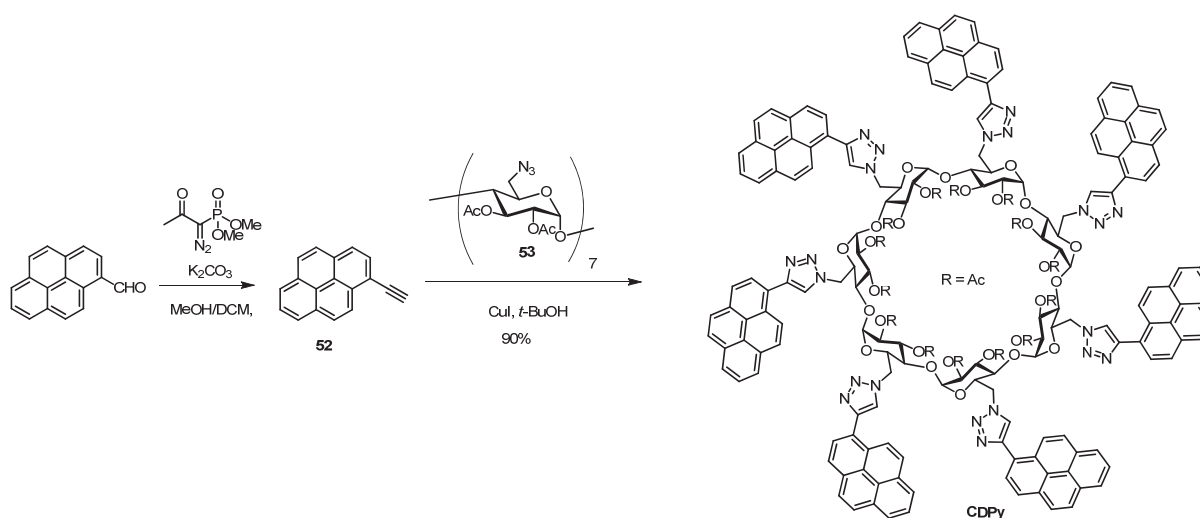
Cyclodextrins (CyDs) are one of the most commonly used building blocks in supramolecular chemistry.^{30,31,32,33,34} They are cyclic oligosaccharides, usually consisting of six to eight glucopyranose units linked by α -1,4-glycosidic bonds, as shown in Scheme 3-6.^{34,35} The shape of CyDs resembles that of a truncated cone, displaying a wider rim composed by 2- and 3-OH groups and narrower rim composed by 6-OH group. The difference in the primary and secondary hydroxyl groups allows the selective functionalization on different rims. Various developed synthetic protocols on CyDs boost their applications in host-guest chemistry. One of the most important properties is their capability of encapsulating various inorganic/organic species within their hydrophobic cavity.^{36,37} The cavity size of CyDs depends on the number of glucopyranose repeating units. For β -CyD, its cavity diameter is 0.62 nm, which is suitable to capture naphthalene molecules. Based on the size match effect, extensive fluorescent chemosensors have been constructed for selective recognition of specific analytes. Besides as the receptors in molecular recognition,³⁸ CyDs are also widely used as building blocks to construct molecular devices.³⁹ Installation of multichromophores onto β -CyD has attracted much attention due to the interesting photophysical properties resulted from the mutual interaction of the chromophores in the ground and excited state. A series of works has been done by Valeur et al to investigate the excitation energy transport among the attached chromophores.^{40,41,42,43} Pyrene represents one of the most versatile aromatic fluorophores due to its unique ratiometric properties based on exchange of monomer and excimer emission.^{44,45} However, rare examples have been reported by integration of multi pyrene fluorophores onto the CyDs rim through covalent bonds. Inspired by our previous work on appending different fluorophores onto CyDs through click chemistry^{46,47} and their interesting spectral behavior to metal ions, herein seven 1-ethynylpyrene units are covalently attached to β -CyD's narrow rim by click reaction. The assembly of the pyrene fluorophore is designed to provide unique spectral properties, constructing an excellent signal transducing platforms for metal ions. Furthermore, the resultant seven triazole groups are located on the narrow rim of β -CyD, forming a preorganized structure and multiple binding sites for metal ions and might possibly increase the sensing selectivity and sensitivity.



Scheme 3-6. Molecular structure of CyDs.

3.4.2. Synthesis of CDPy (by Stéphane Maisonneuve)

As shown in Scheme 3-7, pyrene aldehyde was solubilized in a mixed of MeOH/DCM then reacted with potassium carbonate and Bestmann-Ohira reagent at room temperature. After 3h stirring (TLC monitoring), the mixture was neutralized to pH 7-8 using a HCl 4M solution to afford the pyrene alkyne **52**. Per-(6-azido)- β -CyD **53**, CuI and *t*-BuOH were then added to make a click reaction. After 5h the reaction mixture was treated by EDTA 0.1 M and extracted by DCM. Organic layers were combined and washed with brine, dried over MgSO₄. The solvent were evaporated under vacuum to obtain **CDPy** in a 90% yield.



Scheme 3-7. Synthesis of CDPy.

3.4.3. Photophysical properties of CDPy

Though it has been reported that the position of chromophores is much better spatially defined in the multichromophoric β -CyD, orientation of pyrene moieties may be changed by the surrounding environment such as solvent polarity and hydrogen bonding interaction, which consequently may alter the intramolecular interaction between different pyrene units and the stable assembled structures. Solvatochromism of **CDPy** was carried out in 9 different organic solvents. The results are collected in Table 3-3, Figure 3-36 and Figure 3-37. As can be seen from Table 3-3 and Figure 3-36, **CDPy** consistently exhibits a broad absorption band

at ca. 347 nm. Small blue shift of the absorption band is observed in protic solvents (MeOH and EtOH), which might be attributed to the intermolecular hydrogen bonding interaction between **CDPy** and solvents. The extinction coefficient in MeOH is a little lower than those in toluene and dioxane. Anyhow, the loss of the structured shape of the absorption band is observed when compared with those of unconjugated pyrene chromophores, indicating electronic coupling between pyrene and triazole moieties.

Solvents	λ_{\max}^A [nm]	λ_{\max}^F [nm]	$\Delta\lambda_{F-A}$ [cm ⁻¹]	ϵ_{00} [L.mol ⁻¹ .cm ⁻¹]	Φ_F
MeOH	343	489	8704	1.44×10^5	0.18
EtOH	343	489	8704	nd	0.22
Toluene	346	492	8576	1.59×10^5	0.26
MeCN	345	492	8660	nd	0.14
Dioxane	347	488	8326	1.67×10^5	0.45
DCM	347	492	8493	nd	0.35
CHCl ₃	349	492	8328	1.42×10^5	0.22
DMSO	349	497	8532	nd	0.44
THF	347	492	8493	nd	0.26

Table 3-3. Photophysical data of **CDPy** in different organic solvents, quantum yields were determined using quinine sulfate as reference, nd = not determined.

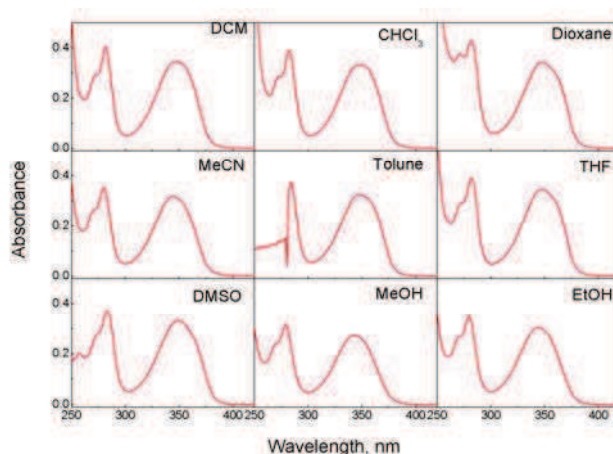


Figure 3-36. Absorption spectra of **CDPy** in different organic solvents; [**CDPy**] = 2 μ M.

As presented in Table 3-3, the maximum emission bands of **CDPy** appear mostly at 492 nm. A little blue shift is observed in MeOH and EtOH, while a little red shift exists in DMSO,

which are consistent with the results of absorption spectra. Distinct differences can be easily found for the emission patterns in different solvents (Figure 3-37). Remarkable monomer emission bands at 388 nm and 410 nm are observed in dioxane, and moderate intensity of monomer emission in THF, toluene and CHCl_3 . In strongly polar solvents like DMSO, MeOH and EtOH, the monomer emission is much less important than that of the excimer. This means that **CDPy** in different solvents may adopt different structural conformations, and in polar solvent pyrene fluorophores stack more strongly than that in less polar solvents. The determined fluorescence quantum yields range from 0.14 to 0.45, with the largest value (0.45) in dioxane and lowest (0.14) in MeCN. The difference in fluorescence quantum yields may be due to the different conformations induced energy transfer and the different strength of the intramolecular interactions.

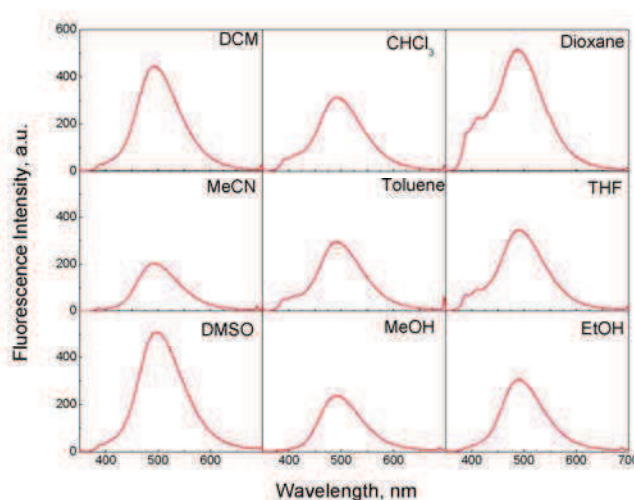


Figure 3-37. Fluorescence spectra of **CDPy** in different organic solvents; [**CDPy**] = 2 μM , excited at corresponding maximum absorption wavelength.

3.4.4. Structural conformation of **CDPy**

It's quite important to obtain the structural information of **CDPy** in solutions before we start to study its complexation properties. The above absorption and emission spectra have already indicated that structural conformation of **CDPy** is dependent on solvent medium. Importantly, excimer emission is always much higher than that of the monomer, suggesting that seven pyrene fluorophores on the narrow rim are very crowded. However, more detailed evidences are highly desirable to understand its conformation in solutions. NMR spectroscopy has become the most important method for structural elucidation of CyD in the solution.⁴⁸ In order to investigate the orientation of pyrene moieties on the rim, NOEs (Nuclear Overhauser effects) experiment was taken to provide information about through space interaction. No

cross coupling is observed between pyrene and CyD (Figure 3-38), indicating that pyrene moieties are out of the CyD cavity. However, due to the large molecular weight of **CDPy** (3482 D), 2D ROESY NMR experiment (suitable molecular weight range: roughly 1000-3000D) needs to be carried out to get more precise information.

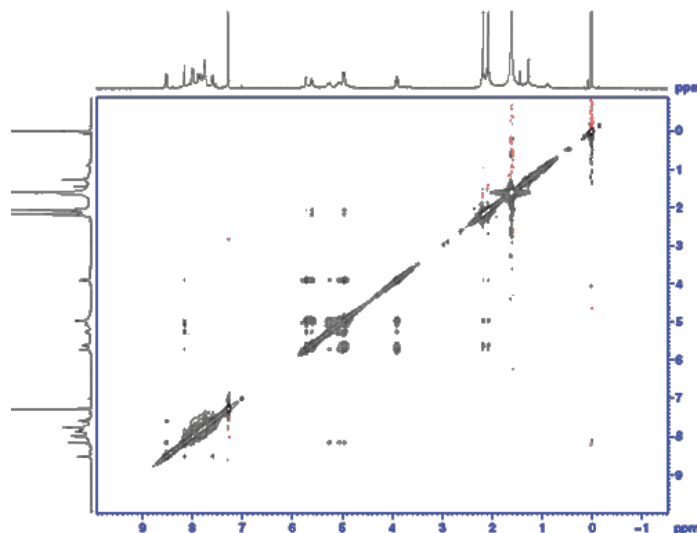


Figure 3-38. NOESY spectra of **CDPy** in CDCl_3 .

Induced circular dichroism (ICD) has been proved to be an efficient spectroscopic tool to study the orientation of the achiral chromophoric guest on CyD rims.^{49,50,51,52} A rule has been established by Harata for the prediction of structure from ICD when the chromophore is included within the CyD. It predicts that ICD signal will be positive when the electronic transition dipole moment is parallel to the principal axis of CyD and negative when the electronic transition dipole moment is perpendicular to the axis. However, according to the treatment of Kodaka, when a chromophore is outside the cavity of CyD, the sign of the ICD will become reverse.⁵⁰ Analysis of NOESY spectra of **CDPy** in CDCl_3 have demonstrated that pyrene chromophores stayed outside of the cavity of CyD. Figure 3-39 shows ICD spectrum and corresponding UV/Vis absorption spectrum of **CDPy** in MeOH. The major electronic transitions of **CDPy** are $^1\text{B}_b$ and $^1\text{L}_a$ peaks observed at 278 and 343 nm, respectively. It's known that $^1\text{B}_b$ transition of pyrene is polarized along the short axis and the $^1\text{L}_a$ transition is polarized along the long axis. **CDPy** exhibits a negative ICD at the $^1\text{L}_a$ transition around 343 nm, indicating that the $^1\text{L}_a$ transition moment of pyrene fluorophores aligns in parallel with primary CyD axis, as shown in the schematic illustration in Scheme 3-8.

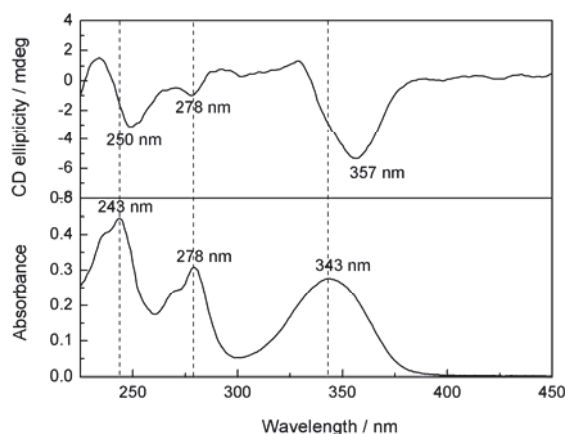
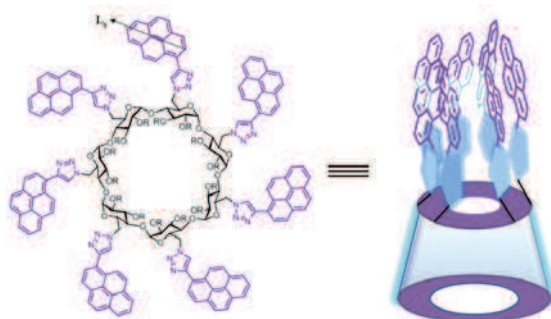


Figure 3-39. Absorption and circular dichroism spectra of **CDPy** in MeOH, $[\text{CDPy}] = 2 \mu\text{M}$.



Scheme 3-8. Schematic illustration of molecular structure of **CDPy**.

Temperature-dependent fluorescence spectra were also recorded to investigate its structure in solution. As shown in Figure 3-40, the ratio of excimer and monomer is almost unchanged under 50°C and decreases with further increasing temperature, demonstrating that increasing the conformational flexibility by heating should increase the distance between pyrene units on the rim. In other words, the pyrene moieties at room temperature should interact with each other in the vicinity more strongly than at high temperature.

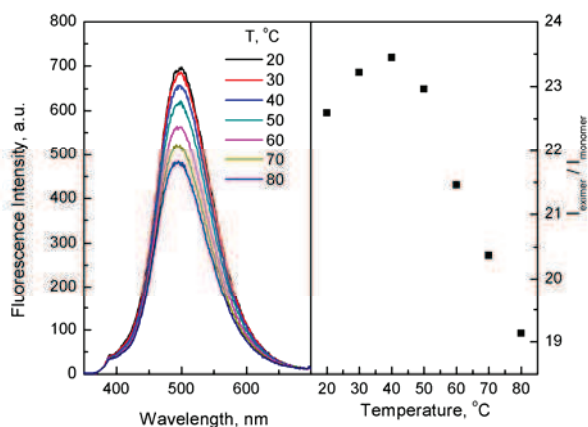


Figure 3-40. Variable-temperature emission spectra of **CDPy** in DMSO, $[\text{CDPy}] = 2 \mu\text{M}$.

3.4.5. Complexation properties of CDPy

The metallo-responsive properties of **CDPy** was examined in MeOH by screening a series of metal ions, such as Hg^{2+} , Cu^{2+} , Zn^{2+} , Pb^{2+} , Cd^{2+} , Ni^{2+} , Co^{2+} , Mn^{2+} , Ag^+ , Fe^{2+} , Mg^{2+} , and Ba^{2+} . As shown in Figure 3-41, the addition of Hg^{2+} causes almost complete quenching of excimer emission and Ag^+ to a lesser extent, while Cu^{2+} leads to a slight quenching and other tested metal ions show no influence on the emission of **CDPy**. Considering the practical applications, competition experiment was also carried out. As presented in Figure 3-41 (c), the presence of excessive competing metal ions shows consistently no interference on the spectral response of **CDPy** to Hg^{2+} except Ag^+ which produces a slight anti-quenching effect.

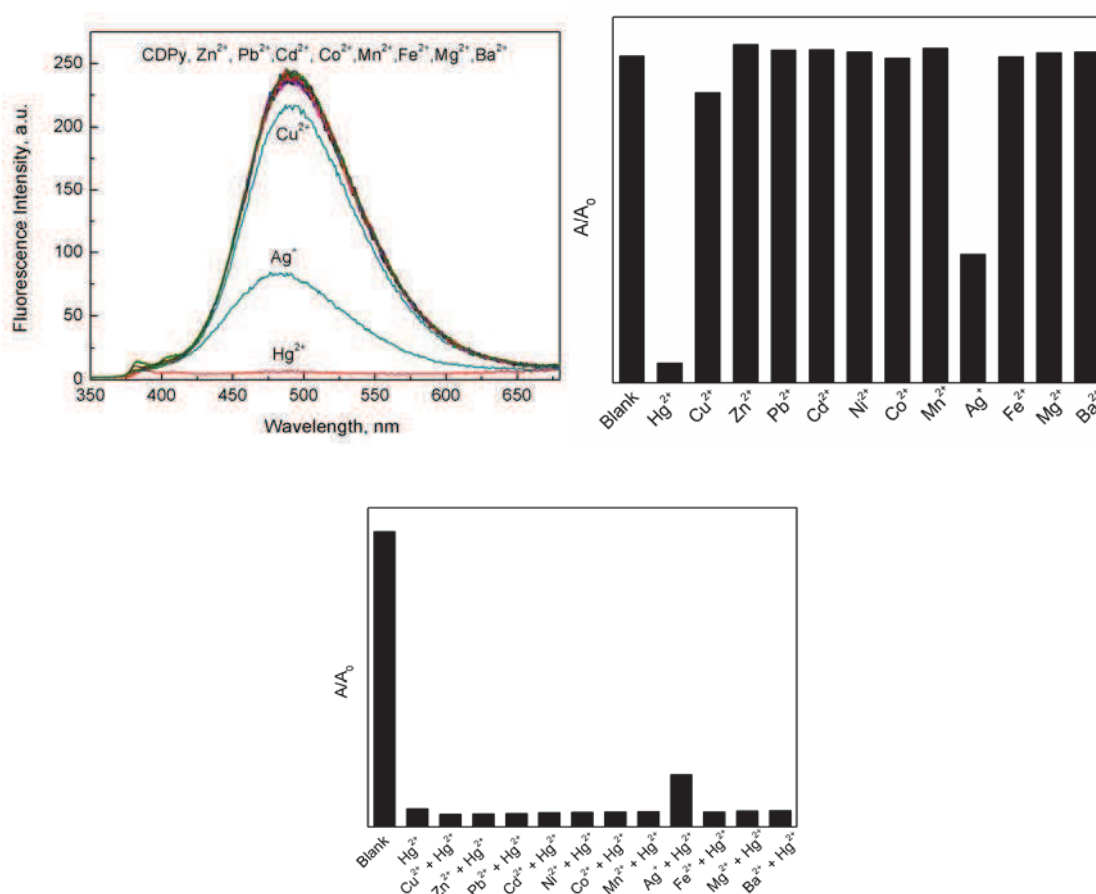


Figure 3-41. Selectivity (top) and competition (bottom) experiments of **CDPy** to a series of cations in MeOH; $[\text{CDPy}] = 2.0 \mu\text{M}$, $[\text{Hg}^{2+}] = 40 \mu\text{M}$, $[\text{M}^{\text{n}+}] = 80 \mu\text{M}$, $\lambda_{\text{ex}} = 343 \text{ nm}$.

Solvatochromic investigation on **CDPy** has demonstrated that different conformations of pyrene moieties on the rims may occur, which might consequently affects the selectivity of **CDPy** to metal ions. Toluene is selected for comparison with MeOH, as we can see that **CDPy** exhibits much more intense monomer emission in toluene than in MeOH. Figure 3-42 shows the selectivity of **CDPy** to metal ions in toluene. Quite similar to the results in MeOH,

the introduction of Hg^{2+} induce the most efficient fluorescence quenching, followed by Ag^+ and Cu^{2+} . Other metal ions exhibit no effects. The similarity of the selectivity indicates that conformational difference between MeOH and toluene is not large enough to create a new geometric binding structure.

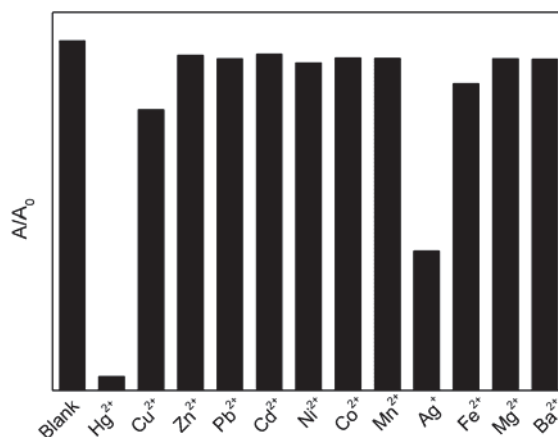


Figure 3-42. Selectivity of **CDPy** to a series of cations in toluene, $[\text{CDPy}] = 2.0 \mu\text{M}$, $[\text{Hg}^{2+}] = 40 \mu\text{M}$, $[\text{M}^{n+}] = 80 \mu\text{M}$, $\lambda_{\text{ex}} = 348 \text{ nm}$.

Although the selectivity of **CDPy** does not differ from MeOH to toluene, the responsive properties of **CDPy** toward Hg^{2+} may be affected by the solvent environment such as the solvation of Hg^{2+} . Figure 3-43 compares the spectral response of **CDPy** to Hg^{2+} in nine different organic solvents from both absorption and fluorescence spectra. No spectral change is observed before and after addition of Hg^{2+} to **CDPy** in DMSO while complete fluorescence quenching is obtained in CH_2Cl_2 , dioxane, toluene, MeOH, and EtOH. In other solvents fluorescence quenching with different extents is observed by following the order: THF < CHCl_3 < MeCN. In accordance with the emission spectra, the absorption bands of **CDPy** in different solvents decrease in the presence of Hg^{2+} . Spectral patterns of the resultant complex are different from each other.

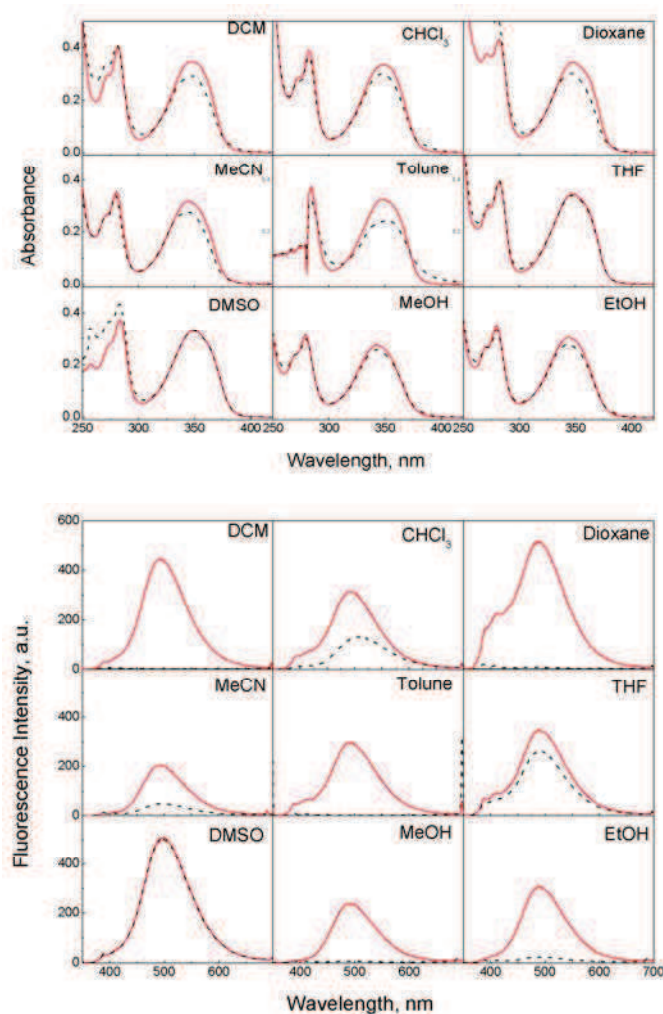


Figure 3-43. Absorption (top) and fluorescence (bottom) spectra of **CDPy** alone (solid line) and **CDPy-Hg²⁺** (dash line) in different organic solvents, [CDPy] = 2.0 μM , [Hg²⁺] = 40 μM , excited at corresponding maximum absorption wavelengths.

In order to get insight into the binding process of **CDPy** to Hg²⁺, spectral titrations were conducted in different solvents. Figure 3-44 depicts the absorption and fluorescence titrations of **CDPy** with the gradual addition of Hg²⁺ in MeOH. When Hg²⁺ concentration is lower than 10 μM , almost no change is observed for both absorption and emission spectra. Further addition of Hg²⁺ then causes decrease of maximum absorption band and dramatic quenching of the excimer emission, and surprisingly, it quickly reaches a plateau after 15 μM . The individual unit concentration of pyrene moiety is calculated to be seven folds of **CDPy**, that is 14 μM , which means that 1 molar Hg²⁺ can quench ca. 1 molar of pyrene.

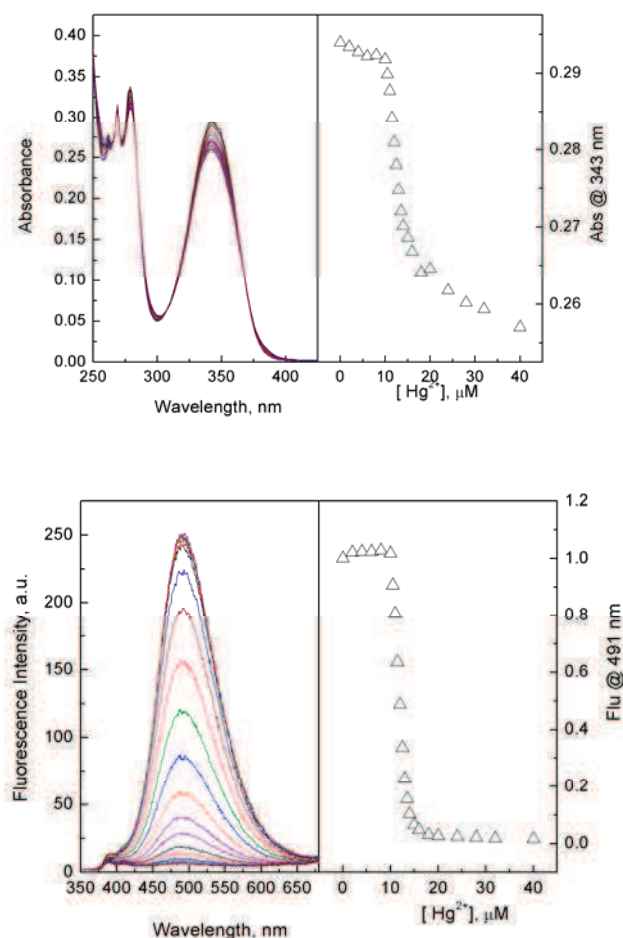


Figure 3-44. Absorption (top) and fluorescence (bottom) spectra of **CDPy** with increasing concentrations of Hg^{2+} in MeOH; $[\text{CDPy}] = 2.0 \mu\text{M}$, $\lambda_{\text{ex}} = 343 \text{ nm}$.

Spectral titration in dioxane was also carried out, as shown in Figure 3-45. **CDPy** exhibits a little more structured absorption band than those in other solvents, accompanying with stronger monomer emission band. With the addition of increasing concentrations of Hg^{2+} , absorbance of the maximum band at 347 nm decreases and two clear isosbestic points are observed at 332 and 380 nm, indicating the interconversion of free ligand and the bound complex. The silent spectral response of **CDPy** to Hg^{2+} in the range of low Hg^{2+} concentration as observed during the titration in MeOH (Figure 3-44) disappears in dioxane. In contrast, it reaches the equilibrium very quickly when the concentration of Hg^{2+} is 5 μM . Therefore 5 μM Hg^{2+} is enough to affect 2 μM **CDPy** with 14 μM pyrene moieties, demonstrating that signal amplification or as called superquenching exists in this system. By assembling seven pyrene units on the CyD primary rim, the exciton may move among different pyrene units due to their close vicinity in the excited state. This phenomenon has been widely reported in fluorescent conjugated polymers, but rarely in the supramolecular structures.

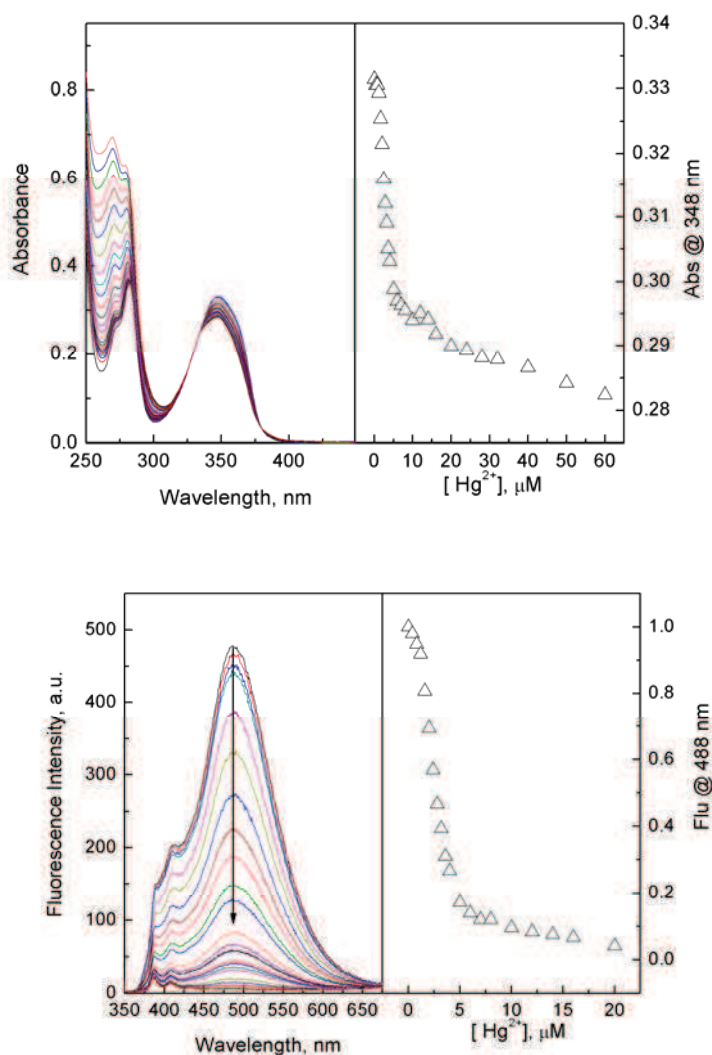


Figure 3-45. Absorption (top) and fluorescence (bottom) spectra of **CDPy** with increasing concentrations of Hg^{2+} in dioxane; $[\text{CDPy}] = 2.0 \mu\text{M}$, $\lambda_{\text{ex}} = 348 \text{ nm}$.

Toluene as an aromatic solvent has been demonstrated to form exciplex with the excited ICT fluorophores.⁵³ Assuming that toluene may insert into the gap between different pyrene moieties and help the exciton transfer, higher sensitivity might be obtained when the titration is performed in toluene medium. As shown in Figure 3-46, complete quenching reaches very fast as in toluene, but at even lower concentrations (4 μM), indicating that the solvent medium may help the excitation transfer in the excited state. The efficiency of signal amplification is then further increased, also giving hints for the design of condense stacking of pyrene as more efficiently sensing platform. On the other hand, the increased quenching efficiency in toluene may be caused by the difference in ionic solvation.

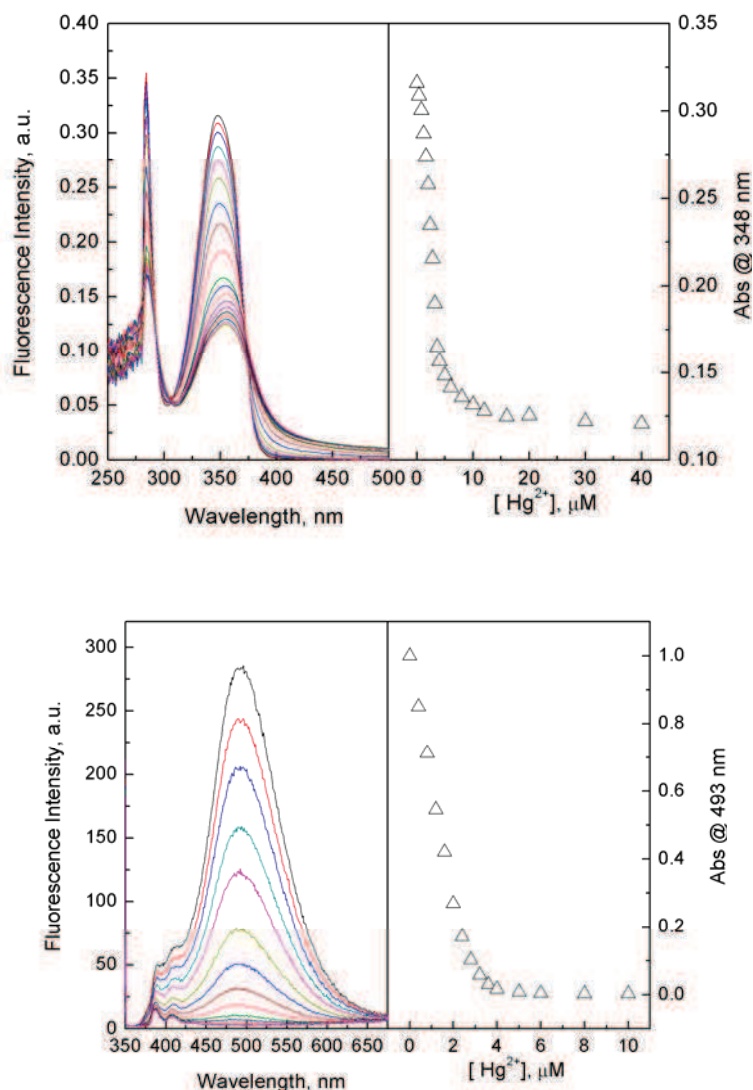


Figure 3-46. Absorption (top) and fluorescence (bottom) spectra of **CDPy** with increasing concentrations of Hg^{2+} in toluene, $[\text{CDPy}] = 2.0 \mu\text{M}$, $\lambda_{\text{ex}} = 348 \text{ nm}$.

Considering the practical applications of **CDPy** in detection of Hg^{2+} , the spectral titrations were further performed in water containing medium. Figure 3-47 demonstrates the titration of **CDPy** with Hg^{2+} in MeOH/ H_2O (9:1, v/v). It's obvious that the addition of Hg^{2+} can cause the fluorescence quenching, however with a much lower sensitivity when compared with that in pure MeOH. As presented in Figure 3-48, titrations in dioxane/ H_2O (9:1, v/v) show the similar spectral behavior as that in dioxane, however, with lower sensing sensitivity. It's therefore that sensitivity of **CDPy** to Hg^{2+} is significantly affected by the solvent medium.

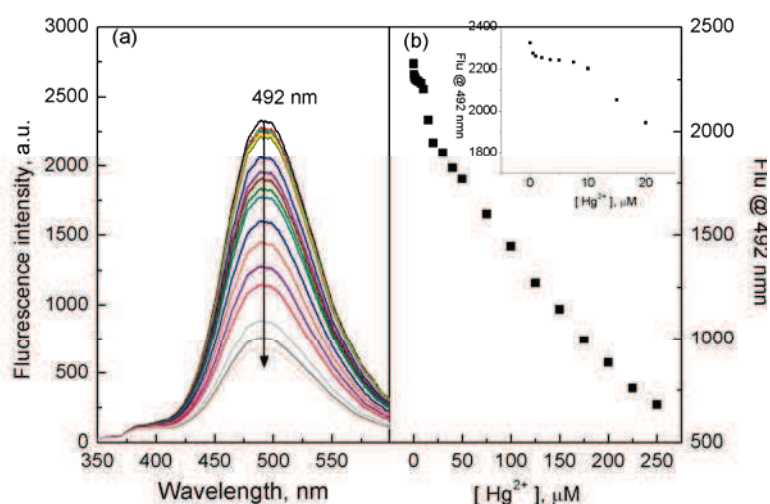


Figure 3-47. (a) Fluorescence spectra of **CDPy** in CH₃OH-H₂O (9:1, v/v) in the presence of various concentration of Hg²⁺. (b) Fluorescence intensity of **CDPy** at 492 nm as a function of Hg²⁺ concentration, $\lambda_{\text{ex}} = 320$ nm, [Hg²⁺] = 0-250 μM , [CDPy] = 2.0 μM .

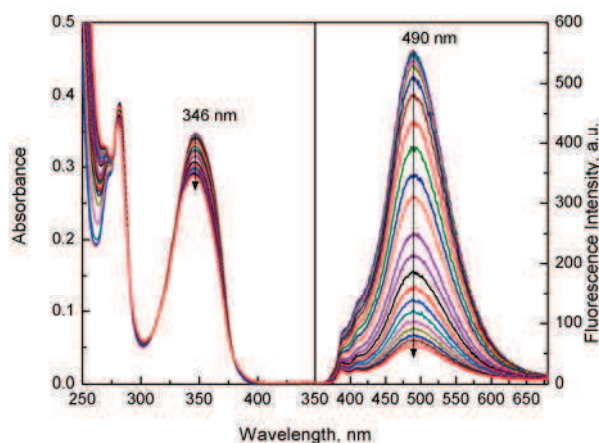


Figure 3-48. Absorption and fluorescence spectra of **CDPy** in dioxane-H₂O (9:1, v/v) in the presence of various concentration of Hg²⁺; $\lambda_{\text{ex}} = 347$ nm, [CDPy] = 2.0 μM .

The binding process of **CDPy** to Hg²⁺ in MeOH was monitored by using circular dichroism spectra, as shown in Figure 3-49. **CDPy** alone shows negative bands at around 357, 278, and 250 nm and a positive band at 233 nm. The induced circular dichroism intensities of positive and negative peaks of **CDPy** enhance with increasing concentrations of Hg²⁺, suggesting that interaction of pyrene units in close proximity becomes stronger or pyrene units are closer to the rim of CyD cavity upon complexation with Hg²⁺.

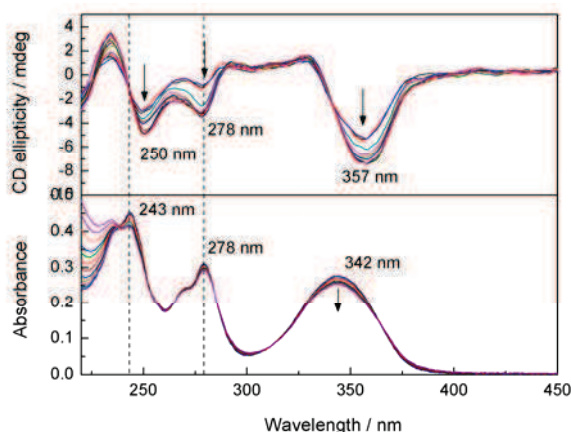


Figure 3-49. Circle dichroism spectra of **CDPy** in presence of increasing concentrations of Hg^{2+} in CH_3OH . $[\text{CDPy}] = 2.0 \mu\text{M}$, $[\text{Hg}^{2+}] = 0\text{-}30 \mu\text{M}$.

Inclusion complexation is one of the most fascinating characters of CyD, based on binding guest molecules into the hydrophobic cavity. Herein, we envision that the introduction of new binding site by an additional ligand can improve the sensing performance of **CDPy**. Meanwhile considering the strong binding ability of carboxylic acid, different aromatic acids which are likely to be included into the CyD cavity were selected to take tests. As shown in Figure 3-50, the hypothesis is examined in MeOH. However, only very little change is observed in the presence of different acids as the second ligand. This may be attributed to the following explanations: (1) acetylation of secondary rim of β -CyD leads to a large steric hindrance and disables the inclusion complexation; (2) **CDPy** shows low binding ability to the tested carboxylic acids due to the mismatch of size; (3) the inclusion complex formation is trivial in methanol; (4) the introduction of additional binding site does not necessarily change the binding processes. More detailed experiments are going to be carried out to get more evidences of this binding process.

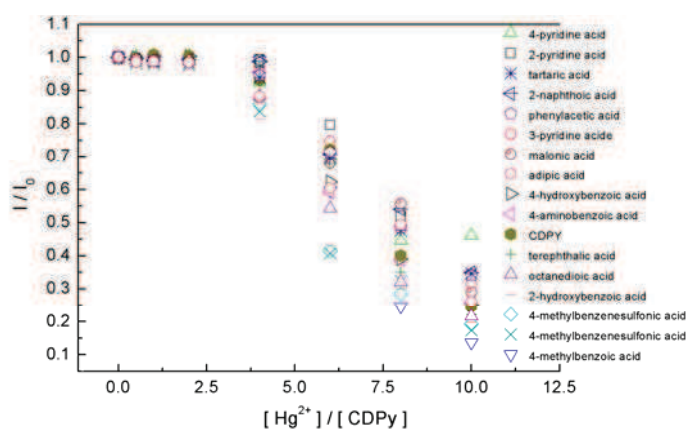


Figure 3-50. Plot of fluorescence intensity **CDPy** at 488 nm as a function of concentrations of Hg^{2+} in CH_3OH in the presence of $2.0 \mu\text{M}$ second ligand, $[\text{CDPy}] = 2.0 \mu\text{M}$, $\lambda_{\text{ex}} = 311 \text{ nm}$.

Finally, the ensemble of **CDPy**- Hg^{2+} complex was utilized to test whether it was capable of discriminating enantiomers of amino acids due to the chirality transfer from CyD to pyrene-triazole moiety, as evidenced from the circular dichroism spectra. As shown in Figure 3-51, addition of either enantiomers (D/L) of cysteine recovers the comparable fluorescence intensity. GSH and homocysteine (HCys) can also almost completely restore the emission. No chiral discrimination of analytes may be due to the strong binding ability of Hg^{2+} to the thiol group in these amino acids.

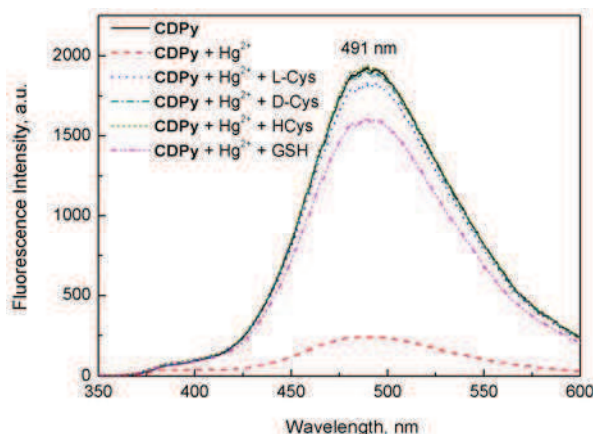


Figure 3-51. Fluorescence spectra of **CD-Py** before and after addition of Hg^{2+} , then L-Cys.HCl, D-Cys.HCl, HCys, GSH. $[\text{CD-Py}] = 2.0 \mu\text{M}$, $[\text{Hg}^{2+}] = 30 \mu\text{M}$, $[\text{Amino Acids}] = 30 \mu\text{M}$.

3.4.6. Conclusion

Click chemistry was utilized to attach pyrene fluorophores to the primary rim of β -CyD to give a novel fluorescent chemosensor **CDPy**. Its structural confirmation has been studied by UV/vis, fluorescence, NOESY NMR and circular dichroism spectra, which demonstrate that pyrene moieties align along the primary axis of β -CyD and strong interaction is observed between different pyrene units in the excited state. Metallo-responsive properties of **CDPy** shows that it exhibits high selectivity to Hg^{2+} in both MeOH and toluene, which was further confirmed by a competition experiment. Investigation of the spectral response of **CDPy** to Hg^{2+} in different solvents demonstrates that sensing sensitivity is strongly depended on the solvent medium. More importantly, signal amplification (superquenching) was inferred from the spectral titrations, suggesting that such an assembling approach may provide a new platform for the sensing applications. More detailed investigations on this system will provide more useful and solid information and promote the further exploration of chemosensors by modification on macrocyclic compounds with click chemistry.

3.5. Benzothiadiazolyl-Triazole based chemosensors

3.5.1. Introduction

With increasing demand in pursuing excellent fluorescent chemosensors for the detection of biologically and environmentally analytes, modular approaches have offered the possibility for rapidly constructing sensor molecular libraries. Among them, Cu(I)-catalyzed Azide-Alkyne Cycloaddition (CuAAC) represents one of the most efficient approaches for chemical transformation to create new fluorescent molecules with desired spectral properties.^{46,18,47,54,55} When the triazolyl moiety is conjugated with chromophores, the extended aromatic systems reduce the energy gap of π - π^* transition, thereby resulting in red shift of the excitation and emission wavelength maxima. As we have discussed in the Chapter 2, the conjugation of triazole with pyridine and benzothiadiazole has led to two new fluorescent chemosensors for the selective recognition of Zn^{2+} and Ni^{2+} , respectively. For the flexible modulation of spectral properties by formation of triazolyl moiety, detailed investigation on the influence of triazole on benzothiadiazolyl moiety will be presented in this section as an example to demonstrate rational design of new fluorophores by click reactions.

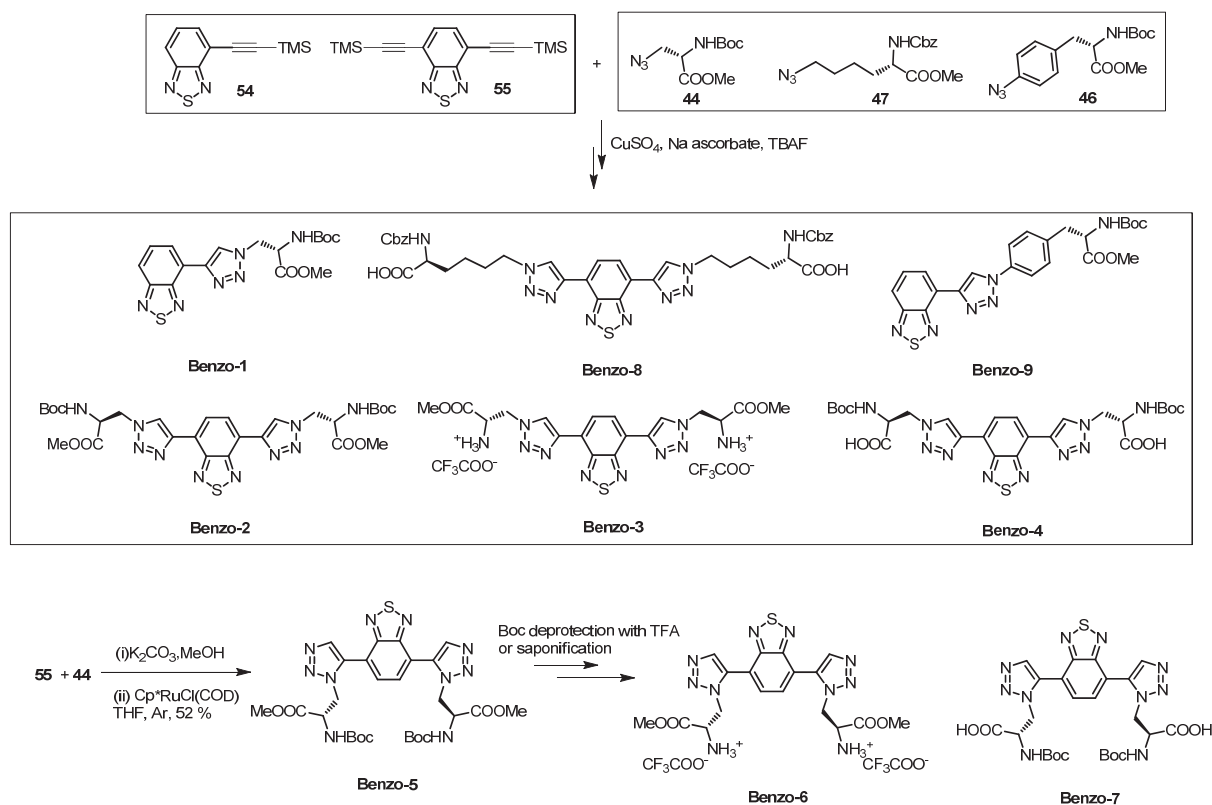
In the last three sections of this chapter, we have focused on the utilization of triazole as the sole binding site and they consistently show selective response to Hg^{2+} . This is quite different from the benzothiadiazole-triazole fluorophore where preorganized structure between benzothiadiazole and triazole forms. It shows response to a series of transition metal ions, such as Cu^{2+} , Ni^{2+} and Hg^{2+} . In order to investigate how the triazole and the terminal binding groups affect the binding properties, spectral investigation based on a series of benzothiadiazole-triazole derivatives was carried out to illustrate a rational design. The molecules involved in this work are presented in Scheme 3-9.

3.5.2. Synthesis of Benzo-x derivatives (by Chun Li and Yanhua Yu)

1,4-Disubstituted 1,2,3-triazole derivatives (**Benzo-1** to **Benzo-4** and **Benzo-8** and **9**) were obtained by click reaction between the corresponding alkyne-functionalised fluorophore with azido aminoesters, catalyzed by $\text{CuSO}_4 \cdot 5\text{H}_2\text{O}$ and Na ascorbate in $\text{CH}_2\text{Cl}_2/\text{H}_2\text{O}$ (1:1).^{56,18}

1,5-Disubstituted 1,2,3-triazole derivatives **Benzo-5** – **Benzo-7** were prepared by reacting alkyne-functionalised fluorophore **55** with azido aminoester **44** catalyzed by

$\text{Cp}^*\text{RuCl}(\text{COD})^{57}$ in dry THF under Ar.



Scheme 3-9. Molecular structures and synthesis of **Benzo-x**.

3.5.3. Photophysical properties of **Benzo-x** series

As we have mentioned above, the incorporation of triazole can extend the conjugation of the aromatic system. In order to rationally design fluorophores containing triazole, investigation on how triazole moiety influences the spectral properties of benzothiadiazole was carried out based on mono-substituted (**Benzo-1**) and bis-substituted 1,4 (**Benzo-2** - **Benzo-4**) and 1,5 (**Benzo-5** - **Benzo-7**) regioisomers. With these molecules in hands, we started to examine spectral properties of various fluorophores.

Photophysical data of **Benzo-1** and **Benzo-2** are collected in Figure 3-52 and Table 3-4. Precursor of click reaction **Benzo-alkyne** exhibits an absorption band at 347 nm and an emission band at 425 nm in MeCN. After transformation of the alkyne group into triazole group by click chemistry, **Benzo-1** shows a red-shift absorption band at 355 nm and an emission band centered at 469 nm with the quantum yield up to 0.61 in MeCN. This is consistent with the fact that formation of triazole moiety enhances aromatic conjugation due to replacement of electron-withdrawing alkyne group by electron-donating triazole group.⁵⁸ Based on the phenomenon, it is supposed that the bis-substituted 1,4-triazolyl benzothiadiazole derivatives may have better spectral properties, with more red-shifted

excitation and emission wavelengths. In line with our assumption, **Benzo-2** with two conjugated triazole groups shows an absorption band at 401 nm and an emission band at 522 nm in MeCN, which are more red-shift than that of **Benzo-1** by 40 nm for absorption spectrum and 53 nm for the emission band. Its quantum yield is determined to be 0.86. This can be attributed to a more reduced energy gap when the second triazole is anchored. Therefore increasing number of triazole moiety directly conjugated with benzothiadiazole leads to the red shift of both absorption and emission spectra while keeping high fluorescence quantum yields.

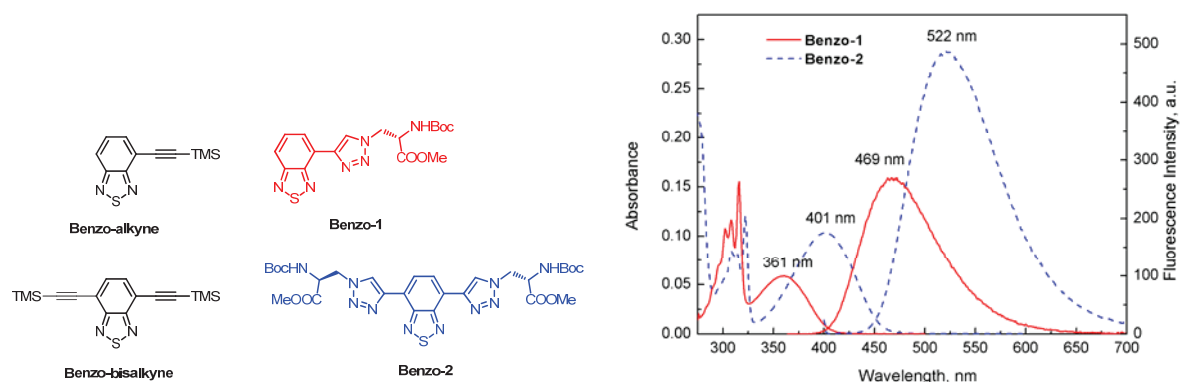


Figure 3-52. Absorption and fluorescence spectra of **Benzo-1** and **Benzo-2** in MeCN; [**Benzo-1**] = [**Benzo-2**] = 10 μ M.

Compounds	λ_{\max}^A [nm]	λ_{\max}^F [nm]	ϵ_{00} [L mol ⁻¹ cm ⁻¹]	Φ_F
Benzo-alkyne	347	427	nd	nd
Benzo-bisalkyne	376	457	nd	nd
Benzo-1	361	469	6.0×10^3	0.61
Benzo-2	401	522	1.06×10^4	0.86

Table 3-4. Photophysical data of **Benzo-alkyne**, **Benzo-bisalkyne**, **Benzo-1** and **Benzo-2** in MeCN; nd: not determined.

Substituent effect of the 1,2,3-triazole can possibly exert some influence on the electronic distribution of the conjugated system. As shown in Figure 3-53 and Table 3-5, regioisomers **Benzo-2** (1,4-disubstituted) and **Benzo-5** (1,5-disubstituted) exhibit very different spectral properties. **Benzo-5** shows an absorption band at 354 nm and an emission band at 475 nm with the fluorescence quantum yield of 0.71. Large blue shifts are observed for both absorption and emission spectra when compared with those of **Benzo-2**. Furthermore, the extinction coefficient of **Benzo-5** is about half (56%) of that of **Benzo-2**. They together

demonstrate that the position of the substituent is of significant importance on the electronic spectra.

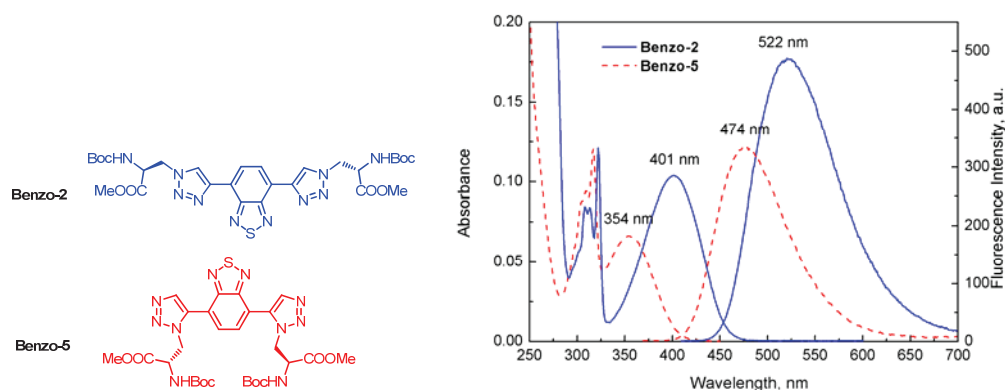


Figure 3-53. Absorption and fluorescence spectra of **Benzo-2** and **Benzo-5** in MeCN; [**Benzo-2**] = [**Benzo-5**] = 10 μ M.

Compounds	λ_{\max}^A [nm]	λ_{\max}^F [nm]	ϵ_{00} [L mol ⁻¹ cm ⁻¹]	Φ_F
Benzo-2	401	522	1.06×10^4	0.86
Benzo-5	354	475	6.0×10^3	0.71

Table 3-5. Photophysical data of **Benzo-2** and **Benzo-5** in MeCN.

Terminal amino acid moiety is another important constituent in this series of benzothiadiazole-triazole derivatives. Investigation on the effect of amino acid moiety imposed on the fluorescent core was also carried out. **Benzo-3** and **Benzo-4** were prepared by deprotection of **Benzo-2**. As shown in Figure 3-54 and Table 3-6, they all show the absorption and emission bands nearly at the same wavelength: *ca.* 400 nm and 522 nm, respectively. However, fluorescence quantum yields and extinction coefficients are a bit reduced after removal of the protection groups. This may be attributed to the formation of intramolecular hydrogen bond between triazole and amino acid moiety. Anyhow, the terminal amino acids moiety exerts little influence on properties of the fluorescent core.

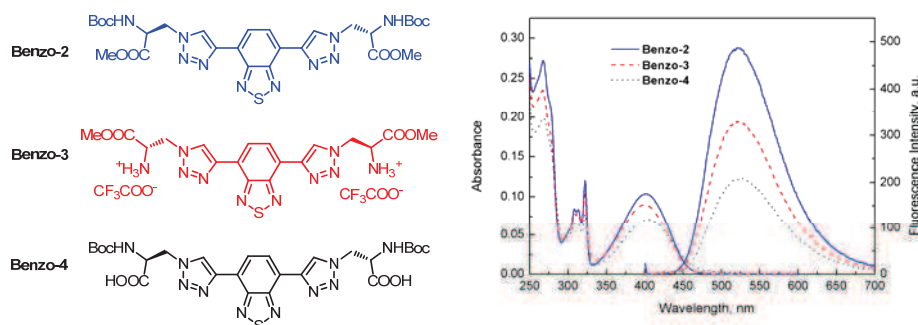


Figure 3-54. Absorption and fluorescence spectra of **Benzo-2**, **Benzo-3** and **Benzo-4** in MeCN; [**Benzo-2**] = [**Benzo-3**] = [**Benzo-4**] = 10 μ M.

Compounds	λ_{\max}^A [nm]	λ_{\max}^F [nm]	ϵ_{00} [L mol ⁻¹ cm ⁻¹]	Φ_F
Benzo-2	401	522	1.06×10^4	0.86
Benzo-3	400	522	8.7×10^3	0.69
Benzo-4	405	525	6.9×10^3	0.38

Table 3-6. Photophysical data of **Benzo-2**, **Benzo-3** and **Benzo-4** in MeCN.

3.5.4. Complexation properties of Benzo-x series

In our previous sections, triazole moiety has been shown to be a flexible binding site for metal ions, especially for Hg²⁺. When it was conjugated with benzothiadiazole, metallo-responsive properties of these ligands changed a lot, as demonstrated by compound **42** in Chapter 2. In order to get insight into the structure-dependent binding selectivity and sensitivity, metallo-responsive properties of a series of **Benzo-x** were examined.

3.5.4.1. Selectivity of Benzo-x series to metal ions

Figure 3-55 depicts fluorescence change of **Benzo-1** in the presence of various metal ions in MeCN. Consistent with our reported results, addition of Co²⁺, Cu²⁺, Hg²⁺ and Ni²⁺ quenches the emission intensity to different extents by following the order of Ni²⁺>Cu²⁺>Hg²⁺~Co²⁺. It is postulated that the coordinate site of **Benzo-1** for transition metal ions is the preorganized binding pocket between benzothiadiazole and triazole. The selectivity of **Benzo-2** was also examined under identical conditions. Consistent with our expectation, **Benzo-2** shows exactly the same metallo-responsive selectivity as that of **Benzo-1**, as illustrated in Figure 3-56. In contrast, **Benzo-5** exhibits a great discrepancy, and only the addition of Hg²⁺ can quench the emission intensity accompanied by a slight blue shift. By comparison of the selectivity in this group, we can demonstrate a structure-dependent selectivity in MeCN: the binding pocket formed between benzothiadiazole and 1,4-substituted triazole shows moderate binding selectivity to Ni²⁺, Cu²⁺, Co²⁺ and Hg²⁺, independent on the number of binding pockets; however, when the preorganized structure is destroyed in **Benzo-5**, the sole triazole moiety shows selective response to Hg²⁺ (Figure 3-57), in accordance with our previous results presented in the last three sections.

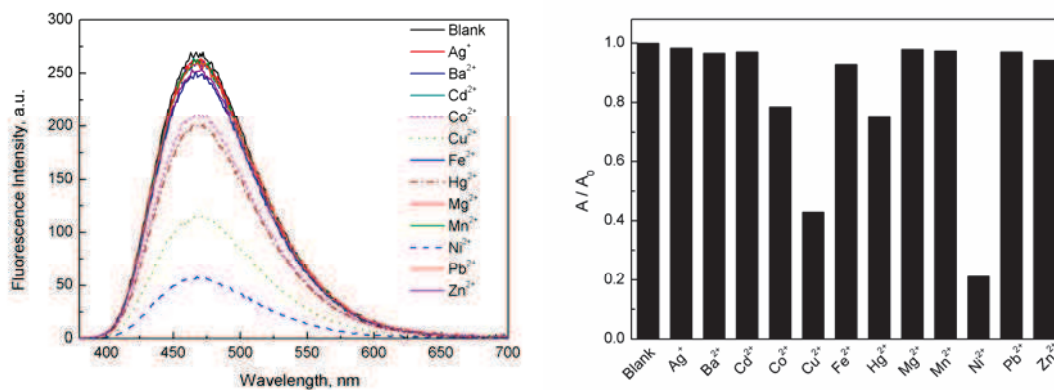


Figure 3-55. Fluorescence spectra of **Benzo-1** in the presence of various metal ions in MeCN; [**Benzo-1**] = 10 μ M, $[M^{n+}] = 0.2$ mM, $\lambda_{ex} = 361$ nm.

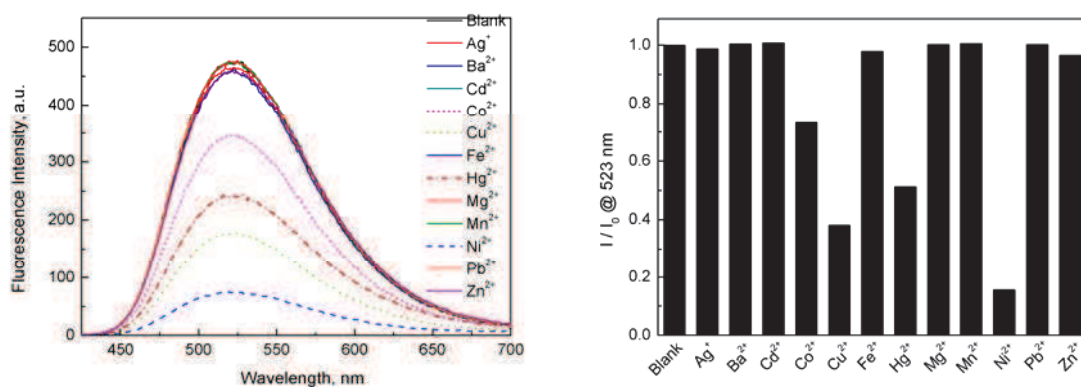


Figure 3-56. Fluorescence spectra of **Benzo-2** in the presence of various metal ions in MeCN; [**Benzo-2**] = 10 μ M, $[M^{n+}] = 0.2$ mM, $\lambda_{ex} = 400$ nm.

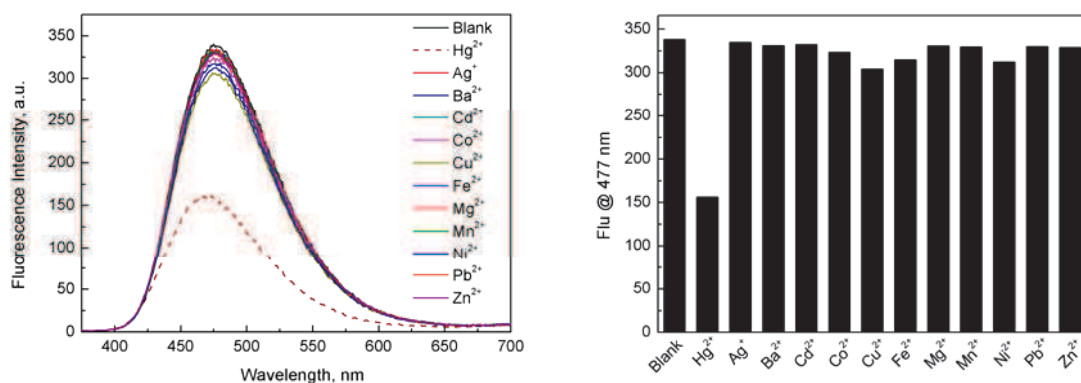


Figure 3-57. Fluorescence spectra of **Benzo-5** in the presence of various metal ions in MeCN; [**Benzo-5**] = 10 μ M, $[M^{n+}] = 0.2$ mM, $\lambda_{ex} = 355$ nm.

Considering the possibility of formation of intramolecular hydrogen bond between triazole and the short arm alanine, **Benzo-3** and **Benzo-4** with partially deprotected alanine were subjected to selectivity screening. As shown in Figure 3-58, **Benzo-3** shows almost the same selectivity as that of **Benzo-2**. Only the addition of Ni^{2+} , Hg^{2+} , Cu^{2+} and Co^{2+} quenches the fluorescence emission. The difference between **Benzo-2** and **Benzo-3** is the quenching ability of Hg^{2+} which shows stronger quenching effect on **Benzo-3**. In contrast, the complexation properties of **Benzo-4**, as presented in Figure 3-59, are more complicated than **Benzo-3**. Beside fluorescence quenching caused by Ni^{2+} , Hg^{2+} , Cu^{2+} and Co^{2+} , the addition of Ag^+ and Fe^{2+} can induce fluorescence enhancement. Anyway, participation of carboxylic acid function to the complexation helps to increase the binding ability to Ni^{2+} and Hg^{2+} as inferred from the stronger fluorescence quenching observed for **Benzo-4**, but reduces meanwhile its selectivity. Therefore, selectivity of **Benzo-x** relies mainly on the preorganized structure and terminal amino acid group is an auxiliary binding site.

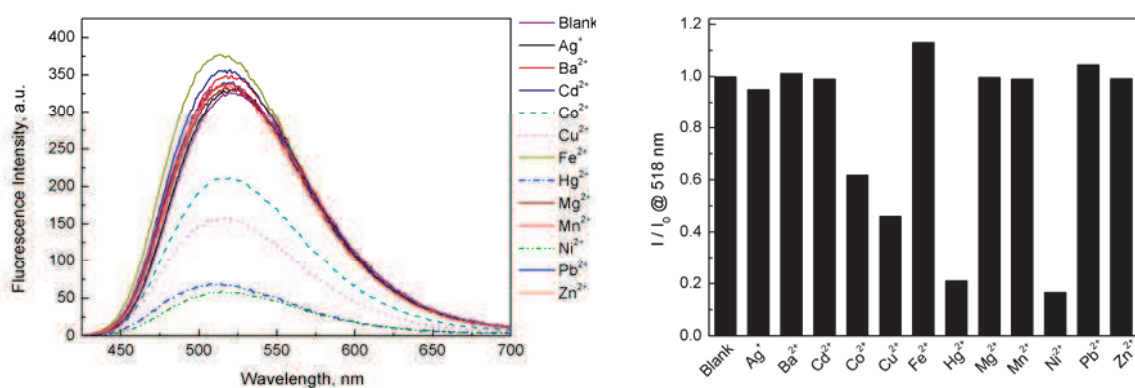


Figure 3-58. Fluorescence spectra of **Benzo-3** in the presence of various metal ions in MeCN; [**Benzo-3**] = 10 μM , $[\text{M}^{\text{n}+}] = 0.2 \text{ mM}$, $\lambda_{\text{ex}} = 400 \text{ nm}$.

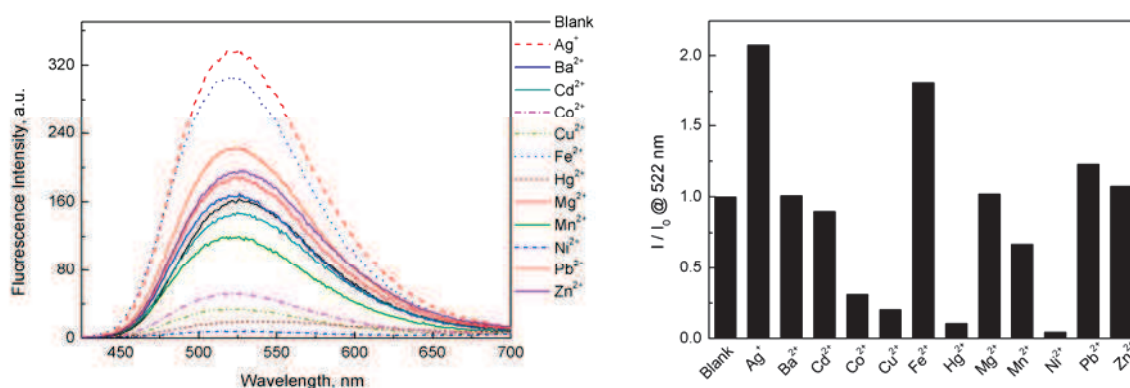


Figure 3-59. Fluorescence spectra of **Benzo-4** in the presence of various metal ions in MeCN; [**Benzo-4**] = 10 μM , $[\text{M}^{\text{n}+}] = 0.2 \text{ mM}$, $\lambda_{\text{ex}} = 405 \text{ nm}$.

The minor contribution of amino acid moiety can be further confirmed by metallo-responsive properties of **Benzo-9**, with more rigid phenylalanine to prevent the co-binding of amino acid group with benzothiadiazole-triazole. As shown in Figure 3-60, **Benzo-9** exhibits the same selectivity as that of **Benzo-1**, however, with lower sensing sensitivity as inferred from the fluorescence quenching percentage.

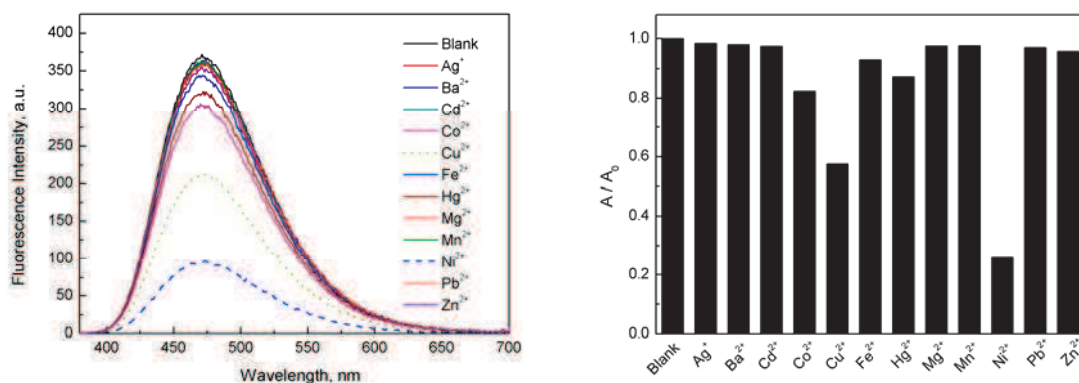


Figure 3-60. Fluorescence spectra of **Benzo-9** in the presence of various metal ions in MeCN; [**Benzo-9**] = 10 μ M, $[M^{n+}] = 0.2$ mM, $\lambda_{\text{ex}} = 361$ nm.

3.5.4.2. Spectral titration of **Benzo-x** series with Cu^{2+} , Hg^{2+} and Ni^{2+}

Spectral titrations were carried out to get insight into the binding process between **Benzo-x** and metal ions. Based on the selectivity screening results, Cu^{2+} , Hg^{2+} and Ni^{2+} were selected as the target cations.

Figure 3-61 presents the evolution of absorption and fluorescence spectra of **Benzo-1** in the presence of increasing concentrations of Cu^{2+} . With the gradual addition of Cu^{2+} , absorption band lower than 300 nm increases dramatically which extends to the main absorption band of **Benzo-1** lying in the range over 350 nm. This leads to the difficulty in identifying the evolution of absorption band at 360 nm. However, it is clear that the addition of Cu^{2+} reduces gradually the fluorescence intensity, with 73% quenched at 0.4 mM. Titration of **Benzo-1** with Hg^{2+} was carried out under same conditions, as shown in Figure 3-62. Only 25% fluorescence intensity is quenched after addition of 0.2 mM Hg^{2+} . Ni^{2+} shows the most remarkable influence on its spectra (Figure 3-63). Upon full complexation with Ni^{2+} , the absorption titration spectra display a 5 nm red shift and about 85% emission intensity is quenched at 0.4 mM Ni^{2+} . Several clear isobestic points were observed during the absorption titration, indicating the interconversion of the free ligand and the bound complex. Non linear regression analysis of the titrations with Cu^{2+} and Ni^{2+} , as presented in Table 3-7, demonstrates that **Benzo-1** shows stronger binding ability to Ni^{2+} ($\log K = 4.30$) than Cu^{2+}

($\log K = 3.77$), which might be related to the size match between metal ions and the preorganized binding pocket. This binding affinity for Ni^{2+} is in the same range as that of compound **40b** ($\log K = 4.48$, Figure 2-9, Chapter 2).⁴⁷ **Benzo-9** with a more rigid terminal amino acid moiety shows the similar binding ability to the three tested metal ions, as depicted in Figures 3-64 to 3-66 and Table 3-7.

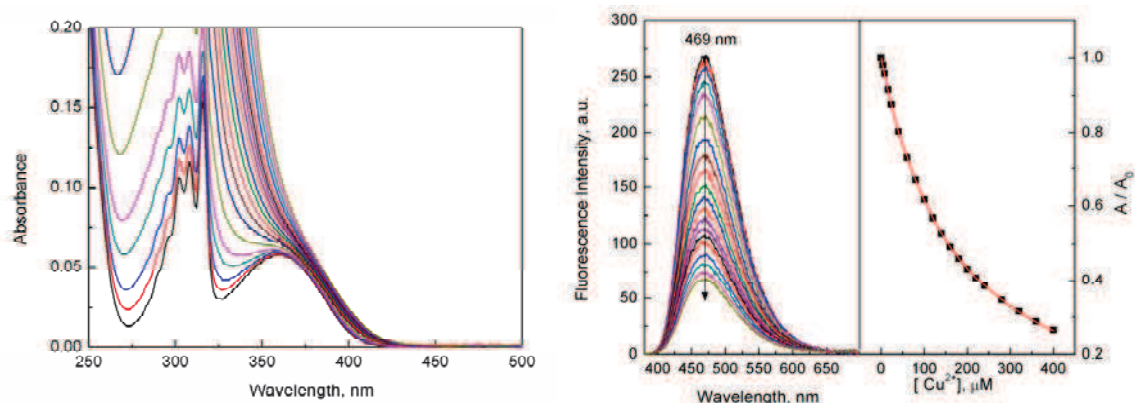


Figure 3-61. Absorption and fluorescence spectra of **Benzo-1** in the presence of increasing concentrations of Cu^{2+} in MeCN; [**Benzo-1**] = 10 μM , $\lambda_{\text{ex}} = 360 \text{ nm}$.

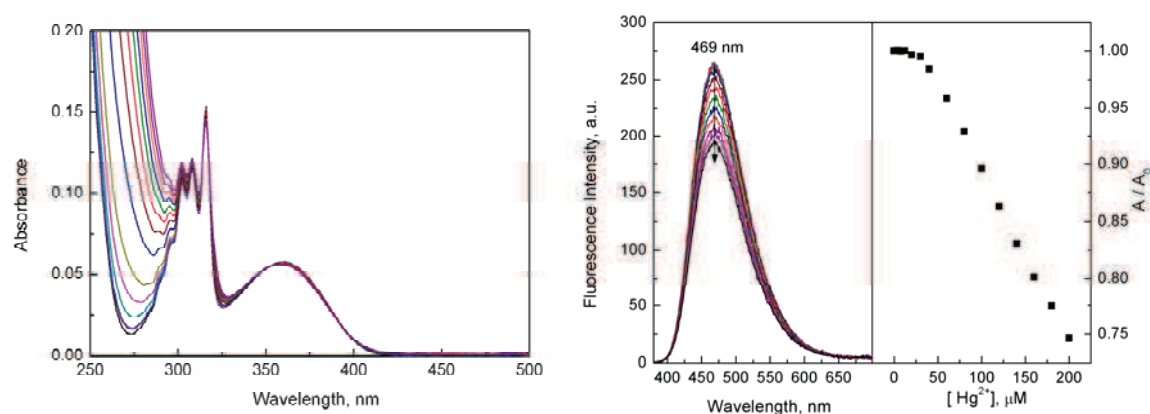


Figure 3-62. Absorption and fluorescence spectra of **Benzo-1** in the presence of increasing concentrations of Hg^{2+} in MeCN; [**Benzo-1**] = 10 μM , $\lambda_{\text{ex}} = 360 \text{ nm}$.

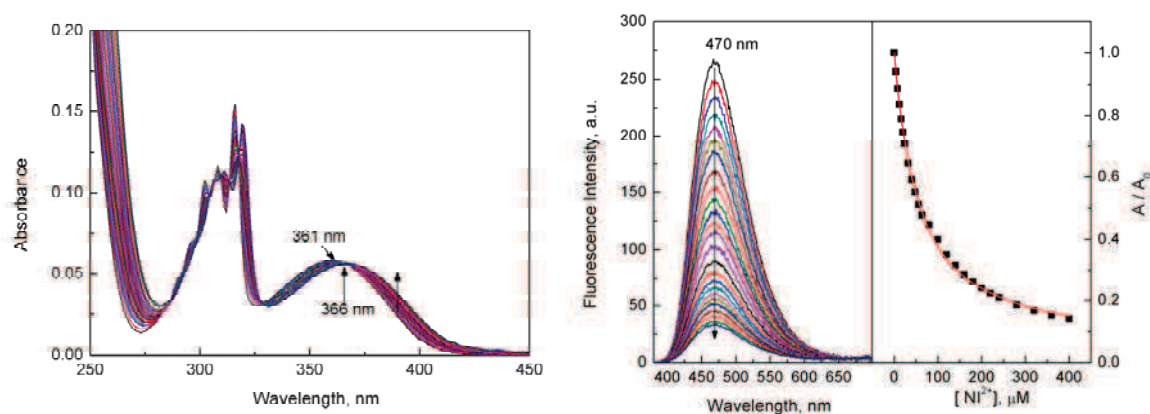


Figure 3-63. Absorption and fluorescence spectra of **Benzo-1** in the presence of increasing concentrations

of Ni^{2+} in MeCN; [**Benzo-1**] = 10 μM , λ_{ex} = 360 nm.

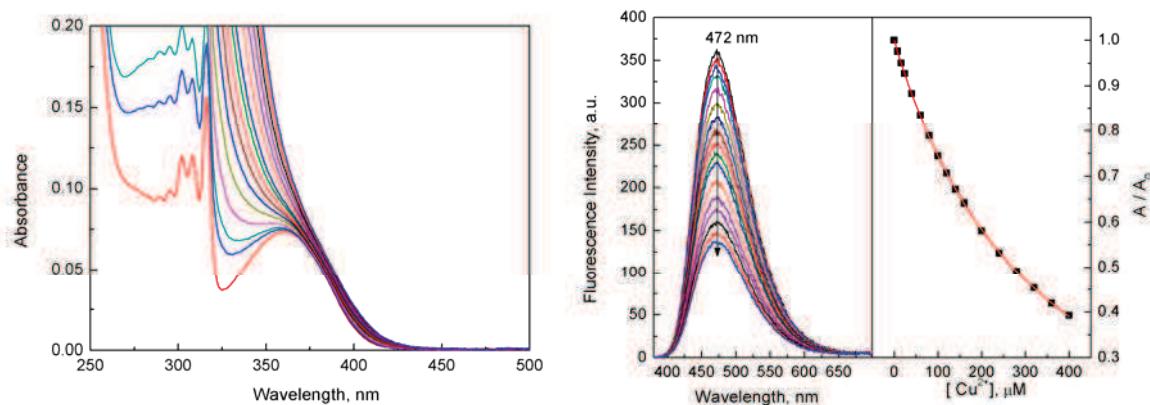


Figure 3-64. Absorption and fluorescence spectra of **Benzo-9** in the presence of increasing concentrations of Cu^{2+} in MeCN; [**Benzo-9**] = 10 μM , λ_{ex} = 360 nm.

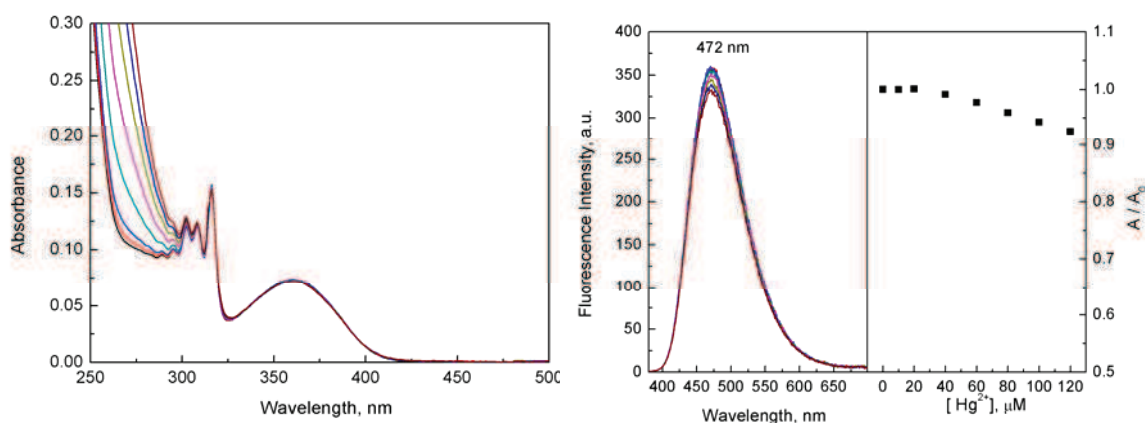


Figure 3-65. Absorption and fluorescence spectra of **Benzo-9** in the presence of increasing concentrations of Hg^{2+} in MeCN; [**Benzo-9**] = 10 μM , λ_{ex} = 360 nm.

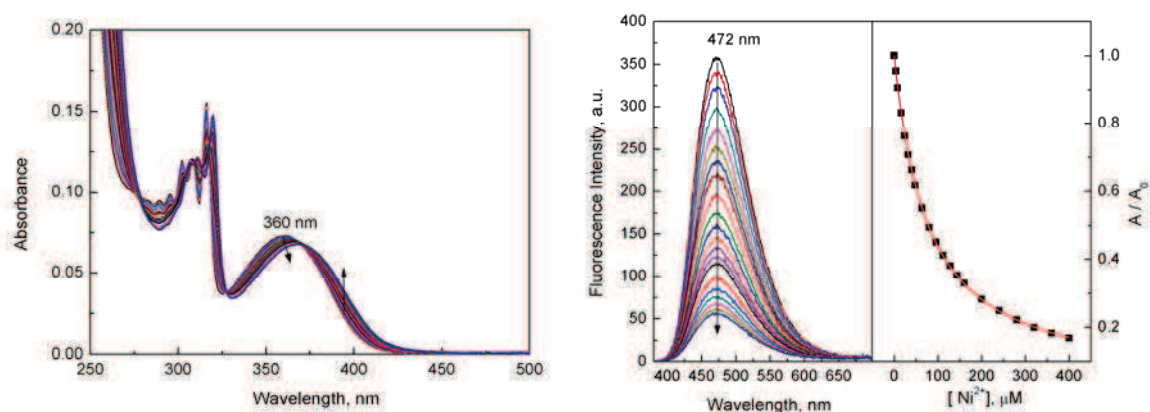


Figure 3-66. Absorption and fluorescence spectra of **Benzo-9** in the presence of increasing concentrations of Ni^{2+} in MeCN; [**Benzo-9**] = 10 μM , λ_{ex} = 360 nm.

Log K	Cu^{2+}	Ni^{2+}
Benzo-1	3.77 ± 0.004	4.30 ± 0.01
Benzo-2	3.93 ± 0.004	4.46 ± 0.01
Benzo-9	3.47 ± 0.01	4.16 ± 0.003

Table 3-7. Binding constants of **Benzo-1** and **Benzo-2** with Cu^{2+} and Ni^{2+} in MeCN.

Spectral titrations of **Benzo-2** with Cu^{2+} , Hg^{2+} and Ni^{2+} were carried out in MeCN. Figure 3-67 depicts the evolutions of absorption and fluorescence spectra in the presence of increasing concentrations of Cu^{2+} . With increasing concentrations of Cu^{2+} , absorption of **Benzo-2** at 402 nm decreases and a new band centered at 417 nm appears, accompanied with a well-defined isosbestic point. Meanwhile, its fluorescence intensity is gradually quenched. As shown in Figure 3-69, Ni^{2+} shows quite similar influence on the spectral properties of **Benzo-2** as that of Cu^{2+} . In contrast, the addition of Hg^{2+} only induced minor decrease of absorbance at 402 nm, accompanied by a less efficient fluorescence quenching (Figure 3-68). Non-linear regression analysis of the fluorescence titrations based on 1:1 binding stoichiometry gave us the binding constants: $\log K = 3.93$ for Cu^{2+} and $\log K = 4.46$ for Ni^{2+} , as shown in Table 3-7. By comparison of the binding constants of different ligands (**Benzo-1**, **Benzo-2** and **Benzo-9**) in Table 3-7, we can demonstrate that the binding ability of **Benzo-x** to metal ions mainly depends on the binding pocket, whereas it's almost independent on the number of separated binding sites and protected terminal amino acid moiety.

We further investigated how deprotected terminal amino acid moieties affected the binding processes. **Benzo-3** with protonated amino group and methyl protected carboxylic acid group was also tested with Cu^{2+} , Hg^{2+} and Ni^{2+} in MeCN (Figures 3-70 to 3-72). In the case of Cu^{2+} , there is a slight decrease of absorbance at 402 nm with an isosbestic point at 432 nm while fluorescence titration reaches the equilibrium at 1 equiv with ca. 43% fluorescence quenching. In the presence of Hg^{2+} , a hypsochromic shift of the absorption band from 402 to 390 nm was observed and fluorescence titration shows that it reaches equilibrium at about 2 equiv, resulting in 78% fluorescence quenching and a blue shift from 520 to 509 nm. Ni^{2+} shows a similar influence on **Benzo-3** as that of Cu^{2+} , however, with a stronger fluorescence quenching effect.

Benzo-4 contains free carboxylic acid and amino group protected by Boc group. Its spectral responses to Cu^{2+} , Hg^{2+} and Ni^{2+} were similarly carried out in MeCN. As shown in Figure 3-73 and Figure 3-75, addition of Ni^{2+} or Cu^{2+} gradually quenches the emission of **Benzo-4**. Worthy

of notice is that the addition of Hg^{2+} exerts quite different impact on its spectral properties (Figure 3-74). When the concentration of Hg^{2+} is lower than 0.5 equiv, it results in fluorescence enhancement; however, when it exceeds 0.5 equiv, addition of Hg^{2+} dramatically quench the fluorescence intensity.

From the above results, we can conclude that amino acid moiety is not the crucial binding site for metal ions, but the free carboxylic acid or amino group will affect the binding ability, especially for Hg^{2+} .

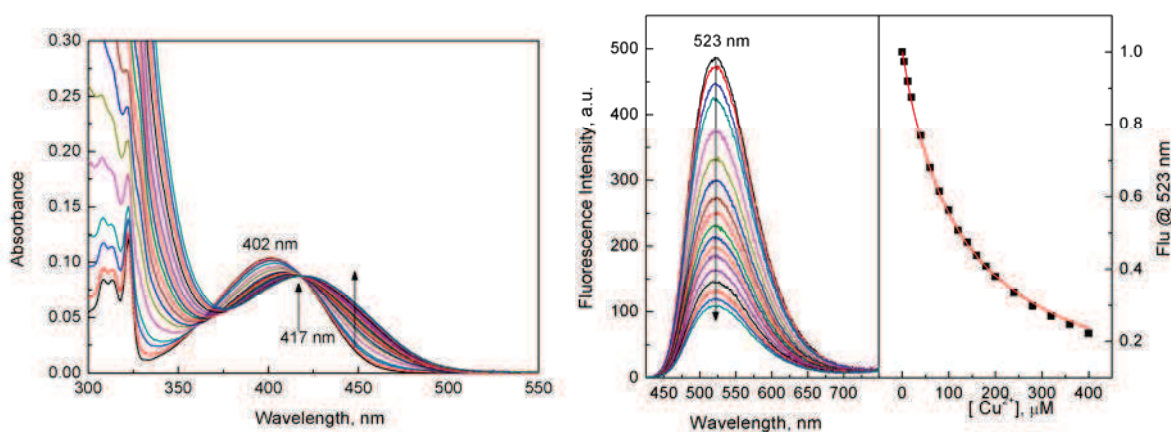


Figure 3-67. Absorption and fluorescence spectra of **Benzo-2** in the presence of increasing concentrations of Cu^{2+} in MeCN; [**Benzo-2**] = 10 μM , λ_{ex} = 400 nm.

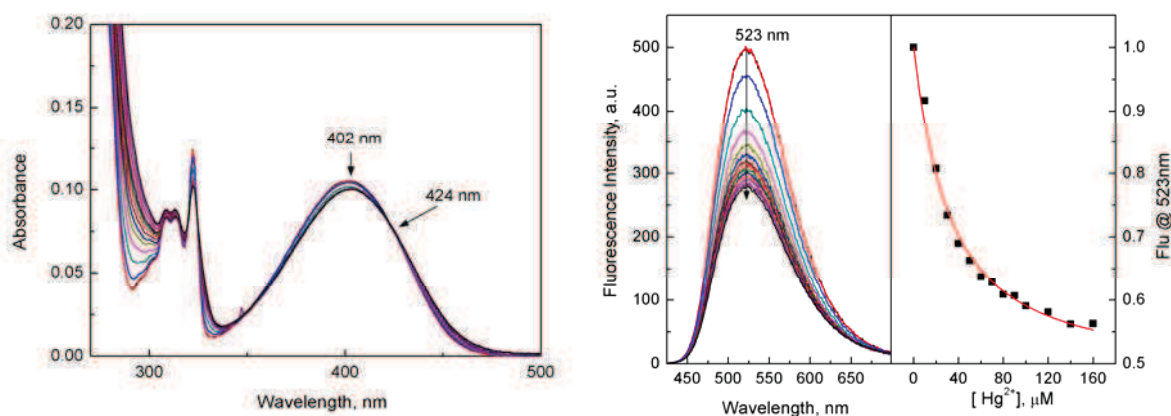


Figure 3-68. Absorption and fluorescence spectra of **Benzo-2** in the presence of increasing concentrations of Hg^{2+} in MeCN; [**Benzo-2**] = 10 μM , λ_{ex} = 400 nm.

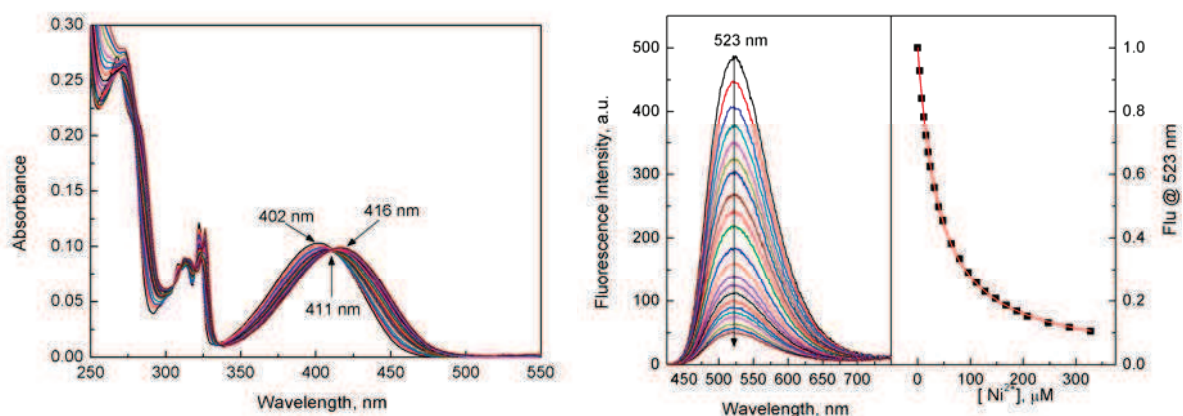


Figure 3-69. Absorption and fluorescence spectra of **Benzo-2** in the presence of increasing concentrations of Ni^{2+} in MeCN; $[\text{Benzo-2}] = 10 \mu\text{M}$, $\lambda_{\text{ex}} = 400 \text{ nm}$.

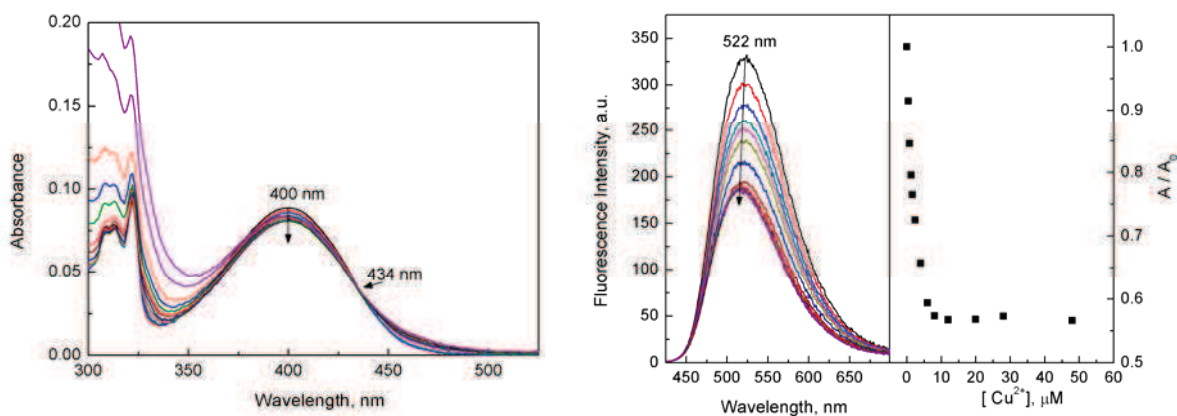


Figure 3-70. Absorption and fluorescence spectra of **Benzo-3** in the presence of increasing concentrations of Cu^{2+} in MeCN; $[\text{Benzo-3}] = 10 \mu\text{M}$, $\lambda_{\text{ex}} = 400 \text{ nm}$.

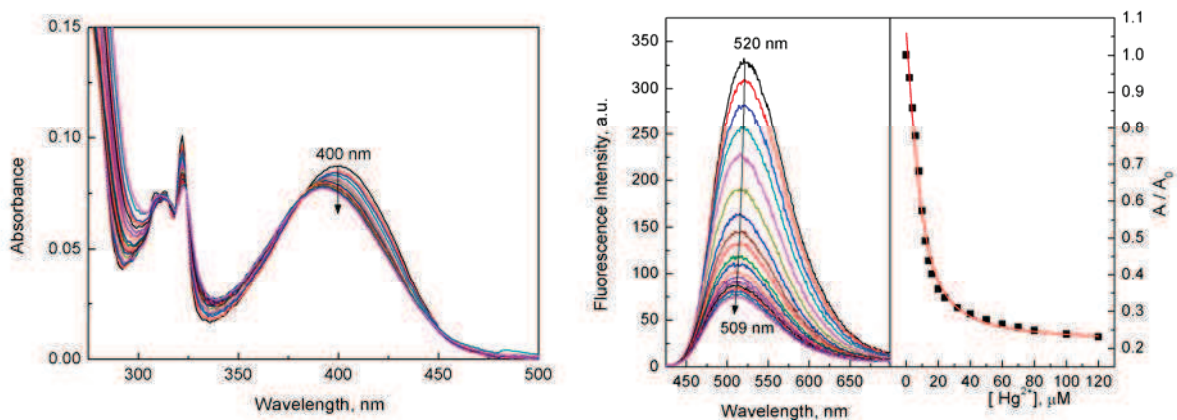


Figure 3-71. Absorption and fluorescence spectra of **Benzo-3** in the presence of increasing concentrations of Hg^{2+} in MeCN; $[\text{Benzo-3}] = 10 \mu\text{M}$, $\lambda_{\text{ex}} = 400 \text{ nm}$.

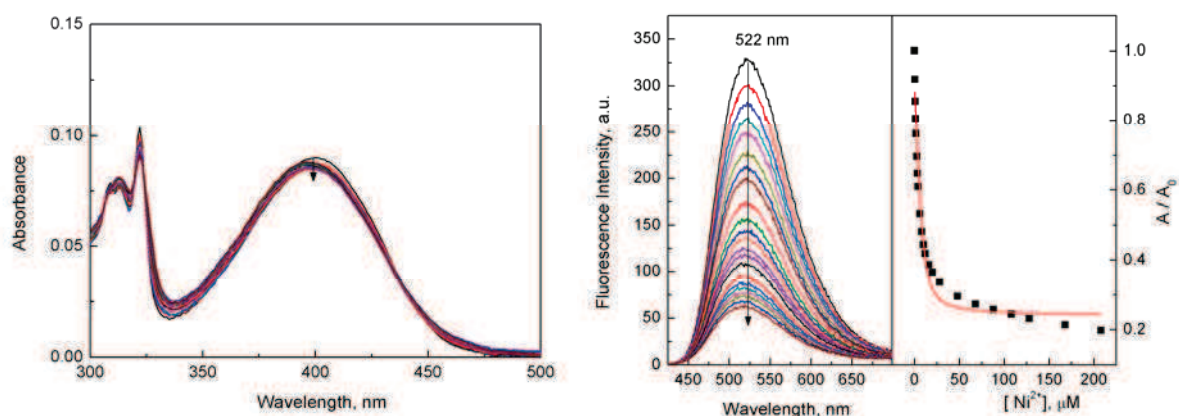


Figure 3-72. Absorption and fluorescence spectra of **Benzo-3** in the presence of increasing concentrations of Ni^{2+} in MeCN; $[\text{Benzo-3}] = 10 \mu\text{M}$, $\lambda_{\text{ex}} = 400 \text{ nm}$.

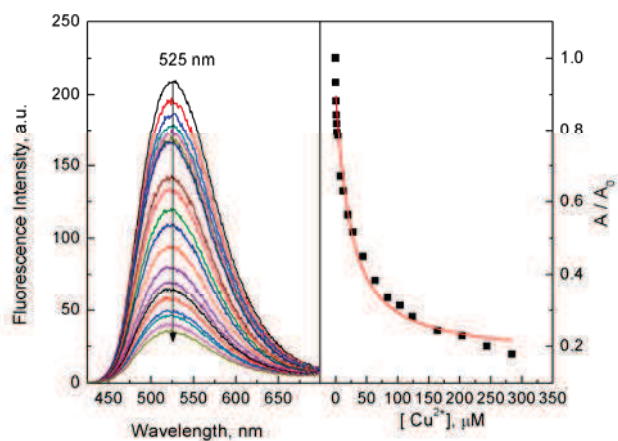


Figure 3-73. Fluorescence spectra of **Benzo-4** in the presence of increasing concentrations of Cu^{2+} in MeCN; $[\text{Benzo-4}] = 10 \mu\text{M}$, $\lambda_{\text{ex}} = 405 \text{ nm}$.

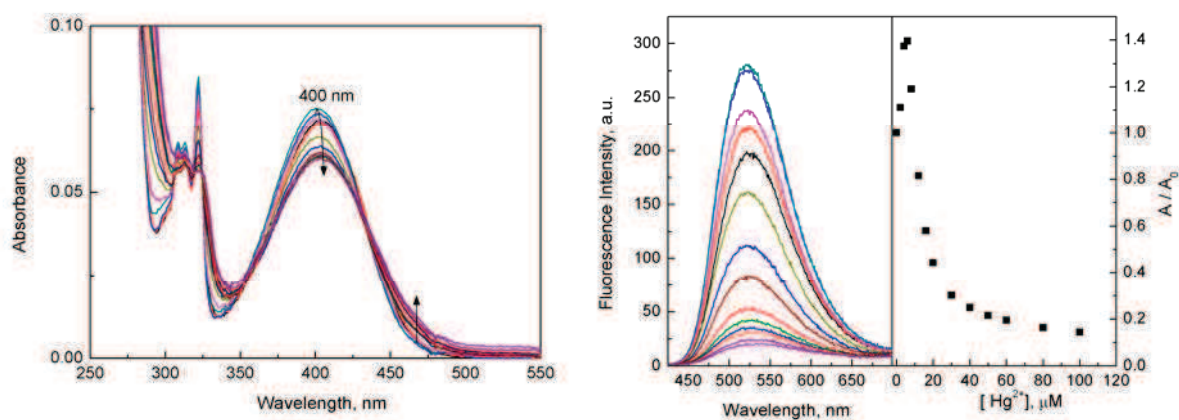


Figure 3-74. Absorption and fluorescence spectra of **Benzo-4** in the presence of increasing concentrations of Hg^{2+} in MeCN; $[\text{Benzo-4}] = 10 \mu\text{M}$, $\lambda_{\text{ex}} = 405 \text{ nm}$.

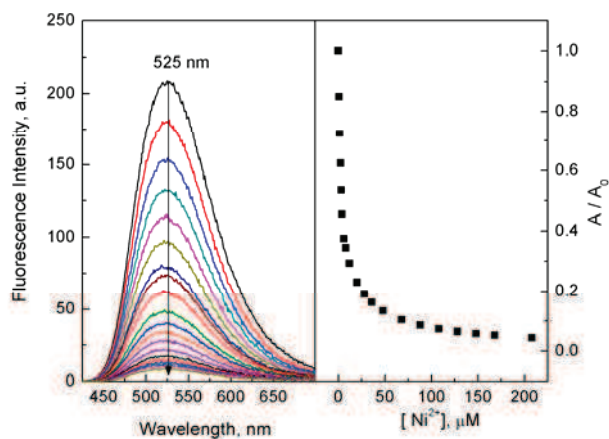


Figure 3-75. Fluorescence spectra of **Benzo-4** in the presence of increasing concentrations of Ni^{2+} in MeCN; $[\text{Benzo-4}] = 10 \mu\text{M}$, $\lambda_{\text{ex}} = 405 \text{ nm}$.

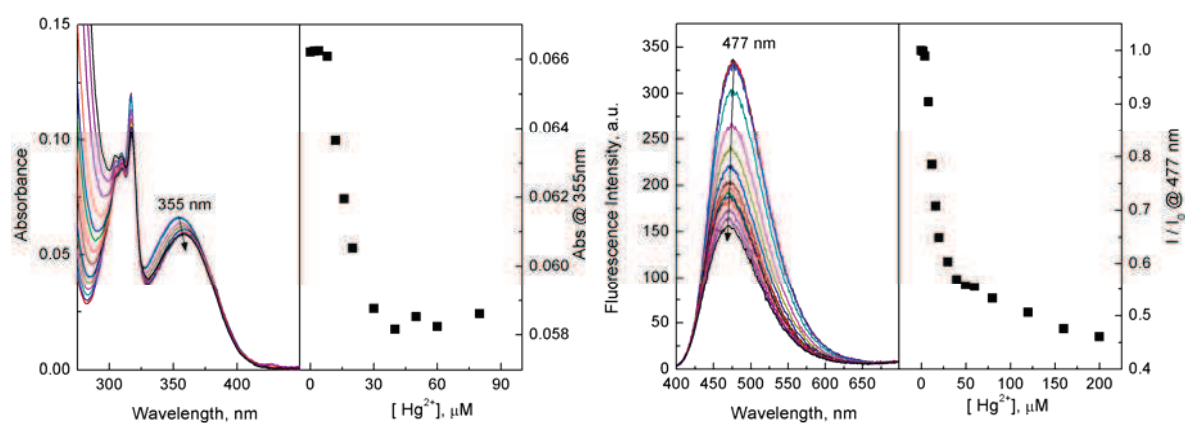


Figure 3-76. Absorption and fluorescence spectra of **Benzo-5** in the presence of increasing concentrations of Hg^{2+} in MeCN; $[\text{Benzo-5}] = 10 \mu\text{M}$, $\lambda_{\text{ex}} = 355 \text{ nm}$.

For the selective response of **Benzo-5** to Hg^{2+} in MeCN, the spectral titration to Hg^{2+} was performed in MeCN. As displayed in Figure 3-76, with the increasing concentrations of Hg^{2+} , the absorbance at 355 nm decreases, accompanying by a slight red shift about 3 nm. Correspondingly, fluorescence quenching and slight blue shift from 477 to 473 nm are observed with increasing concentration of Hg^{2+} . It's worthy of notice that fluorescence quenching commenced with $5 \mu\text{M}$ Hg^{2+} and the further addition of Hg^{2+} leads to 55% fluorescence quenching. The absence of preorganization in 1,5-disubstituted triazole stereoisomer leads to the loss of the cooperative coordination interaction. In this case, the selectivity and sensitivity of **Benzo-5** is dependent on triazole group but not benzothiadiazole.

Based on the results of **Benzo-x** series in organic medium, **Benzo-8** was explored as a chemosensor for Cu^{2+} for the following considerations: firstly, incorporation of two triazoles endows the excitation and emission wavelength in the visible regions; secondly, replacement of the rigid amino group by long flexible lysine may provides additional binding sites; thirdly, deprotection of the protected carbonyl group may facilitate the assay in water. A detailed investigation on **Benzo-8** was carried out as follows.

Benzothiadiazole has been well known for its strong electron-withdrawing character and modulation of its chemical environment would easily change its spectral properties.⁵⁹ It's assumed that in **Benzo-8** an intramolecular charge transfer from triazole to benzothiadiazole occurs. Solvatochromism of **Benzo-8** was thus investigated in different solvents, as shown in Figure 3-77. Its absorption bands show a slight blue shift with increasing solvent polarity (negative solvatochromism) and especially remarkable in protic solvents like CH_3OH and H_2O . But its emissive bands almost keep unchanged except a red shift in H_2O . This might be attributed to intermolecular hydrogen bonding interaction between solvent and solute and different electronic transition states for the absorption and fluorescence.

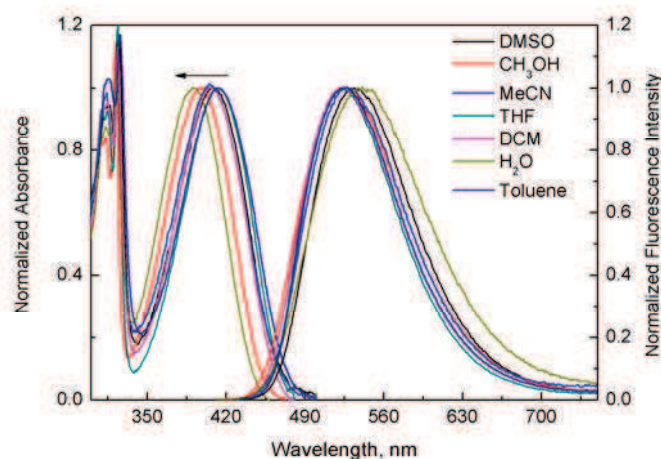


Figure 3-77. Normalized absorption and fluorescence spectra of **Benzo-8** in different solvents.

Selectivity of **Benzo-8** to metal ions was examined in MeCN. As shown in Figure 3-86, very similar to that of **Benzo-4**, remarkable fluorescence quenching is observed in the presence of Ni^{2+} , Cu^{2+} , Hg^{2+} , and Co^{2+} . Except Ag^+ , other metal ions slightly quench its fluorescence intensity. Spectral titrations with Cu^{2+} , Hg^{2+} , and Ni^{2+} in MeCN (Figures 3-79 to 3-81) demonstrate that the long armed terminal amino acid does not affect significantly the binding process.

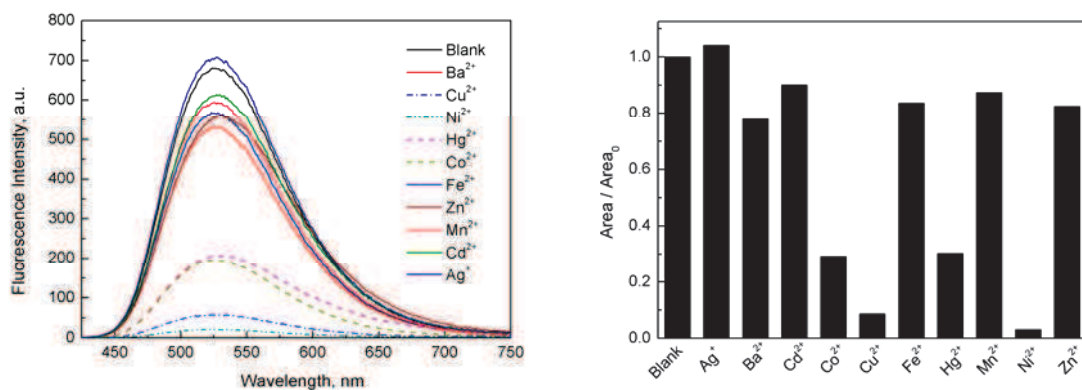


Figure 3-78. Fluorescence spectra of **Benzo-8** in the presence of various metal ions in MeCN; [**Benzo-8**] = 10 μ M, $[M^{n+}] = 0.2$ mM, $\lambda_{\text{ex}} = 405$ nm

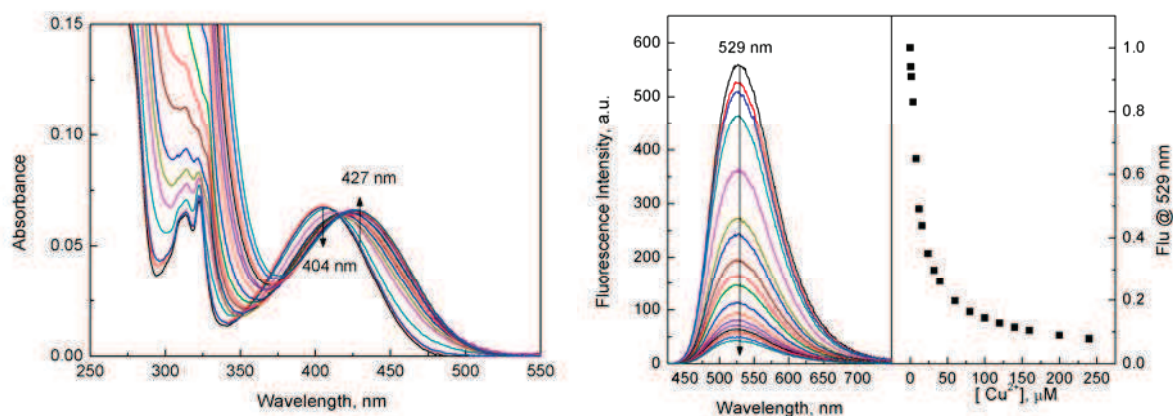


Figure 3-79. Absorption and fluorescence spectra of **Benzo-8** in the presence of increasing concentrations of Cu^{2+} in MeCN; [**Benzo-8**] = 10 μ M, $\lambda_{\text{ex}} = 406$ nm.

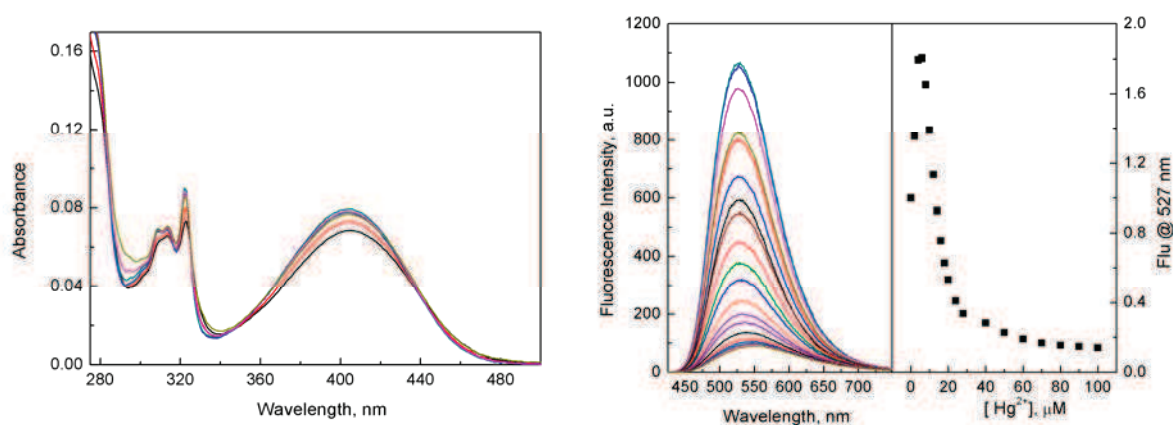


Figure 3-80. Absorption and fluorescence spectra of **Benzo-8** in the presence of increasing concentrations of Hg^{2+} in MeCN; [**Benzo-8**] = 10 μ M, $\lambda_{\text{ex}} = 406$ nm.

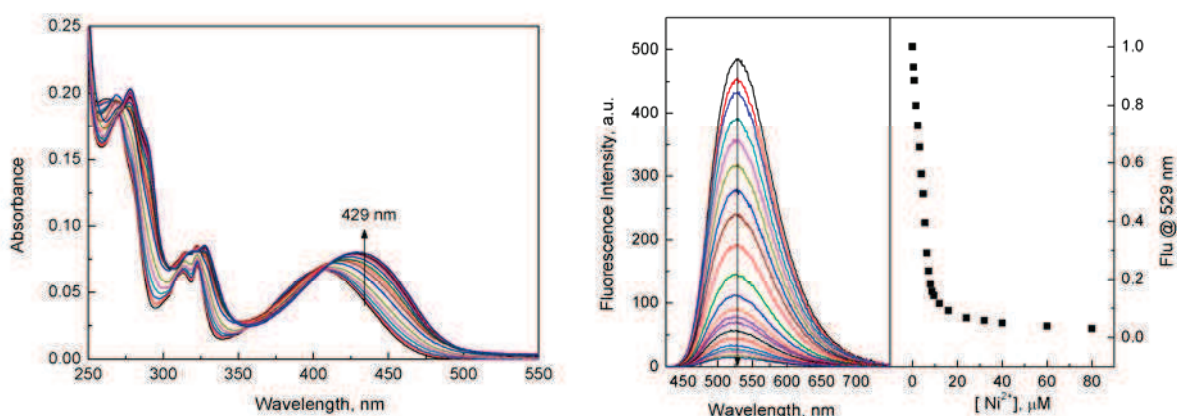


Figure 3-81. Absorption and fluorescence spectra of **Benzo-8** in the presence of increasing concentrations of Ni^{2+} in MeCN; $[\text{Benzo-8}] = 10 \mu\text{M}$, $\lambda_{\text{ex}} = 406 \text{ nm}$.

Considering the practical applications of chemosensors and solvent medium dependent selectivity, we further investigated fluorescence changes of **Benzo-8** in the presence of 20 equiv of selected cations in HEPES buffer solution at pH 7.4. As presented in Figure 3-82 (left), the fluorescence intensity was not affected by Hg^{2+} , Mn^{2+} , Mg^{2+} , Ba^{2+} , Cd^{2+} , Co^{2+} , Zn^{2+} and Pb^{2+} , and slightly quenched by Fe^{2+} , Ag^+ and Ni^{2+} . In contrast, a significant quenching towards Cu^{2+} was observed. The selectivity of **Benzo-8** towards Cu^{2+} was further ascertained by the competition experiment by adding 20 equiv of Cu^{2+} ion to the competing metal ion-ligand mixtures, where the emission was quenched as that in the presence of Cu^{2+} alone (Figure 3-82 (right)). The significantly improved selectivity observed for **Benzo-8** in HEPES buffer solution when compared with that in MeCN, indicates that the selectivity of **Benzo-8** is closely related to solvent medium, which may change both the conformation of the ligand and the metal ions solvation. Additionally, the flexible lysine group in **Benzo-8** may participate into complexation to increase its binding ability to Cu^{2+} by their cooperativity.

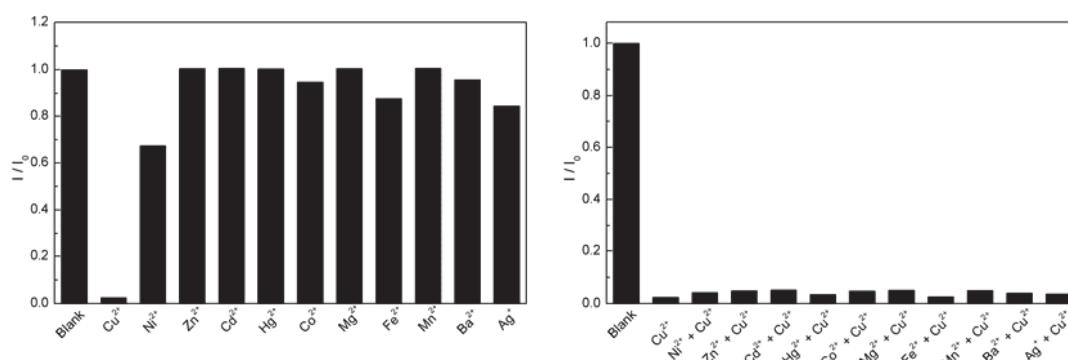


Figure 3-82. Fluorescence intensity change profiles of **Benzo-8** in HEPES buffer solution at pH 7.4 with selected cations in the presence and absence of Cu^{2+} . $[\text{Benzo-8}] = 10 \mu\text{M}$, $[\text{M}^{n+}] = 0.2 \text{ mM}$, $\lambda_{\text{ex}} = 391 \text{ nm}$.

Our previous results have shown that triazole and benzothiadiazole both contributed to the coordination interaction with metal ions. Since the potential binding sites of the nitrogen-containing compounds could be protonated under acidic condition and result in changes of the photophysical properties and binding ability with metal ions, we firstly investigated the pH effect on the free ligand **Benzo-8**. As shown in Figure 3-83, with increasing pH values from 3.2 to 6.2, the absorption of **Benzo-8** shifted from 404 to 392 nm, concomitantly with an enhanced and red-shift emission band from 529 to 552 nm. When the pH value was higher than 6.2, its spectra keep unchanged.

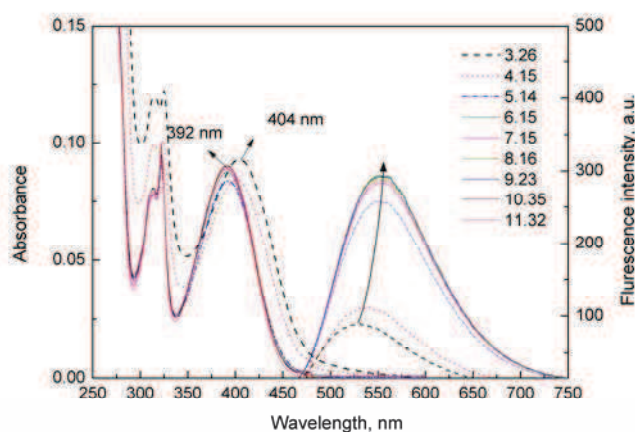


Figure 3-83. Absorption and fluorescence spectra of **Benzo-8** in HEPES solution at different pH. [**Benzo-8**] = 10 μ M, [HEPES] = 10 mM, fluorescence spectra were excited at the maximum absorption wavelength.

The spectral response of **Benzo-8** to Cu^{2+} was tested under different pH conditions. The results in Figure 3-84 demonstrates that at neutral condition, **Benzo-8** showed the most remarkable change before and after addition of 20 equiv Cu^{2+} . This result was explained that under acidic condition, nitrogen atoms could be partially protonated which then prevented the binding between ligand and Cu^{2+} ; while at higher pH, OH^- might compete with ligand **Benzo-8** to bind Cu^{2+} .

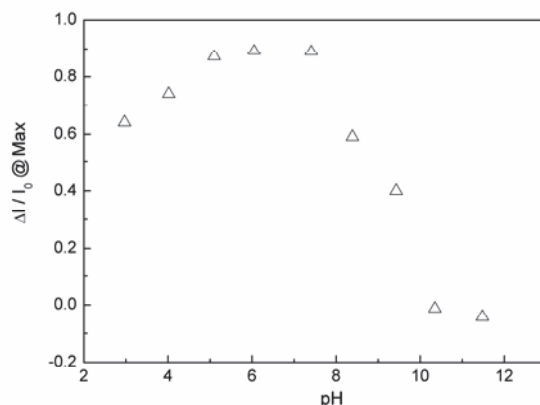


Figure 3-84. The pH effect on the fluorescence response of **Benzo-8** to Cu^{2+} at maximum emission wavelengths in HEPES (10 mM) solution. $[\text{Benzo-8}] = 10 \mu\text{M}$, $[\text{Cu}^{2+}] = 0.2 \text{ mM}$.

According to the pH effect on binding response of **Benzo-8** to Cu^{2+} , spectral titrations of **Benzo-8** with Cu^{2+} were performed in HEPES buffer solution at pH 7.4. As shown in Figure 3-85, with increasing concentration of Cu^{2+} , the absorption band at 391 nm gradually decreases and undergoes a red shift to 418 nm. Meanwhile, a clear isosbestic point at 418 nm was observed which indicated the formation of complex between Cu^{2+} and **Benzo-8**. Fluorescence titration (Figure 3-86) shows that initial addition of Cu^{2+} (concentration lower than 2 equiv), the fluorescence intensity at 542 nm decreased slowly. However, quenching efficiency is enhanced after 2 equiv of Cu^{2+} and it reaches a plateau at 10 equiv. Anyhow, 20 μM Cu^{2+} can quench about 12% fluorescence intensity, which meets with the limit of 20 μM defined by U.S. Environmental Protection Agency.

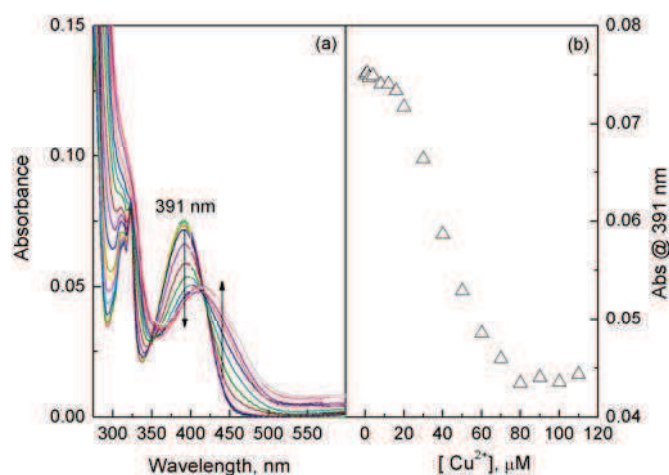


Figure 3-85. (a) Absorption spectra of **Benzo-8** with increasing concentration of Cu^{2+} in HEPES buffer at pH 7.4; (b) plot of absorbance at 391 nm versus Cu^{2+} concentration. $[\text{Benzo-8}] = 10 \mu\text{M}$.

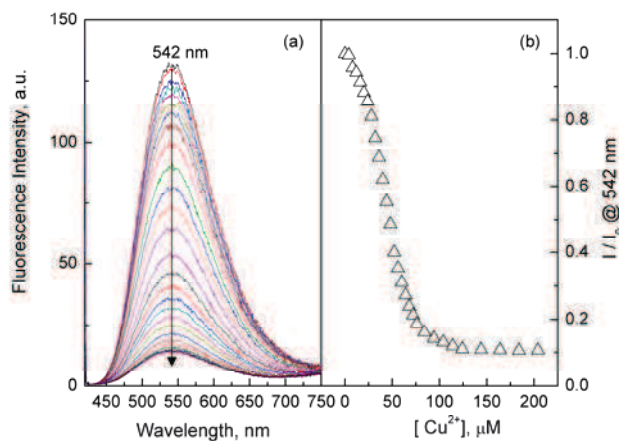


Figure 3-86. (a) Fluorescence spectra of **Benzo-8** with increasing concentration of Cu²⁺ in HEPES buffer at pH 7.4; (b) plot of fluorescence intensity at 542 nm versus Cu²⁺ concentration. [**Benzo-8**] = 10 μM, λ_{ex} = 418 nm.

3.5.5. Conclusion

Systematic investigations on **Benzo-x** derivatives have allowed elucidating the functions of triazole in chemosensors. Firstly, we find that 1,2,3-triazole can be a good selection of auxiliary chromophore. When incorporated into some aromatic chromophores, the spectral properties of the resultant conjugated system are closely related to the number of triazole and the position of the substituents. Especially, incorporation of 1,4-disubstituted 1,2,3-triazole group with benzothiadiazole extended aromatic conjugation system and resulted in the longer excitation and emission wavelengths while keeping high fluorescence quantum yields. Secondly, examination on the selectivity of **Benzo-x** towards metal ions in MeCN demonstrated that preorganized structure between benzothiadiazole and 1,4-disubstituted 1,2,3-triazole mainly determined metallo-responsive properties. In MeCN, 1,4-disubstituted **Benzo-x** series consistently exhibited binding ability to Ni²⁺, Cu²⁺, Hg²⁺ and Co²⁺. The terminal amino acid moiety only slightly affected the affinity of the binding pocket to metal ions. When the preorganized structure is destroyed, as in the stereoisomer with 1,5-disubstituted triazole, **Benzo-5** shows selective response only to Hg²⁺ but no affinity to Ni²⁺, Cu²⁺, and Co²⁺. Detailed spectral titrations confirmed the crucial role of preorganized structure in **Benzo-x** series. Finally, it's worthy of notice that a new ligand **Benzo-8** was successfully explored as a highly selective chemosensor of Cu²⁺ in HEPES buffer solution under physiological pH condition. The high selectivity of **Benzo-8** towards Cu²⁺ was contributed by selection of solvent medium, cooperativity of the binding pocket and terminal flexible amino acid moiety. Future work on mechanical calculations can be carried out to have more solid information for rational design of fluorescent chemosensors based on triazole

moiety. Moreover, due to the high efficiency of Cu(I)-catalyzed alkyne-azide cycloaddition, it allows us to obtain library synthesis for an optimal selection.

References

- [1] Vallee, B. L.; Ulmer, D. D. "Biochemical Effects of Mercury, Cadmium, and Lead." Annual Review of Biochemistry **1972**, *41*, 91-128.
- [2] Nolan, E. M.; Lippard, S. J. "Tools and tactics for the optical detection of mercuric ion." Chemical Reviews **2008**, *108*, 3443-3480.
- [3] Kim, H. N.; Lee, M. H.; Kim, H. J.; Kim, J. S.; Yoon, J. "A new trend in rhodamine-based chemosensors: application of spiro lactam ring-opening to sensing ions." Chemical Society Reviews **2008**, *37*, 1465-1472.
- [4] Liu, J.; Lu, Y. "Rational design of "Turn-On" allosteric DNzyme catalytic beacons for aqueous mercury ions with ultrahigh sensitivity and selectivity." Angewandte Chemie-International Edition **2007**, *46*, 7587-7590.
- [5] Hollenstein, M.; Hipolito, C.; Lam, C.; Dietrich, D.; Perrin, D. M. "A highly selective DNzyme sensor for mercuric ions." Angewandte Chemie-International Edition **2008**, *47*, 4346-4350.
- [6] Lee, J. S.; Han, M. S.; Mirkin, C. A. "Colorimetric detection of mercuric ion (Hg^{2+}) in aqueous media using DNA-functionalized gold nanoparticles." Angewandte Chemie-International Edition **2007**, *46*, 4093-4096.
- [7] Huang, C. C.; Yang, Z.; Lee, K. H.; Chang, H. T. "Synthesis of highly fluorescent gold nanoparticles for sensing Mercury(II)." Angewandte Chemie-International Edition **2007**, *46*, 6824-6828.
- [8] White, B. R.; Liljestrand, H. M.; Holcombe, J. A. "A 'turn-on' FRET peptide sensor based on the mercury binding protein MerP." Analyst **2008**, *133*, 65-70.
- [9] Chen, P.; He, C. A. "A general strategy to convert the MerR family proteins into highly sensitive and selective fluorescent biosensors for metal ions." Journal of the American Chemical Society **2004**, *126*, 728-729.
- [10] Ren, X. S.; Xu, Q. H. "Highly Sensitive and Selective Detection of Mercury Ions by Using Oligonucleotides, DNA Intercalators, and Conjugated Polymers." Langmuir **2009**, *25*, 29-31.
- [11] Liu, X. F.; Tang, Y. L.; Wang, L. H.; Zhang, J.; Song, S. P.; Fan, C. H.; Wang, S. "Optical detection of mercury(II) in aqueous solutions by using conjugated polymers and label-free oligonucleotides." Advanced Materials **2007**, *19*, 1662-1662.
- [12] Stuchbury, T.; Shipton, M.; Norris, R.; Malthouse, J. P. G.; Brocklehurst, K.; Herbert, J. A. L.; Suschitzky, H. "Reporter Group Delivery System with Both Absolute and Selective Specificity for Thiol-Groups and an Improved Fluorescent-Probe Containing 7-Nitrobenzo-2-Oxa-1,3-Diazole Moiety." Biochemical Journal **1975**, *151*, 417-432.
- [13] Jiang, W.; Fu, Q. Q.; Fan, H. Y.; Wang, W. "An NBD fluorophore-based sensitive and selective fluorescent probe for zinc ion." Chemical Communications **2008**, 259-261.
- [14] Ramachandram, B.; Samanta, A. "Transition metal ion induced fluorescence enhancement of 4-(N,N-dimethylethylenediamino)-7-nitrobenz-2-oxa-1,3-diazole." Journal of Physical Chemistry A **1998**, *102*, 10579-10587.
- [15] Kim, S. H.; Kim, J. S.; Park, S. M.; Chang, S. K. " Hg^{2+} -selective OFF-ON and Cu^{2+} -selective ON-OFF type fluoroionophore based upon cyclam." Organic Letters **2006**, *8*,

371-374.

[16] Xu, Z. C.; Kim, G. H.; Han, S. J.; Jou, M. J.; Lee, C.; Shin, I.; Yoon, J. "An NBD-based colorimetric and fluorescent chemosensor for Zn^{2+} and its use for detection of intracellular zinc ions." *Tetrahedron* **2009**, *65*, 2307-2312.

[17] Qian, F.; Zhang, C. L.; Zhang, Y. M.; He, W. J.; Gao, X.; Hu, P.; Guo, Z. J. "Visible Light Excitable Zn^{2+} Fluorescent Sensor Derived from an Intramolecular Charge Transfer Fluorophore and Its in Vitro and in Vivo Application." *Journal of the American Chemical Society* **2009**, *131*, 1460-1468.

[18] Li, C.; Henry, E.; Mani, N. K.; Tang, J.; Brochon, J. C.; Deprez, E.; Xie, J. "Click Chemistry to Fluorescent Amino Esters: Synthesis and Spectroscopic Studies." *European Journal of Organic Chemistry* **2010**, 2395-2405.

[19] Ruan, Y. B.; Maisonneuve, S.; Xie, J. A. "Highly selective fluorescent and colorimetric sensor for Hg^{2+} based on triazole-linked NBD." *Dyes and Pigments* **2011**, *90*, 239-244.

[20] Duong, T. Q.; Kim, J. S. "Fluoro- and Chromogenic Chemodosimeters for Heavy Metal Ion Detection in Solution and Biospecimens." *Chemical Reviews* **2010**, *110*, 6280-6301.

[21] Kim, H.; Lee, S.; Lee, J.; Tae, J. "Rhodamine Triazole-Based Fluorescent Probe for the Detection of Pt^{2+} ." *Organic Letters* **2010**, *12*, 5342-5345.

[22] Lu, H.; Qi, S. L.; Mack, J.; Li, Z. F.; Lei, J. P.; Kobayashi, N.; Shen, Z. "Facile Hg^{2+} detection in water using fluorescent self-assembled monolayers of a rhodamine-based turn-on chemodosimeter formed via a "click" reaction." *Journal of Materials Chemistry* **2011**, *21*, 10878-10882.

[23] Yi, H.; Maisonneuve, S.; Xie, J. "Synthesis of Triazole-Linked Fluorescent Saccharides and Glycosyl Amino Esters." *Synthesis-Stuttgart* **2012**, *44*, 1647-1656.

[24] Fukaminato, T. "Single-molecule fluorescence photoswitching: Design and synthesis of photoswitchable fluorescent molecules." *Journal of Photochemistry and Photobiology C-Photochemistry Reviews* **2011**, *12*, 177-208.

[25] Knauer, K. H.; Gleiter, R. "Photochromism of Rhodamine Derivatives." *Angewandte Chemie-International Edition in English* **1977**, *16*, 113-113.

[26] Belov, V. N.; Wurm, C. A.; Boyarskiy, V. P.; Jakobs, S.; Hell, S. W. "Rhodamines NN: A Novel Class of Caged Fluorescent Dyes." *Angewandte Chemie-International Edition* **2010**, *49*, 3520-3523.

[27] Montenegro, H.; Di Paolo, M.; Capdevila, D.; Aramendia, P. F.; Bossi, M. L. "The mechanism of the photochromic transformation of spirorhodamines." *Photochemical & Photobiological Sciences* **2012**, *11*, 1081-1086.

[28] Lee, Y.; Lee, C.; Yoon, J. "Kinetics and mechanisms of DMSO (dimethylsulfoxide) degradation by UV/ H_2O_2 process." *Water Research* **2004**, *38*, 2579-2588.

[29] Librando, V.; Tringali, G.; Hjorth, J.; Coluccia, S. "OH-initiated oxidation of DMS/DMSO: reaction products at high NO_x levels." *Environmental Pollution* **2004**, *127*, 403-410.

[30] Liu, Y.; Chen, Y. "Cooperative binding and multiple recognition by bridged bis(beta-cyclodextrin)s with functional linkers." *Accounts of Chemical Research* **2006**, *39*, 681-691.

[31] Haider, J. M.; Pikramenou, Z. "Photoactive metallocyclodextrins: sophisticated supramolecular arrays for the construction of light activated miniature devices." *Chemical Society Reviews* **2005**, *34*, 120-132.

- [32]Harada, A.; Takashima, Y.; Yamaguchi, H. "Cyclodextrin-based supramolecular polymers." Chemical Society Reviews **2009**, *38*, 875-882.
- [33]Bellia, F.; La Mendola, D.; Pedone, C.; Rizzarelli, E.; Saviano, M.; Vecchio, G. "Selectively functionalized cyclodextrins and their metal complexes." Chemical Society Reviews **2009**, *38*, 2756-2781.
- [34]Chen, Y.; Liu, Y. "Cyclodextrin-based bioactive supramolecular assemblies." Chemical Society Reviews **2010**, *39*, 495-505.
- [35]Szejtli, J. "Introduction and general overview of cyclodextrin chemistry." Chemical Reviews **1998**, *98*, 1743-1753.
- [36]Li, J.; Loh, X. J. "Cyclodextrin-based supramolecular architectures: Syntheses, structures, and applications for drug and gene delivery." Advanced Drug Delivery Reviews **2008**, *60*, 1000-1017.
- [37]Conn, M. M.; Rebek, J. "Self-assembling capsules." Chemical Reviews **1997**, *97*, 1647-1668.
- [38]Ogoshi, T.; Harada, A. "Chemical sensors based on cyclodextrin derivatives." Sensors **2008**, *8*, 4961-4982.
- [39]Harada, A. "Cyclodextrin-based molecular machines." Accounts of Chemical Research **2001**, *34*, 456-464.
- [40]Jullien, L.; Canceill, J.; Valeur, B.; Bardez, E.; Lehn, J. M. "Antenna Effect in Multichromophoric Cyclodextrins." Angewandte Chemie-International Edition **1994**, *33*, 2438-2439.
- [41]Choppinet, P.; Jullien, L.; Valeur, B. "Multichromophoric cyclodextrins, Part 7 Photophysical and structural features of inclusion complexes with fluorescent dyes." Chemistry-a European Journal **1999**, *5*, 3666-3678.
- [42]Berberansantos, M. N.; Canceill, J.; Brochon, J. C.; Jullien, L.; Lehn, J. M.; Pouget, J.; Tauc, P.; Valeur, B. "Multichromophoric Cyclodextrins .1. Synthesis of O-Naphthoyl-Beta-Cyclodextrins and Investigation of Excimer Formation and Energy Hopping." Journal of the American Chemical Society **1992**, *114*, 6427-6436.
- [43]Jullien, L.; Canceill, J.; Valeur, B.; Bardez, E.; Lefevre, J. P.; Lehn, J. M.; MarchiArtzner, V.; Pansu, R. "Multichromophoric cyclodextrins .4. Light conversion by antenna effect." Journal of the American Chemical Society **1996**, *118*, 5432-5442.
- [44]Karuppannan, S.; Chambron, J. C. "Supramolecular Chemical Sensors Based on Pyrene Monomer-Excimer Dual Luminescence." Chemistry-an Asian Journal **2011**, *6*, 964-984.
- [45]Manandhar, E.; Wallace, K. J. "Host-guest chemistry of pyrene-based molecular receptors." Inorganica Chimica Acta **2012**, *381*, 15-43.
- [46]David, O.; Maisonneuve, S.; Xie, J. "Generation of new fluorophore by Click chemistry: synthesis and properties of beta-cyclodextrin substituted by 2-pyridyl triazole." Tetrahedron Letters **2007**, *48*, 6527-6530.
- [47]Maisonneuve, S.; Fang, Q.; Xie, J. "Benzothiadiazoyl-triazoyl cyclodextrin: a selective fluoroionophore for Ni(II)." Tetrahedron **2008**, *64*, 8716-8720.
- [48]Schneider, H. J.; Hacket, F.; Rudiger, V.; Ikeda, H. "NMR studies of cyclodextrins and cyclodextrin complexes." Chemical Reviews **1998**, *98*, 1755-1785.
- [49]Liu, Y.; Shi, J.; Guo, D. S. "Novel permethylated beta-cyclodextrin derivatives appended with chromophores as efficient fluorescent sensors for the molecular recognition of bile salts."

Journal of Organic Chemistry **2007**, 72, 8227-8234.

[50]Kodaka, M. "*Application of a general rule to induced circular dichroism of naphthalene derivatives complexed with cyclodextrins.*" Journal of Physical Chemistry A **1998**, 102, 8101-8103.

[51]Walla, P.; Arion, V. B.; Brinker, U. H. "*Solvent- and temperature-tuned orientation of ferrocenyl azide inside cyclodextrin.*" Journal of Organic Chemistry **2006**, 71, 3274-3277.

[52]Kodaka, M. "*Sign of Circular-Dichroism Induced by Beta-Cyclodextrin.*" Journal of Physical Chemistry **1991**, 95, 2110-2112.

[53]Leinhos, U.; Kuhnle, W.; Zachariasse, K. A. "*Intramolecular Charge-Transfer and Thermal Exciplex Dissociation with Para-Aminobenzonitriles in Toluene.*" Journal of Physical Chemistry **1991**, 95, 2013-2021.

[54]Garcia, L.; Maisonneuve, S.; Xie, J. A.; Guillot, R.; Dorlet, P.; Riviere, E.; Desmadril, M.; Lambert, F.; Policar, C. "*Sugars to Control Ligand Shape in Metal Complexes: Conformationally Constrained Glycoligands with a Predetermination of Stereochemistry and a Structural Control.*" Inorganic Chemistry **2010**, 49, 7282-7288.

[55]Garcia, L.; Maisonneuve, S.; Marcu, J. O. S.; Guillot, R.; Lambert, F.; Xie, J.; Policar, C. "*Intrinsically Fluorescent Glycoligands To Study Metal Selectivity.*" Inorganic Chemistry **2011**, 50, 11353-11362.

[56]Li, C.; Tang, J.; Xie, J. "*Synthesis of crosslinking amino acids by click chemistry.*" Tetrahedron **2009**, 65, 7935-7941.

[57]Moumne, R.; Larue, V.; Seijo, B.; Lecourt, T.; Micouin, L.; Tisne, C. "*Tether influence on the binding properties of tRNA(3)(Lys) ligands designed by a fragment-based approach.*" Organic & Biomolecular Chemistry **2010**, 8, 1154-1159.

[58]Zhou, Z.; Fahrni, C. J. "*A fluorogenic probe for the copper(I)-catalyzed azide-alkyne ligation reaction: Modulation of the fluorescence emission via (3)(n, π^*)-(1)(π , π^*) inversion.*" Journal of the American Chemical Society **2004**, 126, 8862-8863.

[59]Kato, S.; Matsumoto, T.; Ishi, T.; Thiemann, T.; Shigeiwa, M.; Gorohmaru, H.; Maeda, S.; Yamashita, Y.; Mataka, S. "*Strongly red-fluorescent novel donor- π -bridge-acceptor- π -bridge-donor (D- π -A- π -D) type 2,1,3-benzothiadiazoles with enhanced two-photon absorption cross-sections.*" Chemical Communications **2004**, 2342-2343.

Chapter 4. Fluorescent Calix[4]bisazacrown Based Chemosensors

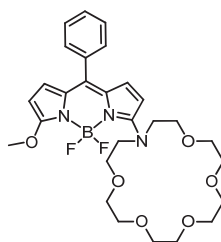
4.1 Fluorescent Calix[4]bisazacrown for selective recognition of potassium

4.1.1. Introduction of selective fluoroionophores of potassium

Potassium as one of the most abundant cations in the human body plays crucial regulatory roles in many biological events.^{1,2} The most challenging issue for the detection of potassium is the interference resulting from Na^+ due to much higher concentrations of Na^+ than K^+ in human extracellular fluid (*e.g.* concentrations of Na^+ and K^+ in blood plasma are 152 mM and 5 mM, respectively).² Therefore, fluorescent ligands with high binding ratio of K^+ vs Na^+ are highly demanded. However, it's a quite difficult task to discriminate alkali metal ion due to the fact that they show similar properties, such as hard and nonpolarisable spheres; little fixed preference for particular coordination geometries; relative high free energies of hydration.³ Anyhow, they still show some discrimination in ionic size with Na^+ 0.97 Å and K^+ 1.33 Å, respectively.³ By utilizing this difference, a number of researches have demonstrated the high efficiency to obtain high selectivity of K^+ over Na^+ . Among them, several binding motifs are mainly developed for this purpose, such as (aza)crown-ether, cryptand and calixarene.

4.1.1.1. Crown ethers

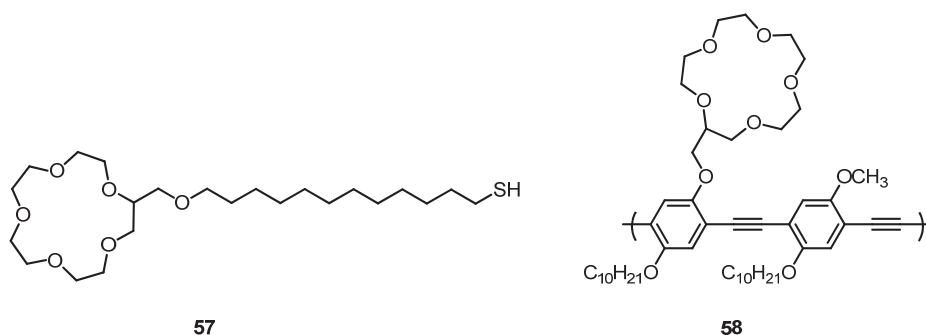
Crown ethers are macrocyclic ligands, usually consisting of oxygen atoms linked by $-\text{CH}_2\text{CH}_2-$.³ They have been widely utilized in supramolecular chemistry as receptors for metal ions. Especially, 18-crown-6 shows optimal binding ability to K^+ when compared with other alkali metal ions due to much better match of ionic size with the crown cavity. When it's incorporated with fluorophores to construct fluorescent chemosensors, they show selective response to K^+ . It has been reported that the aza-18-crown-6 directly linked to BODIPY (4,4-difluoro-4-bora-3a,- 4a-diaza-s-indacene or boron dipyrromethene) **56** showed selective ratiometric response to K^+ in MeCN.⁴ Upon binding to K^+ , intramolecular charge transfer from nitrogen of azacrown to electron deficient BODIPY was partially suppressed and consequently enhance fluorescence intensity of local excited state in MeCN. The results of their quantum mechanism calculations clearly showed that K^+ -induced conformation change with increase of the torsion angle around the chemical bond between carbon atom of the conjugated backbone and the nitrogen atom of azacrown reduced the coupling of the nitrogen atom with BODIPY. Noticeably, the addition of Na^+ almost produced no effect on its spectra.



56

Figure 4-1. Potassium sensor based on aza-18-crown-6.

However, the high flexibility of the macrocycle usually diminishes the variation of the binding constants to different alkali metal ions. Potassium though does not fit very well with the cavity of 15-crown-5; however, it can form a sandwich structure with two 15-crown-5 which has been proved to be a very powerful binding motif to discriminate Na^+ and K^+ . Chromophores or fluorophores such as gold nanoparticles, conjugated polymers, pyrene and tetraphenylethene (TPE) with unique spectroscopic properties in the dimer or aggregated states were widely used to realize the selective detection of potassium. Gold nanoparticles (Au NPs) functionalized with **57** when exposed to 0.1 mM K^+ in H_2O , the solution color immediately changed from red to blue which is indicative of the aggregation of Au nanoparticles. This was attributed to the formation of a sandwich complex of 2:1 between 15-crown-5 moiety and K^+ .⁵ Even in the presence of excessive amount of Na^+ (2.5 mM), it produced slight interference. Due to the intrinsic high sensitivity and selectivity of fluorescence technology, this latter attracts much more attention compared with colorimetric methods. With the attachment of 15-crown-5 to conjugated polymer backbone, the addition of K^+ to **58** solution in THF could also induce the aggregation of polymer to produce enhanced sensitivity and high selectivity to K^+ over Na^+ because of highly diffused excitons along the polymer chain.⁶



57

58

Figure 4-2. Potassium sensor based on 15-crown-5

When one of the ethyl linker in 15-crown-5 is replaced by phenyl group, benzo[15]-crown-5 is obtained with similar binding ability and selectivity to K^+ as that of

15-crown-5. Xia *et al.* developed a fluorescent probe **59**, relying on the fluorescence behavior of distyrylbenzene fluorophore.⁷ In the presence of 10 equiv K^+ in MeCN, the formation a conformationally constrained complex could inhibit *Z-E* isomerization and consequently result in 20-fold fluorescence enhancement. Other alkali metal ions including Na^+ just resulted in very slight change on the emission spectra. When benzo[15]-crown-5 was coupled with pyrene by amido and methylene group, **60** showed quite interesting methylene length dependent K^+ response in the presence of γ -cyclodextrin in H_2O .⁸ With $n=3$, addition of K^+ cause enhanced excimer and diminished monomer and worthy of notice is that the selectivity of K^+ over Na^+ was calculated to be 2600 by apparent association constant. While $n=1$ it showed no response to K^+ and when $n=5$ interference of Na^+ could not be negligible. TPE derivatives were discovered to exhibit unique aggregation induce emission (AIE).⁹ With the symmetrical attachment of four benzo[15]-crown-5 to TPE core, a new turn-on fluorescent chemosensor **61** for K^+ in THF was developed. In the presence of K^+ , a cross-linking complex aggregated by formation of a 2:1 sandwich coordination geometry between benzo[15]-crown-5 and K^+ .

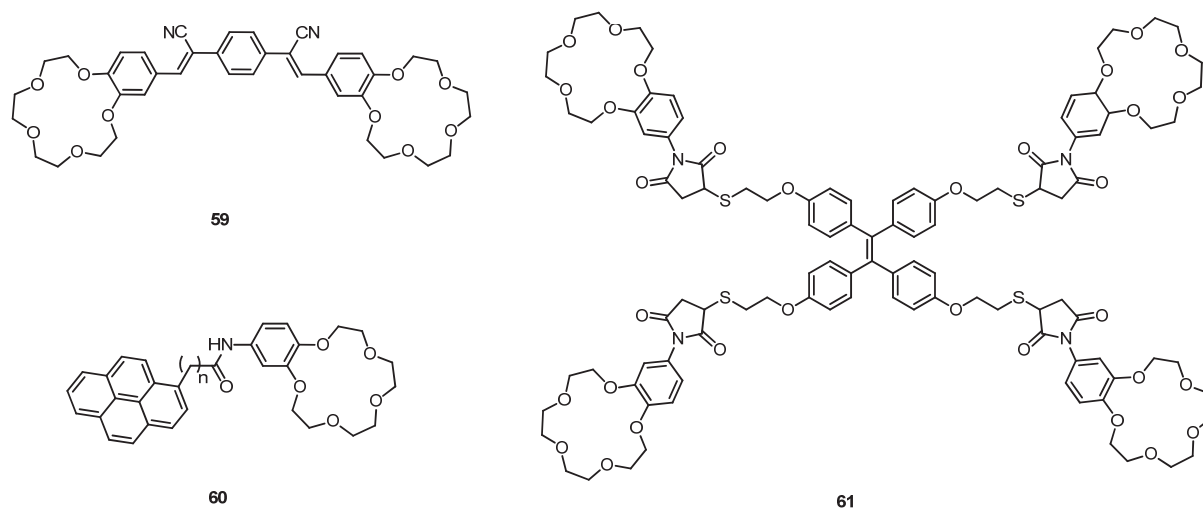


Figure 4-3. Potassium sensor based on benzo[15]-crown-5

4.1.1.2. Cryptand

Cryptand is an analogue of crown ether with three dimensional complexation geometry.³ The additional rigidity and stability given by the additional podand complexation imposed on the crown is supposed to reside the cation into a capsule like binding motif. It requires the precise match between the size of guest cation and the host cavity and thus can be used to improve the cation selectivity and enhancement in ionophore-like transport properties.³ Furthermore, the preorganization of three dimensional cryptand is more favorable for cation binding as less entropy happens during the process that complex adopts the optimum complex

geometry. When a cryptand motif was coupled to a fluorophore, not only it can be used to enhance the binding ability to K^+ but also the nitrogen atom as a trigger of the fluorescence signal. The fusion of [222] cryptand with a coumarin fluorophore showed selective response to K^+ , however suffering from the interference of Na^+ and pH effect.¹⁰ In order to improve the selectivity, triazacryptand was then utilized to couple with 4-aminonaphthalamide fluorophore to construct **62**.¹¹ Aromatization of the three nitrogen atoms alleviates the pH sensitivity and the adjustment of macrocyclic size was more suitable to K^+ with lower binding ability to Na^+ . The free ligand displayed weak fluorescence due to photo-induced electron transfer (PET) from nitrogen of azacryptand to the 4-aminonaphthalamide fluorophore. Upon binding to K^+ , PET process was inhibited and caused fluorescence enhancement in Tris-HEPES buffer at pH 7.4. The coexistence of 160 mM Na^+ just produced slight interference. Keeping the same ionophore, the fluorophore was changed with dicyanomethylene to construct a new pull-push probe **63**.¹² The strong delocalization of electrons decreased the electron density of nitrogen atom of aniline moiety and reduced remarkably its binding ability to K^+ and sensitivity of the intramolecular charge transfer. With the addition of K^+ , the fluorescence intensity increased gradually and its K_d was estimated to be 88 mM. Retaining the selectivity over the other metal ions, it's worthy of notice that it can response to K^+ over a very broad range up to 1600 mM, which was quite meaningful in tracking K^+ in intracellular samples. Imidazolyl group was utilized to replace the phenyl group in triazacryptand to reduce the size of the crown beside the consideration of simplification of the synthesis routine. A new structurally simplified ligand **64** obtained in 5 steps in 53% overall yield was found to show quite selective response to K^+ in HEPES buffer solution at pH 7.¹³

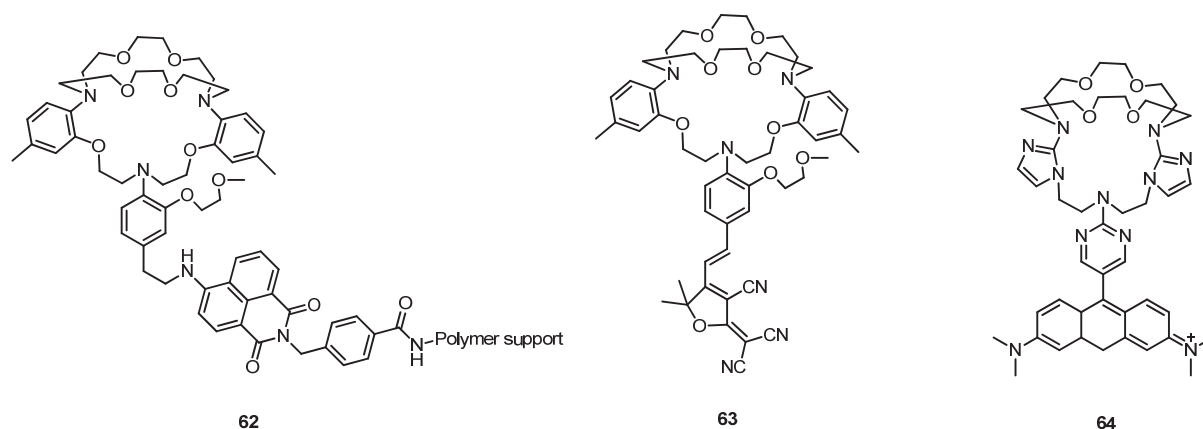


Figure 4-4. Potassium sensor based on cryptan

4.1.1.3. Calixarene

Calixarenes are one of the most popular supramolecular scaffolds which consist of phenol and methylene to form versatile macrocycles, as shown in Figure 4-5.¹⁴ The first cyclic

tetrameric structure of calixarene was proposed by Alois Zinke who then was able to isolate a crystalline product from condensation of *p*-tert-butylphenol with formaldehyde. This assumption was then later confirmed by John Conrforth with the evidence of X-ray crystallography and molecular weight determination. Due to the resemblance of the bowl-shaped conformation of the smaller calixarenes to a Greek vase called a *calix crater*, the structure was then described as “calixarene” by C. David Gutsche.¹⁴

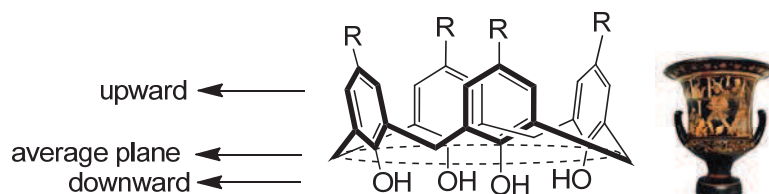


Figure 4-5. Molecular structure of calix[4]arene and a *calix crater*

Stereochemistry of calix[4]arene

The stereochemistry of calixarene following will be illustrated by calix[4]arene. Due to the possible rotation of phenol moiety, there exists four different conformational isomers with various aromatic rings upward and downward relative to an average plane defined by the bridged methylene group. These conformations were named by Gutsche as “cone”, “partial cone” “1,2-alternate” and “1,3-alternate” as shown in Figure 4-6, which are affected by a lot of factors such as solvent polarity and hydrogen bonding interactions.¹⁴ For example, the cone conformer is the most common due to the stabilization of intramolecular hydrogen bonding interaction among the OH groups. However, when all the hydroxyl groups were alkylated, it may adopt different conformations in the solution because of the absence of the hydrogen bonding interaction.

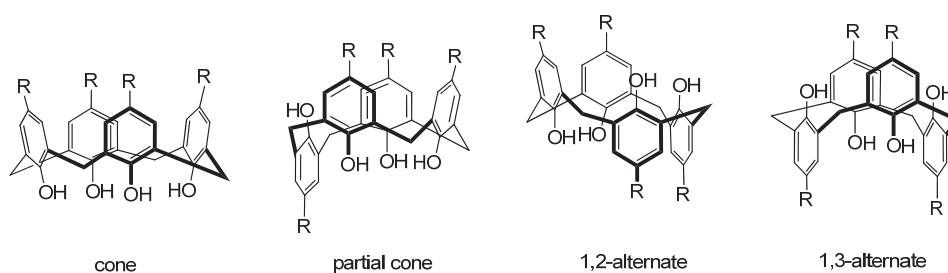


Figure 4-6. Possible conformations of *p*-substituted calix[4]arene.

The functions of calixarene are closely related to their conformations, indicating the importance to study the conformations. The most conclusive and direct evidences are provided by X-Ray crystallography. For example, the first crystal structure of *p*-tert-butylcalix[4]arene was proved to be a perfect C_4 symmetry of cone conformation. However, it's worthy of notice that the conformation of calix[4]arene is flexible and can be

affected by lots of factors. The conformations verified by X-Ray crystallography in the solid state can not represent the ones in the solutions. Most of the applications of calixarene were carried out in solution. Therefore other approaches were quite desirable to determine the conformations of the calixarene in the solution. In 1970s, the studies of temperature-dependent ^1H NMR of *p*-substituted calix[4]arene by Hermann revealed that the conformation of the cyclic tetramers were quite flexible and interconversion of different conformations was possible in solution. From then on, NMR became a standard and the most powerful tool to determine the conformation of calixarene in solution based on the development of high field NMR instruments with advanced pulse techniques (COSY, NOESY, ROESY *et al.*). Three most commonly encountered ^1H NMR resonance patterns of bridged methylene unit in different fixed conformers are shown in Figure 4-7.¹⁴ They exhibit quite remarkable difference from each other with two, eight and one group of split protons for cone, partial cone and 1,3-alternate conformation. Furthermore, the magnitude of the chemical shift ($\Delta\delta$) between the high-field and low-field pairs of resonances resulting from the bridged methylene group is quite helpful in determination of the conformations of calixarene. When the measurement was performed in non-polar solvent like CDCl_3 , $\Delta\delta$ is generally 0.9 ± 0.2 ppm and zero for cone and 1,3-alternate conformation, respectively (Figure 4-8). Between these two extremes, flattened conformations give an intermediate value of $\Delta\delta$ *ca.* 0.5 ± 0.1 ppm. The value of $\Delta\delta$ can provide information about the deviation of the conformation from the two extremes. Noticeably, the $\Delta\delta$ value is also affected by solvent, and generally larger in polar solvent than that in nonpolar solvent. Not only the ^1H NMR provides plenty of information about the conformation, but also can ^{13}C NMR spectra give resonance patterns for different conformations. The resonance of the bridged methylene carbon is at near δ 31 ppm when the attached aryl groups are in *syn* orientation and near 37 ppm when they are arranged in *anti* orientation. Combining the ^1H and ^{13}C NMR spectra, it's easier and more precisely to assign and monitor the conformation changes in the binding processes.

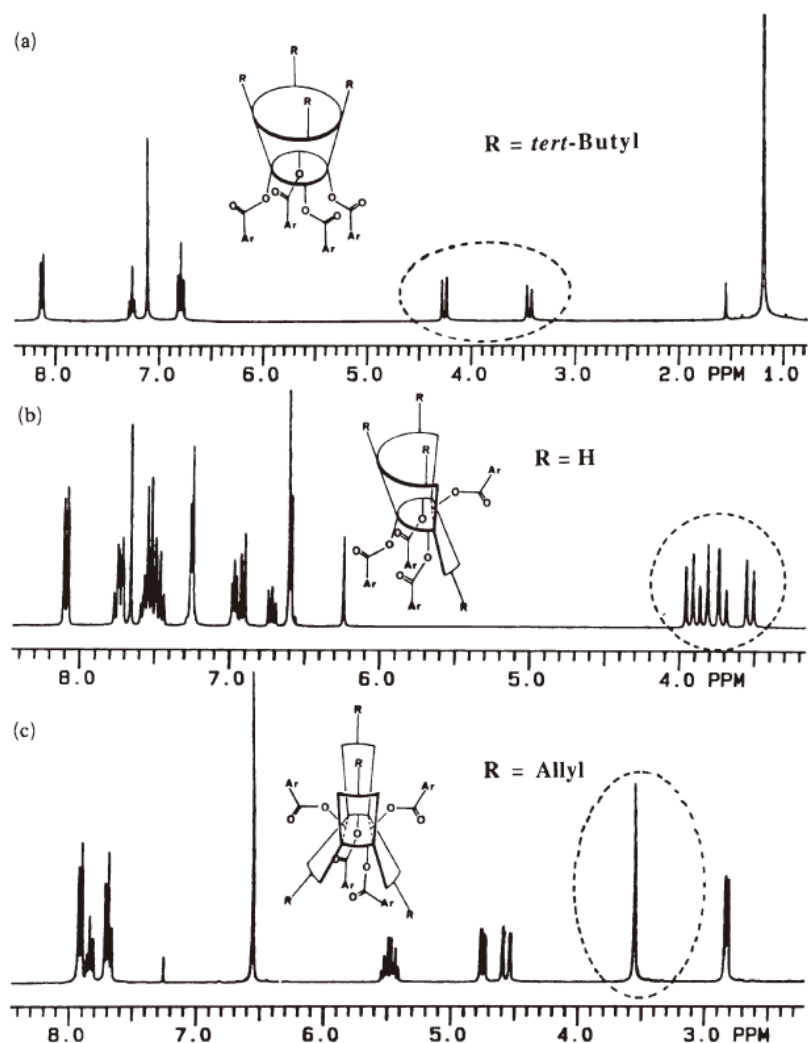


Figure 4-7. ^1H NMR spectra of calix[4]arenes in (a) cone conformation, (b) the partial cone conformation and (c) 1,3-alternate conformation; the circled region represents the patterns of methylene unit.

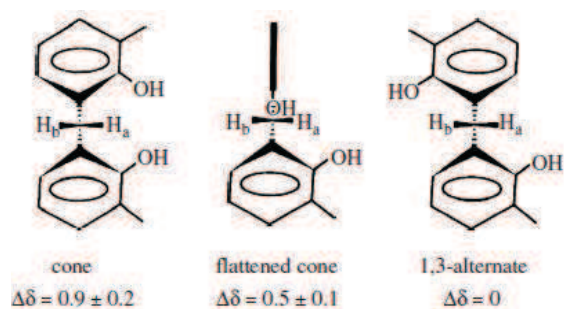


Figure 4-8. Change of chemical between the high-field and low-field pairs of resonance shifts of bridged methylene unit in different conformations.

Complexation of calix[4](aza)crown

Attachments of the functional groups onto the calixarenes have been widely utilized as the frameworks for cations, anions and small organic molecules.^{15,16,17,18} Especially, as shown in

Figure 4-9, calixarene exhibits several advantages in binding alkali metals.¹⁹ For example, phenol moiety with or without alkylation shows binding ability to hard alkali metal ions and hydrophobic aromatic cycles provide additional cation- π interaction. When the chromophores/fluorophores are attached to upper rim or phenolic hydroxyl groups, the binding event can be transduced into electric or optical signals. Many investigations by introduction of four amide, ester or ketone binding sites on the phenolic groups demonstrated that they showed selective response to Na^+ which might be due to the fixation of the cone conformation. Calixcrowns bearing larger binding cavity show preference to larger cations.

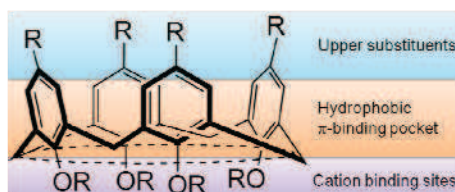
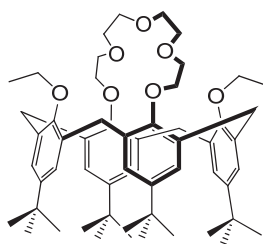


Figure 4-9. Structure analysis of calix[4]arene.

Calix[4]arenes with 1,3-dialkylation of the phenolic OH groups and suitable bridged polyether on the remaining OH groups have been constructed as receptors for K^+ with very higher selectivity over Na^+ . Ungaro and his coworkers have pioneered in construction of calixcrowns since their first introduction of polyethyleneoxy moiety on the endo rim in 1983 to have **65**.²⁰ **65** with different conformations all show high selectivity of K^+ over Na^+ in CDCl_3 which might be attributed to the better size match of the crown and K^+ .¹⁴ Moreover, ligand with partial cone conformation showed most efficient and selective binding to K^+ , conforming to Cram's views that the preorganization often enhance both the efficiency and selectivity in cation complexation.



65

Figure 4-10. Potassium ionophore based on Calix-crown.

After installation of fluorophores onto the calix[4]crowns, fluorescent chemosensors can be developed for the detection of K^+ . A new 1,3-alternate **66** composed of anthracene fluorophores as the signal reporting site and crown as the binding site for K^+ was synthesized.²¹ Under acidic condition when amino group was protonated, the PET process

was blocked and the ligand shows moderate fluorescence quantum yield (0.085). The added K^+ in MeCN/H₂O (99:1) bound with the crown moiety and consequently the repulsion interaction between K^+ and protonated amino group induced the deprotonation which reset the PET and caused fluorescence quenching. The ¹H NMR resonance pattern of protonated **66** in the presence of K^+ almost shifted back to that of the free ligand without protonation, indicating the deprotonation of amino group in the presence of K^+ . The addition of even 100 equiv of Na^+ showed almost no influence on its spectra. With the attachment of two pyrene fluorophores onto 1,3-alternate calix[4]crown by amido group, a new chemosensor **67** with different binding sites was synthesized.²² It exhibited strong excimer emission in solution which was quenched by Pb^{2+} , however, restored by addition of K^+ to the Pb^{2+} complex in MeCN. Such a switchable fluorescent chemosensor also shows moderate selectivity to K^+ over Na^+ .

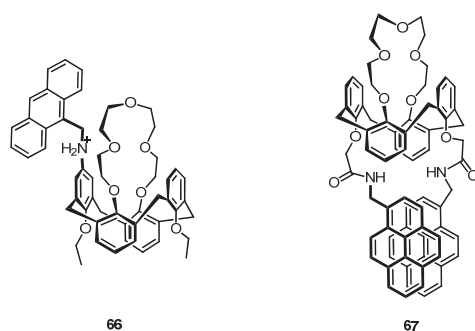


Figure 4-11. Potassium sensor based on calix[4]crown with pyrene and anthracene.

Azacrown ethers are often used as cation-complexing agents and have the accessibility of the modification on the secondary nitrogen atom. The nitrogen atom plays important roles by participation into the complexation and modulation of the spectral properties of the fluorophores. With the attachment of *p*-nitrophenol to the calix[4]azacrown, a new chelating agent **68** was synthesized.²³ Complexation selectivity was first investigated by ¹H NMR. Remarkable chemical shift and splitting patterns were observed in the presence of K^+ when compared with free ligand, indicating the encapsulation of the K^+ in the calixazacrown cavity. This was consistent with the absorption spectral change that significant bathochromic shift from 326 nm to 428 nm was observed in the presence of K^+ . However, no chemical shifts of the ¹H NMR and detectable spectral change were observed after addition of Na^+ to the parent ligand. The calixazacrown possesses high binding selectivity to K^+ over Na^+ . Later, Kim *et al* prepared the first calixarene-based azacrown fluoroionophore **69** by attaching the pyrene to the secondary amine.²⁴ In the absence of cation, fluorescence was quenched via a PET process. With the addition of K^+ to the free ligand in EtOH solution, fluorescence intensity was remarkably enhanced. This could be attributed to complexation of K^+ with nitrogen atom

which suppressed the PET process. Negligible fluorescence change was observed for Na^+ , which further demonstrated that 1,3-alternate calix[4]azacrown was a highly selective ionophore for K^+ over Na^+ .

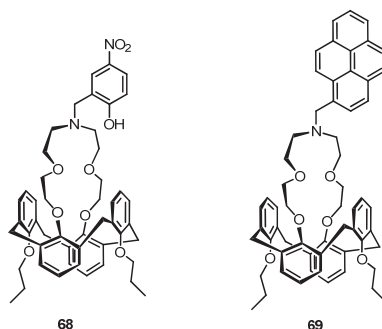


Figure 4-12. Potassium sensor based on calix[4]azacrown with nitrophenol, pyrene and anthracene.

1,3-Alternate calix[4]bis(aza)crown bearing two binding sites on the edges connected by hydrophobic cavity composed of four rotated aryl rings can also provide selective binding to K^+ . By measurement of ^1H NMR, **70** showed much larger association constant to K^+ than Na^+ .²⁵ Additionally, cation tunneling across calix[4]arene cavity was observed about 100°C , which is quite important for the study of cation channels in biological systems. Unsymmetrical crown-azacrown of calix[4]arene **71** was incorporated into polymeric membrane electrode to study its ion-responsive properties.²⁶ Results showed that it exhibited selective response to K^+ over a wide concentration range ($10\ \mu\text{M}$ - $0.1\ \text{M}$) with a detection limit of $2\ \mu\text{M}$ and almost no interference came from Na^+ .

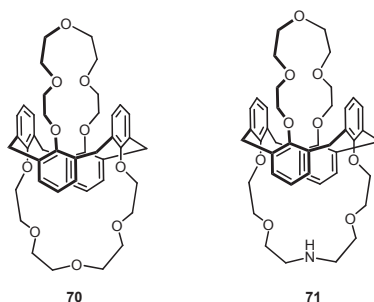


Figure 4-13. Potassium ionophores based on calix[4]bis(aza)crown

Compound **BC6N** was the first example of incorporation of a fluorophore naphthalene into calix[4]biscrown developed in the group of Dr Vicens (Figure 4-14). It showed large binding constant toward K^+ with $\log K$ to be 4.2 in MeCN. However, its spectral response is not sensitive enough for the practical application and it was only examined in organic solvent.²⁷ **Calix-Cou1** and **Calix-Cou2** based on the calix[4]biscrown were synthesized for the selective detection of K^+ and Cs^+ (Figure 4-15).²⁸ 6,7-Dialkoxycoumarin with very good photochemical stability was utilized as the fluorophore. Cation-interrupted intramolecular

charge transfer in these two ligands was expected to produce photophysical changes.

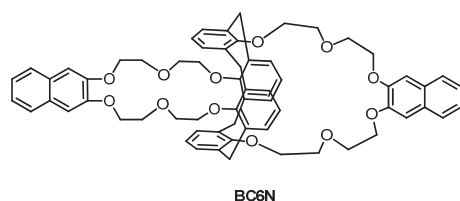


Figure 4-14. Potassium ionophores based on calix[4]bis(aza)crown.

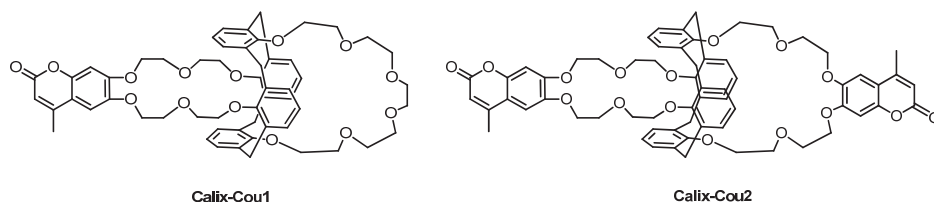


Figure 4-15. Molecular structures of **Calix-cou1** and **Calix-cou2**.

Spectral investigations were carried out in ethanol and acetonitrile. With the addition of K^+ to the solution of **Calix-Cou2**, a slight increase of the absorbance was observed at the maximum wavelength. However, fluorescence changes a lot during the titration of **Calix-Cou2** to K^+ in ethanol, as shown in Figure 4-16. At lower concentrations when the ratio $[K^+]/[Calix-Cou2]$ is lower than 10, moderate and steep fluorescence quenching and blue shift by 3 nm were observed; when the ratio is over 10, gradual fluorescence quenching was observed and the fluorescence quantum yield was reduced from 0.29 to 0.05 at full complexation. Emission of coumarin was resulted from the intramolecular charge transfer. The interaction between K^+ and the oxygen donor decreased the electron-donor character and reduced the intramolecular charge transfer, leading to the blue shift of the fluorescence spectrum and decrease of the fluorescence quantum yield. Similar spectral behavior was observed for **Calix-Cou1**.

Fluorescence titration was analyzed by SPECFIT program. The fitting results demonstrated that two successive complexes were formed during the titration with 1:1 and 2:1 stoichiometry ($K^+ : Calix-Cou2$) and the obtained association constants for $\log K_{11}$ and $\log K_{21}$ were 4.81 and 2.46, as shown in Table 4-1. The ratio of K_{21}/K_{11} was smaller than 1/4, which indicated that anticooperative interaction existed in the binding process. Such an anticooperative interaction was attributed to electrostatic repulsion between the two cations and unfavorable conformational change induced by the first bound cation.

Selectivity of K^+ versus Na^+ when expressed as the ratio of the associate constants was found to be 220 for **Calix-Cou2**. Such selectivity can be explained by the size match effect of

different cations with the crown cavity. The resultant looser complex with Na^+ had larger average distance between the cation and the oxygen atoms and corresponded to the less spectral changes.

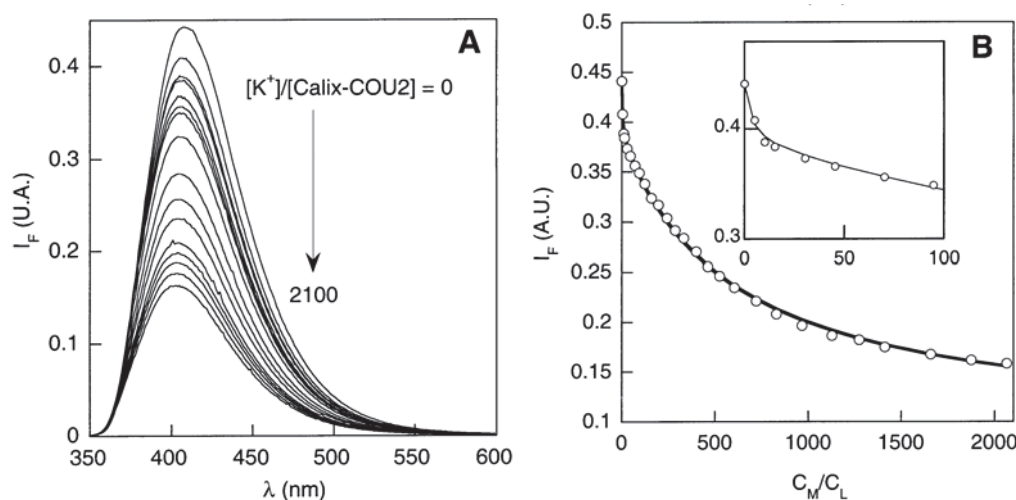


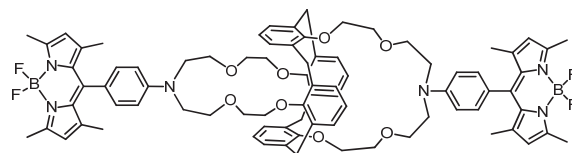
Figure 4-16. Fluorescence spectra of **Calix-Cou2** in the presence of increasing concentrations of KSCN in EtOH and plot of fluorescence intensity as a function of ratio of $[\text{K}^+]/[\text{Calix-Cou2}]$.

	Calix-Cou1		Calix-cou2	
	$\log K_{11}$	$\log K_{12}$	$\log K_{11}$	$\log K_{12}$
Na^+	2.75 ± 0.05	-	2.48 ± 0.06	-
K^+	5.03 ± 0.09	2.47 ± 0.09	4.81 ± 0.07	2.46 ± 0.06

Table 4-1. Binding constants of **Calix-Cou1** and **Calix-Cou2** to Na^+ and K^+ .

Calix-BODIPY bearing 1,3-alternate calix[4]bisazacrown and BODIPY was developed as a highly selective fluorescent chemosensor for detection of potassium in our group (Figure 4-17).²⁹ Its absorption spectrum was insensitive to solvent polarity and no charge transfer band at long wavelength was observed. However, solvatochromism of its emission spectra was quite remarkable. The emission at shorter wavelength was resulted from the local excited state. In solvents more polar than hexane, a broad and unstructured emission band at 630 nm was observed and quite sensitive to solvent polarity. This could be attributed to intramolecular charge transfer, which was further confirmed by time-resolved fluorescence measurement. Spectral investigation was carried out in MeCN and EtOH. Addition of K^+ led to gradual decrease of absorbance at 260 nm in EtOH, which is quite the same as that of protonation of the aniline moiety. Meanwhile, fluorescence intensity was gradually enhanced. The fluorescence titration was analyzed by SPECFIT program. The fraction of the complex with 1:1 and 2:1 (metal:ligand) binding stoichiometry was displayed in Figure 4-18. The selectivity

towards K^+ over other cations was expressed as the ratio of association constant to be higher than 1000. This high selectivity was attributed to the perfect fit of the size between potassium and the azacrown cavity and a cation- π interaction between K^+ and π -base columnar channel composed of four rotated aryl rings. The ratio K_{21}/K_{11} was smaller than 1/4, indicating an anticooperative interaction for the second binding of the potassium.



Calix-BODIPY

Figure 4-17. Molecular structures of **Calix-BODIPY**.

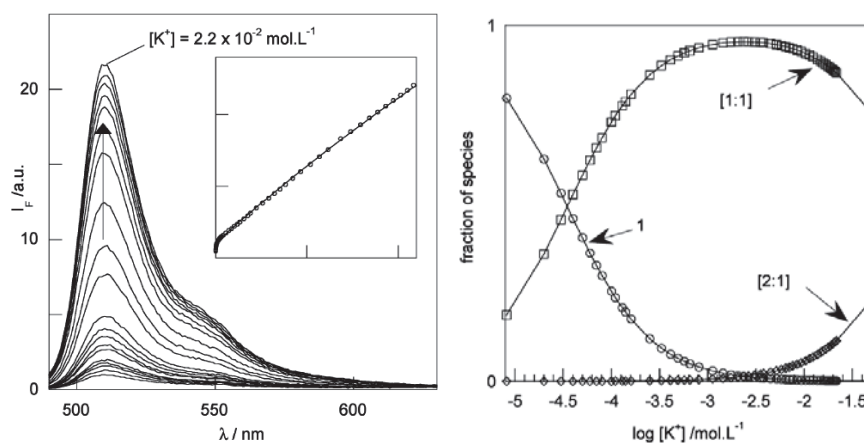
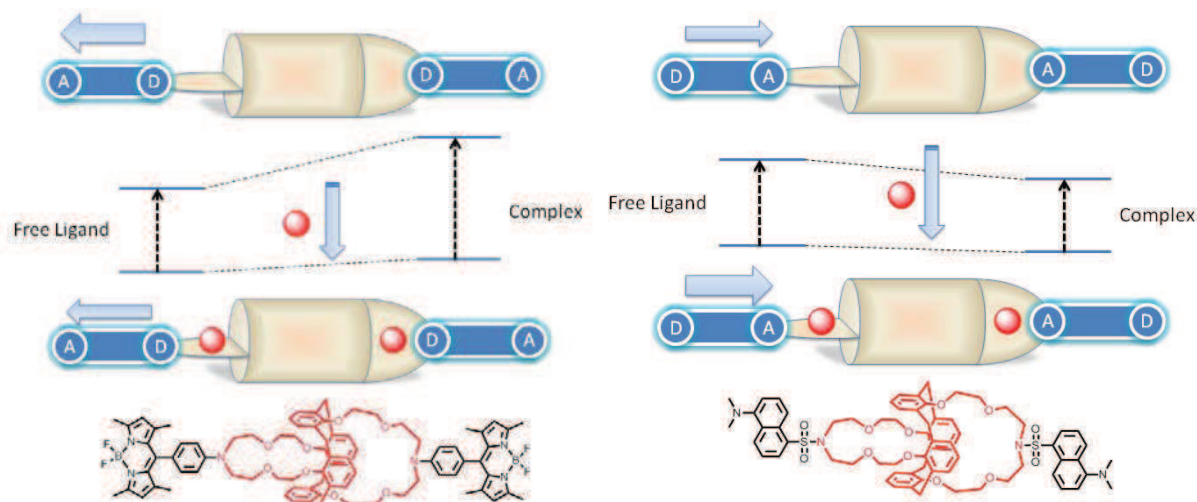


Figure 4-18. Fluorescence spectra of **Calix-BODIPY** in the presence of increasing concentrations of KSCN in EtOH and plot of fluorescence intensity as a function of ratio of $[K^+]/[Calix-BODIPY]$.

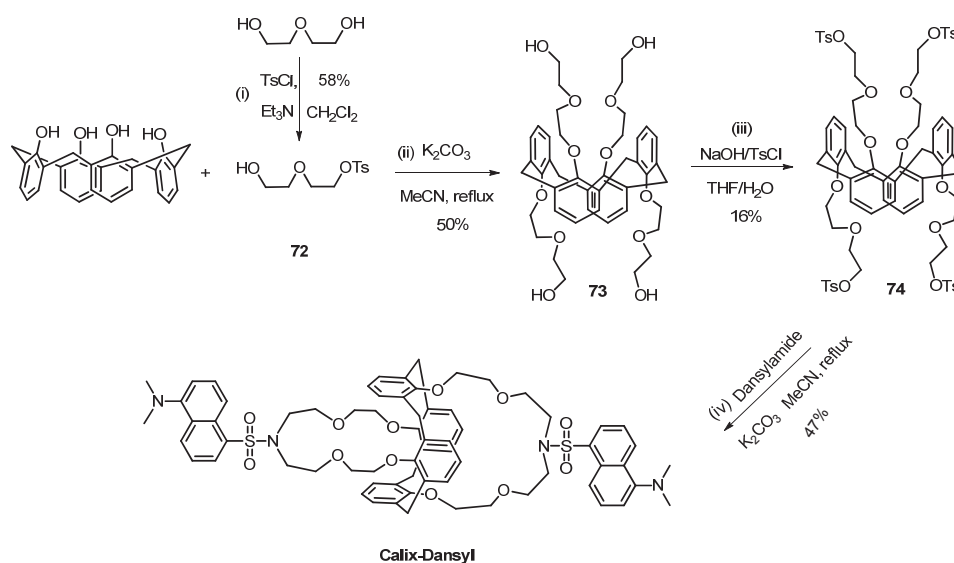
As shown in Scheme 4-1, nitrogen atom in **Calix-BODIPY** plays important roles by acting as the binding site for cation and as the electron donor. In the excited state, the charge transfer will result in partial positive charge on the nitrogen atom which may eject the bound cation out of the crown and reduce the sensing performance. Herein, we envisage to improve the binding ability by reversing the direction of the charge transfer by using dansyl as fluorophore in **Calix-Dansyl**. In the excited state, the charge transfer from dimethylamino group might result in partial negative charge on nitrogen atom of sulfonamide and enhance the binding ability of the azacrown to cations by increase of the electron density of the nitrogen atom.



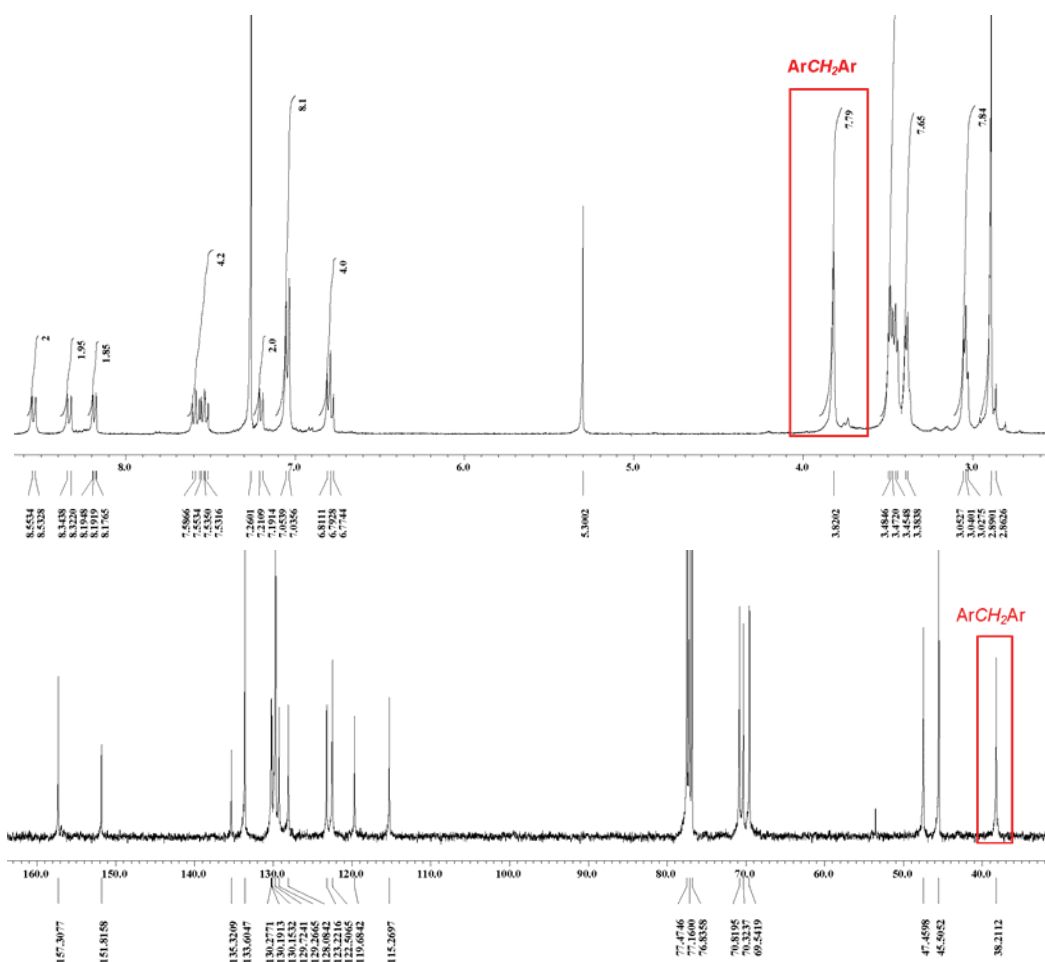
Scheme 4-1. Schematic illustration of **Calix-BODIPY** and **Calix-Dansyl** interaction with cations.

4.1.2. Synthesis of Calix-Dansyl

Scheme 4-2 shows the synthesis of **Calix-Dansyl**. Diethyleneglycol was reacted with 0.25 equiv tosyl chloride in the presence of triethylamine in dry DCM at room temperature overnight. Chromatography on a silica column gave mono-tosylated diethyleneglycol **72** in 58% yield.³⁰ Calix[4]arene in the presence of 7.4 equiv of K_2CO_3 was reacted with mono-tosylated product in refluxing MeCN to give **73** in 50% yield after isolation by column chromatography.³¹ Tosylation of the hydroxyl group was carried out with 5 equiv of tosyl chloride in dry THF for 5 days at room temperature in the presence of NaOH dissolved in H_2O . Chromatography gave ditosylate, tritosylated and tetratosylate **74** in 16% yield. The di- and tritosylated products could further react with tosyl chloride under the same conditions to produce **74**. Dansylamide was then reacted with 0.5 equiv tetratosylated **74** in the presence of 2.5 equiv K_2CO_3 in the refluxing MeCN overnight. The crude product was isolated by chromatography to afford the **Calix-Dansyl** in 47% yield.³² The 1,3-alternate conformation of **Calix-Dansyl** was deduced from the presence of the singlet peak (8H) at 3.82 ppm for the $ArCH_2Ar$ in 1H NMR spectra in $CDCl_3$ (Figure 4-19 (top)). It was further confirmed by peaks at 38.2 ppm for the $ArCH_2Ar$ in ^{13}C NMR spectra (Figure 4-19 (bottom)), indicating that the all the four aryl rings were arranged in *anti* orientation.



Scheme 4-2. Synthesis of Calix-Dansyl.

Figure 4-19. ^1H (top) and ^{13}C (bottom) NMR of Calix-Dansyl in CDCl_3 .

4.1.3. Photophysical properties of Calix-Dansyl

The photophysical properties of **Calix-Dansyl** were investigated in EtOH and MeCN. As shown in Figure 4-20, it exhibits an absorption band centered at 338 nm in MeCN with a molar extinction coefficient of $8898 \text{ mol}^{-1} \text{ L cm}^{-1}$, which is almost twice as large as dansylamide, indicating no significant interaction between the two dansylamide fluorophores in the ground state. When excited at 338 nm, it shows a broad emission band with the maximum wavelength at 532 nm. Its fluorescence quantum yield was determined to be 0.37. Fluorescence time decay profile of **Calix-Dansyl** in MeCN at 533 nm was monoexponential and its lifetime was measured to be 12.9 ns ($\chi_p^2 = 1.25$), which demonstrated that no interaction of the dansylamide fluorophores in the excited states. As displayed in Table 4-2, very similar spectral behavior was observed in EtOH, which might be ascribed to their close polarity and no hydrogen bonding interaction between **Calix-Dansyl** and EtOH.

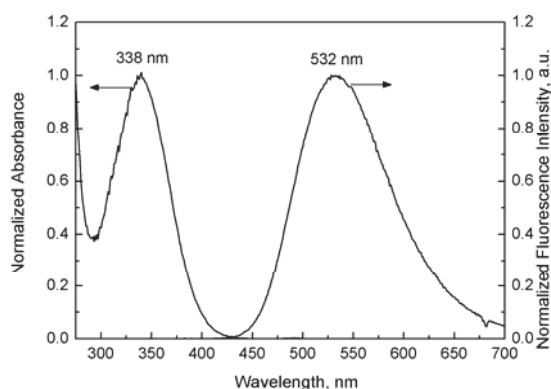


Figure 4-20. Normalized absorption and fluorescence spectra of **Calix-Dansyl** in MeCN, [**Calix-Dansyl**] = 10 μM .

Solvents	$\lambda_{\text{abs}}/\text{nm}$	$\epsilon/\text{mol}^{-1} \text{ L cm}^{-1}$	$\lambda_{\text{em}}/\text{nm}$	ϕ	τ/ns	χ_p^2
MeCN	338	8.9×10^3	532	0.37	12.9	1.25
EtOH	337	nd	533	0.41	13.5	1.24

Table 4-2. Photophysical data of **Calix-Dansyl** in different organic solvents, nd: not determined, using sulfate quinine in 0.5N H_2SO_4 as the reference.

4.1.4. Complexation properties of Calix-Dansyl in organic solvents

The spectral investigation on complexation properties of **Calix-Dansyl** was carried out in MeCN, as presented in Figure 4-21. With the addition of increasing concentrations of KSCN, slightly bathochromic and hyperchromic effects of the absorption band are observed. This

phenomenon can be attributed to the complexation interaction between K^+ and the nitrogen atom of the sulfonamide group. It reduces the electron density of the nitrogen atom and enhanced the electron-withdrawing character of sulfonyl group, thus facilitating the intramolecular charge transfer from dimethylamino group to sulfonyl group. Accordingly, fluorescence quenching and gradually red shift of the emission band are observed. An isoemissive point at 566 nm indicates the interconversion of the free ligand and complex. The fluorescence quenching reaches a plateau when the concentration of KSCN is 10 mM, with 10 nm red shift and about 16% fluorescence intensity quenched. Fluorimetric titration was analyzed by means of SPECFIT program (using global analysis with 361 wavelengths). The successive association constants K_{11} and K_{21} are defined as following:



The global equilibrium for the full complex M_2L is:



The values of the association constants derived from the fluorimetric titration are collected in Table 4-3. It can be seen that K_{11} of **Calix-Dansyl** is about one order of magnitude smaller than that of **Calix-BODIPY**, although they both have the same calix[4]bisazacrown as the binding site. Two possibilities could be proposed for this difference: firstly, electron density of the nitrogen atom in these two ligands is quite different, in **Calix-BODIPY** the nitrogen atom conjugated with the phenyl ring, retaining strong basic character; however, sulfonyl group is much more electron-withdrawing than phenyl group, which reduces the electron density of the nitrogen and decreases the binding ability with cations; on the other hand, due to the distorted tetra-hedral geometry of sulfonyl group that the conformation of **Calix-Dansyl** is in bent conformation which might produce steric effect on the binding process but it does not exist in **Calix-BODIPY** for its more extended and flat conformation. Furthermore, a second step complexation was observed at the high concentration of K^+ and was assumed to form a 2:1 (metal:ligand) stoichiometry complex. This is consistent with the previous report that the second step binding constant (K_{21}) is much lower than the first step (K_{11}), indicating that binding of the second cation is more difficult than the first one. The ratio of K_{21}/K_{11} (~ 0.014) is much lower than statistical value 1/4 when the two binding processes are independent, indicative of the anticooperative binding.²⁹ Several reasons can be proposed to explain this phenomenon. Firstly, the first binding cation in one crown produces electrostatic repulsion

interaction with sequent binding cation; secondly, it has been reported that the binding K^+ show tunneling behavior through the hydrophobic cavity of calixarene with the help of cation- π interaction; thirdly, the first binding event might induce the conformation change of the calixarene, which is unfavorable for the second binding process.

Compounds	Solvent	$\text{Log}K_{11}$	$\text{Log}K_{21}$	$\text{Log}\beta_{21}$
Calix-Dansyl	MeCN	2.95 ± 0.04	1.11 ± 0.04	4.06 ± 0.04
	EtOH	2.92 ± 0.19	1.75 ± 0.25	4.67 ± 0.37
Calix-BODIPY	MeCN	4.32 ± 0.04	1.73 ± 0.04	6.05 ± 0.04
	EtOH	4.47 ± 0.14	0.78 ± 0.14	5.26 ± 0.14

Table 4-3. Association constants of **Calix-Dansyl** and **Calix-BODIPY** with K^+ in MeCN and EtOH.

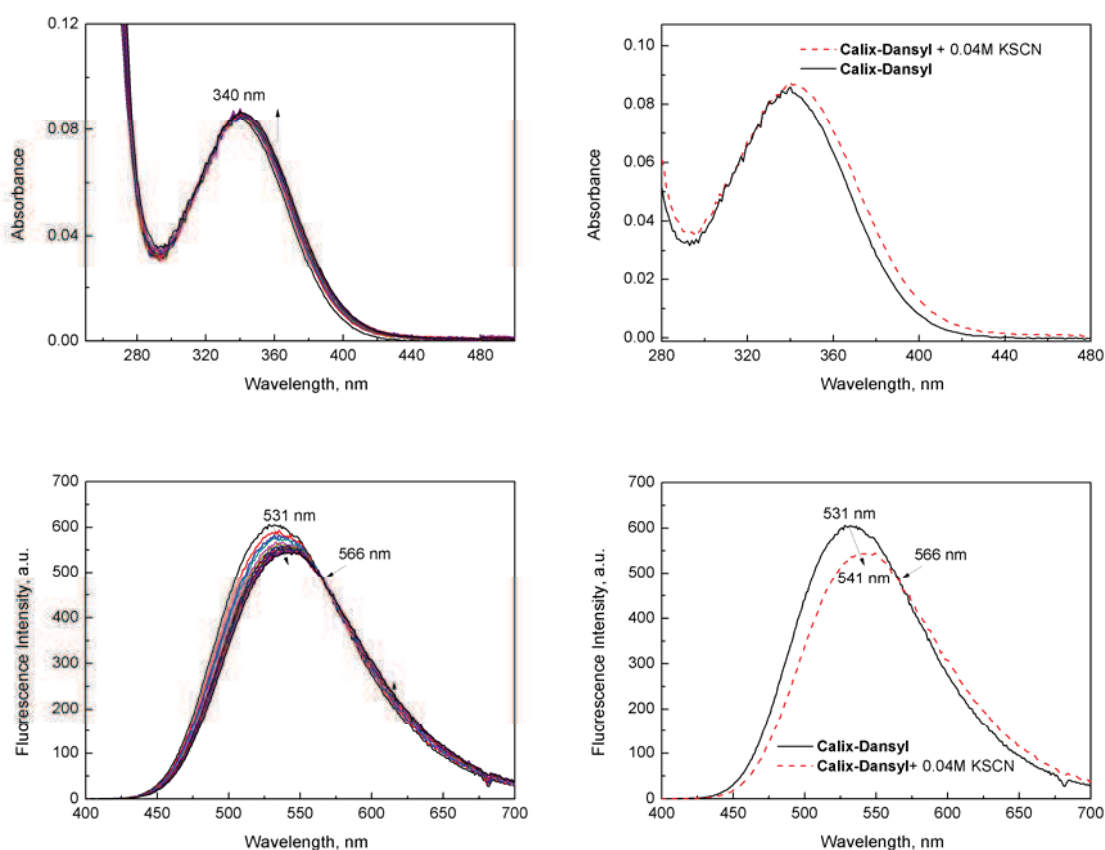


Figure 4-21. Absorption (top) and fluorescence (bottom) of **Calix-Dansyl** with increasing concentrations of KSCN in MeCN. [**Calix-Dansyl**] = 10 μM , λ_{ex} = 340 nm.

The fraction of different species in the solution during the titration with K^+ was analyzed by SPECFIT program. As shown in Figure 4-22 (left), when the concentration of K^+ is lower

than 3 mM, the dominant species are 1:1 complex and free ligand. Then with increasing concentrations of K^+ , the free ligand is further transformed into the complex and meanwhile the 1:1 complex is decreased due to the gradual formation of 2:1 complex. The extrapolated fluorescence spectra of the 1:1 and 2:1 complex are displayed in Figure 4-22 (right). Inferred from the fluorescence intensity, the second binding of K^+ just produces slight fluorescence quenching on the fluorophore in MeCN.

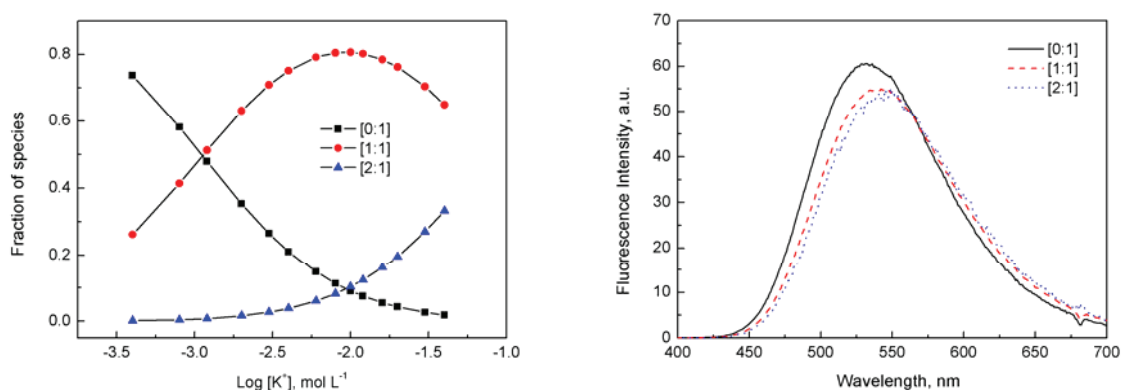


Figure 4-22. Specfit analysis of **Calix-Dansyl** fluorometric titration with K^+ in MeCN, the fraction of different species during the titration (left); extrapolated fluorescence spectra (right).

Spectral titration of **Calix-Dansyl** with K^+ was also carried out in EtOH. As shown in Figure 4-23, it shows quite similar behavior to that in MeCN. Slightly bathochromic and hyperchromic effects were observed for the absorption band and fluorescence quenching and red shift for fluorescence spectra. The isoemissive point is at 580 nm, a little red-shifted compared with that in MeCN. The binding constants shown in Table 4-3 illustrated that the association constant K_{11} is almost the same, indicative of no discrimination of the binding ability in the first step in these two solvents. However, the K_{21} is a bit larger than that in MeCN, indicating that the second binding of K^+ in EtOH is easier than that in MeCN. The ratio of K_{21}/K_{11} (~ 0.067) is much lower than statistical value $1/4$, indicative of the anticooperative binding. Figure 4-24 (left) presents analysis of the fractions of different species in solution during the titration, illustrating that the formation of M_2L in EtOH is much more quickly than that in MeCN. The extrapolated fluorescence spectra of 1:1 and 2:1 complex in EtOH shown in Figure 4-24 (right) indicate that the second binding of K^+ could induce almost the same fluorescence quenching as the first binding by comparison of the ratio of the fluorescence intensity.

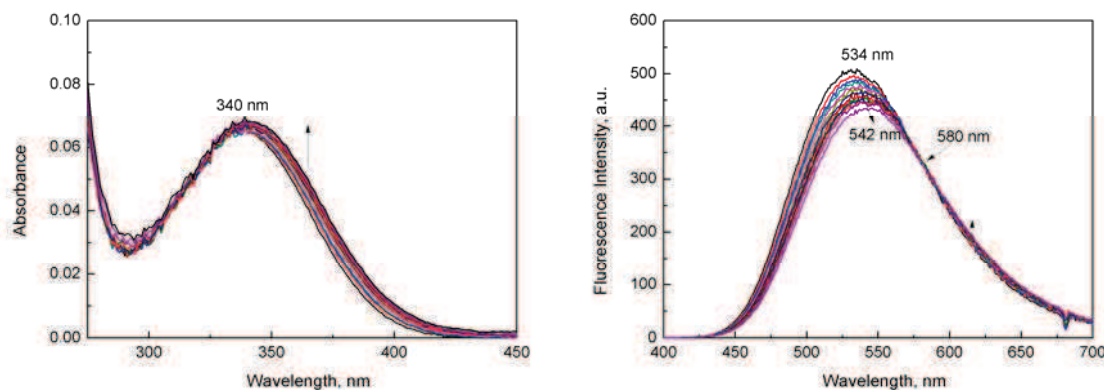


Figure 4-23. Absorption and fluorescence of **Calix-Dansyl** with increasing concentrations of KSCN in EtOH. [**Calix-Dansyl**] = 10 μ M, λ_{ex} = 340 nm.

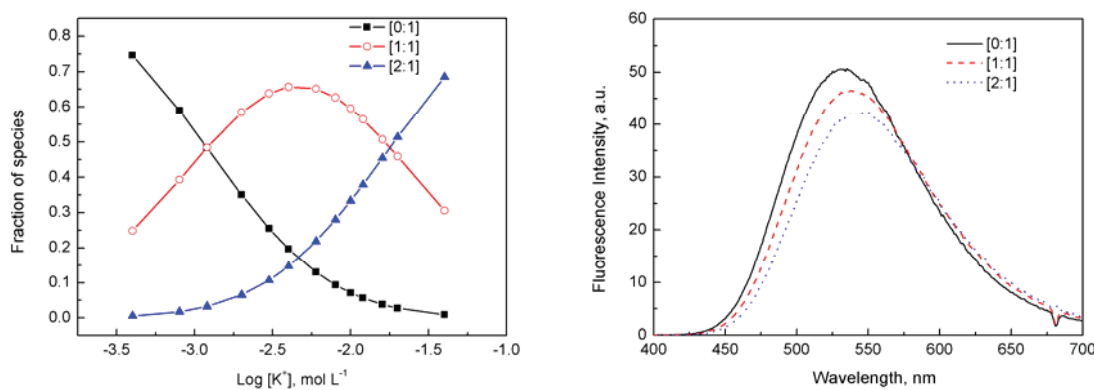


Figure 4-24. Specfit results from the titration of **Calix-Dansyl** to K^+ in EtOH, the fraction of different species during the titration (left); extrapolated fluorescence spectra (right).

Time decay profiles of **Calix-Dansyl** in the absence and presence of potassium were then recorded in different solvents, as shown in Table 4-4 and Figure 4-25. Mono-exponential model can give satisfactory fitting results with a value of 12.9 ns in MeCN and 13.5 ns in EtOH. In the presence of large excess amounts of K^+ , bi-exponential model gives a major component of free ligand and a minor component with slightly shorter lifetime at 10.2 ns (23%) in MeCN and 9.8 ns (32%) in EtOH, respectively, which indicates a relatively low efficient coordination of K^+ to **Calix-Dansyl**.

Solvent	$\tau_{\text{(Free ligand)}}$, ns	$\tau_{\text{(Complex)}}$, ns
MeCN	12.9	12.9 (77%), 10.2 (23%)
EtOH	13.5	13.5 (68%), 9.8 (32%)

Table 4-4. Lifetimes of **Calix-Dansyl** in the absence and presence of K^+ in MeCN and EtOH, [**Calix-Dansyl**] = 5 μ M, [KSCN] = 20 mM.

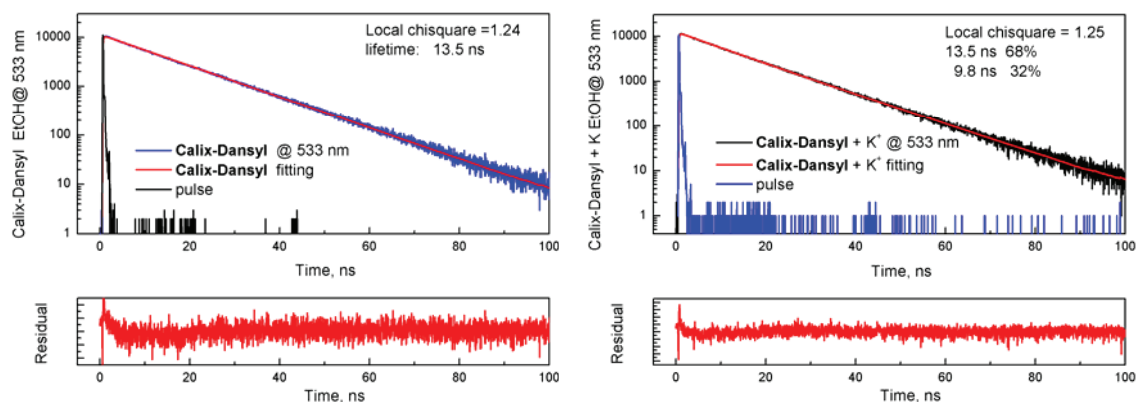


Figure 4-25. Time decay profiles of **Calix-Dansyl** in the absence and presence of K^+ EtOH, $[\text{Calix-Dansyl}] = 5 \mu\text{M}$, $[\text{KSCN}] = 20 \text{ mM}$.

^1H NMR is one of the most powerful tools for the investigation of interaction between host and guest. The assignment of the protons was accomplished by two dimension corrected spectra COSY. As shown in Figure 4-26, aromatic protons of dansylamide are located in the range between 7.25 and 8.75 ppm; while the ones of calix[4]arene moiety with symmetrical 1,3-alternate conformation appear at 6.79 and 7.04 ppm; and protons of crown ethers fall in the range of 3.0 over 3.5 ppm. ^1H NMR spectra of **Calix-Dansyl** in the presence of varying concentrations of KSCN were recorded in CD_3CN at room temperature (293K), as shown in Figure 4-26. With the increasing concentrations of KSCN, the down field shift and broadening of calix[4]arene aromatic and glycolic crown ether peaks were observed. To be clear, the molar ratio of $[\text{K}^+]/[\text{Calix-Dansyl}]$ was expressed as “R” and the variations of chemical shifts of protons on calix[4]arene moiety are plotted against R value, as shown in Figure 4-27. About 0.16 ppm down-field shifts were observed for both *m*- and *l*-H and they reached a plateau when R is over 2. More importantly, gradually down-field shift and remarkable broadening of the aromatic protons on calix[4]arene moiety during the titration indicated metal binding to π -basic cavity of calix[4]arene and the rapid metal exchange between the free ligand and complex within the NMR time scale.³³ On the contrast, protons H_h linked to sulfonamido group at 3.04 ppm does not shift when R is lower than 1.0 but its integration is gradually decreases and disappears when R is 1.0, demonstrating the initial formation of 1:1 complex. After the disappearance of peak at 3.04, a new broad peak at 3.6 ppm appears and its integration increases with increasing concentrations of K^+ when the R is over 1.0. This clearly demonstrates that the stepwise and quantitative formation of 1:1 complex and 2:1 complex during the titration. Aromatic protons of dansyl moiety show much smaller shift ($\Delta\delta = 0.05 \text{ ppm}$) when compared with calix[4]arene moiety. Based on these

observations, here we propose the binding model between **Calix-Dansyl** and K^+ , as shown in Scheme 4-3.

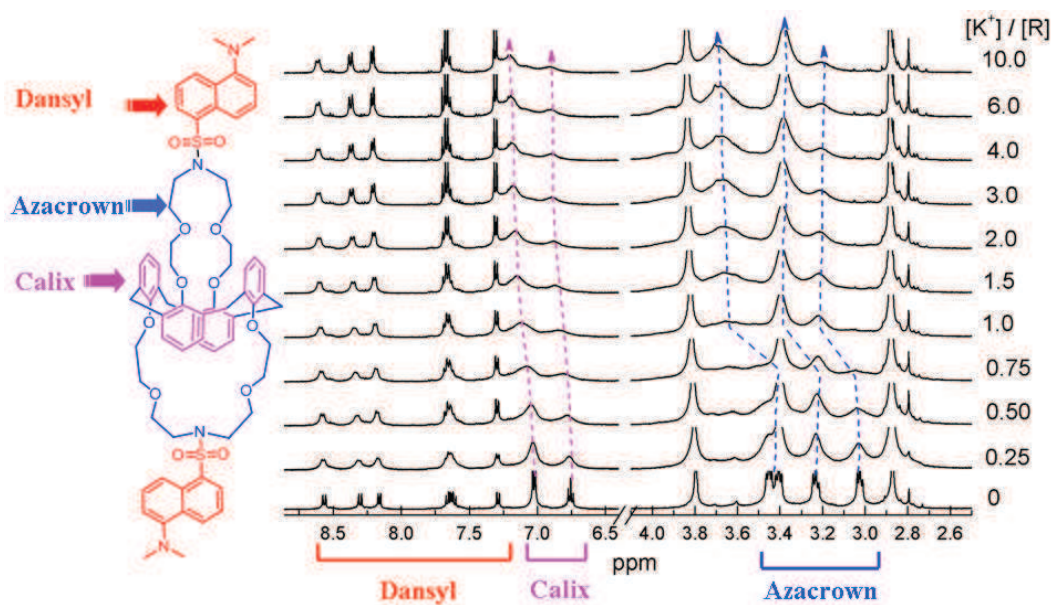


Figure 4-26. ^1H NMR titration of **Calix-Dansyl** with KSCN in CD_3CN .

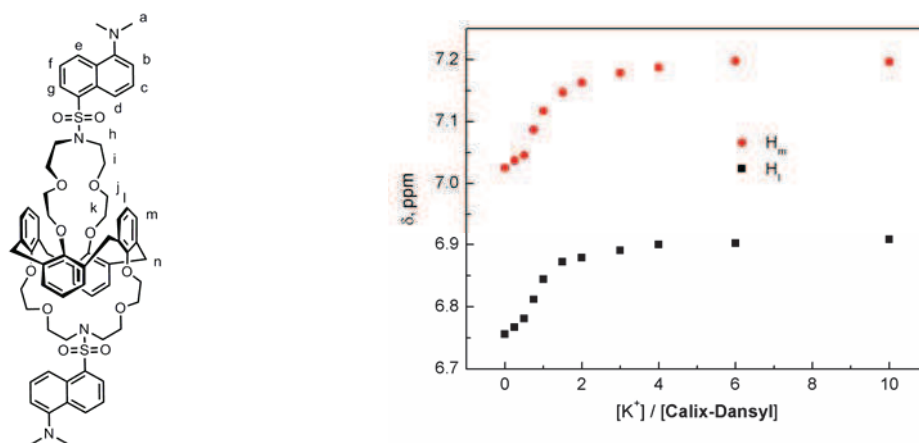
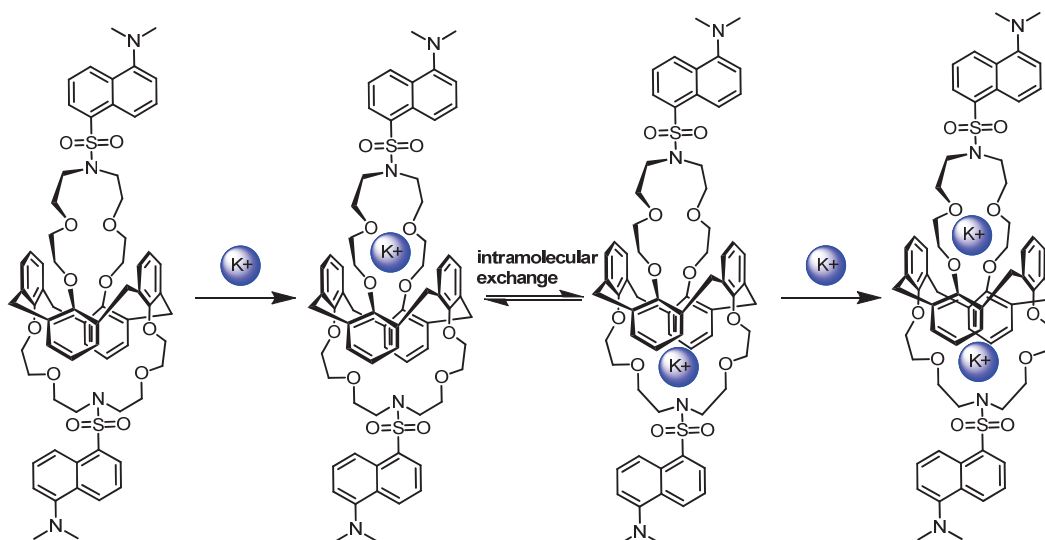


Figure 4-27. Plots of chemical shift as a function of ratio of $[K^+]$ and **Calix-Dansyl** in CD_3CN .



Scheme 4-3. Proposed binding model for **Calix-Dansyl** and KSCN.

In order to examine the practical application of **Calix-Dansyl**, selectivity was tested for K^+ over the other metal ions such as Na^+ , Mg^{2+} , Ca^{2+} , Ba^{2+} , Ag^+ , Cd^{2+} , Co^{2+} , Cu^{2+} , Fe^{2+} , Hg^{2+} , Pb^{2+} , Ni^{2+} , Mn^{2+} , Zn^{2+} in different organic solvents. As shown in Figure 4-28, several metal ions show remarkable influence on the spectra of **Calix-Dansyl**. Besides K^+ , the addition of Cu^{2+} induced decrease of the absorption band at 340 nm and complete fluorescence quenching. It's worthy of notice that the spectral change could not be recovered by the addition of CN^- , which indicated the process was irreversible. We supposed that Cu^{2+} with high oxidation potential in MeCN reacted with dansyl fluorophore and destroyed the intramolecular charge transfer.^{34,35,36,37,38,39} The addition of Hg^{2+} shows similarity in the fluorescence change, however, the absorption spectrum of the resultant complex is significantly different from that of Cu^{2+} . It exhibits new absorption bands at 280 and 320 nm, the same spectral pattern as that of protonation of dimethylamino group, which may indicate that interaction between dimethylamino group of dansyl and Hg^{2+} . The introduction of Fe^{2+} shows an identical spectral change, however to a lesser extent when compared with Hg^{2+} . Thereafter, the selectivity experiment was also performed in MeCN/ H_2O mixed solution at pH 4.0 adjusted by $HClO_4$, as shown in Figure 4-29. And only the addition of Hg^{2+} induces slight fluorescence quenching and other metal ions show no influence on its fluorescence, which can be attributed to the strong solvation of the metal ions in MeCN/ H_2O which significantly reduces their binding ability to **Calix-Dansyl**.

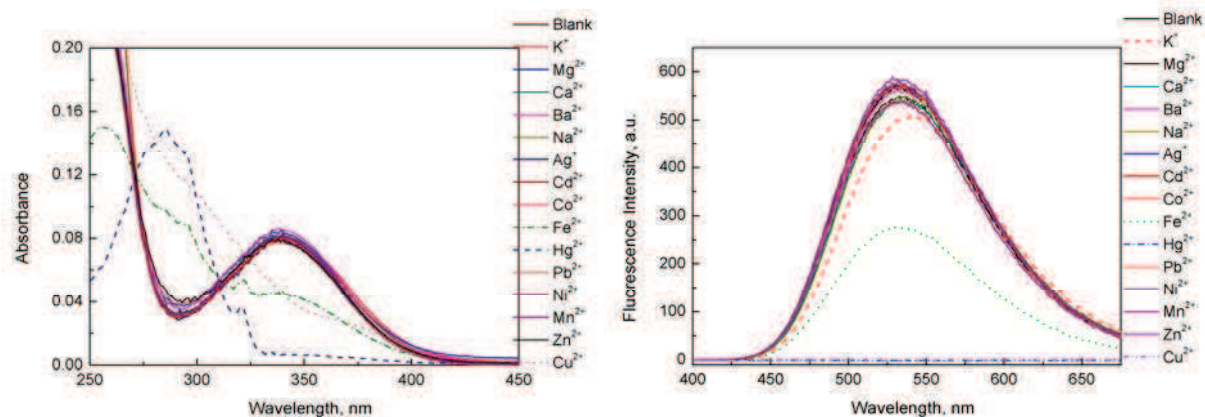


Figure 4-28. Absorption (left) and fluorescence (right) of **CalixDansyl** in the presence of different metal ions in MeCN. [Calix-Dansyl] = 10 μ M, alkyl and alkyl earth metal ions 0.01M, transition metal ions 80 μ M, λ_{ex} = 340 nm.

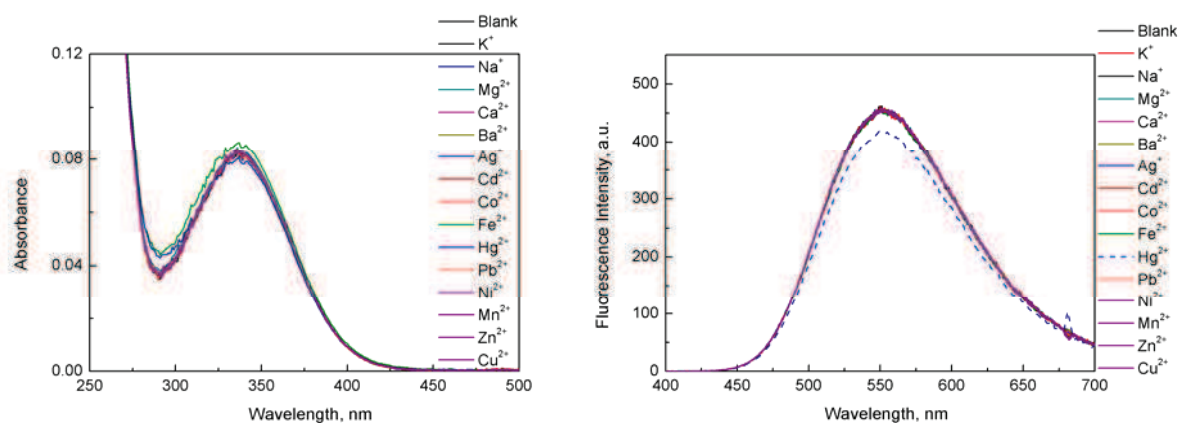


Figure 4-29. Absorption and fluorescence of **CalixDansyl** in the presence of different metal ions in MeCN/H₂O (v/v = 3:2, pH 4.0 adjusted by HClO₄). [CalixDansyl] = 10 μ M, alkyl and alkyl earth metal ions 0.01M, transition metal ions 80 μ M, λ_{ex} = 340 nm.

Figure 4-30 presents selectivity of **Calix-Dansyl** to metal ions in EtOH. Quite different from the behavior in MeCN, only the presence of Hg²⁺ and K⁺ cause some different influence on the spectral properties of **Calix-Dansyl**. Hg²⁺ caused fluorescence quenching without shift while K⁺ induced fluorescence quenching with 8 nm red shift. No spectral response was observed in the presence of Cu²⁺, which was attributed to the low oxidation potential of Cu²⁺ in EtOH and further confirmed our assumption that fluorescence quenching induced by Cu²⁺ in MeCN was a redox-reaction based process.³⁸ By using the ratio of fluorescence area 400-580 nm and 580-675 nm, the high selectivity of **Calix-Dansyl** to K⁺ over the other metal ions was obtained. The most common interference coming from Na⁺ was negligible. The high selectivity of K⁺ over Na⁺ can be explained by the fact that the much better size fit of K⁺ to azacrown than Na⁺ and the preferential cation- π interaction of K⁺ with rotated phenyl ring of

1,3-alternate calix[4]arene. The effect of alkali and alkaline earth metal ions was further investigated in EtOH/H₂O (v:v = 3:1), as shown in Figure 4-31. Still, no spectral response was observed due to strong solvation of the metal ion in water-containing medium.

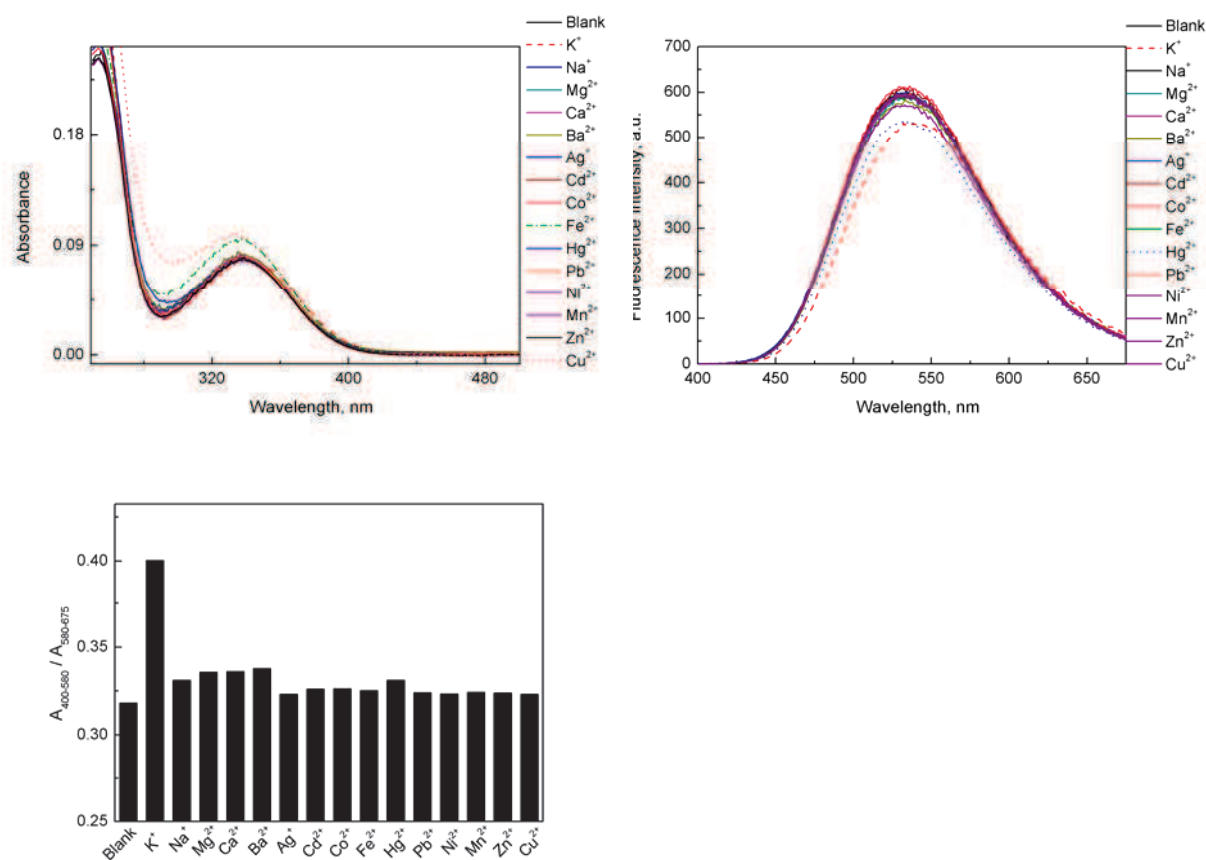


Figure 4-30. Absorption and fluorescence of **CalixDansyl** in the presence of different metal ions in EtOH. [CalixDansyl] = 10 μ M, alkyl and alkyl earth metal ions 0.01M, transition metal ions 80 μ M, λ_{ex} = 340 nm.

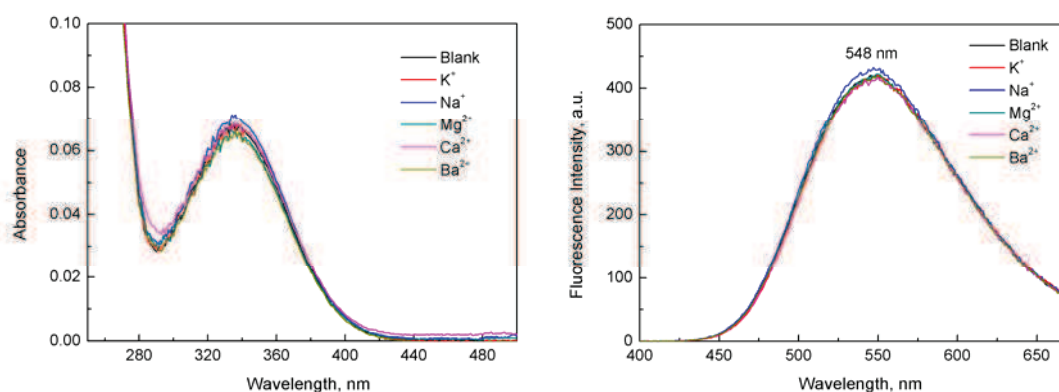


Figure 4-31. Absorption and fluorescence of **CalixDansyl** in the presence of different metal ions in EtOH/H₂O (v/v = 3:1). [CalixDansyl] = 10 μ M, alkyl and alkyl earth metal ions 0.01M, λ_{ex} = 340 nm.

4.1.5. Conclusion

A new fluoroionophore **Calix-Dansyl** bearing dansylamide fluorophore and calix[4]bisazacrown was synthesized and fully characterized. It was found to show selective response to K^+ over the other tested metal ions in EtOH. Complexation with K^+ induced fluorescence quenching accompanied by about 8 nm red shift. Analysis of the fluorescence titration by using SPECFIT program indicated a stepwise formation of 1:1 and 2:1 complex, with an anticooperative interaction in the second binding step. 1H NMR titration in CD_3CN confirmed the stepwise binding mechanism. Consistent with our assumption, due to the good size match of the cation with azacrown and preferential cation- π interaction with the phenyl rings of calix[4]azacrown, **Calix-Dansyl** retained a high selectivity to K^+ over Na^+ , which is of instructive significance for the design of fluorescent chemosensor for K^+ . However, the binding constants of **Calix-Dansyl** to K^+ were insufficient, which was attributed to the strong electron-withdrawing character of sulfonyl group and possibly steric effect from fluorophores. It's therefore herein we demonstrate that selection of fluorophores is quite important to affect detecting sensitivity, not only its signal transduction efficiency but also its influence on the binding ability of azacrown to K^+ . Future work on this project should pay attention to increasing the binding ability without interruption of the nitrogen atom in azacrown and avoiding steric effect by using rigid linker.

4.2. Sulfonated Fluorescent Calix[4]bisazacrown for Selective Detection of Aluminum(III)

4.2.1. Introduction of selective fluoroionophores of aluminum(III)

Aluminum is the most abundant metallic element in the Earth's crust. Due to its good physical and chemical properties, it has been widely used in our daily life and thus its health concerns are considerably important. Extremely low acute toxicity was reported; however, exposure to high dose of Al^{3+} can lead to neurotoxicity and deposit in bone and central nervous system.^{40,41,42,43} For example, it's considered that Alzheimer's disease is closely connected to the accumulation of Al^{3+} in the human body. High concentrations of Al^{3+} especially in acidic soils when absorbed by the plants can also reduce the growth. According to the WHO's reports, the average daily intake of Al^{3+} is estimated to be 3-10 mg kg^{-1} of body weight and the limited concentration of Al^{3+} in drinking water is 200 $\mu g L^{-1}$ (7.4 μM).⁴⁴

Advanced techniques are thus highly demanded to study biological and environmental roles of Al^{3+} . Conventional methods such as graphite furnace atomic absorption spectrometry and inductively coupled plasma atomic emission spectroscopy have been utilized to detect elemental aluminum with very high sensitivity and selectivity. However, several disadvantages like requirement of expensive instruments and complicated sample preparation processes make them unsuitable for the on-site detection. Fluorescent chemosensors have been well developed for the detection of important analytes in biological and environmental samples. They exhibit several advantages when compared with the conventional methods, such as the low cost, easy sample preparation, on-site detection and biological imaging applications in *vivo/vitro* samples. Due to the intrinsic high sensitivity and selectivity of fluorescence technique, several typical binding motifs have been coupled with efficient chromophore/fluorophores like small organic molecules, conjugated polymer, nano materials for the detection of Al^{3+} in environmental systems, and some of them were used for biological imaging.

Salicylic-Schiff as binding sites

Salicylic schiff base can be very easily synthesized by direct condensation between salicylic aldehyde and amine. Due to the flexible coordination chemistry, it has been widely applied in catalysis, material science and biological applications.⁴⁵ Its strong binding ability to metal ions is mainly contributed by the participation of nitrogen atom of imine group and

oxygen atom of phenolic group based on the formation of a six-membered ring.^{46,47} Compound **75** (Figure 4-32) directly coupled between 2-hydroxyaniline and salicylaldehyde was designed for the selective detection of Al^{3+} .⁴⁸ Upon treatment with Al^{3+} , fluorescence intensity was significantly enhanced under neutral pH condition. This was attributed to the formation of 1:1 complex between Al^{3+} and **75**, which was verified by mass spectra, ^1H NMR titration and job's plot. Worthy of notice is that such a simple ligand worked efficiently to fluorescently visualize intracellular Al^{3+} . By retaining the binding motif, several modified probes have also been reported based on different sensing mechanisms.^{49,50,51,52} Al^{3+} could form complexes with tridentate ligands (**77**, **78**) and inhibit the *trans-cis* isomerization along the imine ($\text{C}=\text{N}$) bond. As a result, non-radiative decay process was suppressed and the fluorescence intensity was enhanced. Fluorescence resonance energy transfer (FRET) dyad **80** was constructed by combination of coumarin 343 as acceptor and 3,5-bis(o-hydroxyphenyl)-1,2,4-triazole substituted benzoic acid as donor (Figure 4-32). In the presence of Al^{3+} , emission spectra of donor overlap with the absorption of coumarin 343 and therefore fluorescence of coumarin moiety was enhanced through energy transfer. Other metal ions except Cu^{2+} and Fe^{3+} showed noninterference. Other salicylic schiff based fluoroionophores (**76**, **79**) could also be used as quite selective chemosensors with turn-on fluorescence for the detection of Al^{3+} (Figure 4-32).

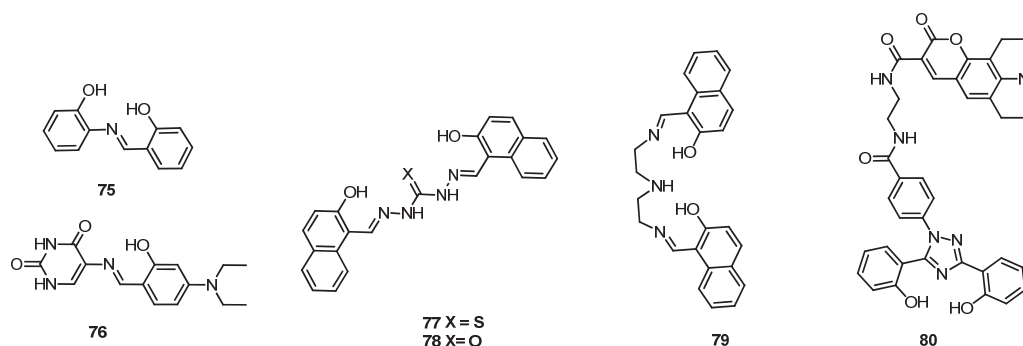


Figure 4-32. Al^{3+} chemosensors based on salicylic schiff base six-membered ring.

Salicylic-amino as binding sites

Salicylic amino derivatives can be synthesized from the reduction of salicylic schiff base with NaBH_4 . In the absence of imine bond ($\text{C}=\text{N}$), photophysical properties of the attached fluorophores can behave quite differently due to the possible photo-induced electron transfer from amino group to fluorophore and thus dramatically quench their fluorescence. Several selective fluorescent chemosensors based on the salicylic-amino binding motif were designed to detect aluminum (Figure 4-33). For **81**, complexation with Al^{3+} induced fluorescence enhancement and no influence was observed for the other metal ions.⁵³ Moreover, **81** showed

strongly solvent-dependent spectral behavior to Al^{3+} . In MeOH/ H_2O (1:99) medium, treatment with Al^{3+} caused slight fluorescence enhancement for the monomer and strong increase for the excimer. Ratio of the fluorescence intensity between excimer and monomer facilitated this ligand for ratiometric detection of Al^{3+} in aqueous solution. Detailed ^1H NMR titration demonstrated that the incorporation of the hydroxyl, amino and carboxylic group together contributed to its high selectivity to Al^{3+} . By changing the amino carboxylic acid to amino alcohol, **82** still showed selectively turn-on fluorescent response to Al^{3+} in MeOH.⁵⁴ This fact demonstrated that the preorganization of three binding sites including OH, NH, and COOH (OH) to form a tridentate binding motif is crucial for the selective interaction with Al^{3+} . Double electron donors comprised of nitrogen and sulfur atom were attached to 1,2-dihydroxyanthraquinone to create a turn-on fluorescent probe **83**.⁵⁵ It showed quite weak fluorescence under neutral pH condition due to the photoinduced electron transfer. Upon complexation with Al^{3+} , 110-fold fluorescence enhancement was triggered due to the inhibition of the PET process from the lone electron pair of nitrogen and sulfur atom.

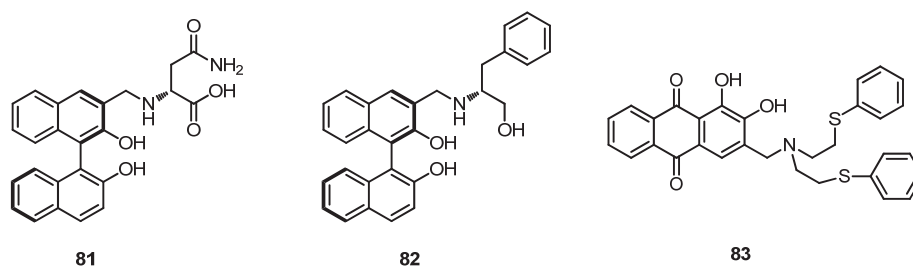


Figure 4-33. Al^{3+} chemosensors based on salicyclic amino six-membered ring.

Triazole as binding sites

1,2,3-Triazolyl moiety can be easily obtained with very high yields and good regioselectivity by Cu(I) catalyzed alkyne-azide cycloaddition (CuAAC) click reaction, which has been widely utilized in organic synthesis, material science and bioconjugation chemistry. Its incorporation with fluorophores has been designed to be fluorescent chemosensors for different species. However, only rare examples have been reported for the selective detection of Al^{3+} . Three ligands **84**, **85**, and **86** containing triazolyl moiety and different fluorophores were synthesized in Govindaraju's group for the detection of Al^{3+} (Figure 4-34).^{56,57,58} Constraining bipyridyl-dansyl linked by triazole, **84** showed distinct spectral behavior to Al^{3+} with fluorescence quenching at 532 nm and appearance of new peak at 446 nm. The initial fluorescence quenching and blue shift of the emission band was attributed to complexation of Al^{3+} with dimethylamino group of dansyl moiety which reduced its electron-donating character and suppressed the intramolecular charge transfer, causing the blue shift and fluorescence quenching. The further addition of Al^{3+} coordinated to nitrogen atom on the

bipyridyl-triazole moiety and consequently blocked the photo-induced electron transfer and led to fluorescence enhancement. This binding process had been verified by chemical shifts of **84** in the presence of Al^{3+} . In another piece of later work, by keeping the bipyridyl-triazole binding sites, dansyl fluorophore was changed into coumarin to have compound **85**. High selectivity for Al^{3+} was retained in this system. The addition of Al^{3+} induced red shift of absorption band to 324 nm and concomitantly with large fluorescence enhancement at 443 nm in MeCN. The formation of 1:1 complex was illustrated by ^1H NMR titration and MALDI/TOF mass spectra. It should be noted that though these two ligands (**84**, **85**) consisted of different fluorophores, absorption and emission spectra of the final complex was quite similar, indicating the key binding sites bipyridyl-triazole might also be the fluorophore of the complex. Recently Govindaraju et al reported **86**, a conjugation of two fluorophores (coumarin and hydroxyquinoline), as a ratiometric sensor for Al^{3+} . In the presence of Al^{3+} , fluorescence intensity of ligand **86** at 400 nm was quenched and a new band at 484 nm appeared in MeCN/ H_2O (9:1) mixed solution. Comparison of ^1H NMR between free ligand and 1:1 complex suggested that Al^{3+} coordinated to coumarin, triazole and hydroxyquinoline. The above three pieces of works demonstrated that incorporation of triazole in chemosensors can potentially selectively response to Al^{3+} ; however, many of them still suffered from the limitation in organic solvent medium.

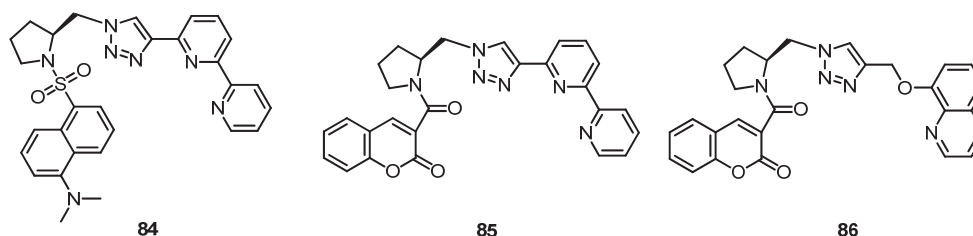


Figure 4-34. Al^{3+} chemosensors based on triazolyl group.

Ion pair interaction

Compared with metal complexation interaction, ion pair interaction usually provides great advantages to overcome the limitation in organic solvents. Au NPs functionalized with pentapeptide CALNN **87** (Figure 4-35) showed distinct response to Al^{3+} when compared with other metal ions.⁵⁹ Addition of Al^{3+} induced red shift of surface plasmon band and resulted in solution color change from purple to blue, strongly indicative of aggregation of Au NPs in the presence of Al^{3+} . Modified protected ligands were used to demonstrate that the selectivity was both coming from sequence of the peptide and terminal carboxylic acid group. Detection limit with 0.2 μM was achieved and this approach was successfully applied for quantitative analysis of cellular Al^{3+} . A new water soluble ligand **88** was found to exhibit aggregation induced emission (AIE) in THF/ H_2O medium with increasing fraction of H_2O (Figure 4-35).⁶⁰

excimer emission at around 475 nm and a weak monomer emission at 375 nm, which indicated that the close proximity of two pyrene moieties in the solution and intramolecular π - π stacking interaction. In the presence of increasing concentrations of Al^{3+} in MeCN, a fluorescent ratiometry with enhanced monomer and quenched excimer was observed due to the less efficient overlap of π - π stacking interaction interrupted by Al^{3+} . However, selectivity of these ligands to Al^{3+} through the polyether was not good enough since they also showed efficient quenching to Pb^{2+} .

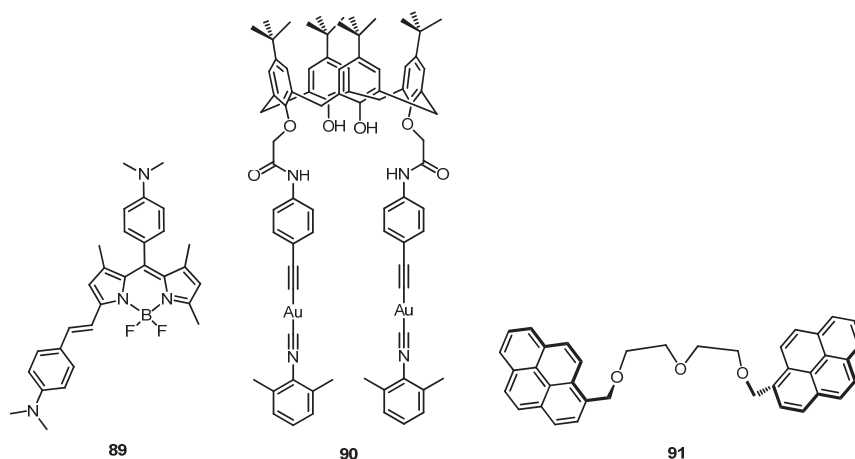


Figure 4-36. Al^{3+} chemosensors based on atypical binding sites.

The introduction mentioned above has demonstrated that ions pair approach possesses several advantages when compared with others. They generally work well in aqueous solutions and show high selectivity to Al^{3+} with little interference from other metal ions. However, there are still rare examples by utilization of ion pair interactions to detect aluminum with satisfactory results. Investigations on interaction of surfactant containing sulfonate with Al^{3+} have shown that the strong electrostatic interaction could lead to precipitation which was quite markedly influenced by pH.⁶⁴ Their results indicated that the competition among sulfonate monomers, micelles and hydroxyl ions for Al species control the behavior of the system. For continuous work on the program of developing fluorescent chemosensors based on the framework of calix[4]arene, we envisage to introduce the sulfonate groups on to the calix[4]arene moiety. On one hand we intend to study the effect of the additional sulfonate group on the binding ability of azacrown to K^+ and on the other hand the strong interaction between sulfonate and aluminum could lead to form aggregates and consequently influence photophysical properties of dansyl fluorophore. **SulfCalix-Dansyl** is shown in Scheme 4-4.

polar micro-environment for ICT type fluorophores.

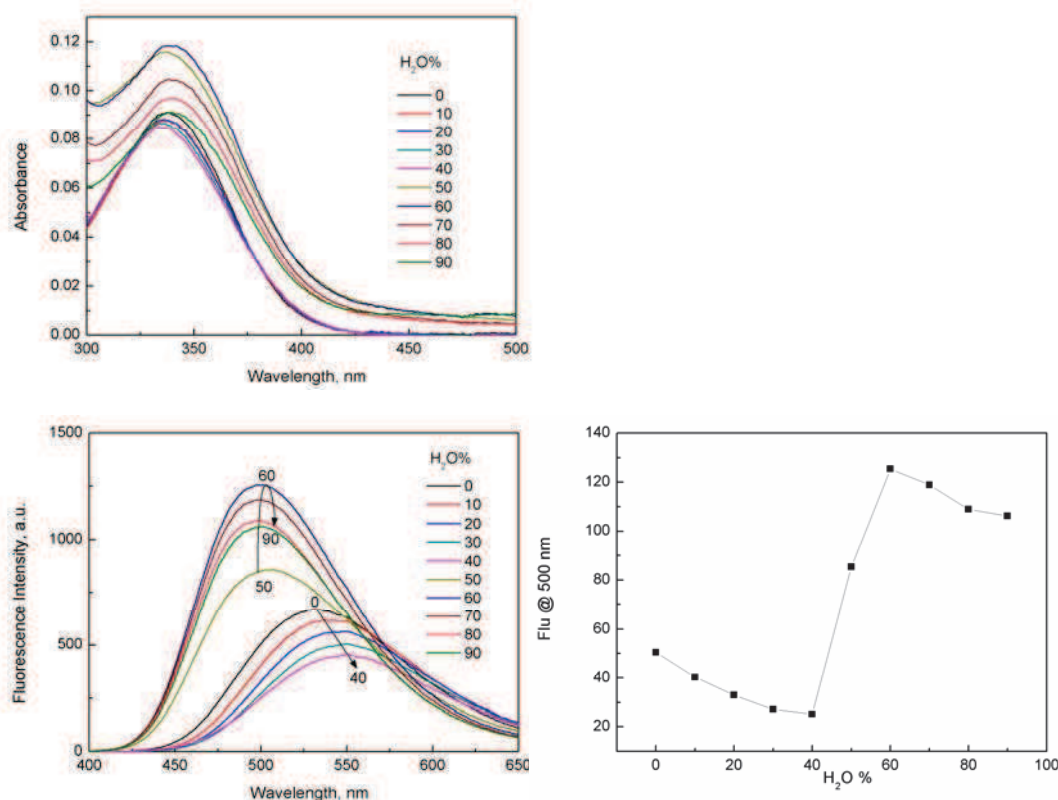


Figure 4-37. Absorption (top) and fluorescence (bottom) spectra of **Calix-Dansyl** in EtOH and milli-Q water mixed solution; [**Calix-Dansyl**] = 10 μ M, λ_{ex} = 338 nm.

4.2.4. Photophysical properties of SulfCalix-Dansyl

Spectral properties of **SulfCalix-Dansyl** were investigated in H₂O. As shown in Figure 4-38, it exhibits a broad absorption band centered at 328 nm and an emission band at 579 nm under neutral and basic condition, which can be attributed to intramolecular charge transfer from dimethylamino group to sulfonyl group. By decreasing pH of the solution with the addition of HClO₄, absorption band at 328 nm decreases and new peaks at 320 and 285 nm appear, which is characteristic of dansyl fluorophore when its dimethylamino group is protonated. Meanwhile, gradual decrease of the fluorescence intensity at 579 nm was observed. Protonation of the dimethylamino group blocks the intramolecular charge transfer. The pK_a of **SulfCalix-Dansyl** in H₂O was obtained by fitting from the titration to be 4.7. Molecular geometry in solution was investigated by ROESY spectra. As displayed in Figure 4-39, protons at 3.4 ppm of glycol couple with protons of dansyl at 8.1 ppm and protons of dimethylamino group of dansyl at 2.7 ppm couple with protons of calixarene at 7.4 ppm. The results indicate that dansyl fluorophores are in close proximity to calixarene moiety due to pyramidalization of nitrogen atom and distorted tetra-hedral geometry of sulfonyl group, resulting two of sulfonate anions completely exposed to water.

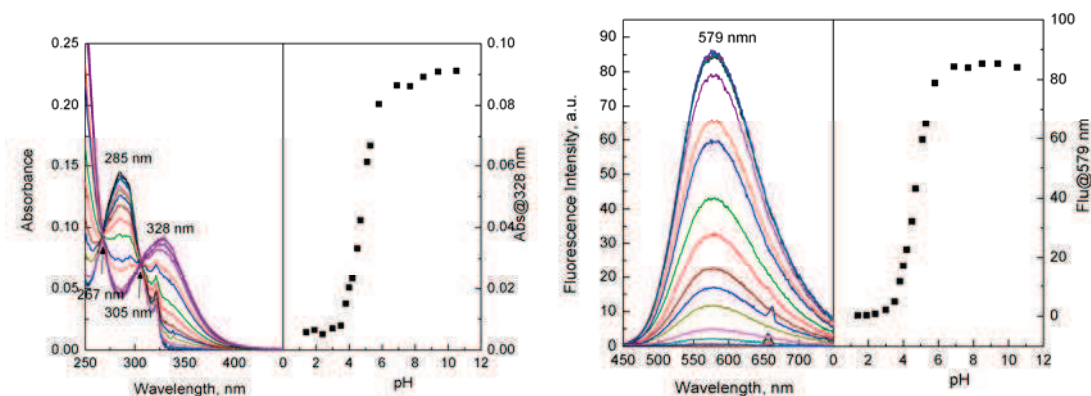


Figure 4-38. Absorption and fluorescence of **SulfCalix-Dansyl** at different pH in milli-Q water, pH was adjusted by HClO₄ and NaOH, [SulfCalix-Dansyl] = 10 μM.

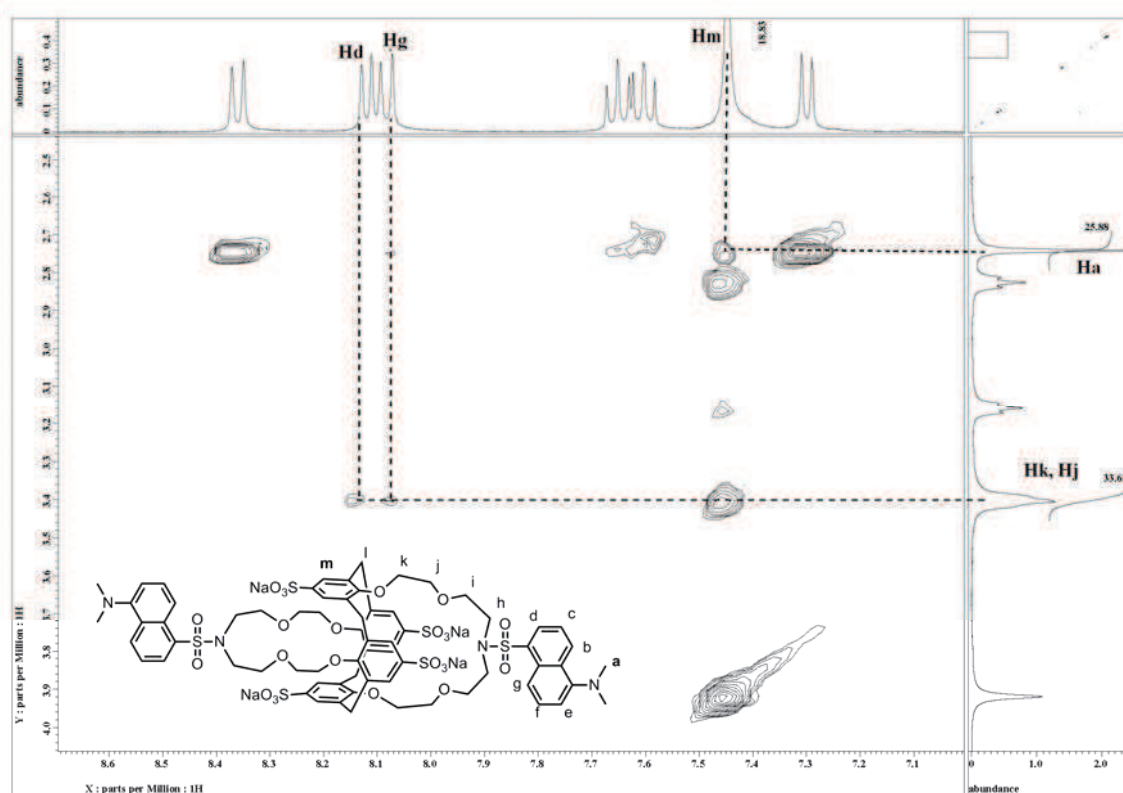


Figure 4-39. ROESY of **SulfCalix-Dansyl** in D₂O.

In order to examine how the introduction of four sulfonate groups affect the photophysical properties of fluorescent core dansylamide, firstly their absorption and fluorescence spectra were recorded in MeCN/H₂O (v:v = 3:2). As shown in Figure 4-40, the normalized spectra illustrate that the introduction of four sulfonate groups cause about 6 nm blue shift for the absorption spectra and 5 nm red shift for the emission spectra. More detailed investigation

was again performed in EtOH/H₂O (v:v = 9:1), as displayed in Table 4-5. The blue shift of the absorption band in this medium is 8 nm, a bit larger than that in MeCN/H₂O (v:v = 3:2). However, no wavelength shift was observed for the emission spectra. They both show almost the same extinction coefficients and fluorescence quantum yield in EtOH/H₂O (v:v = 9:1). Therefore the introduction of four sulfonate groups on the calix[4]arene does not affect significantly radiative processes but makes it very soluble in water. It's also assumed that it may affect the binding ability of the azacrown moiety to cations.

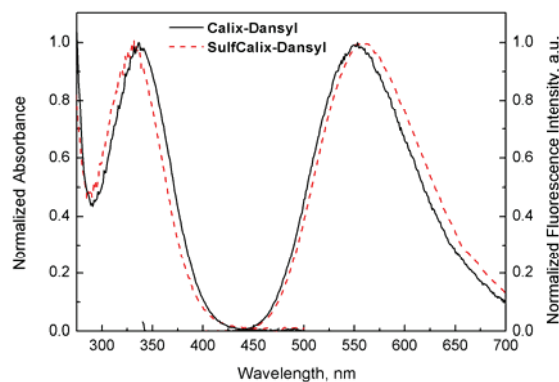


Figure 4-40. Normalized absorption and fluorescence spectra of **Calix-Dansyl** and **SulfCalix-Dansyl** in MeCN/H₂O (v/v = 3:2).

Compound	λ_{\max}^A [nm]	λ_{\max}^F [nm]	$\Delta\lambda_{F-A}$ [cm ⁻¹]	ϵ_{00} [L.mol ⁻¹ .cm ⁻¹]	Φ_F
Calix-Dansyl	338	539	11033	8910	0.39
SulfCalix-Dansyl	330	540	11601	9038	0.34

Table 4-5. Photophysical data of **Calix-Dansyl** and **SulfCalix-Dansyl** in EtOH/H₂O(v:v = 9:1), using sulfate quinine in 0.5N H₂SO₄ as the reference.

4.2.5. Complexation of SulfCalix-Dansyl in buffer solutions

Spectral response of **SulfCalix-Dansyl** to a wide range of metal ions was then screened in lutidine buffer solution at pH 6.0. As shown in Figure 4-41, the addition of very high concentrations of alkali metals Na⁺, K⁺, Li⁺, alkaline earth metal Mg²⁺, Ca²⁺, Ba²⁺ at 10 mM level and transition metal ions Eu³⁺, La³⁺, Cd²⁺, Co²⁺, Cu²⁺, Fe²⁺, Hg²⁺, Mn²⁺, Ni²⁺, Pb²⁺ and Zn²⁺ at 0.1 mM show almost no effect on the spectral properties of **SulfCalix-Dansyl**. In contrast, the addition of Al³⁺ (0.1 mM) induces remarkable fluorescence enhancement concomitant with large blue shift from 576 to 530 nm and fluorescence color change from yellow to green. The addition of Fe³⁺ (0.1 mM), however, decreases the fluorescence intensity without wavelength shift. Concerning the absorption spectra, almost no change was observed

for all the tested metal ions except Al^{3+} and Fe^{3+} . In the presence of Fe^{3+} it shows a quite strong absorption band at 340 nm where it significantly overlaps with the excitation wavelength. Thus the fluorescence quenching caused by Fe^{3+} quite probably comes from the inner filtering effect. The level-off tail absorption band in the longer wavelength range is observed in the presence of Al^{3+} , strongly indicating the formation of small particles in solutions. Considering the large blue shift of the wavelength with respect to Al^{3+} , selectivity is expressed as the ratio of fluorescence intensity at 540 nm and 640 nm, as shown in Figure 4-43. It further confirms that **SulfCalix-Dansyl** shows very high selectivity to Al^{3+} over other metal ions and the interference from Fe^{3+} was reduced to a large extent when compared with the selectivity expressed as fluorescence intensity at single wavelength. Ratiometric detection not only has a built-in correction for the environmental effects but also reduces the interference behaving in the way of fluorescence intensity variation at single wavelength.

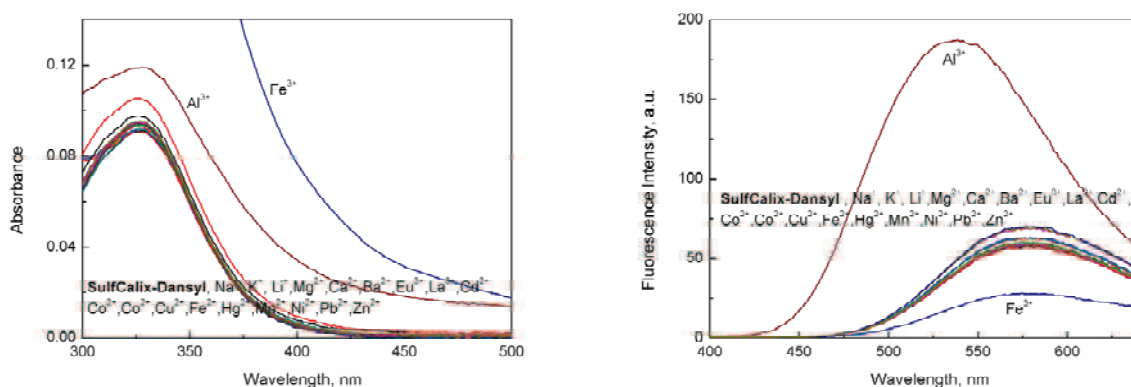


Figure 4-41. Absorption and fluorescence spectra of **SulfCalix-Dansyl** in the presence of various metal ions in lutidine buffer solution (pH = 6.0, 10 mM); [**SulfCalix-Dansyl**] = 10 μM , alkali and alkaline earth metal ions were 10 mM, and the others were 0.1 mM, $\lambda_{\text{ex}} = 328$ nm.

To examine the practical application of our protocol, we investigated the spectral response of **SulfCalix-Dansyl** to Al^{3+} in the presence of other competing metal ions. As shown in Figure 4-42, even the presence of high concentrations of alkali metals Na^+ , K^+ , Li^+ , (10 mM), alkaline earth metal Mg^{2+} , Ca^{2+} , Ba^{2+} , (10 mM), they did not influence the detection of Al^{3+} . For transition metal ions, except Cu^{2+} and Fe^{3+} all the others almost show no interference. The presence of Cu^{2+} and Fe^{3+} induced remarkable fluorescence quenching but to different extents; however, it's worthy of notice that they all show large blue shift compared with **SulfCalix-Dansyl**. We believe that the presence of Cu^{2+} does not interrupt the first binding process but quenches the fluorescence of the resultant “green” complex (**SulfCalix-Dansyl**- Al^{3+}) by heavy atom effect or electron/energy transfer. The major quenching of Fe^{3+} is attributed to the inner filter effect. When the ratio of fluorescence intensity at 540 nm and 640

nm was used to establish the competition experiment, the interference of Cu^{2+} was eliminated and Fe^{3+} was reduced, as shown in Figure 4-43. Therefore **SulfCalix-Dansyl** was demonstrated to be a promising selective fluorescent chemosensor for aluminum in complex samples.

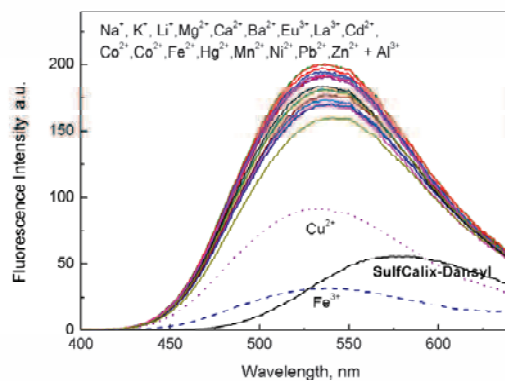


Figure 4-42. Fluorescence spectra of **SulfCalix-Dansyl** in the coexistence of various metal ions and Al^{3+} in lutidine buffer solution (pH = 6.0, 10 mM); [**SulfCalix-Dansyl**] = 10 μM , alkali and alkaline earth metal ions were 10 mM, and the others were 0.1 mM, $\lambda_{\text{ex}} = 328 \text{ nm}$.

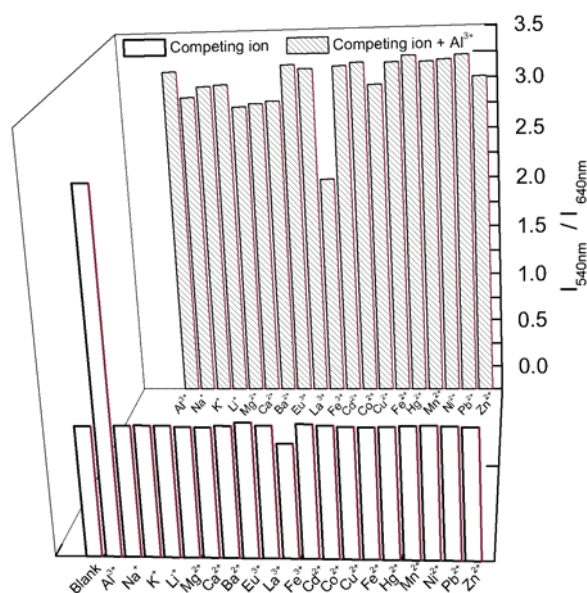
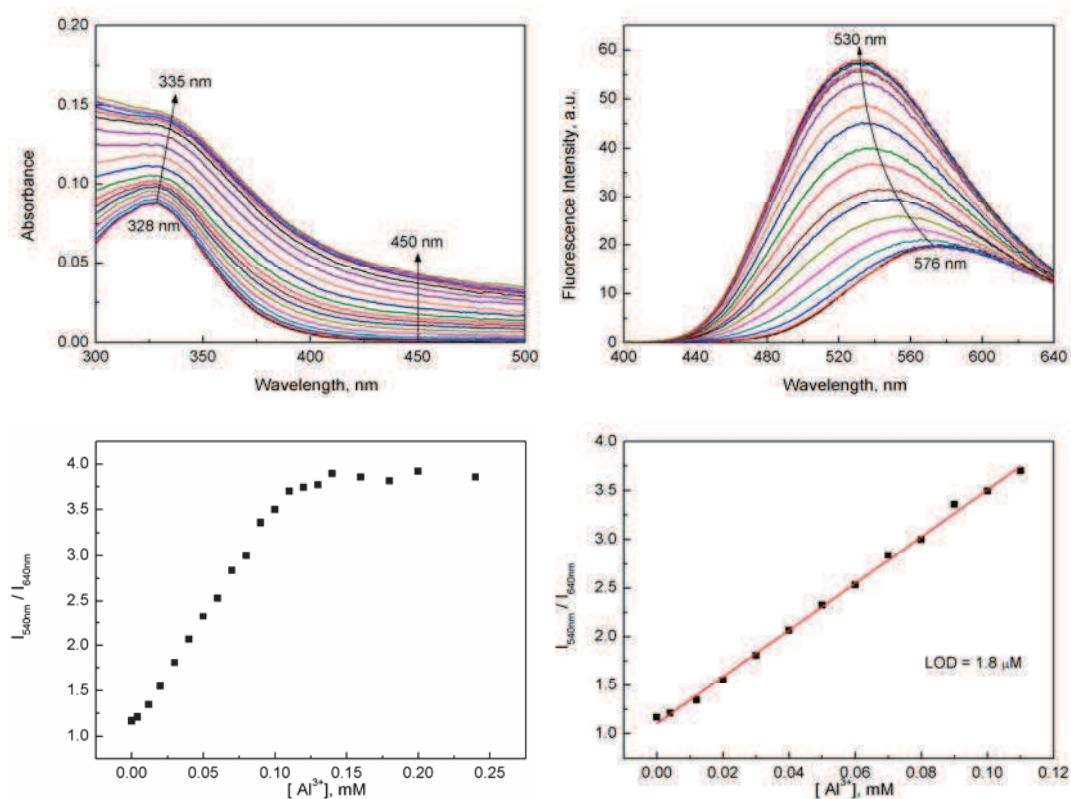


Figure 4-43. Ratiometric response I_{540}/I_{640} of **SulfCalix-Dansyl** in the presence of selected metal ions in lutidine buffer solution (pH = 6.0, 10 mM). The light bars represent the response of **SulfCalix-Dansyl** in the presence of selected cations; the dense bars represent the response upon an addition of Al^{3+} to a solution of **SulfCalix-Dansyl** in the presence of selected cations; [**SulfCalix-Dansyl**] = 10 μM , alkali and alkaline earth metal ions were 10 mM, and the others were 0.1 mM, $\lambda_{\text{ex}} = 328 \text{ nm}$.

As shown in Figure 4-44 (top), the absorption and fluorescence titration of **SulfCalix-Dansyl** to Al^{3+} were then carried out in lutidine buffer solution at pH 6.0. Upon addition of increasing concentrations of Al^{3+} , the absorption band at 328 nm shows a little red

shift to 335 nm, which is quite close to that of **Calix-Dansyl** and indicates that partial negative charges were neutralized by Al^{3+} . Meanwhile, level-off tail absorption band ranging in long wavelength region increases due to scattering effect from the incremental formation of aggregates/particles. With respect to the fluorescence titration, when the concentration of Al^{3+} is lower than 0.1 mM, there is a gradual fluorescence enhancement and emission band blue shift from 576 nm to 530 nm. It reaches a plateau when the concentration is over 0.1 mM. Due to 46 nm blue shift, it's possible for us to detect Al^{3+} in ratiometric method. Ratio of fluorescence intensity at 540 and 640 nm as the functions of concentrations of added Al^{3+} is plotted, as shown in Figure 4-44 (middle). A nice linear dependence is obtained ranging from 0 to 0.1 mM. According to the $3\sigma/k$, the detection limit in this approach was calculated to be $1.8 \mu\text{M}$, meeting with the requirement of WHO with a limit of $7.41 \mu\text{M}$ Al^{3+} in drinking water. We also try to make a plot by integration fluorescence area from 400 to 640 nm versus concentration of Al^{3+} , as displayed in Figure 4-44 (bottom). However, the linear dependence is not as good as the ratiometric methods. In order to test the validation of this approach under physiological conditions, the titration was also conducted at pH 7.0, as shown in Figure 4-45. It shows very similar spectral response to Al^{3+} as that under pH 6.0. However, the solution was not stable, especially when the concentration of Al^{3+} was over 0.1 mM.



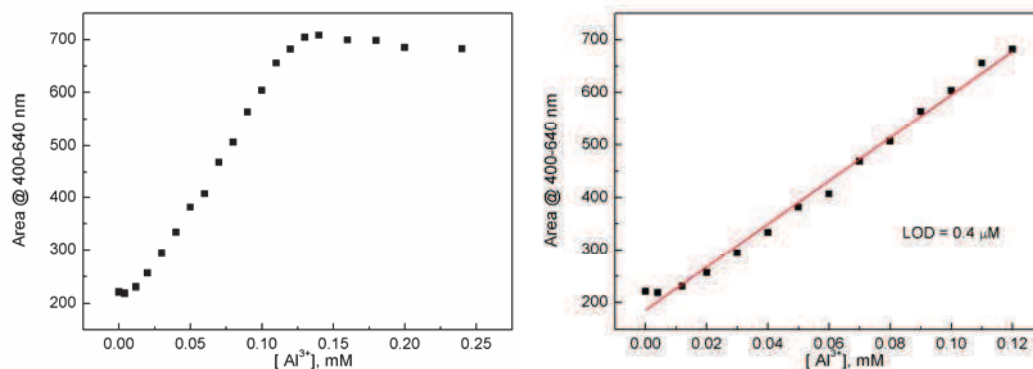


Figure 4-44. Absorption and fluorescence spectra of **SulfCalix-Dansyl** in the presence of increasing concentrations of Al^{3+} in lutidine buffer solution (pH = 6.0, 10 mM); $[\text{SulfCalix-Dansyl}] = 10 \mu\text{M}$, $\lambda_{\text{ex}} = 330 \text{ nm}$.

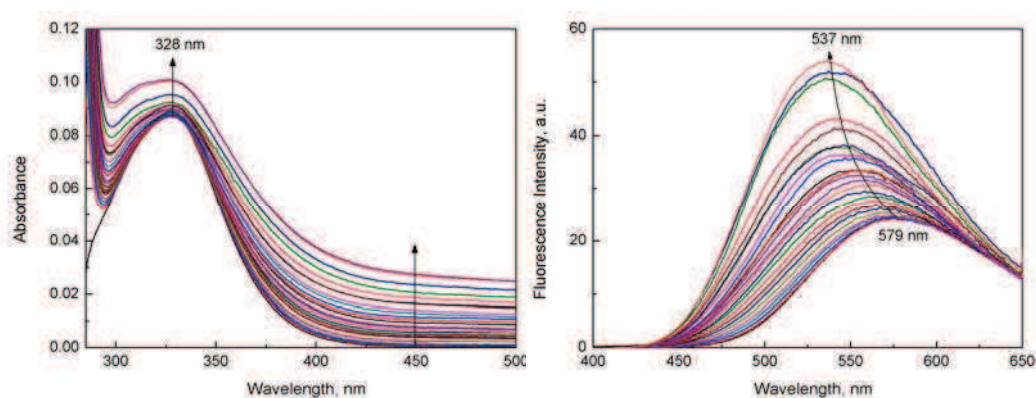


Figure 4-45. Absorption and fluorescence spectra of **SulfCalix-Dansyl** in the presence of increasing concentrations of Al^{3+} in lutidine buffer solution (pH = 7.0, 10 mM); $[\text{SulfCalix-Dansyl}] = 10 \mu\text{M}$, $\lambda_{\text{ex}} = 330 \text{ nm}$.

Reversibility is one of the most important parameters of chemosensors. The reversible binding process between **SulfCalix-Dansyl** and Al^{3+} was investigated in lutidine buffer solution both at pH 6.0, as illustrated in Figure 4-46. With the addition of 2 equiv of Na_2EDTA or NaF with respect to Al^{3+} , fluorescence spectra of **SulfCalix-Dansyl** were recovered and nearly overlapped with free ligand. This is due to much stronger binding ability of $\text{EDTA}^{2-}/\text{F}^-$ to Al^{3+} compared with sulfonate anion. Regeneration of free ligand is important for the fabrication of devices to sense Al^{3+} .

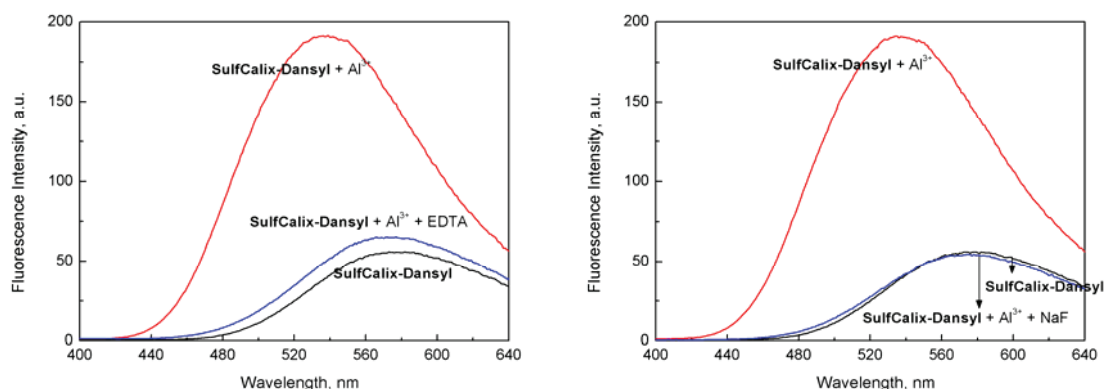


Figure 4-46. Reversibility **SulfCalix-Dansyl** - Al^{3+} in lutidine buffer solution (pH = 6.0, 10 mM); [**SulfCalix-Dansyl**] = 10 μM , [Al^{3+}] = 0.1 mM, [EDTA] = [NaF] = 0.2 mM, λ_{ex} = 328 nm.

In Figure 4-44, with the increasing concentrations of Al^{3+} , the increment of absorption tail (450-500 nm) resulted from the scattering effect indicates large particle was formed during the titration. Two possibilities can be proposed for this phenomenon: one is the addition of Al^{3+} could coordinate with sulfonate ion to form metal coordination polymers, which subsequently form aggregates; the other is Al^{3+} itself at pH 6 hydrolyzes into $\text{Al}(\text{OH})_3$ and suspends in solution.

In order to get insight into sensing mechanism of our protocol, we then first investigated the pH effect on the binding ability of **SulfCalix-Dansyl** to Al^{3+} . As mentioned above, dansylamide fluorophore is sensitive to pH change.⁶⁵ Protonation on the dimethylamino group inhibits intramolecular charge transfer and decreases its emission intensity. However, no wavelength shift for ICT band is observed in the tested pH range (4-9) and thus ratio of fluorescence intensity at 540 nm and 640 nm keeps constant under different pH conditions, as shown in Figure 4-47 (left). While in the presence of Al^{3+} , the ratio of resultant complex shows maximum at pH 6 and decreases dramatically when pH deviates 6. When pH is lower than 5 or higher than 8, the presence of Al^{3+} almost shows no influence on the ratio value. It's well known that the existing forms of aluminum change with pH, as shown in Figure 4-47 (right). In pure water, when the pH is lower than 4, 90% of aluminum exists as the free $[\text{Al}(\text{H}_2\text{O})_6]^{3+}$; with increase of pH but lower than 7, aluminum hydrolyzes to produce precipitate $\text{Al}(\text{OH})_3$; and when the pH is higher than 7, $\text{Al}(\text{OH})_3$ is again transferred into $\text{Al}(\text{OH})_4^-$.⁶⁶ The pH effect on the spectral response of **SulfCalix-Dansyl** to Al^{3+} is a bit like the curve of fraction distribution of $\text{Al}(\text{OH})_3$ in water under different pH, though with a narrower half-peak width. It's supposed that **SulfCalix-Dansyl** with four negative charge can be adsorbed onto the $\text{Al}(\text{OH})_3$ colloid surface covered with positive charge through

electrostatic interaction. From pH 5 to 6, there may exist species with positive charge such as Al^{3+} , $\text{Al}(\text{OH})^{2+}$ and $\text{Al}(\text{OH})_2^+$, which result in the strong adsorption of **SulfCalix-Dansyl**; however when pH further increases, density of the positive charge on the surface will be reduced quickly, which might be the reason why it shows narrower half-peak width. Micro-environmental polarity of the dansylamide changes a lot when **SulfCalix-Dansyl** was adsorbed onto the colloid surface. As we know, decrease of the polarity will induce blue shift and fluorescence enhancement. This explanation is consistent with our results.

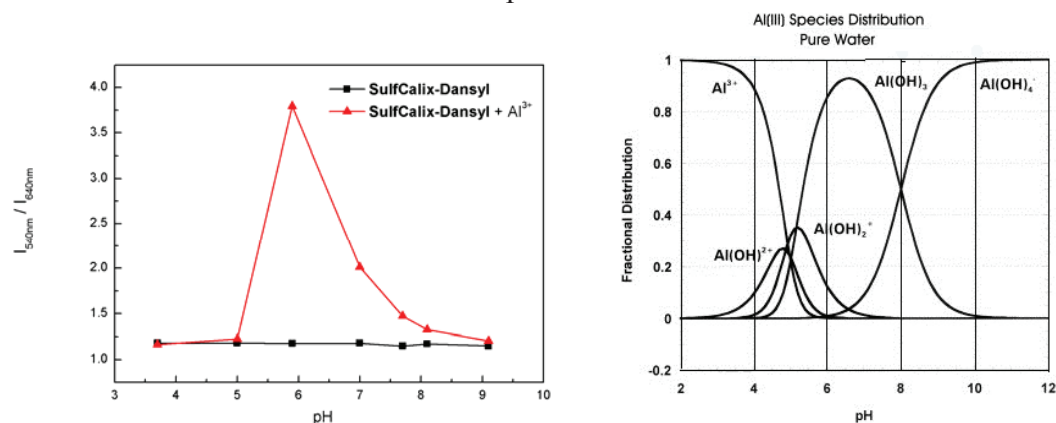


Figure 4-47. The pH effect on the change of fluorescence intensity at 533 nm of **SulfCalix-Dansyl** before and after addition of Al^{3+} in lutidine solution (10 mM), $\lambda_{\text{ex}} = 328 \text{ nm}$; [**SulfCalix-Dansyl**] = 10 μM and the pH effect of species of Al^{3+} in pure water; right: Al(III) species distribution in pure water⁶⁶.

Resonance light scattering spectrometry plays important roles in physical chemistry, colloid chemistry and macromolecule chemistry, mainly providing important information on molecular weight, radius of rotation, shape and size of particle.^{67,68} Theory of light scattering may be categorized into two theoretical frameworks.⁶⁹ One is Rayleigh scattering when diameter of particle is much smaller than incident light wavelength; and the other is Mie scattering when particle size is about the same or larger than wavelength of incident light. Though versatile theories have been developed for analytical calculations, herein it's difficult for us to obtain information about the size and shape of the particles formed in-situ. Rayleigh approximation is then simply used to describe our system, from which we can see the light intensity is proportional to diameter of particles with sixth power orders dependence.⁷⁰ Anyhow, variation of resonance light scattering can still qualitatively indicate the change of particles size. As displayed in Figure 4-48, both Al^{3+} and **SulfCalix-Dansyl** in lutidine buffer at pH 6.0 show very weak signal. However, with addition of Al^{3+} to the solution of **SulfCalix-Dansyl**, a quite strong resonance relay scattering was observed from 300 nm to 500 nm. This demonstrates that interaction between Al^{3+} and **SulfCalix-Dansyl** promotes to form a large particle in solution and the absorption of **SulfCalix-Dansyl** in this range induces the resonance light scattering and greatly enhances the signal. No change is observed in the case

of Zn^{2+} , while addition of Fe^{3+} causes an enhancement but to a lesser extent when compared with Al^{3+} (Figure 4-48).

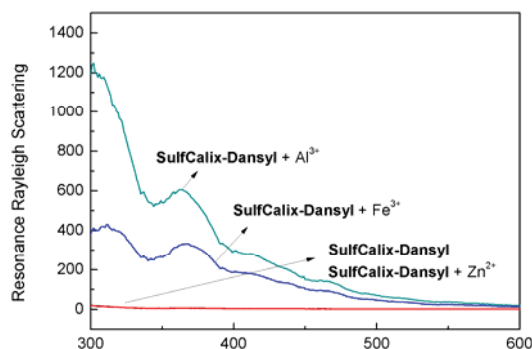


Figure 4-48. Resonance Rayleigh scattering of **SulfCalix-Dansyl** in the presence of various metal ions in lutidine buffer solution (pH = 6.0, 10 mM); [**SulfCalix-Dansyl**] = 10 μM , metal ions were 0.1 mM.

Anisotropy measurement has been proved to be a robust approach to obtain information on size and shape of macromolecules or assemblies or the rigidity of molecular environment. It's significantly affected by several factors, among which rotational diffusion is the most common cause. Assuming no other processes result in loss of anisotropy, the expected anisotropy can be given by Perrin equation:

$$r = \frac{r_0}{1 + (\tau / \theta)}$$

where r_0 is the anisotropy measured in the absence of rotational diffusion, and τ is lifetime of the fluorophore, and θ is the rotational correlation time for the diffusion process.⁷¹ Therefore larger anisotropy would be obtained when the rotational diffusion time is increased by attaching the fluorophore to large particles.⁷² ⁷³We then carried out the anisotropy measurement of our sensing systems. As can be seen from Figure 4-49, the free **SulfCalix-Dansyl** shows very small anisotropy with the average value at 0.05 from 560 to 600 nm, due to the rapid rotation of fluorophore in its lifetime scale. It's quite surprising to find that with the addition of 10 equiv of Al^{3+} , anisotropy of the resultant complex was increased to 0.23 from 520 to 560 nm. The significant increase of the anisotropy strongly demonstrates that **SulfCalix-Dansyl** is attached to large particles which results in decrease of the rotational diffusion rate. This is consistent with our results from the light resonance scattering.

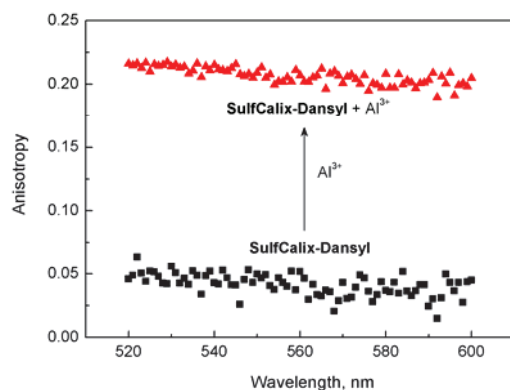


Figure 4-49. Anisotropy of **SulfCalix-Dansyl** in the absence and presence of Al^{3+} in lutidine buffer solution (pH = 6.0, 10 mM); [**SulfCalix-Dansyl**] = 10 μM , [Al^{3+}] = 0.1 mM, λ_{ex} = 328 nm.

Reference compound **Calix-Dansyl** without sulfonate groups was further utilized to verify the role of electrostatic interactions in the binding process. Under the identical conditions, spectral response of **Calix-Dansyl** and **SulfCalix-Dansyl** to Al^{3+} was examined. Considering the different solubility of both ligands, it was carried out in EtOH and lutidine (pH = 6.0, 10 mM) mixed solution ($v_{\text{EtOH}}:v_{\text{Lutidine}} = 9:1$). As shown in Figure 4-50, with addition of 10 equiv Al^{3+} , there is a fluorescence enhancement and slight blue shift for **SulfCalix-Dansyl** while no influence on **Calix-Dansyl**. The smaller blue shift and less fluorescence enhancement can be attributed to the less variation of polarity of dansyl fluorophore before and after adsorption onto the colloid $\text{Al}(\text{OH})_3$. This phenomenon confirms our assumption that the electrostatic interaction plays an important role in the binding process and the azacrown in **SulfCalix-Dansyl** seems to act as a linker not a binding site.

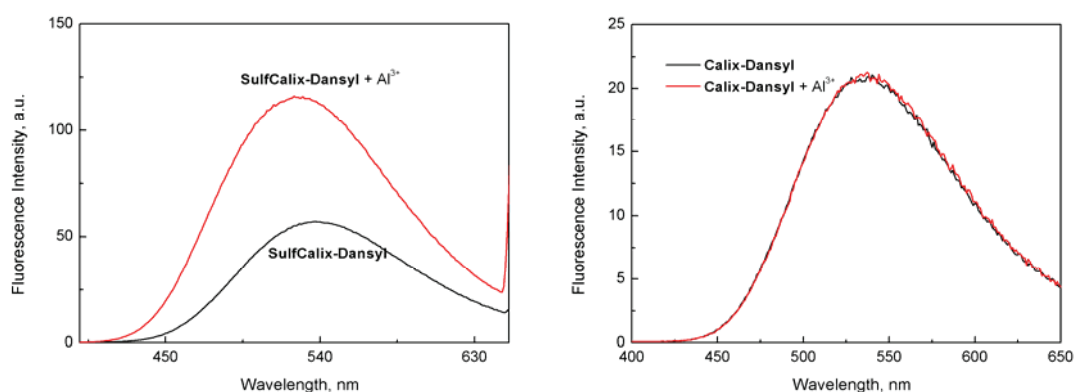


Figure 4-50. Fluorescence spectra of **SulfCalix-Dansyl** and **Calix-Dansyl** in the absence and presence of Al^{3+} in EtOH and lutidine buffer solution (pH = 6.0, 10 mM) mixed solution ($v_{\text{EtOH}}:v_{\text{Lutidine}} = 9:1$); [**SulfCalix-Dansyl**] = 10 μM , [Al^{3+}] = 0.1 mM, λ_{ex} = 328 nm for **SulfCalix-Dansyl** and , λ_{ex} = 338 nm for **Calix-Dansyl**.

Finally naked eye detection is fascinating due to its great simplicity. There is a blue shift by 40 nm from 579 to 537 nm with the fluorescence change from dark yellow to bright green under illumination of 365 nm (Figure 4-51). When the resultant complex was kept still for another two hours, very obvious flocs with bright fluorescence were observed at the bottom of cuvette, indicating the agglomeration of destabilized particles into large size.

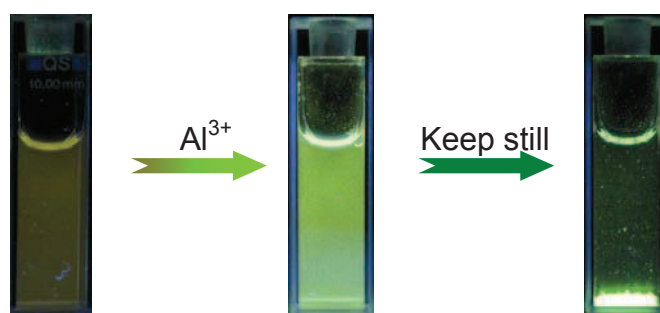
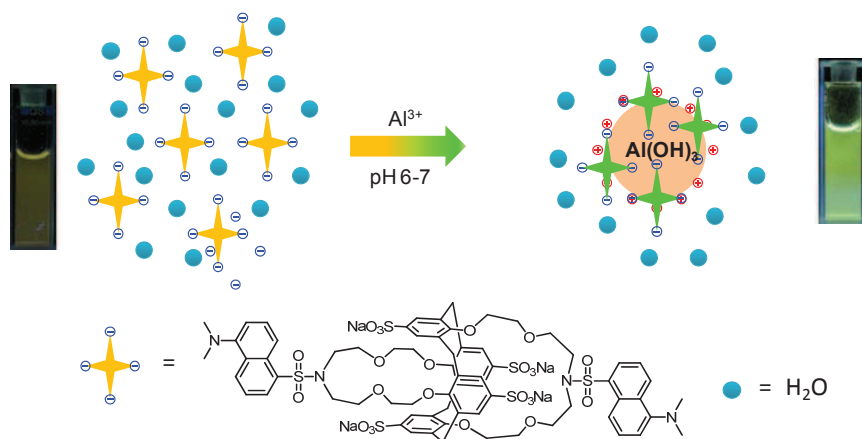


Figure 4-51. Photographs of **SulfCalix-Dansyl** in the absence and presence of Al^{3+} in lutidine buffer solution (pH = 7.0, 10 mM); [**SulfCalix-Dansyl**] = 10 μM .

4.2.6. Conclusion

In this section, we have presented that sulfonated **SulfCalix-Dansyl** exhibited very high selectivity to Al^{3+} under weak acid condition pH 6.0. Remarkable fluorescence blue shift and about 3-fold enhancement were observed due to the adsorption of **SulfCalix-Dansyl** to colloid particle of $\text{Al}(\text{OH})_3$ with positive charge on its surface, as illustrated in Scheme 4-5. This assumption was verified by the increase of absorption tail band, pH effect, resonance light scattering, anisotropy measurement and also flocculation formation. The change of the micro-environmental polarity of ICT characteristic dansyl fluorophore results in the fluorescence enhancement and blue shift. It should be noted that many reported investigations on fluorescent Al^{3+} chemosensors have been conducted under weak acidic condition, however without consideration of the distribution of different species of Al^{3+} may cause misunderstanding of the binding process. From our results above, it's already known that the selectivity stems from the unique character of Al^{3+} , thus the vast choices of the indicators may largely and easily extend our strategy by using different ICT characteristic chromophore/fluorophores for the selective detection of aluminum.



Scheme 4-5. Schematic illustration of interaction between **SulfCalix-Dansyl** and Al^{3+} .

References

- [1] Sterns, R. H.; Cox, M.; Feig, P. U.; Singer, I. "Internal Potassium-Balance and the Control of the Plasma Potassium Concentration." Medicine **1981**, *60*, 339-354.
- [2] Minta, A.; Tsien, R. Y. "Fluorescent Indicators for Cytosolic Sodium." Journal of Biological Chemistry **1989**, *264*, 19449-19457.
- [3] Steed, J. W.; Atwood, J. L. "Supramolecular Chemistry, 2nd edition" John Wiley & Sons, **2009**.
- [4] Baruah, M.; Qin, W. W.; Vallee, R. A. L.; Beljonne, D.; Rohand, T.; Dehaen, W.; Boens, N. "A highly potassium-selective ratiometric fluorescent indicator based on BODIPY azacrown ether excitable with visible light." Organic Letters **2005**, *7*, 4377-4380.
- [5] Lin, S. Y.; Liu, S. W.; Lin, C. M.; Chen, C. H. "Recognition of potassium ion in water by 15-crown-5 functionalized gold nanoparticles." Analytical Chemistry **2002**, *74*, 330-335.
- [6] Kim, J.; McQuade, D. T.; McHugh, S. K.; Swager, T. M. "Ion-specific aggregation in conjugated polymers: Highly sensitive and selective fluorescent ion chemosensors." Angewandte Chemie-International Edition **2000**, *39*, 3868-3872.
- [7] Xia, W. S.; Schmehl, R. H.; Li, C. J. "A highly selective fluorescent chemosensor for K^+ from a bis-15-crown-5 derivative." Journal of the American Chemical Society **1999**, *121*, 5599-5600.
- [8] Yamauchi, A.; Hayashita, T.; Kato, A.; Nishizawa, S.; Watanabe, M.; Teramae, N. "Selective potassium ion recognition by benzo-15-crown-5 fluoroionophore/ γ -cyclodextrin complex sensors in water." Analytical Chemistry **2000**, *72*, 5841-5846.
- [9] Wang, X. R.; Hu, J. M.; Liu, T.; Zhang, G. Y.; Liu, S. Y. "Highly sensitive and selective fluorometric off-on K^+ probe constructed via host-guest molecular recognition and aggregation-induced emission." Journal of Materials Chemistry **2012**, *22*, 8622-8628.
- [10] Lehn, D. B.; Sauvage, J. P.; Blanzat, J. "Cryptates—X: Syntheses et propriétés physiques de systèmes diaza-polyoxa-macrobicycliques." Tetrahedron **1973**, *29*, 1629-1645.
- [11] He, H. R.; Mortellaro, M. A.; Leiner, M. J. P.; Fraatz, R. J.; Tusa, J. K. "A fluorescent sensor with high selectivity and sensitivity for potassium in water." Journal of the American Chemical Society **2003**, *125*, 1468-1469.
- [12] Zhou, X. F.; Su, F. Y.; Tian, Y. Q.; Youngbull, C.; Johnson, R. H.; Meldrum, D. R. "A New Highly Selective Fluorescent K^+ Sensor." Journal of the American Chemical Society **2011**, *133*, 18530-18533.
- [13] Carpenter, R. D.; Verkman, A. S. "Synthesis of a Sensitive and Selective Potassium-Sensing Fluoroionophore." Organic Letters **2010**, *12*, 1160-1163.
- [14] Gutsche, C. D. "Calixarenes An Introduction 2nd Edition" The Royal Society of Chemistry, **2008**.
- [15] Valeur, B.; Leray, I. "Ion-responsive supramolecular fluorescent systems based on multichromophoric calixarenes: A review." Inorganica Chimica Acta **2007**, *360*, 765-774.
- [16] Kim, J. S.; Quang, D. T. "Calixarene-derived fluorescent probes." Chemical Reviews **2007**, *107*, 3780-3799.
- [17] Joseph, R.; Rao, C. P. "Ion and Molecular Recognition by Lower Rim 1,3-Di-conjugates of Calix[4]arene as Receptors." Chemical Reviews **2011**, *111*, 4658-4702.

- [18] Oueslati, I. "Calix(aza)crowns: synthesis, recognition, and coordination. A mini review." *Tetrahedron* **2007**, *63*, 10840-10851.
- [19] Ikeda, A.; Shinkai, S. "Novel cavity design using calix[n]arene skeletons: Toward molecular recognition and metal binding." *Chemical Reviews* **1997**, *97*, 1713-1734.
- [20] Alfieri, C.; Dradi, E.; Pochini, A.; Ungaro, R.; Andreetti, G. D. "Synthesis, and X-Ray Crystal and Molecular-Structure of a Novel Macrobicyclic Ligand - Crowned Para-Tert-Butyl-Calix[4]Arene." *Journal of the Chemical Society-Chemical Communications* **1983**, 1075-1077.
- [21] Bu, J. H.; Zheng, Q. Y.; Chen, C. F.; Huang, Z. T. "New fluorescence-quenching process through resumption of PET process induced by complexation of alkali metal ion." *Organic Letters* **2004**, *6*, 3301-3303.
- [22] Kim, S. K.; Lee, S. H.; Lee, J. Y.; Lee, J. Y.; Bartsch, R. A.; Kim, J. S. "An excimer-based, binuclear, on-off switchable calix[4]crown chemosensor." *Journal of the American Chemical Society* **2004**, *126*, 16499-16506.
- [23] Kim, J. S.; Shon, O. J.; Ko, J. W.; Cho, M. H.; Yu, I. Y.; Vicens, J. "Synthesis and metal ion complexation studies of proton-ionizable calix[4]azacrown ethers in the 1,3-alternate conformation." *Journal of Organic Chemistry* **2000**, *65*, 2386-2392.
- [24] Kim, J. S.; Shon, O. J.; Rim, J. A.; Kim, S. K.; Yoon, J. "Pyrene-armed calix[4]azacrowns as new fluorescent ionophores: "Molecular taekowndo" process via fluorescence change." *Journal of Organic Chemistry* **2002**, *67*, 2348-2351.
- [25] Koh, K. N.; Araki, K.; Shinkai, S.; Asfari, Z.; Vicens, J. "Cation-Binding Properties of a Novel 1,3-Alternate Calix[4]Biscrown - Formation of 1/1-Complex and 1/2-Complex and Unique Cation Tunneling across a Calix[4]Arene Cavity." *Tetrahedron Letters* **1995**, *36*, 6095-6098.
- [26] Kim, S. G.; Kim, H.; Noh, K. H.; Lee, S. H.; Kim, S. K.; Kim, J. S. "Potassium ion-selective membrane electrodes based on 1,3-alternatecalix[4]crown-5-azacrown-5." *Talanta* **2003**, *61*, 709-716.
- [27] ArnaudNeu, F.; Asfari, Z.; Souley, B.; Vicens, J. "Binding properties of calix[4]-bis-crowns towards alkali cations." *New Journal of Chemistry* **1996**, *20*, 453-463.
- [28] Leray, I.; Asfari, Z.; Vicens, J.; Valeur, B. "Synthesis and binding properties of calix[4]biscrown-based fluorescent molecular sensors for caesium or potassium ions." *Journal of the Chemical Society-Perkin Transactions 2* **2002**, 1429-1434.
- [29] Malval, J. P.; Leray, I.; Valeur, B. "A highly selective fluorescent molecular sensor for potassium based on a calix[4]bisazacrown bearing boron-dipyrromethene fluorophores." *New Journal of Chemistry* **2005**, *29*, 1089-1094.
- [30] van Ameijde, J.; Liskamp, R. M. J. "Synthesis of novel trivalent amino acid glycoconjugates based on the cyclotrimeratrylene ('CTV') scaffold." *Organic & Biomolecular Chemistry* **2003**, *1*, 2661-2669.
- [31] Kim, S. K.; Sim, W.; Vicens, J.; Kim, J. S. "Modular chemistry. Double- and multi-1,3-alternate-calixcrowns." *Tetrahedron Letters* **2003**, *44*, 805-809.
- [32] Kim, J. S.; Lee, W. K.; No, K.; Asfari, Z.; Vicens, J. "Two novel 1,3-calix[4]azacrowns." *Tetrahedron Letters* **2000**, *41*, 3345-3348.
- [33] Haddadi, H.; Alizadeh, N.; Shamsipur, M.; Asfari, Z.; Lippolis, V.; Bazzicalupi, C. "Cation- π Interaction in Complex Formation Between Tl^+ Ion and Calix[4]crown-6 and

- Some Calix[4]biscrown-6 Derivatives: Thallium-203 NMR, Proton NMR, and X-ray Evidence.* Inorganic Chemistry **2010**, *49*, 6874-6882.
- [34]Zatko, D. A.; Kratochv.B "Copper (2) Oxidation of Thioureas in Acetonitrile." Analytical Chemistry **1968**, *40*, 2120-2013.
- [35]Kratochv.B; Zatko, D. A.; Markusze.R "Copper(2) as an Analytical Oxidant in Acetonitrile." Analytical Chemistry **1966**, *38*, 770-772.
- [36]Kratochv.B; Zatko, D. A. "Oxidation of Some Arylamines by Copper(2) in Acetonitrile." Analytical Chemistry **1968**, *40*, 422-424.
- [37]Li, A. F.; He, H.; Ruan, Y. B.; Wen, Z. C.; Zhao, J. S.; Jiang, Q. J.; Jiang, Y. B. "Oxidative cyclization of N-acylhydrazones. Development of highly selective turn-on fluorescent chemodosimeters for Cu²⁺." Organic & Biomolecular Chemistry **2009**, *7*, 193-200.
- [38]Rodriguez-Morgade, M. S.; Planells, M.; Torres, T.; Ballester, P.; Palomares, E. "A colorimetric molecular probe for Cu(II) ions based on the redox properties of Ru(II) phthalocyanines." Journal of Materials Chemistry **2008**, *18*, 176-181.
- [39]Wang, D. P.; Shiraishi, Y.; Hirai, T. "A BODIPY-based fluorescent chemodosimeter for Cu(II) driven by an oxidative dehydrogenation mechanism." Chemical Communications **2011**, *47*, 2673-2675.
- [40]Kawahara, M.; Muramoto, K.; Kobayashi, K.; Mori, H.; Kuroda, Y. "Aluminum Promotes the Aggregation of Alzheimers Amyloid Beta-Protein in-Vitro." Biochemical and Biophysical Research Communications **1994**, *198*, 531-535.
- [41]Paik, S. R.; Lee, J. H.; Kim, D. H.; Chang, C. S.; Kim, J. "Aluminum-induced structural alterations of the precursor of the non-A beta component of Alzheimer's disease amyloid." Archives of Biochemistry and Biophysics **1997**, *344*, 325-334.
- [42]Lin, J. L.; Kou, M. T.; Leu, M. L. "Effect of long-term low-dose aluminum-containing agents on hemoglobin synthesis in patients with chronic renal insufficiency." Nephron **1996**, *74*, 33-38.
- [43]Good, P. F.; Olanow, C. W.; Perl, D. P. "Neuromelanin-Containing Neurons of the Substantia-Nigra Accumulate Iron and Aluminum in Parkinsons-Disease - a Lamma Study." Brain Research **1992**, *593*, 343-346.
- [44]Geneva, W. W. H. O. "Guidelines for drinking water quality 4th edition", **2011**.
- [45]Kumar, S.; Dhar, D. N.; Saxena, P. N. "Applications of metal complexes of Schiff bases-A review." Journal of Scientific & Industrial Research **2009**, *68*, 181-187.
- [46]Su, Z. A.; Chen, K. Y.; Guo, Y. A.; Qi, H. P.; Yang, X. F.; Zhao, M. L. "A Coumarin-Based Fluorescent Chemosensor for Zn²⁺ in Aqueous Ethanol Media." Journal of Fluorescence **2010**, *20*, 851-856.
- [47]Hisaindee, S.; Zahid, O.; Meetani, M. A.; Graham, J. "Fluorescent Studies of Salicylaldehyde and Other Related Carbonyl Compounds for the Selective and Sensitive Detection of Zinc(II) Ions in Aqueous Solution." Journal of Fluorescence **2012**, *22*, 677-683.
- [48]Kim, S.; Noh, J. Y.; Kim, K. Y.; Kim, J. H.; Kang, H. K.; Nam, S. W.; Kim, S. H.; Park, S.; Kim, C.; Kim, J. "Salicylimine-Based Fluorescent Chemosensor for Aluminum Ions and Application to Bioimaging." Inorganic Chemistry **2012**, *51*, 3597-3602.
- [49]Upadhyay, K. K.; Kumar, A. "Pyrimidine based highly sensitive fluorescent receptor for Al³⁺ showing dual signalling mechanism." Organic & Biomolecular Chemistry **2010**, *8*, 4892-4897.

- [50] Maity, D.; Govindaraju, T. "Naphthaldehyde-Urea/Thiourea Conjugates as Turn-On Fluorescent Probes for Al^{3+} Based on Restricted $C = N$ Isomerization." European Journal of Inorganic Chemistry **2011**, 5479-5485.
- [51] Sahana, A.; Banerjee, A.; Das, S.; Lohar, S.; Karak, D.; Sarkar, B.; Mukhopadhyay, S. K.; Mukherjee, A. K.; Das, D. "A naphthalene-based Al^{3+} selective fluorescent sensor for living cell imaging." Organic & Biomolecular Chemistry **2011**, 9, 5523-5529.
- [52] Arduini, M.; Felluga, F.; Mancin, F.; Rossi, P.; Tecilla, P.; Tonellato, U.; Valentinuzzib, N. "Aluminium fluorescence detection with a FRET amplified chemosensor." Chemical Communications **2003**, 1606-1607.
- [53] Ma, T. H.; Dong, M.; Dong, Y. M.; Wang, Y. W.; Peng, Y. "A Unique Water-Tuning Dual-Channel Fluorescence-Enhanced Sensor for Aluminum Ions Based on a Hybrid Ligand from a 1,1'-Binaphthyl Scaffold and an Amino Acid." Chemistry-a European Journal **2010**, 16, 10313-10318.
- [54] Dong, M.; Dong, Y. M.; Ma, T. H.; Wang, Y. W.; Peng, Y. "A highly selective fluorescence-enhanced chemosensor for Al^{3+} in aqueous solution based on a hybrid ligand from BINOL scaffold and beta-amino alcohol." Inorganica Chimica Acta **2012**, 381, 137-142.
- [55] Lu, Y.; Huang, S. S.; Liu, Y. Y.; He, S.; Zhao, L. C.; Zeng, X. S. "Highly Selective and Sensitive Fluorescent Turn-on Chemosensor for Al^{3+} Based on a Novel Photoinduced Electron Transfer Approach." Organic Letters **2011**, 13, 5274-5277.
- [56] Maity, D.; Govindaraju, T. "Pyrrolidine constrained bipyridyl-dansyl click fluoroionophore as selective Al^{3+} sensor." Chemical Communications **2010**, 46, 4499-4501.
- [57] Maity, D.; Govindaraju, T. "Conformationally Constrained (Coumarin-Triazolyl-Bipyridyl) Click Fluoroionophore as a Selective Al^{3+} Sensor." Inorganic Chemistry **2010**, 49, 7229-7231.
- [58] Maity, D.; Govindaraju, T. "A differentially selective sensor with fluorescence turn-on response to Zn^{2+} and dual-mode ratiometric response to Al^{3+} in aqueous media." Chemical Communications **2012**, 48, 1039-1041.
- [59] Li, X. K.; Wang, J. N.; Sun, L. L.; Wang, Z. X. "Gold nanoparticle-based colorimetric assay for selective detection of aluminium cation on living cellular surfaces." Chemical Communications **2010**, 46, 988-990.
- [60] Han, T. Y.; Feng, X.; Tong, B.; Shi, J. B.; Chen, L.; Zhi, J. G.; Dong, Y. P. "A novel "turn-on" fluorescent chemosensor for the selective detection of Al^{3+} based on aggregation-induced emission." Chemical Communications **2012**, 48, 416-418.
- [61] Wang, Y. W.; Yu, M. X.; Yu, Y. H.; Bai, Z. P.; Shen, Z.; Li, F. Y.; You, X. Z. "A colorimetric and fluorescent turn-on chemosensor for Al^{3+} and its application in bioimaging." Tetrahedron Letters **2009**, 50, 6169-6172.
- [62] Hau, F. K. W.; He, X. M.; Lam, W. H.; Yam, V. W. W. "Highly selective ion probe for Al^{3+} based on Au(I) center dot center dot center dot Au(I) interactions in a bis-alkynyl calix[4]arene Au(I) isocyanide scaffold." Chemical Communications **2011**, 47, 8778-8780.
- [63] Kim, H. J.; Kim, S. H.; Quang, D. T.; Kim, J. H.; Suh, I. H.; Kim, J. S. "Highly selective fluorescent signaling for Al^{3+} in bispyrenyl polyether." Bulletin of the Korean Chemical Society **2007**, 28, 811-815.
- [64] Somasundaran, P.; Ananthapadmanabhan, K. P.; Celik, M. S. "Precipitation Redissolution Phenomena in Sulfonate $AlCl_3$ Solutions." Langmuir **1988**, 4, 1061-1063.

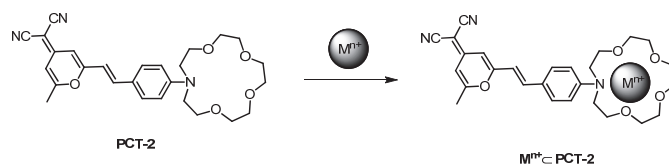
- [65]Metivier, R.; Leray, I.; Valeur, B. "*Photophysics of calixarenes bearing two or four dansyl fluorophores: charge, proton and energy transfers.*" Photochemical & Photobiological Sciences **2004**, *3*, 374-380.
- [66]Elkins, K. M.; Nelson, D. J. "*Spectroscopic approaches to the study of the interaction of aluminum with humic substances.*" Coordination Chemistry Reviews **2002**, *228*, 205-225.
- [67]Collings, P. J.; Gibbs, E. J.; Starr, T. E.; Vafek, O.; Yee, C.; Pomerance, L. A.; Pasternack, R. F. "*Resonance light scattering and its application in determining the size, shape, and aggregation number for supramolecular assemblies of chromophores.*" Journal of Physical Chemistry B **1999**, *103*, 8474-8481.
- [68]Wu, J. J.; Li, N.; Li, K. A.; Liu, F. "*J-aggregates of diprotonated tetrakis(4-sulfonatophenyl)porphyrin induced by ionic liquid 1-butyl-3-methylimidazolium tetrafluoroborate.*" Journal of Physical Chemistry B **2008**, *112*, 8134-8138.
- [69]Brar, S. K.; Verma, M. "*Measurement of nanoparticles by light-scattering techniques.*" Trac-Trends in Analytical Chemistry **2011**, *30*, 4-17.
- [70]Barnett, C. E. "*Some Applications of Wave-length Turbidimetry in the Infrared.*" Journal of Physical chemistry **1942**, *46*, 69-75.
- [71]Valeur, B. "*Molecular Fluorescence: Principles and Applications*" Wiley-VCH Verlag GmbH, **2001**.
- [72]Sowmiya, M.; Purkayastha, P.; Tiwari, A. K.; Jaffer, S. S.; Saha, S. K. "*Characterization of guest molecule concentration dependent nanotubes of beta-cyclodextrin and their secondary assembly: Study with trans-2-[4(dimethylamino)styryl]benzothiazole, a TICT-fluorescence probe.*" Journal of Photochemistry and Photobiology a-Chemistry **2009**, *205*, 186-196.
- [73]Liu, B.; Bao, Y. Y.; Wang, H.; Du, F. F.; Tian, J.; Li, Q. B.; Wang, T. S.; Bai, R. K. "*An efficient conjugated polymer sensor based on the aggregation-induced fluorescence quenching mechanism for the specific detection of palladium and platinum ions.*" Journal of Materials Chemistry **2012**, *22*, 3555-3561.

**Chapter 5. Preliminary Investigation on Modulation of Cation
Binding in the Excited State**

5.1. Preliminary investigation on cation photoejection based on a fullerene-azacrown dyad

5.1.1. Introduction

Discovery of crown ether has significantly promoted the development of supramolecular chemistry of macrocyclic compounds.^{1,2} Due to its high binding affinity and selectivity to inorganic ions, it has been widely used in fluoroionophres as the receptor.^{3,4} The abrupt change of the spectral properties of the fluorophores upon complexation with cation then gives great advantage in serving as fluorescent chemosensors in determination of trace amount of metal ions. Of those reported approaches, the most fascinated probably is the n,π -conjugation between one (or more) heteroatom of the macrocycle and the chromophore fragment. Early studies on such chromophores by using ethylenediaminetetraacetic acid revealed unusual change in fluorescence spectra of some compounds upon complexation. The shift of the fluorescence maxima was abnormally small when compared with those of the absorption maxima.⁵ The first detailed study by using monoaza-15-crown-5-ether as the binding site was based on compound **PCT-2**, as shown in Scheme 5-1.^{6,7,8,9,10} With the addition of metal ions to the solution of **PCT-2** in MeCN, solution color changed from orange-red to yellow but the fluorescence maximum did not shift.⁶ For example upon full complexation with Ca^{2+} , the hypsochromic shift of the absorption maximum was 3600 cm^{-1} , whereas the shift of the fluorescence maximum was ten times smaller. The normalized fluorescence of the complex overlapped very well with that of the free ligand. Moreover, the lifetime of the complex showed only slight difference from the free ligand. Relaxed intramolecular charge transfer (RICT) was proposed to explain the spectral features of **PCT-2** to cations. Photoinduced intramolecular charge transfer could lead to the positive polarization of the chromophoric heteroatom of the macrocycle, resulting in the Coulomb repulsion between the heteroatom and metal ions present in the cavity. Furthermore, the reduced electron density of the heteroatom due to charge transfer would weaken the coordination bond. Together, they both bring the recoordination of the metal ions in the cavity, and in some cases the metal ions would be completely ejected from the crown cavity to the bulk solution.² The mechanism of this phenomenon was mainly studied by picosecond transient absorption spectra. It should be pointed out that this discovery is important for the design of fluorescent chemosensors for metal ions, molecular switch and other photodevices.¹¹ Based on the reversible binding, the accumulation process can increase the signal-to-noise (S/N) ratio.⁹



Scheme 5-1. Fluoroionophore **PCT-2** based on aza-15-crown-5.

Successive investigations on the photoejection of cations from their complex with **PCT-2** were carried out. Strong evidences from the transient absorption spectra were obtained to verify the photoejection processes. To be clear, here release of calcium from its complex with **PCT-2** is taken as an example. Femtosecond transient absorption spectroscopy was used for this purpose.⁹ Within the timescale of hundred femtoseconds, appearance of the structured stimulated emission band from 525 nm to 750 nm was observed and attributed to the locally excited (LE) state of the complex, as shown in Figure 5-1 (a). The vibrational structure disappeared in 300 fs accompanied by its red shift and concomitant blue shift of the excited state absorption, indicating the primary interruption of bond linking the cation to the nitrogen atom of the azacrown. On a picosecond timescale (Figure 5-1 (b)), the rise of an absorption band at 530 nm was assigned to intraligand charge transfer state, resulted from the LE state of the free-like ligand. The isosbestic point in the simulated emission band confirmed the evolution of LE state to CT states. In a few hundred picoseconds time scale (Figure 5-1 (c)), the red shift of the stimulated emission stemmed from the further motion of the cation away from nitrogen atom of the crown while the CT reaction proceeded. When the delay ranged from 250 ps to 1.2 ns (Figure 5-1 (d)), the differential absorbance decayed in the whole spectral range and the simulated emission band kept shifting to the red and reached a maximum at 1.2 ns, indicating the photoejection cation moved away to the bulk solution. For strontium, the formation of ultra-loose complex from the charge transfer complex in about 400 ps and the cation rebinding in the ground state proceed after nearly 110 ns.⁸ It was calculated that only 5%-10% of ultra-loose complex underwent dissociation with the release of cation. Since the lifetime of **PCT-2** in the excited state is about 2 ns, it is not long enough for the complete release of the cation from the azacrown. In search for a highly efficient photoinduced cation release system, a photoinduced charge separated state with a long lifetime is much more favorable.

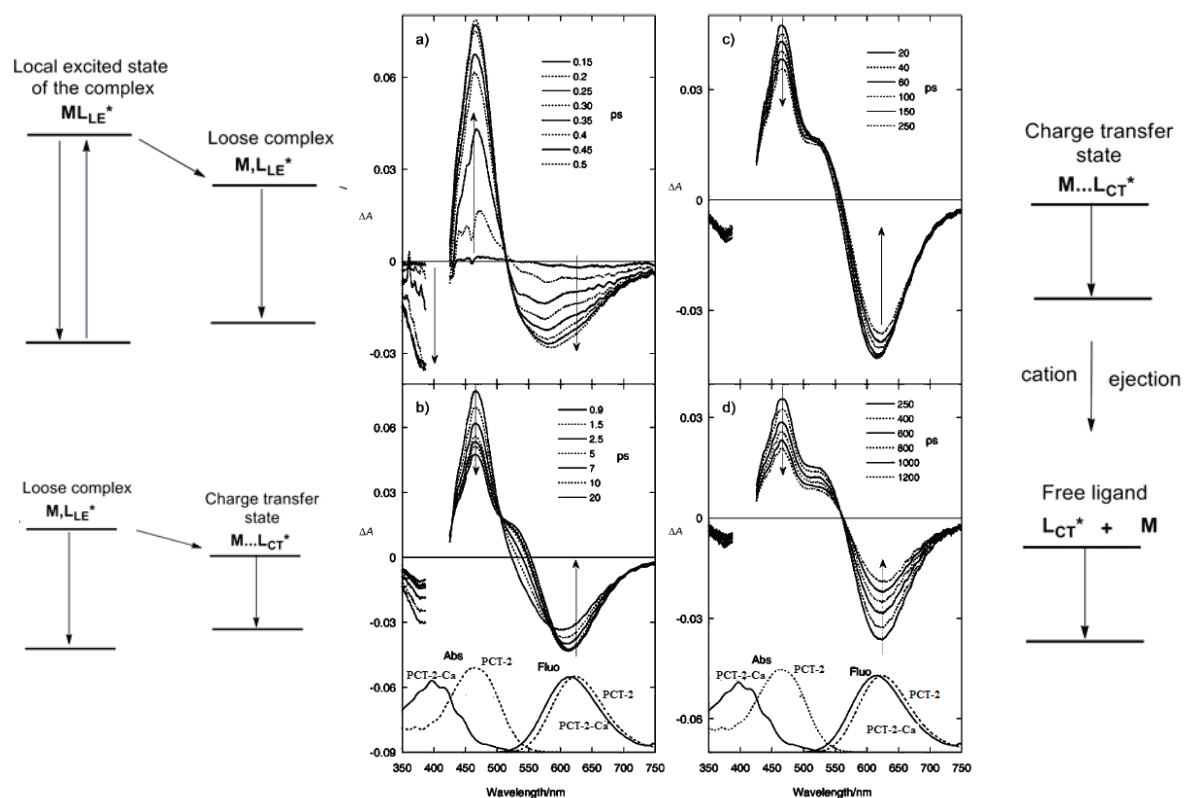


Figure 5-1. Transient absorption spectra of **PCT-2-Ca** complex in MeCN upon excitation with a 50 fs laser pulse at 405 nm, pump-probe delay time a) 0.15 ps and 0.5 ps, b) 0.9 and 20 ps; c) 20 and 250 ps and d) 250 and 1200 ps.⁹

In pursuing of long-live excited state for the cation release, Lewis et al have developed a novel platform based on crown-containing complex (bpy)Re^I(CO)₃L (bpy represents bipyridine) whose lifetime is in the order of tens and hundreds of nanoseconds, as shown in Figure 5-2.^{12,13}

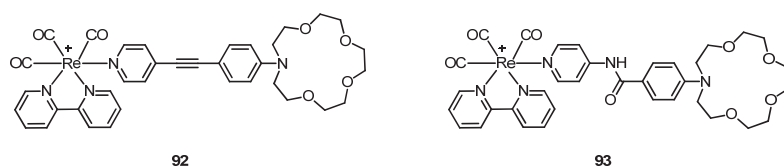


Figure 5-2. Photoinduced cation release based on Re complexes.

Complex of **92** with Ba²⁺ was studied by transient absorption spectra on the nanosecond and microsecond time scales.¹² The H-analogue of compound **92** gave a characteristic MLCT excited state with a lifetime of 260 ns. For compound **92**, its lifetime was dramatically decreased to lower than 5 ns, which was explained by the ultrafast electron transfer from the nitrogen atom of the azacrown to Re^{II}, resulting in a ligand-to-ligand charge-transfer (LLCT) excited state. Upon binding to Ba²⁺, the resulting complex **92-Ba²⁺** after excitation at 355 nm

gave a constant transient absorption band with the time delay larger than 20 ns and it consisted of a bleach at 340-360 nm and an absorption band at 410 nm which matched very well with the difference spectrum by subtracting the steady state absorption spectrum of **92**-Ba²⁺ from that of **92** (Figure 5-3), demonstrating the release of Ba²⁺ after 20 ns and the ground state of **92** formed after 20 ns.

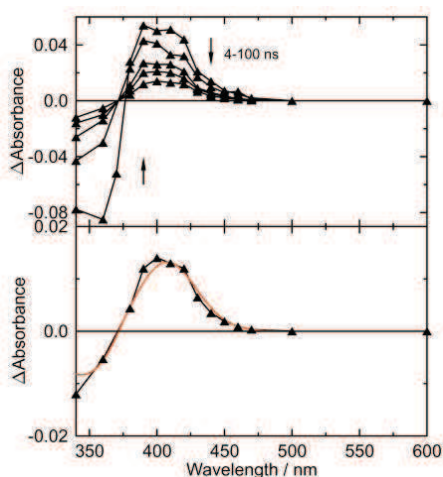


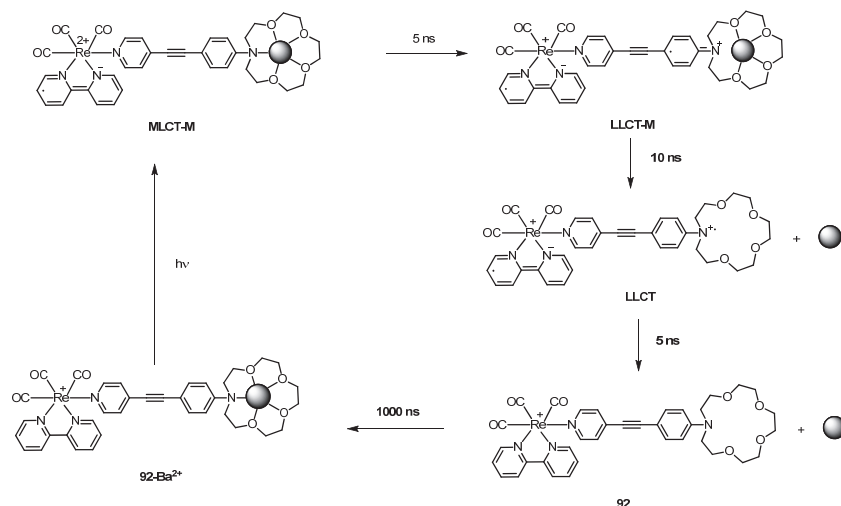
Figure 5-3. (Top): Transient absorption spectra of **92**-Ba²⁺ in MeCN at different delay times; (bottom) : comparison of transient absorption spectra of **92**-Ba²⁺ at 100 ns overlaid with the difference spectrum obtained by subtracting the steady state absorption spectrum of **92**-Ba²⁺ from that of **92**.

Scheme 5-2 depicts the photochemical mechanism of **92**-Ba²⁺ upon exposure to UV illumination.² Excitation of **92**-Ba²⁺ at 355 nm leads to the formation of MLCT state, where an electron is transferred from Re^I to bipyridine. Subsequent electron transfer from nitrogen atom of azacrown to Re^{II} results in a LLCT-M state, which produces a positive charge on nitrogen atom and consequently ejects the cation present in the crown within 10 ns. The free ligand is generated after deactivation of LLCT state, which is inferred from the similarity of transient absorption spectra after 20 ns as the difference absorption between compound **92** and **92**-Ba²⁺. The rebinding of cation shows a bimolecular constant of $9.3 \times 10^7 \text{ L mol}^{-1} \text{ s}^{-1}$, which takes from 100 to 1000 ns depending on the concentration of Ba²⁺ in the solution.

When the linking alkyne group in **92** is replaced by amide group, compound **93** upon complexation with metal ions showed a similar photochemical path to that of **92** with a larger time scale.¹³ Photorelease of the metal ions strongly depended on metal ions charge density: Li⁺ and Na⁺ released faster than Ca²⁺ and Ba²⁺, while no release of Mg²⁺ was observed. The cation rebinding takes a few microsecond to reach a thermal equilibrium.

Free ligand **93** exhibited an absorption band at 344 nm, which was attributed to the ILCT

state and masked a weaker MLCT band at 350 nm. Excitation of the ligand **93** at 355 nm led to a MLCT state which was quenched by LLCT in nearly 500 ps. Upon complexation with metal ions, such as Ba^{2+} , the lifetime of MLCT state increased considerably to 47 ns. Transient absorption spectra when recorded with a time delay shorter than 50 ns, resembled to pattern of protonated form, indicating a slow formation of LLCT state. As the delay time increased to 50-200 ns, the spectra of complex with Ba^{2+} changed significantly. Photoejection of Ba^{2+} is inferred from the similarity of transient absorption spectra after 200 ns as the difference absorption between compound **93** and **93-Ba²⁺** (Figure 5-4). The lifetime of LLCT state of the free ligand was about 19 ns; during this time interval Ba^{2+} travel distance from 57 Å. Transient absorption spectra recorded in 1 - 100 μs indicate the existence of exclusive complex, where the cation was far away from the equilibrium position of macrocycle. Cation rebinding Ba^{2+} to a thermal equilibrium shows a bimolecular rate constant with $5 \times 10^7 \text{ L mol}^{-1} \text{ s}^{-1}$, lower than that of **92**.



Scheme 5-2. Photochemical mechanism for **92-Ba²⁺**.

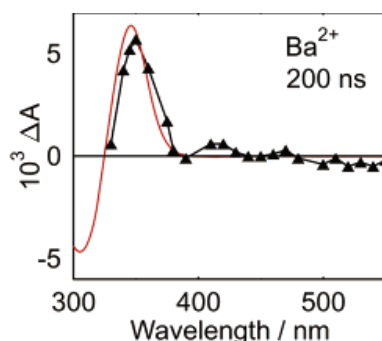


Figure 5-4. Comparison of transient absorption spectra of **93-Ba²⁺** at 100 ns overlaid with the difference spectrum obtained by subtracting the steady state absorption spectrum of **93-Ba²⁺** from that of **93**.

New photoinduced intra-/intermolecular electron-transfer systems based on fullerenes and

their derivatives are attractive for their wide applications in light-driven molecular systems including artificial photosynthetic models.^{14,15,16} Fullerenes display very promising features as a three-dimensional electron acceptor, which in principle could be utilized as an electron accumulator and electron relay.^{17,18,19} Its promising properties as an electron acceptor are mainly due to the small reorganization energy (λ).¹⁷ Various electron donors have been used to couple with fullerenes, such as aromatic amines, ferrocenes, oligovinylenes, tertathiafulvalene derivatives and porphyrins, phthalocyanines.¹⁸ In the case of aromatic amine, when linked with a long rigid spacer to C₆₀, a novel dyad **94** was constructed (Figure 5-5).²⁰ Its low fluorescence quantum yield and short fluorescence lifetime in PhCN and THF indicated that charge separation took place via the singlet excited state with a quite fast rate and very high efficiency. The nanosecond transient absorption spectra exhibited two broad bands at 880 nm and 1100 nm, which were assigned as the radical cation of aromatic amine and radical anion of fullerene moiety. This charge separated state decayed with a lifetime of 330 ns in PhCN. The long-live charge separated state of this dyad is quite intriguing for its potential application in cation release.

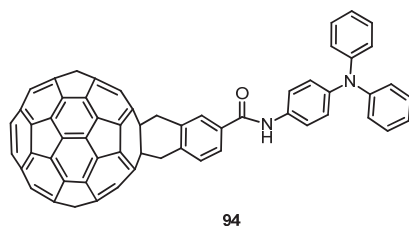


Figure 5-5. Molecular structure of **94**.

It is assumed that if the long-live charge separated state can be kept in the cation release system, then an efficient and reversible cation release system can be constructed. In order to realize the hypothesis, a new dyad **Full-aza** (Figure 5-6) with monoazacrown as metal binding site and meanwhile its conjugation with aromatic system is used as the electron donor and fullerene C₆₀ as the electron acceptor can be established. Upon excitation, the highly charge separated and long-live species can eject the metal ions present in the cavity of crown to the bulk solution very completely.

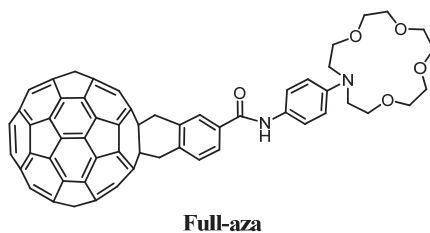
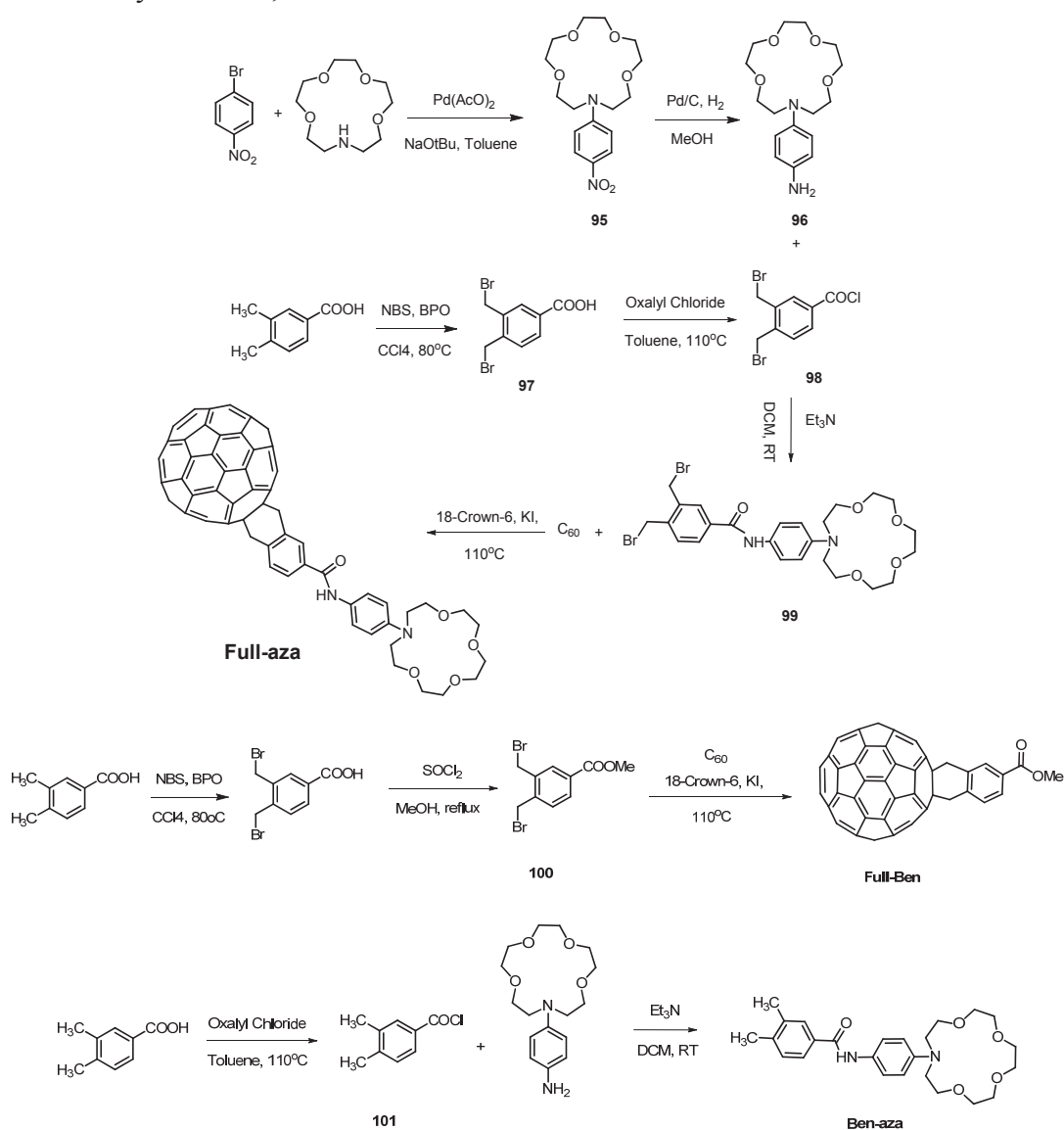


Figure 5-6. Molecular structure of **Full-aza**.

5.1.2. Synthesis of Full-aza

Synthetic routine of **Full-aza** is shown in Scheme 5-3. The coupling between 1-bromo-4-nitrobenzene with aza-15-crown-5 under the catalysis of Pd(AcO)₂ in the presence of NaOtBu afford **95** in 78% yield.²¹ **95** was reduced by hydrogen using Pd/C as the catalyst to give the amine **96** in 90% yield.²² 3,4-Dimethylbenzoic acid was brominated with NBS in the presence of BPO (benzoyl peroxide) to afford **97** in 38% yield.²³ The coupling between amine **96** and **98** in the presence of Et₃N then give the amide **99** in 67% yield. Diels-Alder reaction of **99** and C₆₀ in refluxing toluene afforded **Full-aza** in 10% yield.²⁰ **Full-aza** was characterized by ¹H NMR, ¹³C NMR and HRMS. Reference compound **Full-Ben** was synthesized according to the reported procedure.²³ And **Ben-aza** was obtained by direct coupling between amine **96** and **101** in the presence of Et₃N in 38% yield. It was characterized by ¹H NMR, ¹³C NMR and HRMS.



Scheme 5-3. Synthesis of ligand **Full-aza** and reference compounds **Full-Ben** and **Ben-aza**.

5.1.3. Photophysical properties of Full-aza

Figure 5-7 shows the steady spectra of **Full-aza** and its reference compounds in polar solvent THF. Two characteristic absorption bands stemming from C_{60} with $58-\pi$ conjugated system are observed at 639 and 706 nm.²⁰ It should be noted that the whole absorption spectra of **Full-aza** is very similar to the sum of both reference compounds **Full-Ben** and **Ben-aza**. Especially, its absorption pattern above 400 nm matches very well with that of **Full-Ben**, indicating no significant interaction between C_{60} moiety and aromatic amine in the ground state. With respect to the fluorescence spectra, **Full-aza** shows a very weak emission band with a maximum at 713 nm. When compared with **Full-Ben**, they both emit at the same wavelength 713 nm, indicating the observed fluorescence is resulting from C_{60} moiety; however, **Full-aza** has much lower fluorescence intensity, which is due to the electron transfer from aromatic amine to C_{60} moiety in the excited state. This can be further confirmed by the spectral properties of **Full-aza** in toluene (Figure 5-8), where it still has almost the same absorption spectra as that of **Full-Ben** above 400 nm but it provides a higher fluorescence intensity than that in THF. This is can be explained by the fact the charge separated species are more stable in polar solvent THF than non-polar solvent toluene.

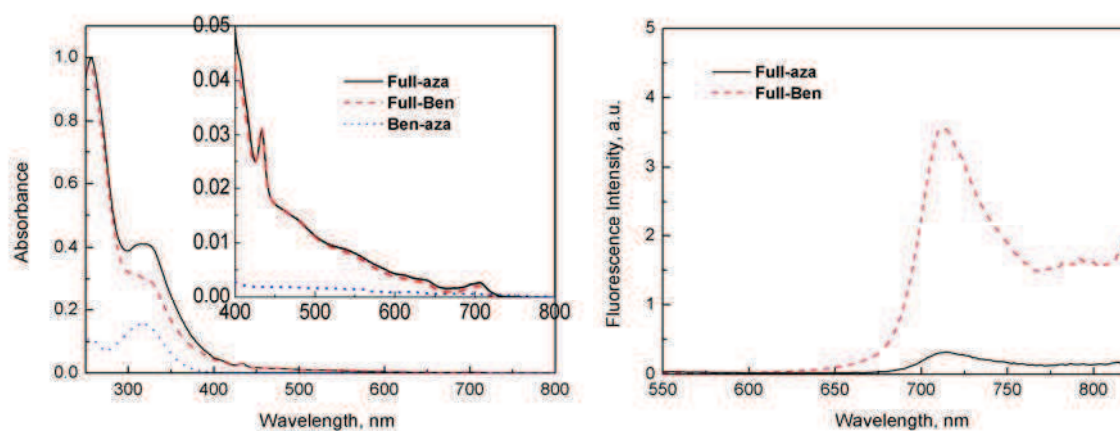


Figure 5-7. Absorption (left) and fluorescence (right) spectra of **Full-aza**, **Full-Ben** and **Ben-aza** in THF, $\lambda_{\text{ex}} = 432 \text{ nm}$, $[\text{Full-aza}] = [\text{Full-Ben}] = [\text{Ben-aza}] = 10 \mu\text{M}$.

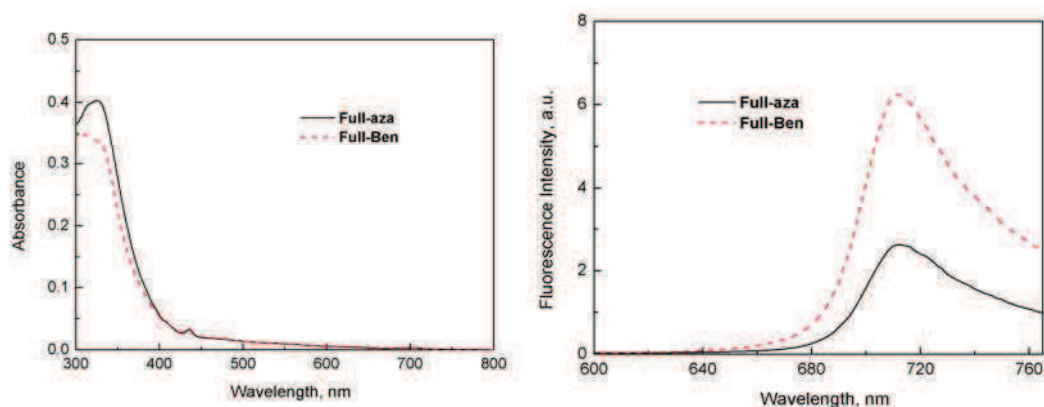


Figure 5-8. Absorption (left) and fluorescence (right) spectra of **Full-aza** and **Full-Ben** in toluene, $\lambda_{\text{ex}} = 432 \text{ nm}$, $[\text{Full-aza}] = [\text{Full-Ben}] = 10 \mu\text{M}$.

Nanosecond transient absorption spectra of **Full-aza** were acquired under Ar by laser excitation at 432 nm in PhCN. Due to instrumental limitation, they were recorded in the range of 475 to 850 nm. As shown in Figure 5-9, it exhibits a structured absorption band between 475 nm and 650 nm, which was firstly assigned as the absorption of radical cation of aromatic amine moiety. The decay profile at 575 nm gives the lifetime of the charge-separated state of 165 ns at room temperature. In order to verify that attribution of absorption band in the transient state, **Ben-aza** was chemically oxidized by $\text{Cu}(\text{ClO}_4)_2$ in MeCN under Ar at room temperature (Scheme 5-4).²⁴ As shown in Figure 5-10, a new structured absorption band between 450 nm and 650 nm appears, which results from the radical cation of aromatic amine. The normalized absorption spectra of the oxidative product of **Ben-aza** and the transient charge separated species of **Full-aza** match very well with each other (Figure 5-10 (right)), demonstrating that the electron transfer in the excited state affords long-live charge separated species. Characteristic absorption band of radical anion $\text{C60}^{\bullet-}$ generally locates at around 1000 nm.²⁰ An advanced instrument with larger wavelength window should be used in order to observe the decay of radical anion of $\text{C60}^{\bullet-}$.

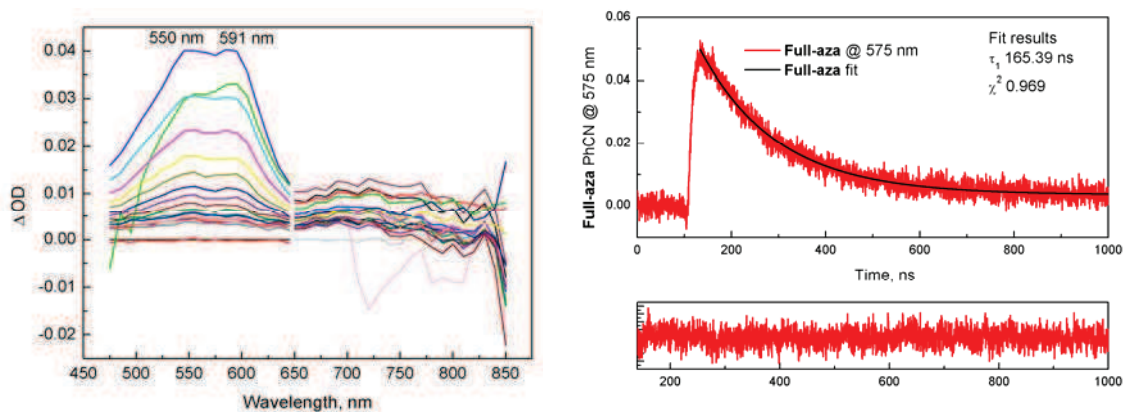


Figure 5-9. Transient absorption spectra of **Full-aza** in PhCN under Ar, laser excitation at 432 nm, $[\text{Full-aza}] = 0.16 \text{ mM}$.

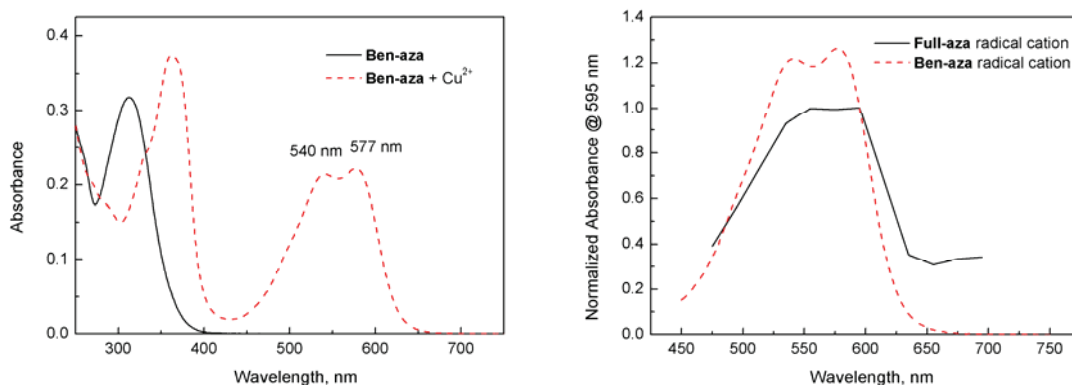
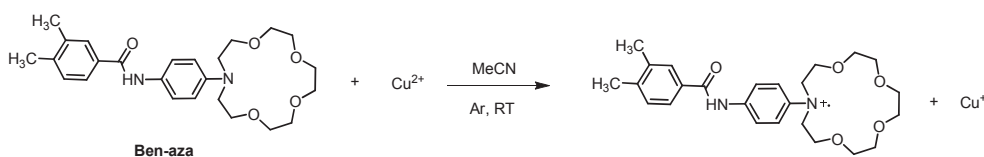


Figure 5-10. Absorption spectra of **Ben-aza** in the absence and presence of Cu^{2+} under Ar in MeCN/THF(98:2). $[\text{Ben-aza}] = 20 \mu\text{M}$, $[\text{Cu}^{2+}] = 80 \mu\text{M}$ and comparison of radical cation of **Full-aza** and **Ben-aza**.

5.1.4. Complexation properties of Full-aza

Consistent with our assumption, long-live charge separated species with positive charge on the nitrogen atom of azacrown was obtained based on the dyad **Full-aza**. Next, we investigated the spectral response of **Full-aza** to metal ions in PhCN. For example, as shown in Figure 5-11, with the addition of increasing concentrations of Ca^{2+} to the solution of **Full-aza** in PhCN, absorption band at 329 nm decreases gradually and an isosbestic point at 306 nm is observed which indicates that the equilibrium between free ligand and the complex. However, no spectral change is observed for the absorption ranging above 400 nm, which illustrates that binding site of **Full-aza** is on the azacrown moiety shared with the aromatic amine. This can be further confirmed by the the spectral response of **Ben-aza** to Ca^{2+} in MeCN (Figure 5-12), in which the absorption band at 313 nm decreases in the presence of increasing concentrations of Ca^{2+} , consistent with that of **Full-aza**. Regarding the fluorescence titration, fluorescence enhancement can be observed during the titration process. This is generally explained by the complexation-suppressed photoinduced electron transfer from aromatic amine to C_{60} . Non linear regression analysis of the spectral titration based on 1:1 binding stoichiometry gives large binding constants ($\log K = 5.5$) in both the ground state and excited state. Spectral titrations with other metal ions such as Li^+ , Mg^{2+} , Ba^{2+} and Sr^{2+} were carried out. They all consistently exhibited similar influence on the spectra of **Full-aza**,

with decreased absorbance of aniline moiety (Figure 5-13) and enhanced fluorescence of C₆₀ moiety at 714 nm. The binding constant of **Full-aza** with various metal ions are collected in Table 5-1, which is consistent with the reported results.¹³ The addition of CF₃COOH also has the same effect as that of the tested metal ions (Figure 5-14).

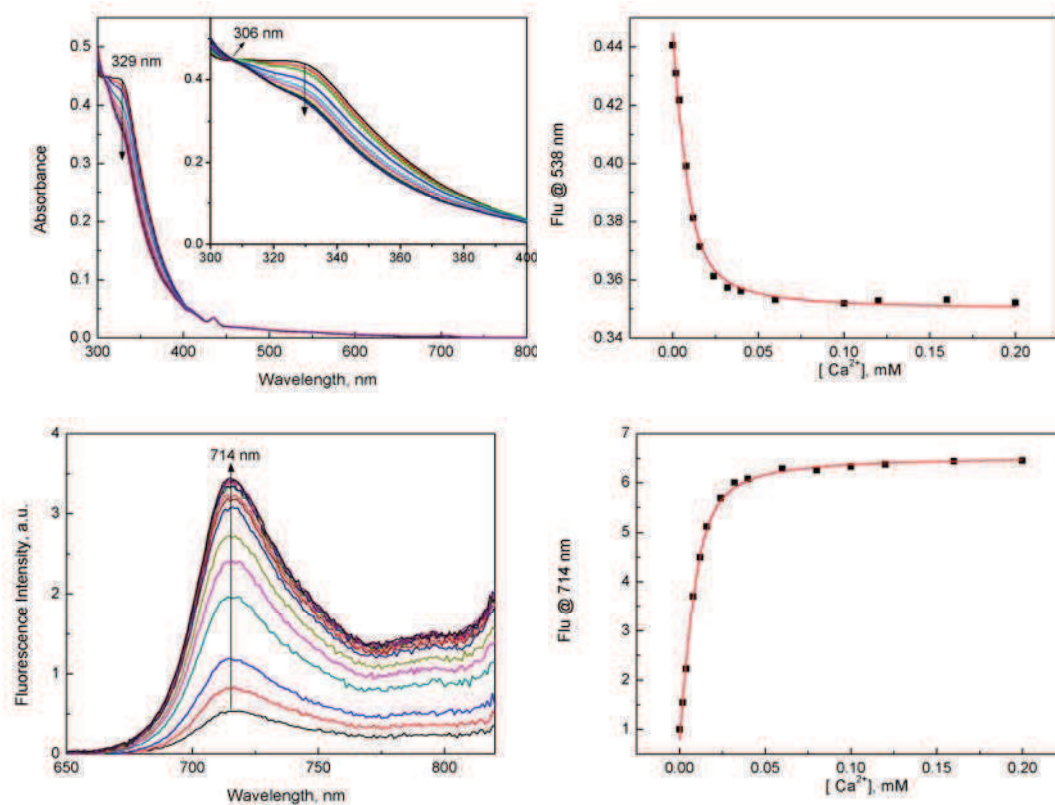


Figure 5-11. Absorption (top) and fluorescence (bottom) spectra of **Full-aza** in the presence of increasing concentrations of Ca²⁺ in PhCN, $\lambda_{\text{ex}} = 432$ nm, [Full-aza] = 10 μM .

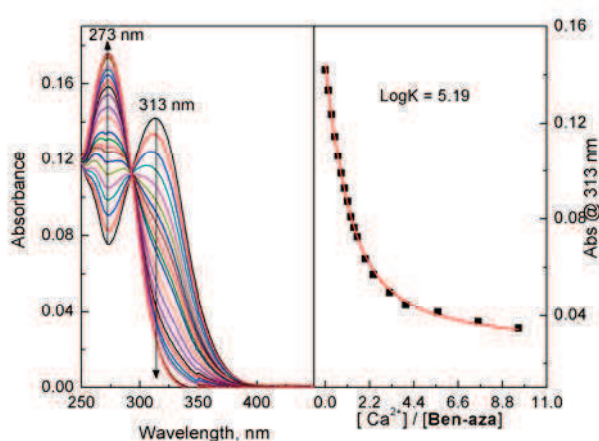


Figure 5-12. Absorption spectra of **Ben-aza** in the presence of increasing concentrations of Ca²⁺ in MeCN, [Ben-aza] = 10 μM .

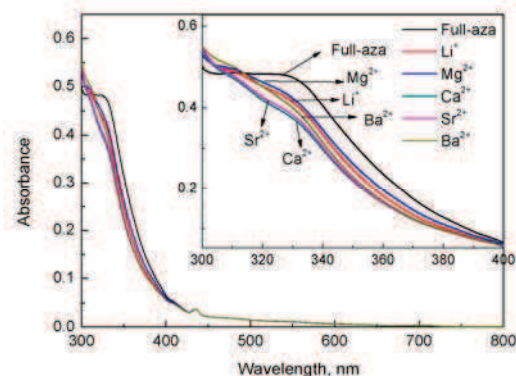


Figure 5-13. Absorption spectra of **Full-aza** in the presence of various metal, $[\text{Full-aza}] = 10 \mu\text{M}$, $[\text{M}^{n+}] = 0.2 \text{ mM}$.

	$\text{Log}K_{(\text{Absorption})}$	$\text{Log}K_{(\text{Fluorescence})}$	Ion Diameter [\AA]	Charge Density [q \AA^{-1}]
Li^+	4.48 ± 0.01	4.46 ± 0.01	1.52	1.31
Mg^{2+}	3.76 ± 0.01	3.86 ± 0.03	1.44	2.78
Ca^{2+}	5.56 ± 0.06	5.52 ± 0.04	2.00	2.00
Sr^{2+}	5.15 ± 0.02	5.10 ± 0.02	2.36	1.69
Ba^{2+}	5.32 ± 0.01	5.32 ± 0.02	2.70	1.48

Table 5-1. Binding constant of **Full-aza** to metal ions in PhCN; ionic diameters are from Handbook of Chemistry and Physics, 84th ed.; CRC Press LLC: D. R. Lide, 2003-2004.

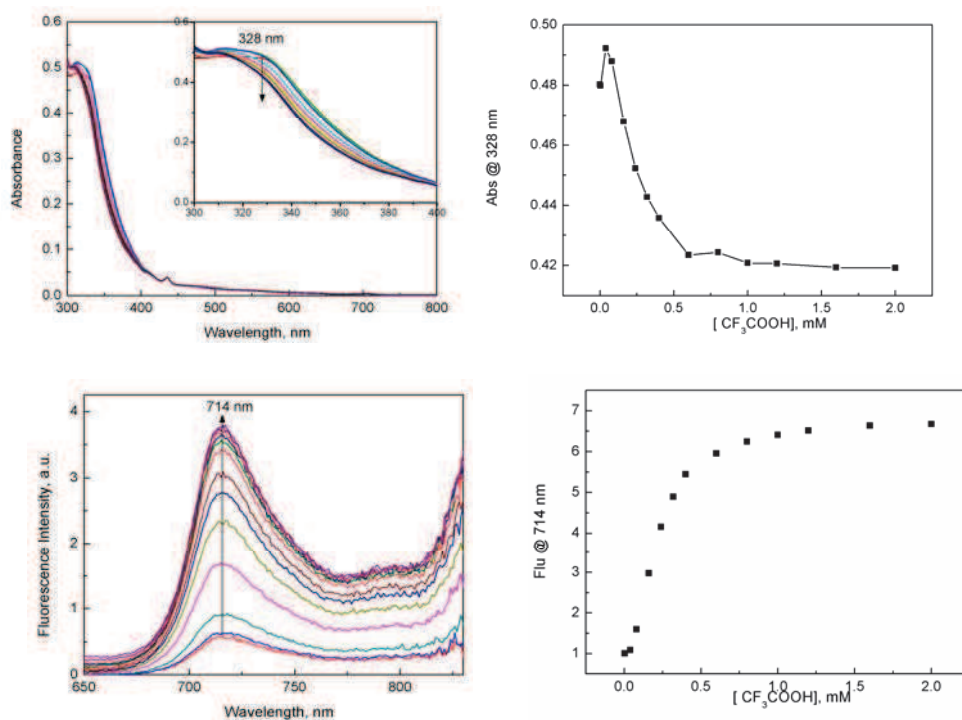


Figure 5-14. Absorption (top) and fluorescence (bottom) spectra of **Full-aza** in the presence of increasing concentrations of CF_3COOH in PhCN, $\lambda_{\text{ex}} = 432 \text{ nm}$, $[\text{Full-aza}] = 10 \mu\text{M}$.

Nanosecond transient absorption spectra of **Full-aza** complex was recorded in PhCN, as shown in Figure 5-15 (right). Under the laser excitation at 432 nm, a broad absorption band at 700 nm is observed. According to the reported data, this band can be assigned as the triplet state C_{60} (${}^3C_{60}^*$).¹⁷ No absorption band peaked at 550 and 591 nm is observed any more, which may indicate no charge separated species after complexation with Ca^{2+} . Transient absorption spectra of other **Full-aza** complexes with Ba^{2+} and Sr^{2+} were acquired under the identical conditions (Figure 5-16 and 5-17). They all show almost the identical absorption band as that of Ca^{2+} . It is postulated that due to suppression of the electron transfer by complexation, no more charge separated species can be generated and the subsequent cation release is unable to occur. We then also try to excite **Full-aza- Ba^{2+}** complex at 260 nm (Figure 5-18), the maximum of the aromatic amine moiety after complexation with Ba^{2+} ; however, no signal was observed in the range from 475 to 825 nm.

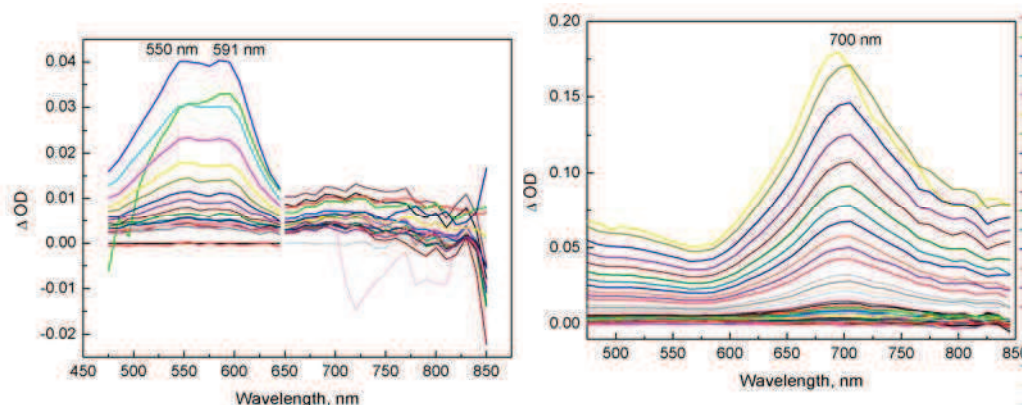


Figure 5-15. Transient absorption spectra of **Full-aza** in the absence (left) and presence (right) of $Ca(ClO_4)_2$ in PhCN under Ar, laser excitation at 432 nm, $[Full-aza] = 0.16$ mM, $[Ca^{2+}] = 16.5$ mM.

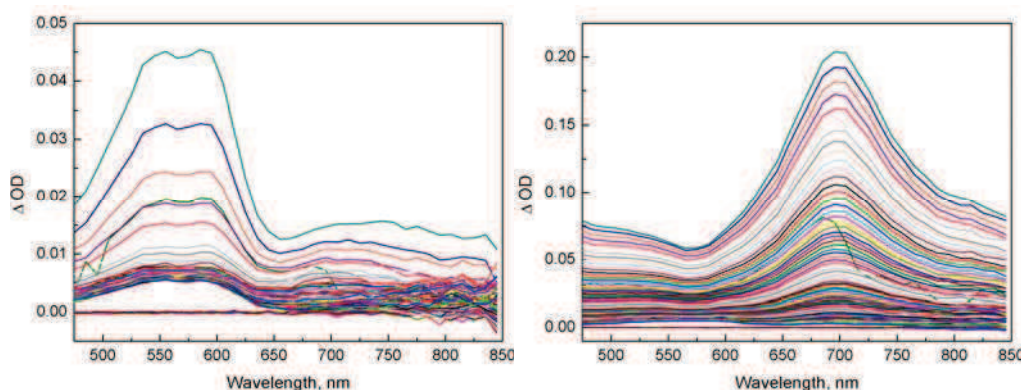


Figure 5-16. Transient absorption spectra of **Full-aza** in the absence (left) and presence (right) of $Ba(ClO_4)_2$ in PhCN under Ar, laser excitation at 432 nm, $[Full-aza] = 0.2$ mM, $[Ba^{2+}] = 20.0$ mM.

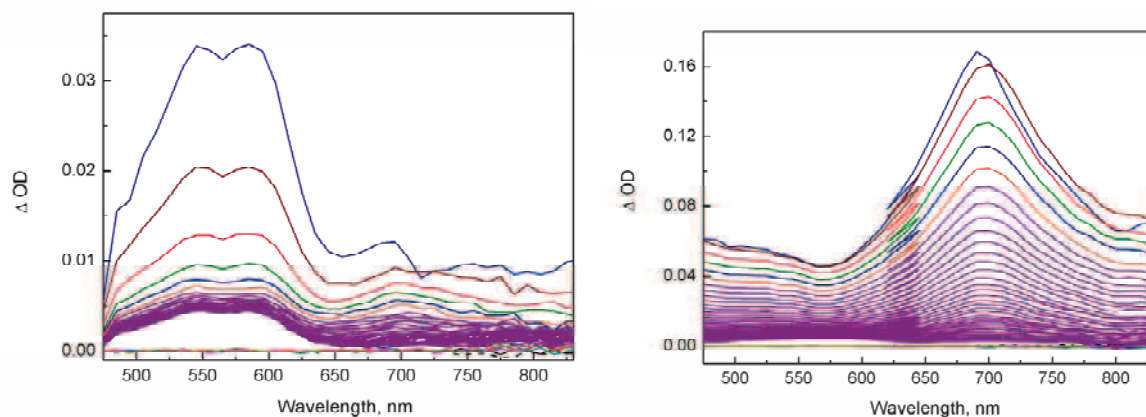


Figure 5-17. Transient absorption spectra of **Full-aza** in the absence (left) and presence (right) of $\text{Sr}(\text{ClO}_4)_2$ in PhCN under Ar, laser excitation at 432 nm, $[\text{Full-aza}] = 0.2 \text{ mM}$, $[\text{Sr}^{2+}] = 20.0 \text{ mM}$.

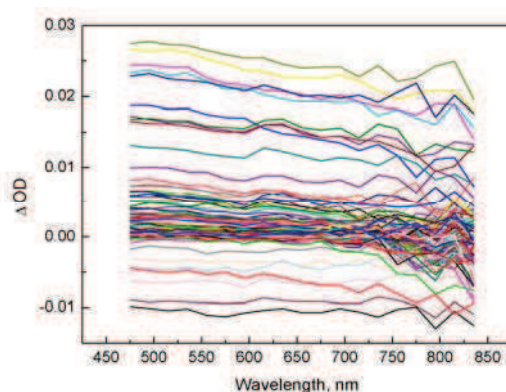
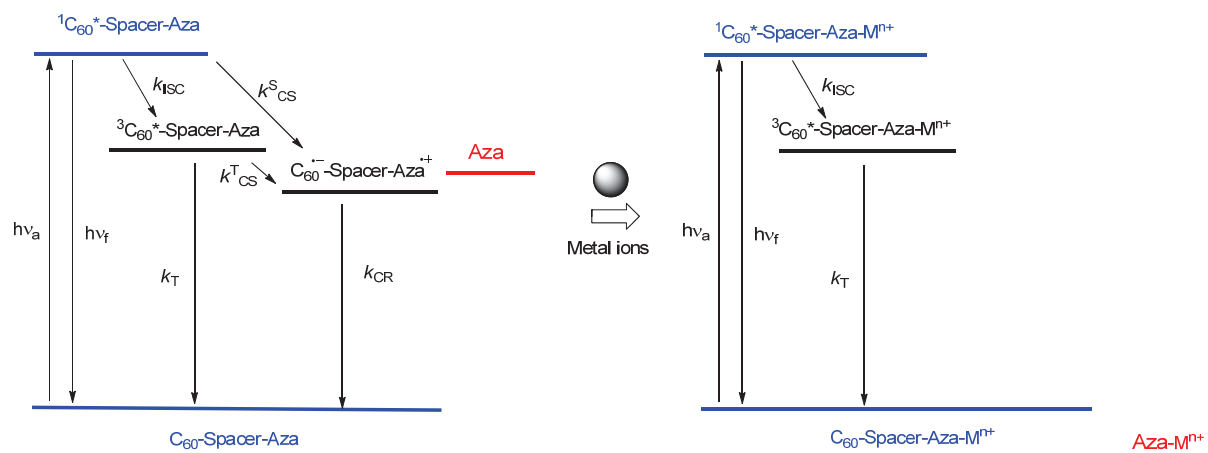


Figure 5-18. Transient absorption spectra of **Full-aza** in the presence of $\text{Ba}(\text{ClO}_4)_2$ in PhCN under Ar, laser excitation at 260 nm, $[\text{Full-aza}] = 0.2 \text{ mM}$, $[\text{Ba}^{2+}] = 20.0 \text{ mM}$.

As shown in Scheme 5-5, an energy diagram is proposed to explain the electronic transition of **Full-aza** and its complex when the 432 nm laser is used as the excitation light. In the free ligand, the charge separated state mainly takes place via ${}^1\text{C}_{60}^*$ -Spacer-Aza, inferred from strong fluorescence quenching, short fluorescence lifetime and no appearance of ${}^3\text{C}_{60}^*$ absorption band. Upon complexation with metal ions, the energy level of the aromatic amine is reduced to lower than ground state of C_{60} -Spacer-Aza. No electron transfer is possible under this condition and the ${}^1\text{C}_{60}^*$ -Spacer-Aza could deactivate through either by fluorescence emission or intersystem crossing. It's therefore that fluorescence enhancement and absorption band of ${}^3\text{C}_{60}^*$ at 700 nm are both observed in the complex.



Scheme 5-5. Schematic energy diagram for the electron transfer in PhCN before and after complexation with metal ions.

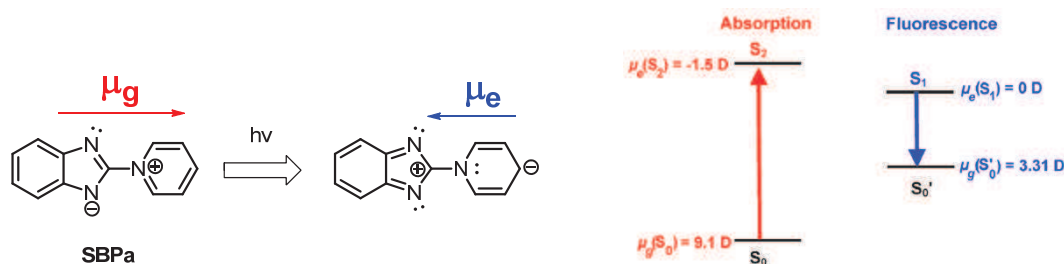
5.1.5. Conclusion

A new C₆₀-azacrown dyad **Full-aza** was readily constructed. Photoinduced charge separation via ¹C₆₀*-Spacer-Aza was observed in PhCN at room temperature with a lifetime of 165 ns. Meanwhile, **Full-aza** shows strong binding ability to Ca²⁺, Ba²⁺ and Sr²⁺ in PhCN. Investigation on its complex by using nanosecond transient absorption showed that no charge separated species was detected and the main deactivation of ¹C₆₀*-Spacer-Aza was intersystem crossing and fluorescence emission. The absence of the charge separated absorption band in the complex may indicate that cation release based on dyad **Full-aza** is not accessible. Further work on designing the long-live charge separated species should focus on these systems involving strong intramolecular charge transfer.

5.2. Preliminary investigation on metal ions translocation based on betaine pyridinium-azacrown dyad

5.2.1. Introduction

Heterocyclic betaine pyridinium derivatives, as one of the most important intramolecular charge transfer molecule,^{25,26} hold great potential in the development of non-linear optics (NLO).^{27,28,29} Among them, (1-pyridinio)benzimidazolot, abbreviated as **SBPa**, has been the object of intensive investigations.^{27,29} As shown in Scheme 5-6, in the ground state, **SBPa** is a zwitterionic molecule, with negative charge localized on benzimidazole moiety and positive charge localized on pyridinium moiety. Its dipole moment in the ground state has been obtained as 10.33 D by both experimental determination and advanced MP2 calculation.^{30,31} Upon photoexcitation, an intramolecular charge transfer involving a displacement of the π charge from benzimidazole moiety to pyridinium moiety results in a large dipole moment inversion. This leads to a particularly large negative first-order hyperpolarizability (β) $(115\pm 25)10^{-30}$ esu,²⁷ which is 5-fold larger than that of 4-nitroaniline in chloroform. A deep knowledge of its photophysical properties is crucial for its various applications. Recently, a comprehensive investigation on the solvatochromism and photoinduced ICT properties of **SBPa** was carried out by Aloïse et al to obtain a reliable evaluation of the dipole moment involved in the charge transfer transition by both steady and time-resolved optical spectroscopic techniques.^{32,33,34} A clear negative solvatochromism was observed for **SBPa**'s absorption spectra while no such an effect for its emission spectra, as shown in Figure 5-20 (top). As illustrated in Scheme 5-6, the different solvatochromic effect on absorption and fluorescence spectra of **SBPa** was attributed to the fact that that its absorption band stemmed from the $S_0 \rightarrow S_2$ transition while emission band from $S_1 \rightarrow S_0'$. Dipole moments in aprotic solvents were determined with $\mu_g(S_0) = +9.1$ D, $\mu_e(S_2) = -1.5$ D, $\mu_e(S_1) = 0$ D, $\mu_g(S_0') = +3.3$ D, which clearly indicated a dipole inversion in the excited state.



Scheme 5-6. Photoinduced dipole moment inversion in **SBPa**.

Benzimidazole moiety has been commonly utilized as the molecular recognition site for cation, anion and neutral molecules due to its unique spectral properties and good versatile coordination chemistry.^{35,36} As shown in Figure 5-19, when the benzimidazole moiety were appended onto the calix[4]arene, a novel molecule **102** was constructed to be a Hg^{2+} selective sensor in an 50% aqueous solution with a fluorescence turn-off manner. $^1\text{H-NMR}$ demonstrated that nitrogen atom in the benzimidazole and oxygen atom of the amide group contributed as the binding site for Hg^{2+} .³⁷ Compound **103** based on rhodamine B and benzimidazole moiety exhibited high selectivity to Cu^{2+} in $\text{CH}_3\text{CN/HEPES}$ (v/v = 2:3) solution at pH 7.0 based on complexation-induced ring-opening of rhodamine lactam. It was postulated that coordination of oxygen atom of carbonyl group as well as nitrogen atom of the benzimidazole moiety to Cu^{2+} led to the ring-opening of **103**.³⁸ To date, most of the reports have focused on its neutral form, which exhibits interesting binding response to Hg^{2+} and Cu^{2+} et al.³⁵ However, no data are available for the complexation properties of its anion form.

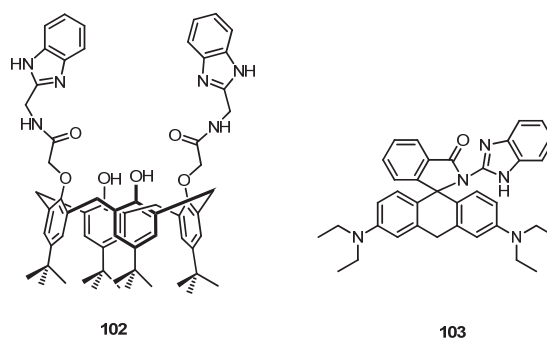
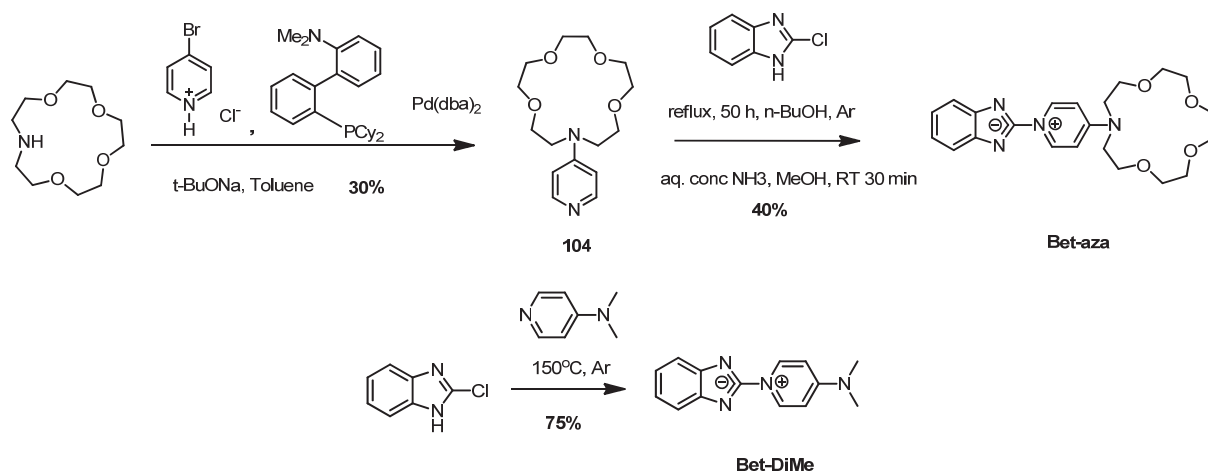


Figure 5-19. Fluorescent chemosensors based on benzimidazole.

A new ligand **Bet-aza** (Scheme 5-7) with an aza-15-crown-5 attached to the pyridinium moiety is designed and synthesized to investigate the photoinduced metal motion in the excited state for these considerations: (1) nitrogen atom of benzimidazole shows strong binding affinity to metal ions, especially in polar organic solvents; (2) in addition, aza-15-crown-5 is one of the most important binding motif in the supramolecular chemistry and can compete with benzimidazole moiety to bind metal ions; (3) upon photoexcitation, a large dipole moment inversion of betaine pyridinium occurs, which means the significant redistribution of the charge in the excited state and consequently changes the binding ability of different moieties in **Bet-aza**. Therefore, such kind of novel ligands can be used to study cation translocation in the excited state.

5.2.2. Synthesis of **Bet-aza** and **Bet-DiMe**

Synthesis of **Bet-aza** is shown in Scheme 5-7. **104** was achieved by palladium-catalyzed coupling of aza-15-crown-5 with 4-bromopyridine hydrochloride in toluene with a 30% yield.³⁹ **Bet-aza** was then prepared by coupling 2-chlorobenzimidazole and **104** in n-BuOH under Ar, followed by deprotonation in concentrated NH₃ solution with a 40% yield.⁴⁰ Reference compound **Bet-DiMe** was directly obtained from the coupling between 2-chlorobenzimidazole and excessive 4-dimethylaminopyridine (DMAP) in 75% yield.⁴¹ These two new compounds were characterized by ¹H and ¹³C NMR, HRMS.



Scheme 5-7. Synthesis of **Bet-aza** and **Bet-DiMe**.

5.2.3. Photophysical properties of **Bet-aza**

Solvatochromic effect of **Bet-aza** was investigated in different organic solvents. Figure 5-20 (bottom) depicts the steady absorption and fluorescence spectra of **Bet-aza** in toluene, THF, MeCN and MeOH. A very clear negative solvatochromism is observed for the absorption spectra with a maximum at 386 nm in toluene and 347 nm in MeOH. In contrast, it exhibits the emission band at the same wavelength of 533 nm except a blue shift to 509 nm in MeOH which is probably due to the intermolecular hydrogen bonding interaction between solute and solvent. According to the reported results of **SBPa** (Figure 5-20 (top)), we can identically attribute the absorption band stemming from $S_0 \rightarrow S_2$ and emission band from $S_1 \rightarrow S_0'$.³² Though no detailed determination of the dipole moment of **Bet-aza**, we can postulate from the negative solvatochromism of the absorption spectra that dipole moment inversion occurs upon photoexcitation. Additionally, when compared with the spectral properties of **SBPa**, remarkable blue shift are both observed for the absorption (33 nm in MeCN) and fluorescence spectra (154 nm in MeCN). This is due to the introduction of strong electron-donating amino group on the 4-position of pyridinium moiety induced reduction of the charge transfer from benzimidazole moiety to pyridinium part.

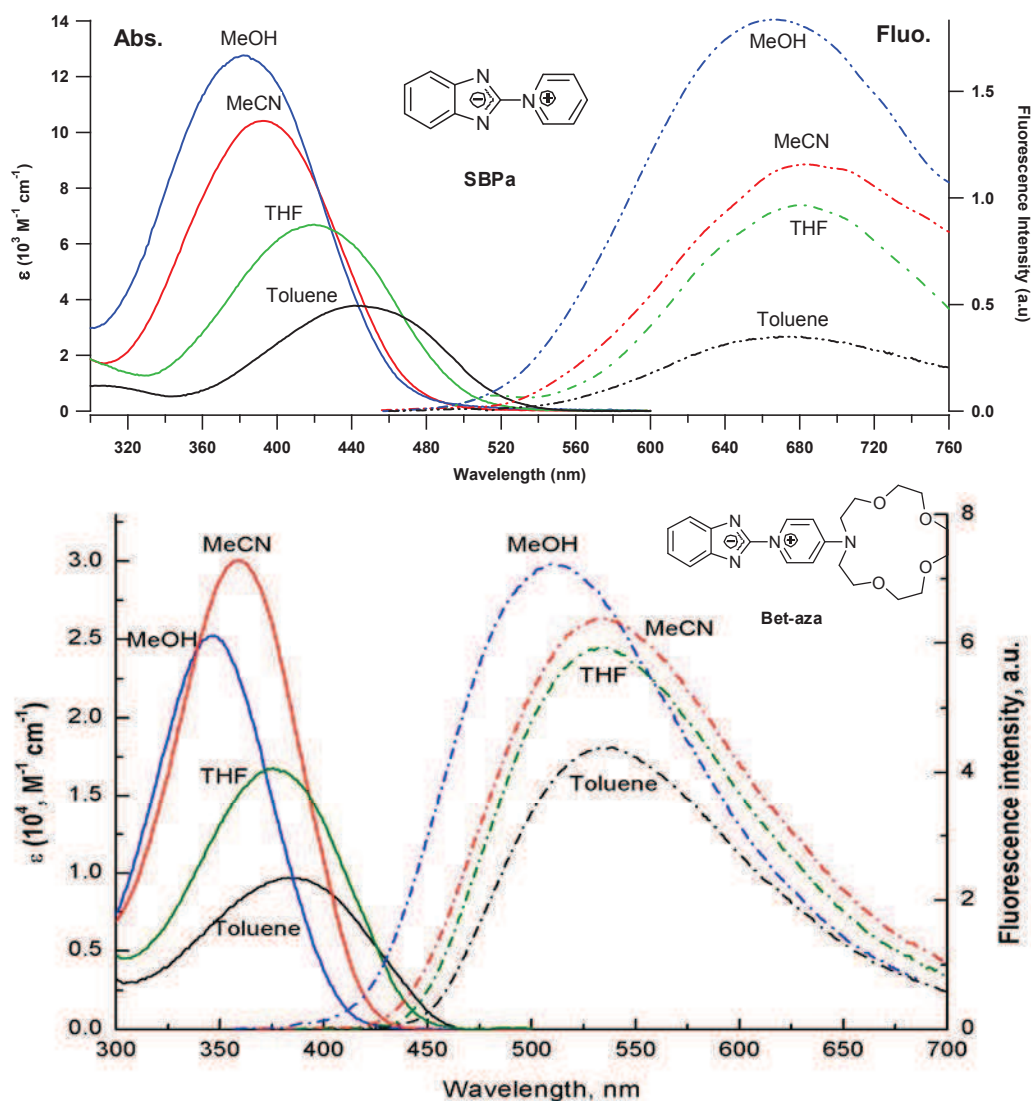


Figure 5-20. Solvatochromism of **SBPa** (top) and **Bet-Aza** (bottom); [**Bet-Aza**] = 5 μM , fluorescence spectra were recorded under excitation at their maximum absorption wavelengths; data of **SBPa** cited from literature.³²

Solvent-dependent spectral shift are often described by using Lippert-Magata equation,^{42,43,44} however, it's available only when the dipole moments in the Frank-Condon and the relaxed state are identical. In our case, the absorption transition and the emission transition come from two different states and therefore this equation is not suitable for analyzing solvatochromism of **Bet-Aza**. Alternative approach has to be used to treat the solvatochromic data.

$E_T(30)$ values are defined as molar transition energy (in kcal/mol; 1 kcal = 4.184 kJ) of the standard betaine dye **105**, as shown in Figure 5-21. It is derived from solvatochromic measurement in solvents of different polarity at room temperature (25°C) and normal pressure

(1 bar), as calculated in eq. 5-2:

$$E_T(30)(\text{kcal/mol}) = hcv_{\text{max}} N_A = (2.8591 \times 10^{-3}) v_{\text{max}} (\text{cm}^{-1}) = 28591 / \lambda_{\text{max}} (\text{nm}) \quad (\text{eq. 5-2})$$

where v_{max} is the wavenumber and λ_{max} the wavelength of the maximum of the long-wavelength solvatochromic intramolecular CT absorption band of betaine dye **105**, and h , c , and N_A represent Planck's constant, the speed of light and Avogadro's constant, respectively. According to Figure 5-21, high $E_T(30)$ values correspond to high solvent polarity.⁴⁵

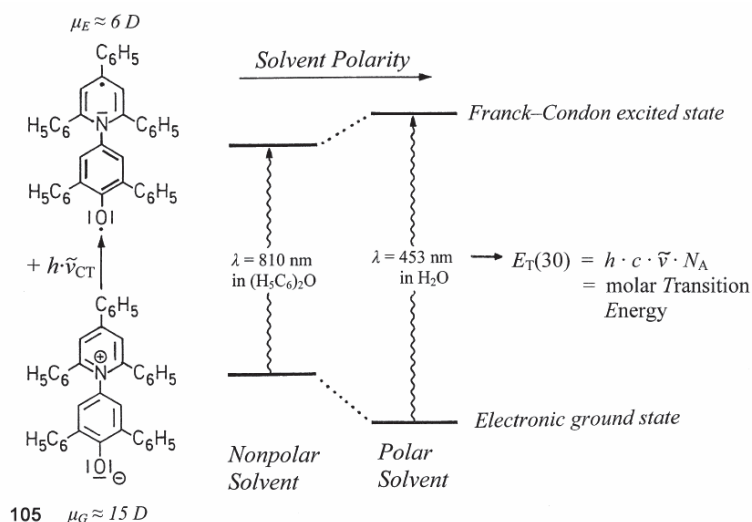


Figure 5-21. Definition of $E_T(30)$ value as molar transition energy of **105**.

The related photophysical data of **Bet-aza** are collected in Table 5-2 and then the solvatochromic data including the absorption and fluorescence maximum bands as a function of $E_T(30)$ values are plotted in Figure 5-22. For the absorption, it is analyzed by using the whole set of solvents, which shows a good linear correlation from nonpolar solvents to polar solvent and aprotic polar solvents. This demonstrates that the solvatochromic effect of **Bet-aza** in the ground state is closely related to solvent polarity. By contrast, a clear distinction between protic and aprotic solvents is observed for emission. The emission wavenumber of **Bet-aza** keeps constant in aprotic solvents and protic solvents, respectively (Figure 5-22). However, blue shift was observed in protic solvent when compared with that in aprotic solvents. This indicates that **Bet-aza** in the excited state is not dependent on the solvent polarity but affected by specific interaction like hydrogen bonding between solute and solvents. The no dependence on the solvent polarity may indicate that the dipole moment of **Bet-aza** in the excited state is 0 D.

No.	Solvents	ET(30) [kcal.mol ⁻¹]	ϵ	n	α	β	π	λ_{\max}^A [nm]	ν^A [cm ⁻¹]	λ_{\max}^F [nm]	ν^F [cm ⁻¹]	Φ_F
1	Toluene	33.9	2.38	1.494	0	0.11	0.54	386	25907	534	18727	0.23
2	THF	37.4	7.58	1.405	0	0.55	0.58	380	26316	533	18762	0.19
3	DCM	40.7	8.93	1.421	0.13	0.1	0.82	367	27248	532	18797	0.20
4	PhCN	41.5	26.00	1.528	0	0.37	0.90	369	27100	529	18904	0.28
5	Acetone	42.2	20.56	1.356	0.08	0.43	0.71	365	27397	533	18762	0.15
6	DMF	43.2	36.71	1.428	0	0.69	0.88	365	27397	528	18939	0.18
7	MeCN	45.6	35.94	1.341	0.19	0.4	0.75	360	27778	533	18762	0.12
8	BuOH	50.2	17.8	1.399	0.84	0.84	0.47	357	28011	511	19569	0.27
9	EtOH	51.9	24.55	1.359	0.86	0.75	0.54	353	28329	512	19531	0.21
10	MeOH	55.4	32.66	1.326	0.98	0.66	0.6	347	28818	509	19646	0.17
11	H ₂ O	63.1	78.36	1.333	1.17	0.47	1.09	341	29325	512	19531	0.04

Table 5-2. Photophysical data of **Bet-aza** in different solvents, solvent properties (Dimroth-Reichardt $E_T(30)$ parameter, dielectric constant ϵ , refractive index n , Kamlet-Taft α , β and π^* parameters) are given; fluorescence quantum yields were determined using Comarine 153 in EtOH ($\Phi = 0.53$) as a reference.⁴⁶

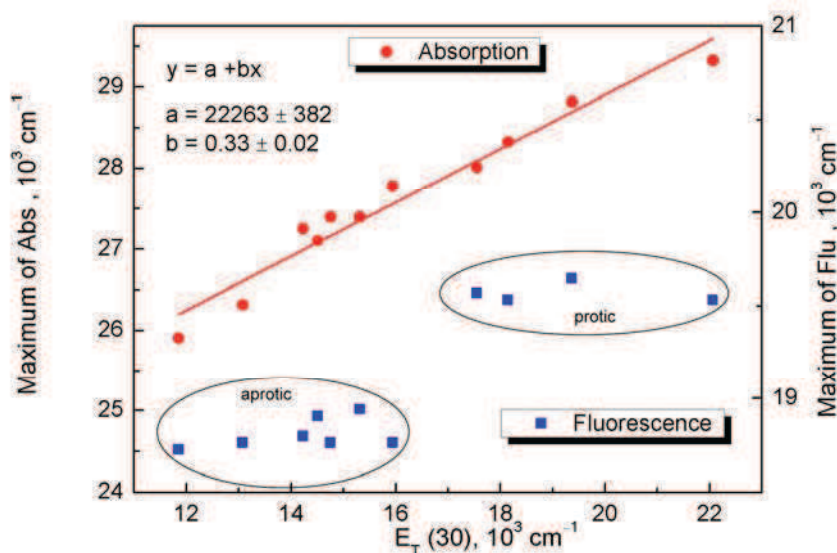


Figure 5-22. Solvatochromic plot for absorption spectra as a function of the $E_T(30)$ polarity index.

Kamlet-Taft correlation has been successfully applied to treat the absorption and fluorescence solvatochromism of **SBPa** separately.³² It can give directly the contribution of electrostatic interaction and specific hydrogen bonding interaction between solute and solvent. According to Kamlet-Taft correlation, the solvent-dependent spectral shift can be linearly

corrected with empirical Kamlet-Taft solvatochromic parameter π^* , α and β as follow:^{47,48}

$$\nu = \nu_0 + p\pi^* + a\alpha + b\beta \quad (\text{eq. 5-1})$$

Where π^* represents a measurement of nonspecific solvent polarity and polarizability, α and β are the solvent hydrogen bond donating (donate a proton) and accepting (donate an electron pair) properties; ν_0 , p , a , and b are solvent independent correction coefficients. Their magnitude and sign provide measure of the influence of the corresponding solute-solvent interaction on the wavenumber of the maximum of the electronic transition band, which can be determined by multiple linear regression analysis. As presented in Table 5-3, Kamlet-Taft correlation coefficients of **Bet-aza** were determined from absorption and emission solvatochromic data. In the case of absorption, coefficient p is larger than a and b , demonstrating that electrostatic interaction dominates the solvatochromism; however, the specific hydrogen bonding interaction is not negligible. In the other case of emission, p is almost negligible when compared with a and b , that is the excited state of **Bet-aza** is insensitive to solvent polarity but mainly controlled by hydrogen bonding interaction. Moreover, when we compare the ratio of coefficients a/b , it's almost the same no matter in the ground state or in the excited state, which might indicate that the same molecular group involved into the absorption and emission.

		Kamlet-Taft correlation coefficients				
	Solvent NO.	ν_0	a	b	p	R^2
Absorption	1-11	25128 ± 612	1684 ± 303	826 ± 613	1979 ± 658	0.86
Fluorescence	1-11	18675 ± 166	689 ± 82	386 ± 167	-65 ± 179	0.93

Table 5-3. Corresponding Kamlet-Taft correlation coefficients obtained from the multiple linear regressions of solvatochromic data of **Bet-aza**.

In order to investigate the conformation of **Bet-aza** in solution, its ^1H NMR spectra were acquired in CD_3OD , CD_3CN and CDCl_3 , as shown in Figure 5-24. The assignment of protons of **Bet-aza** was accomplished through ^1H and ^{13}C NMR, ^1H - ^1H COSY (Figure 5-23). The proton H_c , in the *ortho* position to the pyridinium nitrogen, locates at the highest chemical shift due to the strong deshielding by the positive charge on pyridinium and the intramolecular hydrogen bonding interaction with benzimidazole moiety. From the ^1H - ^1H COSY, H_d locates at the lowest chemical shift because the strong electron-donating amino

group increases shielding effect. Protons H_a and H_b on benzimidazole moiety locate between H_c and H_d . Chemical shift of H_c increases from 8.9 ppm in CD_3OD to 9.2 ppm in CD_3CN then 9.4 ppm in $CDCl_3$, which correlates with the hydrogen bonding ability of solvent $\alpha_{KT}-\beta_{KT}$. This demonstrates that specific interaction between solute and solvent interrupts intramolecular hydrogen bond between H_c and nitrogen atom of imidazole moiety. In contrast when compared with those in CD_3OD , protons H_b , H_a , and H_d shift to the high field in MeCN from 7.5, 7.3, 7.0 ppm to 7.4, 7.0, 6.9 ppm, respectively, which can be explained by the electrostatic interaction.³²

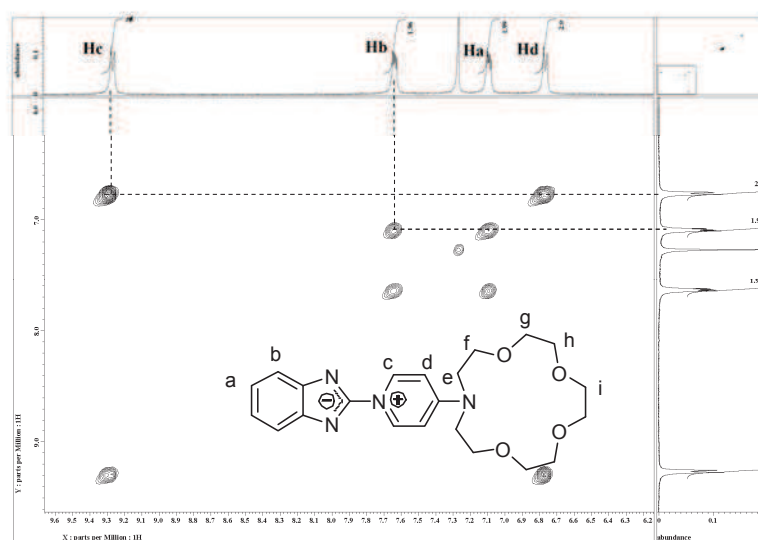


Figure 5-23. COSY spectra of **Bet-aza** in $CDCl_3$.

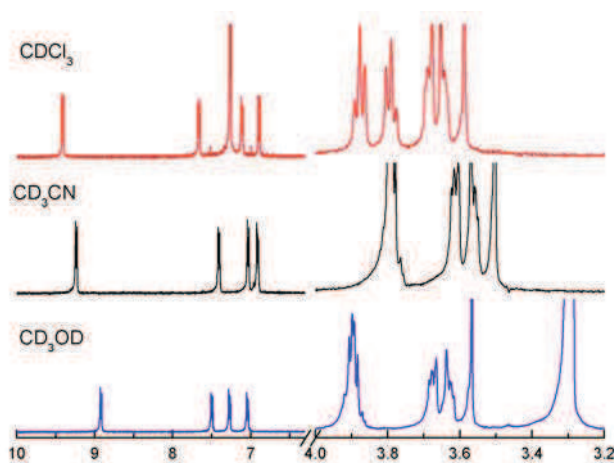


Figure 5-24. 1H NMR spectra of **Bet-aza** in different deuterated solvents.

5.2.4. Complexation properties of **Bet-aza**

Spectral response of **Bet-aza** to metal ions was also examined in MeCN. As shown in Figure 5-25, the addition of Na^+ and K^+ almost does not affect the spectral properties of **Bet-aza**; while the introduction of alkaline earth metal ions causes fluorescence quenching at

534 nm and enhancement at 450 nm to different extents. For Mg^{2+} and Ca^{2+} , 1 equiv is enough to reach equilibrium. This may be attributed to the high charge density of these two metal ions when compared with other tested ions and might indicate the electrostatic interaction between **Bet-aza** and metal ions. Due to the strong binding ability, following experiments focus on investigating the interaction between **Bet-aza** and Ca^{2+} .

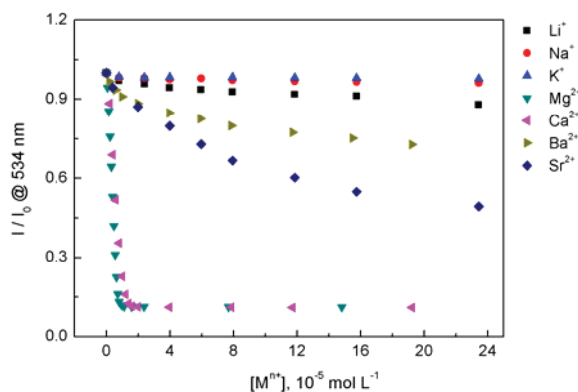


Figure 5-25. Absorption and fluorescence spectra of **Bet-aza** in the presence of increasing concentrations of metal ions in MeCN, [**Bet-aza**] = 10 μM , λ_{ex} = 359 nm.

Figure 5-26 (a) and (b) shows the evolution of absorption and fluorescence spectra of **Bet-aza** in the presence of increasing concentrations of Ca^{2+} in MeCN. With the addition of the Ca^{2+} to the solution of **Bet-aza**, gradual decrease of the absorption maximum at 359 nm are observed, concomitantly with appearance of a new peak at 335 nm. A well-defined isosbestic point at 353 nm indicates the interconversion of free ligand and the complex during the titration. Blue shift is also observed for fluorescence spectra from 534 nm to 450 nm, with a clear isoemissive point at 462 nm indicating only two emissive species in the solution. Both the absorption and fluorescence spectra reach a plateau after 1 equiv of Ca^{2+} is introduced to the solution of **Bet-aza**, demonstrating that the stoichiometry of the complex is 1:1. Nonlinear regression analysis of the spectral titrations based on 1:1 binding ratio then gave the binding constants between **Bet-aza** and Ca^{2+} with $\text{Log } K$ equal to 8.2 in the ground state and 7.9 in the excited state, as presented in Table 5-4. However, it should be noted that our further investigation on kinetics indicates that the binding constants are even larger.

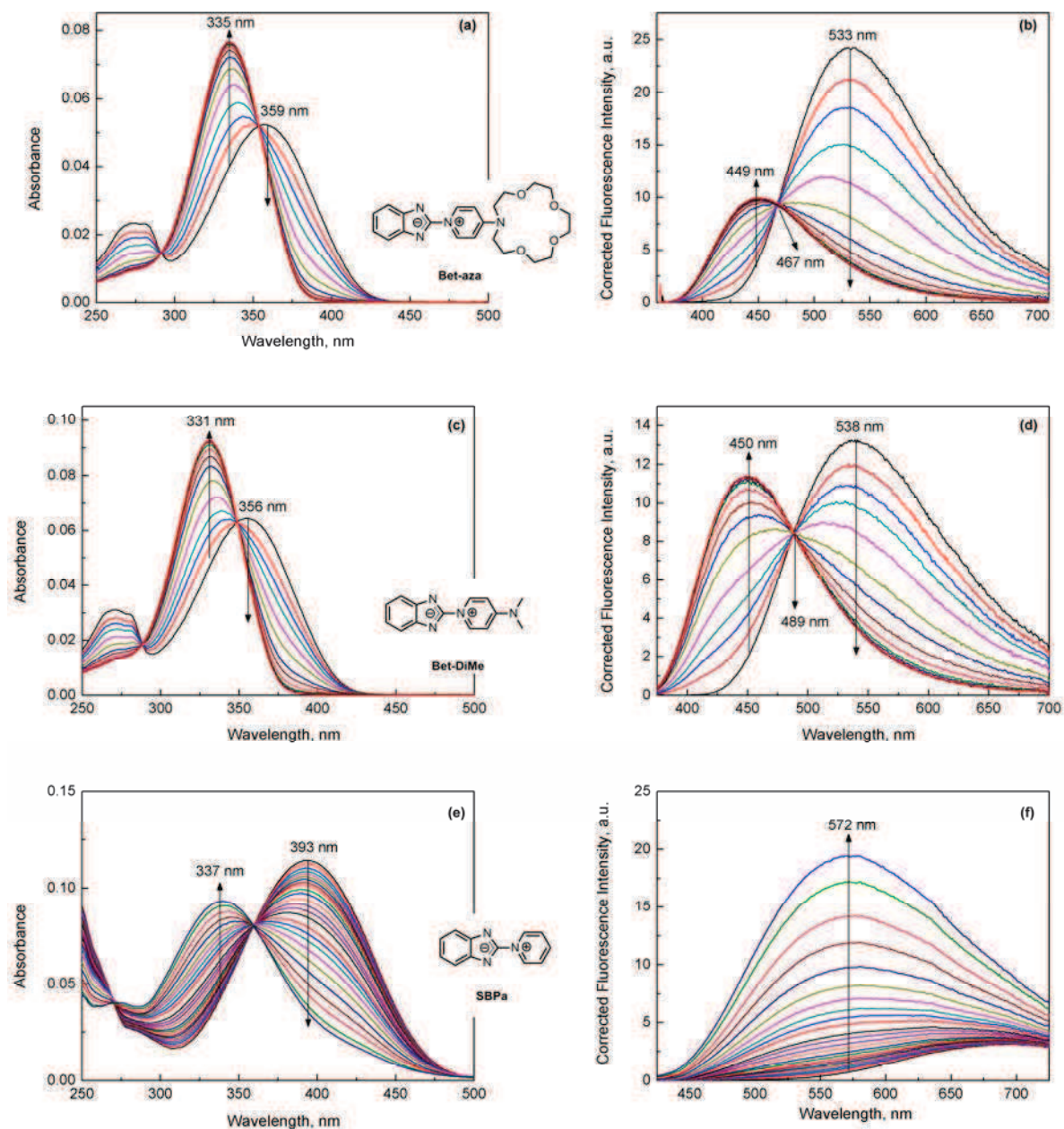


Figure 5-26. Absorption (a, c, e) and fluorescence (b, d, f) spectra of **Bet-aza**, **Bet-DiMe** and **SBPa** in the presence of increasing concentrations of Ca^{2+} in MeCN; (a, b) [**Bet-aza**] = 2.5 μM , λ_{ex} = 359 nm; (c, d) [**Bet-DiMe**] = 2.5 μM , λ_{ex} = 354 nm; (e, f) [**SBPa**] = 10 μM , λ_{ex} = 393 nm.

		Abs			Fluo		
		Ligand	Complex		Ligand	Complex	
		λ_{\max} (nm)	λ_{\max} (nm)	$\text{Log}K^a$	λ_{\max} (nm)	λ_{\max} (nm)	$\text{Log}K^a$
SBPa	MeCN	393	339	3.4	693(br)	570	3.4
Bet-DiMe	MeCN	356	331	7.0	539	450	7.1
Bet-aza	MeCN	359	335	8.2	534	450	7.9
Bet-aza	MeOH	348	336	3.5	508	459	3.5

Table 5-4. Photophysical data of **SBPa**, **Bet-DiMe** and **Bet-aza**; their 1:1 complex with Ca^{2+} and the binding constants from spectral titrations; *a*: it should be noted that the observed binding constants $\text{Log}K$ given here without considering the kinetics effect, therefore the real binding constants are even larger.

It's well known that complexation kinetics usually proceed very fast. However, in our case, it's quite surprising to find a relatively long response time of **Bet-aza** to Ca^{2+} in MeCN by accident. As shown in Figure 5-27, with increasing concentrations of Ca^{2+} when the **Bet-aza** was kept at 2.5 μM , the response time can be slightly reduced. When the concentration of Ca^{2+} is 12 μM , the equilibrium can be reached in 5 min. Figure 5-28 presents the fluorescence spectra of **Bet-aza** in the presence of various concentrations of Ca^{2+} recorded after sufficient equilibrium. It reached a plateau after introduction of 1 equiv Ca^{2+} . Non linear regression analysis of this titration based on 1:1 binding ratio, however, did not give a satisfactory fitting; however, it's definitely that the binding constant for the complex is very large ($\text{Log} K > 7$).

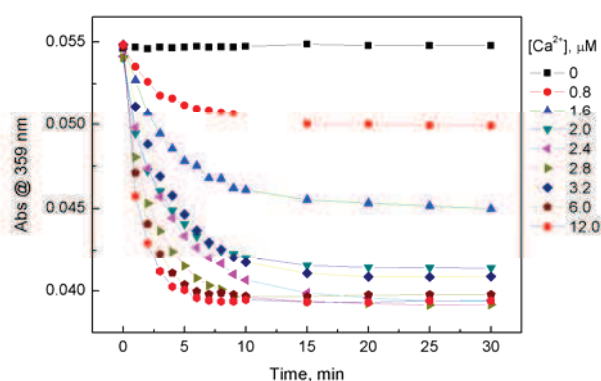


Figure 5-27. Kinetics profile of **Bet-aza** in the absence and presence of different concentrations of $\text{Ca}(\text{ClO}_4)_2$ in MeCN at 359 nm, $[\text{Bet-aza}] = 2.5 \mu\text{M}$, $[\text{Ca}^{2+}] = 0, 0.8, 1.6, 2.0, 2.4, 2.8, 3.2, 6.0, 12.0 \mu\text{M}$.

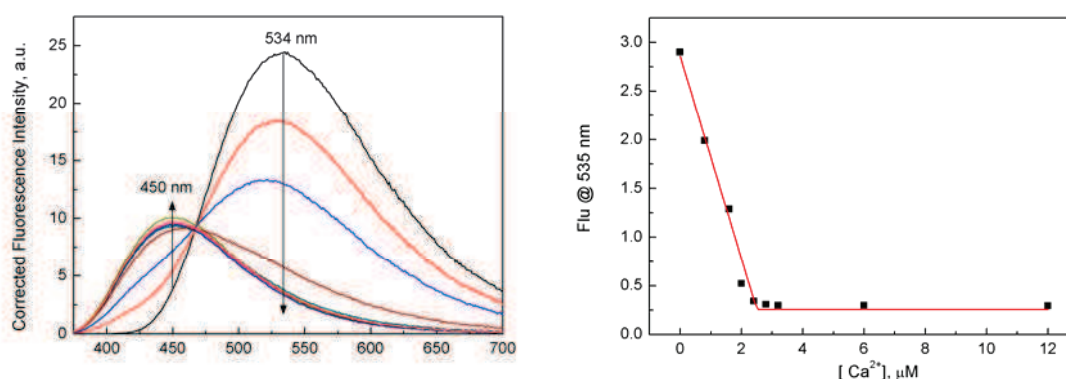


Figure 5-28. Fluorescence spectra of **Bet-aza**, recorded 30 min after the addition of different concentrations of $\text{Ca}(\text{ClO}_4)_2$ in MeCN, $[\text{Bet-aza}] = 2.5 \mu\text{M}$, $[\text{Ca}^{2+}] = 0, 0.8, 1.6, 2.0, 2.4, 2.8, 3.2, 6.0, 12.0 \mu\text{M}$, $\lambda_{\text{ex}} = 359 \text{ nm}$.

Kinetic study on the absorbance variation at 359 nm of **Bet-aza** with the addition of Ca^{2+} was analyzed based on the 1:1 complex, as shown in Figure 5-29. The fitting results give $k_1 = 1.77 \times 10^5 \text{ M}^{-1} \text{ s}^{-1}$ and $k_2 = 0.0245 \text{ s}^{-1}$, and thus binding constant can be calculated by following: $K = k_1/k_2 = 7.22 \times 10^6 \text{ M}^{-1}$, that is $\log K = 6.85$. This is consistent with the strong complexation between **Bet-aza** and Ca^{2+} obtained from the absorption and fluorescence titrations.

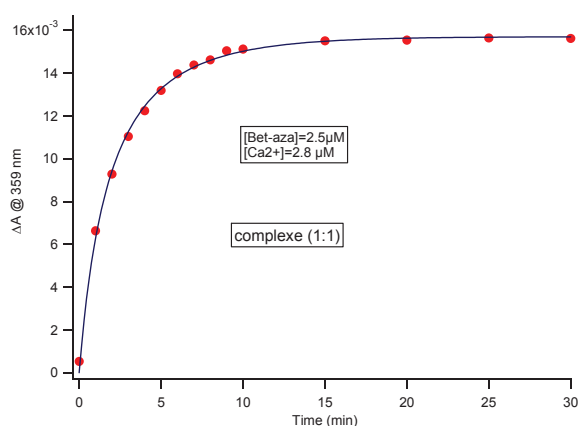
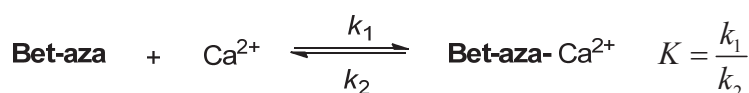


Figure 5-29. Kinetic profile of **Bet-aza** with the addition of $\text{Ca}(\text{ClO}_4)_2$ in MeCN, $[\text{Bet-aza}] = 2.5 \mu\text{M}$, $[\text{Ca}^{2+}] = 2.8 \mu\text{M}$, ΔA denotes the variation of absorbance at 359 nm.

There are two potential binding sites for metal cations in **Bet-aza**: benzimidazole moiety and aza-15-crown-5 moiety. In order to get insight into the binding process, ^1H NMR titration of **Bet-aza** with Ca^{2+} was then carried out in CD_3CN . As shown in Figure 5-30, upon

complexation with Ca^{2+} , proton H_c exhibits a remarkable up-field shift, while H_d shows a down-field shift. Protons of H_a and H_b also exhibit a slight down-field shift as compared with H_d . However, it's surprising to find that the addition of Ca^{2+} almost does not affect the chemical shifts of aza-15-crown-5 moiety, which has been widely reported to bind strongly with metal ions. Anyhow, in our case the ^1H NMR titration demonstrates that Ca^{2+} strongly binds to benzimidazole moiety rather than aza-15-crown-5. This can be explained by the positive charge on the pyridinium ring strongly reduce the electron density of nitrogen atom in aza-15-crown-5 moiety. The mesomeric structure of **Bet-aza** (Scheme 5-8) indeed demonstrates that the partial positive charge on this nitrogen atom results in the loss of its binding ability to cations.⁴⁹ The up-field shift of the proton H_c could be explained by the destroy of the intramolecular hydrogen bonding between H_c and benzimidazole upon complexation with Ca^{2+} .⁵⁰ The slight down-field shift of protons H_a and H_b were due to Ca^{2+} complexation with benzimidazole, as shown in Scheme 5-8. The remarkable blue shift of the absorption and fluorescence bands in the complex indicates that the weaker intramolecular charge transfer as compared with the free ligand, which further confirm complexation of Ca^{2+} with benzimidazole. The complexation-induced destroy of intramolecular hydrogen bonding interaction may explain the long kinetics (5 min) of **Bet-aza** to Ca^{2+} .

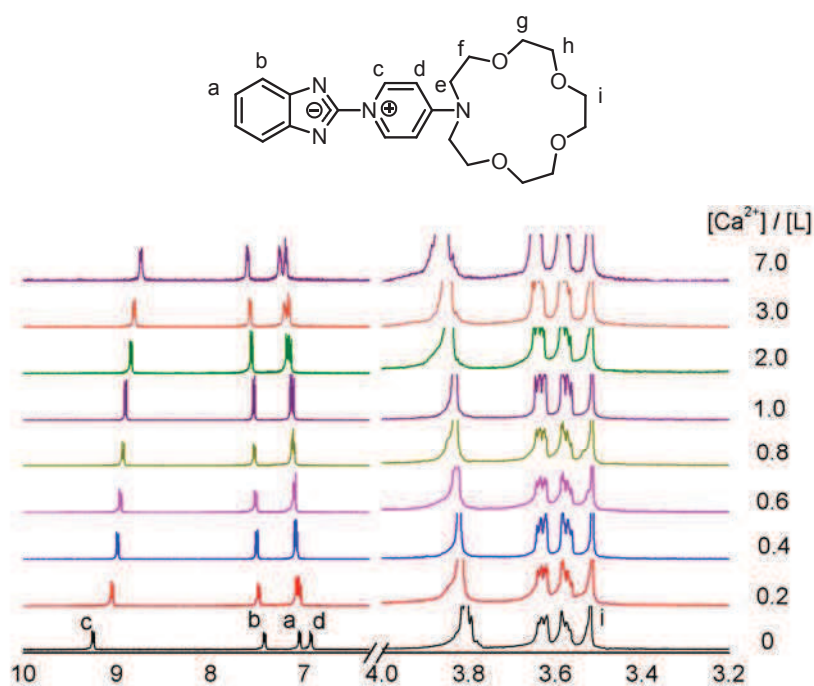
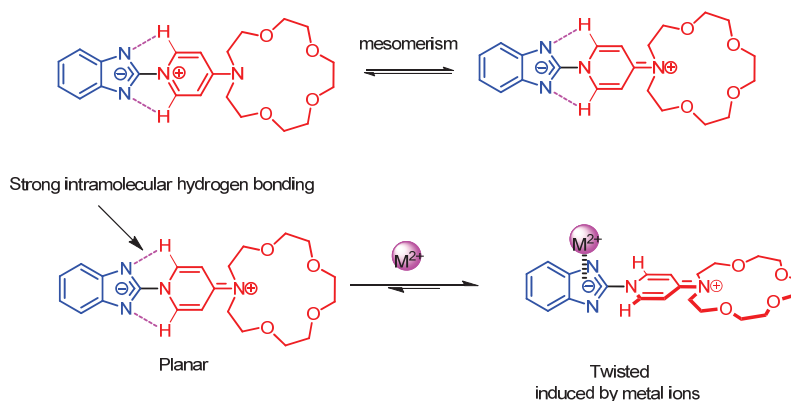


Figure 5-30. ^1H NMR spectra of **Bet-aza** in presence of different concentrations of $\text{Ca}(\text{ClO}_4)_2$ in CD_3CN .



Scheme 5-8. Schematic illustration of mesomerism of **Bet-aza** and its interaction with metal ions.

In order to verify the proposed binding mechanism, a new ligand **Bet-DiMe** without aza-15-crown-5 was synthesized. As shown in Table 5-4, it exhibits an absorption band centered at 356 nm, about 4 nm blue shift as compared with **Bet-aza**; while its fluorescence band at 539 nm is about 6 nm red shift. Spectral titrations (Figure 5-26 (c) and (d)) were carried out in MeCN under identical conditions. Upon addition of increasing concentrations of Ca^{2+} to the solution of **Bet-DiMe**, blue shift of the absorption band from 356 nm to 331 nm and emission band from 539 nm to 450 nm are observed. The clear isosbestic point at 348 nm and isoemissive point at 481 nm demonstrate the equilibrium between free ligand and complex during the titration. Additionally, kinetics of **Bet-DiMe** to Ca^{2+} in MeCN is almost the same as that of **Bet-aza**, as presented in Figure 5-31. In the presence of 12 μM Ca^{2+} when **Bet-DiMe** is 2.5 μM , it reaches equilibrium in 5 min. When the fluorescence spectra of **Bet-DiMe** in the presence of Ca^{2+} were recorded after sufficient equilibrium, it reached a plateau at 1 equiv (Figure 5-32). Non linear regression analysis of the titration based on 1:1 binding ratio, however, did not give a satisfactory fitting due to the quite large binding constant ($\text{Log } K > 7$) for the complex, as shown in Figure 5-32. These evidences strongly confirm that benzimidazole moiety in **Bet-aza** plays a crucial role in binding to metal ions; however, more precise binding constants need to be obtained in order to evaluate the effect of the azacrown on the binding process.

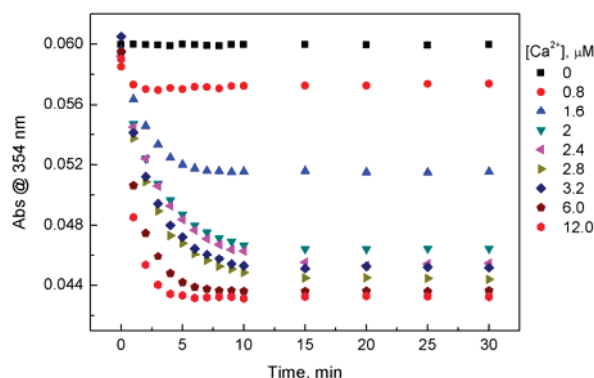


Figure 5-31. Kinetics profile of **Bet-DiMe** in the absence and presence of different concentrations of $\text{Ca}(\text{ClO}_4)_2$ in MeCN at 354 nm, $[\text{Bet-DiMe}] = 2.5 \mu\text{M}$, $[\text{Ca}^{2+}] = 0, 0.8, 1.6, 2.0, 2.4, 2.8, 3.2, 6.0, 12.0 \mu\text{M}$.

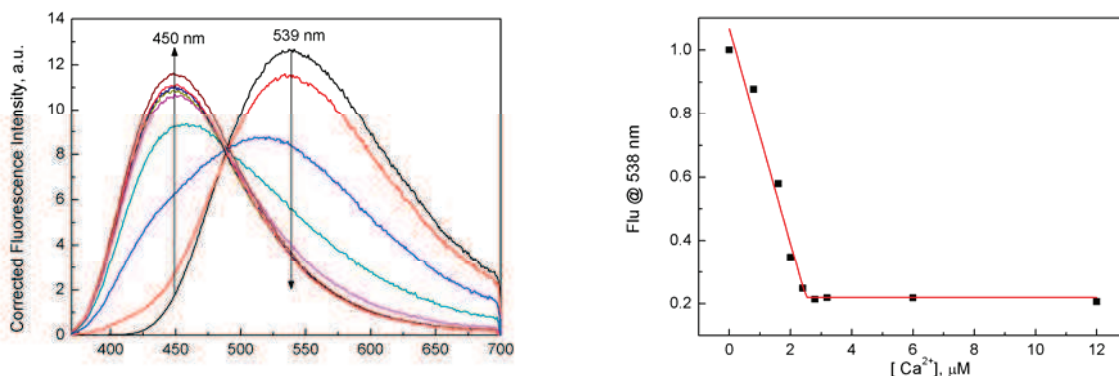


Figure 5-32. Fluorescence spectra of **Bet-DiMe**, recorded 30 min after the addition of different concentrations of $\text{Ca}(\text{ClO}_4)_2$ in MeCN, $[\text{Bet-DiMe}] = 2.5 \mu\text{M}$, $[\text{Ca}^{2+}] = 0, 0.8, 1.6, 2.0, 2.4, 2.8, 3.2, 6.0, 12.0 \mu\text{M}$, $\lambda_{\text{ex}} = 354 \text{ nm}$.

As we points out above that benzimidazole in **Bet-aza** acts as the coordination sites for metal ions,³⁵ the spectral response of **SBPa** to Ca^{2+} was also performed in MeCN in order to investigate the effect of amino group appended to pyridinium moiety on the complexation properties of benzimidazole moiety. As presented in Figure 5-26 (e) and (f), the addition of increasing concentrations of Ca^{2+} induces the blue shift for both the absorption band from 393 nm to 337 nm and emission band from 693 nm to 570 nm. This is consistent with our assumption that complexation of benzimidazole moiety to Ca^{2+} would lead to a weaker intramolecular charge transfer. However, nonlinear regression analysis of fluorescence titration gives the binding constant with $\text{Log } K = 3.39$, which is several orders of magnitude lower than that of **Bet-aza** and **Bet-DiMe**. This is probably because electrostatic repulsion between pyridinium moiety of **SBPa** and metal ions is much stronger than that in the complex of **Bet-aza** and **Bet-DiMe**. In latter case, the mesomeric effect may push partial positive

charge on pyridinium moiety to nitrogen atom and thus reduce the electrostatic repulsion between pyridinium moiety and Ca^{2+} .

Spectral response of **Bet-aza** to CF_3COOH was also investigated in MeCN. As we can see from the Figure 5-33, the addition of CF_3COOH has exactly the same effect with Ca^{2+} . Both absorption and fluorescence spectra of protonated **Bet-aza** overlap with those of **Bet-aza** complex with Ca^{2+} . This further demonstrates that benzimidazole moiety in **Bet-aza** is the binding site to Ca^{2+} .

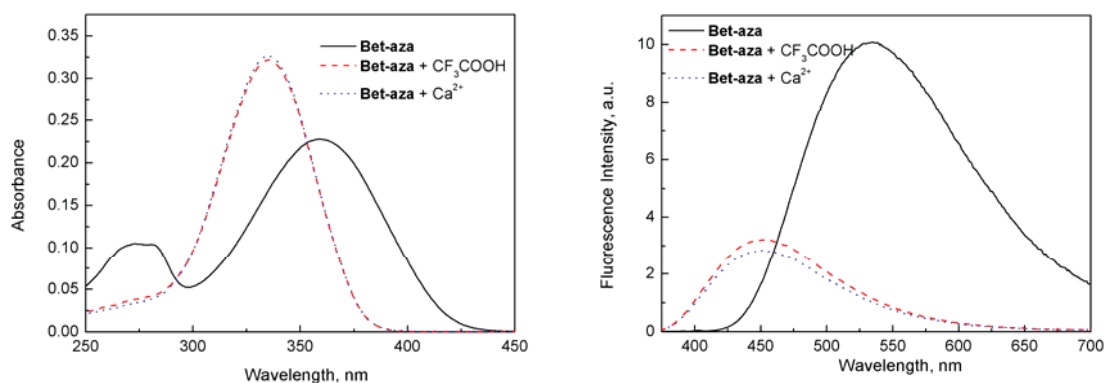
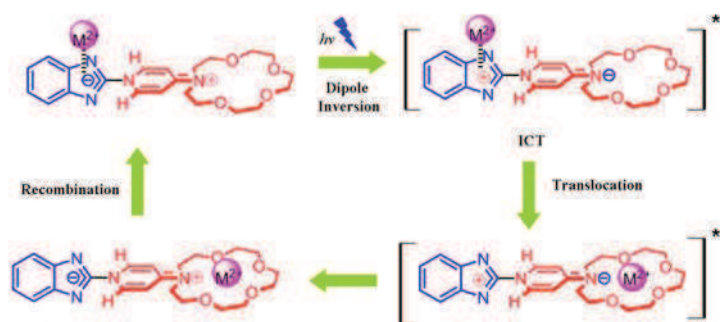


Figure 5-33. Absorption and fluorescence spectra of **Bet-aza** in the absence and presence of CF_3COOH in MeCN, $[\text{Bet-aza}] = 10 \mu\text{M}$, $[\text{CF}_3\text{COOH}] = 12.0 \mu\text{M}$, $[\text{Ca}^{2+}] = 20.0 \mu\text{M}$, $\lambda_{\text{ex}} = 359 \text{ nm}$.

5.2.5. Conclusion

A new ligand **Bet-aza** bearing betaine pyridinium and aza-15-crown-5 was synthesized. Solvatochromism of **Bet-aza** indicated that its absorption band stemmed from $S_0 \rightarrow S_2$ electronic transition while emission band from $S_1 \rightarrow S_0'$ transition. Dipole moment inversion in the excited state can be inferred from negative solvatochromism of absorption spectra. Treatment of the solvatochromic data of **Bet-aza** with $E_T(30)$ and Kamlet-Taft correlation demonstrated: (1) solvatochromism of **Bet-aza** in the ground state was dominated by solvent polarity; however, specific hydrogen bonding interaction should not be negligible; (2) solvatochromism of **Bet-aza** in the excited state was independent on the solvent polarity, indicating the dipole moment of **Bet-aza** in the excited state was 0 D. Strong intramolecular hydrogen bonding interaction in **Bet-aza** was also verified by ^1H NMR in different solvents. Addition of metal ions to the solution of **Bet-aza** led to remarkable blue shift of absorption and fluorescence spectra, which was explained by the coordination of benzimidazole moiety in **Bet-aza** to metal ions. The proposed binding mode was verified by ^1H NMR titration, metallo-responsive properties of reference compounds **Bet-DiMe** and **SBPa**, protonation of

Bet-aza. Based on these results, we believe that dipole moment inversion of **Bet-aza** in the excited state will in one aspect decrease the binding ability of its benzimidazole moiety to Ca^{2+} and in the other aspect there will be an increase of electron density on the nitrogen atom of aza-15-crown-5 to enhance its affinity to Ca^{2+} . They both cooperatively realize the translocation of metal ions from benzimidazole moiety to aza-15-crown-5 moiety in the excited state, as shown in Scheme 5-9. Transient absorption technique will be used to monitor the each step in the excited state.



Scheme 5-9. Schematic illustration of translocations of Ca^{2+} in the excited state.

Reference

- [1] Steed, J. W.; Atwood, J. L. "*Supramolecular Chemistry, 2nd edition*" John Wiley & Sons, 2009.
- [2] Rusalov, M. V.; Uzhinov, B. M.; Alfimov, M. V.; Gromov, S. P. "*Photoinduced recoordination of metal cations in complexes with chromogenic crown ethers.*" Russian Chemical Reviews **2010**, 79, 1099-1121.
- [3] Lewis, J. D.; Moore, J. N. "*Cation sensors containing a (bpy)Re(CO)(3) group linked to an azacrown ether via an alkenyl or alkynyl spacer: synthesis, characterisation, and complexation with metal cations in solution.*" Dalton Transactions **2004**, 1376-1385.
- [4] de Silva, A. P.; Gunaratne, H. Q. N.; Gunlaugsson, T.; Huxley, A. J. M.; McCoy, C. P.; Rademacher, J. T.; Rice, T. E. "*Signaling recognition events with fluorescent sensors and switches.*" Chemical Reviews **1997**, 97, 1515-1566.
- [5] Valeur, B.; Leray, I. "*Design principles of fluorescent molecular sensors for cation recognition.*" Coordination Chemistry Reviews **2000**, 205, 3-40.
- [6] Bourson, J.; Valeur, B. "*Ion-Responsive Fluorescent Compounds .2. Cation-Steered Intramolecular Charge-Transfer in a Crowned Merocyanine.*" Journal of Physical Chemistry **1989**, 93, 3871-3876.
- [7] Martin, M. M.; Plaza, P.; Hung, N. D.; Meyer, Y. H.; Bourson, J.; Valeur, B. "*Photoejection of Cations from Complexes with a Crown-Ether-Linked Merocyanine Evidenced by Ultrafast Spectroscopy.*" Chemical Physics Letters **1993**, 202, 425-430.
- [8] Plaza, P.; Leray, I.; Changenet-Barret, P.; Martin, M. M.; Valeur, B. "*Reversible bulk photorelease of strontium ion from a crown ether-linked merocyanine.*" Chemphyschem **2002**, 3, 668-674.
- [9] Ley, C.; Lacombat, F.; Plaza, P.; Martin, M. M.; Leray, I.; Valeur, B. "*Femtosecond to Subnanosecond Multistep Calcium Photoejection from a Crown Ether-Linked Merocyanine.*" Chemphyschem **2009**, 10, 276-281.
- [10] Martin, M. M.; Plaza, P.; Meyer, Y. H.; Badaoui, F.; Bourson, J.; Lefevre, J. P.; Valeur, B. "*Steady-state and picosecond spectroscopy of Li⁺ or Ca²⁺ complexes with a crowned merocyanine. Reversible photorelease of cations.*" Journal of Physical Chemistry **1996**, 100, 6879-6888.
- [11] Feringa, B. L.; Browne, W. R. "*Molecular Switches, 2nd*" Wiley-VCH, Weinheim, 2011.
- [12] Lewis, J. D.; Moore, J. N. "*Photoinduced Ba²⁺ release and thermal rebinding by an azacrown ether linked by an alkynyl pyridine to a (bpy)Re(CO)(3) group.*" Chemical Communications **2003**, 2858-2859.
- [13] Lewis, J. D.; Perutz, R. N.; Moore, J. N. "*Light-controlled ion switching: Direct observation of the complete nanosecond release and microsecond recapture cycle of an azacrown-substituted [(bpy)Re(CO)(3)L](+) complex.*" Journal of Physical Chemistry A **2004**, 108, 9037-9047.
- [14] Gust, D.; Moore, T. A.; Moore, A. L. "*Mimicking photosynthetic solar energy transduction.*" Accounts of Chemical Research **2001**, 34, 40-48.
- [15] Nierengarten, J. F.; Armaroli, N.; Accorsi, G.; Rio, Y.; Eckert, J. F. "*[60]Fullerene: A*

versatile photoactive core for dendrimer chemistry." Chemistry-a European Journal **2003**, *9*, 37-41.

[16] Imahori, H.; Mori, Y.; Matano, Y. "Nanostructured artificial photosynthesis." Journal of Photochemistry and Photobiology C-Photochemistry Reviews **2003**, *4*, 51-83.

[17] Guldi, D. M.; Prato, M. "Excited-state properties of C-60 fullerene derivatives." Accounts of Chemical Research **2000**, *33*, 695-703.

[18] Araki, Y.; Ito, O. "Factors controlling lifetimes of photoinduced charge-separated states of fullerene-donor molecular systems." Journal of Photochemistry and Photobiology C-Photochemistry Reviews **2008**, *9*, 93-110.

[19] Komamine, S.; Fujitsuka, M.; Ito, O.; Moriwaki, K.; Miyata, T.; Ohno, T. "Photoinduced charge separation and recombination in a novel methanofullerene-triarylamine dyad molecule." Journal of Physical Chemistry A **2000**, *104*, 11497-11504.

[20] Rajkumar, G. A.; Sandanayaka, A. S. D.; Ikeshita, K.; Ito, M.; Araki, Y.; Furusho, Y.; Kihara, N.; Ito, O.; Takata, T. "Photoinduced intramolecular electron-transfer processes in [60]fullerene-(spacer)-N,N-bis(biphenyl)aniline dyad in solutions." Journal of Physical Chemistry A **2005**, *109*, 2428-2435.

[21] Witulski, B. "Palladium-catalyzed synthesis of N-aryl- and N-heteroaryl-aza-crown ethers via cross-coupling reactions of aryl- and heteroaryl bromides with aza-crown ethers." Synlett **1999**, 1223-1226.

[22] Kelly, D. P.; Bateman, S. A.; Martin, R. F.; Reum, M. E.; Rose, M.; Whittaker, A. R. D. "DNA-Binding Compounds .5. Synthesis and Characterization of Boron-Containing Bibenzimidazoles Related to the DNA Minor-Groove Binder, Hoechst-33258." Australian Journal of Chemistry **1994**, *47*, 247-262.

[23] Belik, P.; Gugel, A.; Kraus, A.; Walter, M.; Mullen, K. "Diels-Alder Adduct of C-60 and 4-Carboxy-O-Quinodimethane - Synthesis and Chemical-Transformations." Journal of Organic Chemistry **1995**, *60*, 3307-3310.

[24] Kratochv.B; Zatkan, D. A. "Oxidation of Some Arylamines by Copper(2) in Acetonitrile." Analytical Chemistry **1968**, *40*, 422-424.

[25] Reichardt, C. "Solvatochromism, Thermochromism, Piezochromism, Halochromism, and Chiro-Solvatochromism of Pyridinium N-Phenoxide Betaine Dyes." Chemical Society Reviews **1992**, *21*, 147-153.

[26] Reichardt, C. "Solvatochromic Dyes as Solvent Polarity Indicators." Chemical Reviews **1994**, *94*, 2319-2358.

[27] Abe, J.; Shirai, Y.; Nemoto, N.; Miyata, F.; Nagase, Y. "Heterocyclic pyridinium betaines, a new class of second-order nonlinear optical materials: Combined theoretical and experimental investigation of first-order hyperpolarizability through *ab initio*, INDO/S, and Hyper-Rayleigh scattering." Journal of Physical Chemistry B **1997**, *101*, 576-582.

[28] Nemoto, N.; Abe, J.; Miyata, F.; Shirai, Y.; Nagase, Y. "New class of second-order non-linear optical material: stilbazolium benzimidazolone derived from alkylsulfonyl substituted stilbazole." Journal of Materials Chemistry **1998**, *8*, 1193-1197.

[29] Abe, J.; Shirai, Y.; Nemoto, N.; Nagase, Y. "Manipulation of dipole moment and hyperpolarizability based on heterocyclic pyridinium betaine structures: *Ab initio* and INDO/S MO calculations." Journal of Physical Chemistry B **1997**, *101*, 1910-1915.

[30] Alcalde, E.; Dinares, I.; Elguero, J.; Fayet, J. P.; Vertut, M. C.; Miravittles, C.; Molins, E.

"Azinium Azolate Inner Salts - Synthesis and Structural Studies." Journal of Organic Chemistry **1987**, *52*, 5009-5015.

[31]Abe, J.; Shirai, Y. "Heterocyclic betaines exhibiting extremely large first hyperpolarizability: *Ab initio* and INDO/S calculations." Journal of the American Chemical Society **1996**, *118*, 4705-4706.

[32]Pawlowska, Z.; Lietard, A.; Aloise, S.; Sliwa, M.; Idrissi, A.; Poizat, O.; Buntinx, G.; Delbaere, S.; Perrier, A.; Maurel, F.; Jacques, P.; Abe, J. "The excited state dipole moments of betaine pyridinium investigated by an innovative solvatochromic analysis and TDDFT calculations." Physical Chemistry Chemical Physics **2011**, *13*, 13185-13195.

[33]Aloise, S.; Pawlowska, Z.; Ruckebusch, C.; Sliwa, M.; Dubois, J.; Poizat, O.; Buntinx, G.; Perrier, A.; Maurel, F.; Jacques, P.; Malval, J. P.; Poisson, L.; Piani, G.; Abe, J. "A two-step ICT process for solvatochromic betaine pyridinium revealed by ultrafast spectroscopy, multivariate curve resolution, and TDDFT calculations." Physical Chemistry Chemical Physics **2012**, *14*, 1945-1956.

[34]Perrier, A.; Aloise, S.; Pawlowska, Z.; Sliwa, M.; Maurel, F.; Abe, J. "Photoinduced intramolecular charge transfer process of betaine pyridinium: A theoretical spectroscopic study." Chemical Physics Letters **2011**, *515*, 42-48.

[35]Molina, P.; Tarraga, A.; Oton, F. "Imidazole derivatives: A comprehensive survey of their recognition properties." Organic & Biomolecular Chemistry **2012**, *10*, 1711-1724.

[36]Xu, Z.; Kim, S. K.; Yoon, J. "Revisit to imidazolium receptors for the recognition of anions: highlighted research during 2006-2009." Chemical Society Reviews **2010**, *39*, 1457-1466.

[37]Joseph, R.; Ramanujam, B.; Acharya, A.; Khutia, A.; Rao, C. P. "Experimental and computational studies of selective recognition of Hg(2+) by amide linked lower rim 1,3-dibenzimidazole derivative of calix[4]arene: Species characterization in solution and that in the isolated complex, including the delineation of the nanostructures." Journal of Organic Chemistry **2008**, *73*, 5745-5758.

[38]Tang, L. J.; Li, F. F.; Liu, M. H.; Nandhakumar, R. "A New Rhodamine B Derivative As a Colorimetric Chemosensor for Recognition of Copper(II) Ion." Bulletin of the Korean Chemical Society **2010**, *31*, 3212-3216.

[39]Chi, K. W.; Addicott, C.; Stang, P. J. "Incorporation of a flexible, pyridine-functionalized diaza-crown ether into discrete supramolecules via coordination-driven self-assembly." Journal of Organic Chemistry **2004**, *69*, 2910-2912.

[40]Nemoto, N.; Abe, J.; Miyata, F.; Shirai, Y.; Nagase, Y. "A new class of second-order non-linear optical material: Stilbazolium benzimidazolate covalently bound to polymer backbone." Journal of Materials Chemistry **1997**, *7*, 1389-1393.

[41]Alcalde, E.; Perezgarcia, L.; Dinares, I.; Coombs, G. H.; Frigola, J. "Synthesis and Antitrichomonal Activity of Azinium (Azolium) 4-Nitrobenzimidazolate Betaines and Their Derivatives." European Journal of Medicinal Chemistry **1992**, *27*, 171-176.

[42]Mataga, N.; Kaifu, Y.; Koizumi, M. "The Solvent Effect on Fluorescence Spectrum - Change of Solute-Solvent Interaction during the Lifetime of Excited Solute Molecule." Bulletin of the Chemical Society of Japan **1955**, *28*, 690-691.

[43]Valeur, B. "Molecular Fluorescence: Principles and Applications" Wiley-VCH Verlag GmbH, **2001**.

- [44]Mataga, N.; Kaifu, Y.; Koizumi, M. "*Solvent Effects Upon Fluorescence Spectra and the Dipolemoments of Excited Molecules.*" Bulletin of the Chemical Society of Japan **1956**, *29*, 465-470.
- [45]Reichardt, C. "*Pyridinium N-phenolate betaine dyes as empirical indicators of solvent polarity: Some new findings.*" Pure and Applied Chemistry **2004**, *76*, 1903-1919.
- [46]Grabolle, M.; Spieles, M.; Lesnyak, V.; Gaponik, N.; Eychmuller, A.; Resch-Genger, U. "*Determination of the Fluorescence Quantum Yield of Quantum Dots: Suitable Procedures and Achievable Uncertainties.*" Analytical Chemistry **2009**, *81*, 6285-6294.
- [47]Kamlet, M. J.; Abboud, J. L. M.; Abraham, M. H.; Taft, R. W. "*Linear Solvation Energy Relationships .23. A Comprehensive Collection of the Solvatochromic Parameters, Pi-Star, Alpha and Beta, and Some Methods for Simplifying the Generalized Solvatochromic Equation.*" Journal of Organic Chemistry **1983**, *48*, 2877-2887.
- [48]Marcus, Y. "*The Properties of Organic Liquids That Are Relevant to Their Use as Solvating Solvents.*" Chemical Society Reviews **1993**, *22*, 409-416.
- [49]Abe, J.; Nemoto, N.; Nagase, Y.; Shirai, Y. "*Ab initio MO investigations of molecular structures in the ground and first excited states of heterocyclic pyridinium betaine.*" Chemical Physics Letters **1996**, *261*, 18-22.
- [50]Boz, I.; Schaarschmidt, D.; Ruffer, T.; Lang, H.; Spange, S. "*A Pyridinium-Barbiturate-Betaine Dye with Pronounced Negative Solvatochromism: A New Approach for Molecular Recognition.*" Angewandte Chemie-International Edition **2009**, *48*, 7440-7443.

General Conclusions and Perspectives

General conclusions and perspectives

The related works in this dissertation are focused on rational design, synthesis and spectroscopic evaluation of fluorescent chemosensors for Hg^{2+} , Ni^{2+} , Cu^{2+} based on triazole moiety and K^+ , Al^{3+} based on calix[4]bisazacrown moiety. Preliminary investigations on modulation of cation binding in the excited state have also been carried out.

1. Fluorescent chemosensors based on 1,2,3-triazole

Comprehensively photophysical and complexing investigations on a series of “click” fluoroionophores were performed to elucidate the roles of 1,2,3-triazole moiety in fluorescent chemosensors, concluded as following:

1.1. Triazole as a linker

Fluorescein derivative **Flu-1** showed selective response to Hg^{2+} over a range of metal ions in THF in a fluorescence turn-on manner. While in the presence of protic solvent ($V_{\text{DCM}}/V_{\text{MeOH}}=9:1$), its fluorescence changed in a ratiometric manner with gradual addition of Hg^{2+} . ^1H NMR titration and IR spectra suggested that specific spectral behavior was due to the complexation between carbonyl group of xanthene moiety and Hg^{2+} . When triazole was grafted on xanthene moiety, **Flu-2** exhibited almost the same spectral behavior as that of **Flu-1**, indicating that triazole moiety was just a linker. This result provides us the possibility to incorporate an internal reference by click reaction or to construct a FRET pair to realize a ratiometric detection of analytes. However, limitation of our probes in pure organic solvent medium suggests that the carbonyl group is not a good binding site. Replacement of oxygen atom of the carbonyl group with nitrogen or sulfur atom with strong binding ability to metal ions should be considered to further utilization of metal modulated spectral properties of fluorescein core.

Cu^{2+} -catalyzed Fenton reaction is well known to yield hydroxide and hydroxyl radical very efficiently. **Flu-3** and **Flu-4** containing fluorescein lactone were capable of highly sensitive detection of Cu^{2+} based on a ring-opening process, induced by the hydroxide stemming from Cu^{2+} -catalyzed Fenton reaction. Triazole moieties in **Flu-3** and **Flu-4** were demonstrated to be linkers. Exploration of biologically important catalytic reactions for the detection of analytes is highly attractive for its good sensitivity; however, the limitation of our approach is that spectral change was induced by the pH change. To realize the application

of our approach in real samples under physiological conditions, indicators that are sensitive to hydroxyl radical can be used.

1.2. Triazole acts as sole or important binding sites

NBD-1 showed selective spectral response to Hg^{2+} in EtOH/ H_2O mixed solution at pH 7.4. in a fluorescence turn-off manner. ^1H NMR titration demonstrated that 1,2,3-triazole was the sole binding site for **NBD-1** to Hg^{2+} . The fluorescence quenching and red shift were postulated to be caused by the increase of the local polarity of the fluorophore and the possible photoinduced electron transfer. **NBD-2** with a more rigid terminal amino acid moiety responded to Hg^{2+} in a similar way.

Rho-1 with sugar unit attached to rhodamine fluorophore was linked by triazole moiety. It showed selective response to Hg^{2+} in MeCN/DMSO (99:1), which took 26 h to reach the equilibrium at room temperature. Surprisingly, photochromic approach was able to reduce the response time to 2 min. Insightful investigation demonstrated that small amount of DMSO played an important role in promoting the ring-opening of rhodamine lactame, which was supposed to react with the excited **Rho-1**- Hg^{2+} complex. **Rho-2** with a disaccharide units displayed similar spectral changes in the presence of metal ions as that of **Rho-1**. Although the Hg^{2+} induced ring-opening process was limited in MeCN/DMSO (99:1) medium, it demonstrates a new approach to improve the sensing performance of chemosensors.

1.3. Assemble of triazoles as the binding sites

By grafting seven triazole units on the narrow rim of β -CyD, the assembled **CDPy** exhibited strong excimer emission and low monomer emission in various solvents, indicating the close proximity of pyrene fluorophores in the excited state. Its structural conformation was evidenced by NOESY NMR and circular dichroism spectra. Investigation on the metallo-responsive properties demonstrated that **CDPy** showed moderately selective affinity to Hg^{2+} and more interestingly a signal amplification process occurred during the titration with Hg^{2+} in THF and toluene. This phenomenon would be instructive for using CyD scaffold for chemical sensing.

1.4. Triazoles as conjugated fluorophores and co-binding sites

The incorporation of two 1,2,3-triazoles into benzothiadiazole can extend the conjugated system and subsequently change the spectral properties, which are dependent on the position of the substituents on the triazole, the number of triazole unit but almost independent on the

terminal amino acids moiety. Spectral response of **Benzo-x** to metal ions mainly related to the preorganized structure between benzothiadiazole and triazole moiety. For 1,4-disubstituted **Benzo-2** showed binding ability to Ni^{2+} , Cu^{2+} , Hg^{2+} and Co^{2+} in MeCN. In contrast, 1,5-disubstituted **Benzo-5** showed selective response to Hg^{2+} but no affinity to Ni^{2+} , Cu^{2+} , and Co^{2+} . Finally 1,4-disubstituted **Benzo-8** was successfully developed as a highly selective chemosensor of Cu^{2+} in HEPES buffer solution under physiological pH condition by a judicious selection of solvent medium and molecular structure.

From the above, we can conclude that 1,2,3-triazole shows flexible coordination chemistry in organic solvent. However, its binding ability to metal ions is dramatically decreased in water containing system, which limits its application as chemosensors in real samples. Therefore the incorporation of other complementary binding sites to improve the binding affinity in aqueous solution is more promising than just a sole triazole.

2. Fluorescent chemosensors based on calix[4]bisazacrown

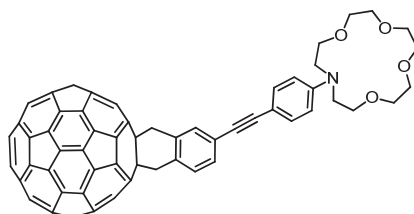
Calix-Dansyl bearing bisazacrown showed selective response to K^+ over Na^+ in EtOH. ^1H NMR titration in CD_3CN demonstrated that the binding was attributed to the good match of the cation size with the azacrown and preferential cation- π interaction with the phenyl rings of calix[4]azacrown. The unsatisfying binding constant of **Calix-Dansyl** to K^+ was due to the strong electron-withdrawing character of sulfonyl group and possibly some steric effect from dansylamide fluorophores. Enhancement of the charge density of nitrogen atom in azacrown should be considered for the improvement of sensing sensitivity.

Among various metal ions, Al^{3+} shows a unique character with formation of colloid particles $\text{Al}(\text{OH})_3$ with positive charge on its surface under weak acid condition pH 6.0. **SulfCalix-Dansyl** with four negative charges could be efficiently adsorbed by electrostatic interaction. Dramatic change of the microenvironmental polarity caused fluorescence enhancement, concomitantly with blue shift of its maximum. The sensing mechanism was verified by the increase of absorption tail band, pH effect, resonance light scattering, anisotropy measurement and also flocculation formation. By virtue of unique character of Al^{3+} , negative charged ICT chromophore/fluorophores may be explored for the detection of Al^{3+} under weak acidic condition.

3. Modulation of Cation Binding in the Excited State

Constructing a dyad by using fullerene C_{60} as an electron acceptor and aniline moiety as electron donor, we were able to get a long-live charge separated state with a lifetime of 165 ns,

providing the possibility of complete cation release in the excited state. In the other aspect, steady state spectral investigation demonstrated that **Full-aza** exhibited strong binding ability to divalent cations in PhCN. Transient absorption spectra of the complex, however, did not display absorption band of the radical cation any more. Instead, the deactivation of excited state mainly occurred by intersystem crossing and fluorescence emission, inferred from the strong triplet state absorption of ${}^3\text{C}_{60}^*$ and enhancement of fluorescence emission. This was attributed to the complexation inhibiting PET process and consequently no charge separated species would be detected. It seems that cations release does not work based on **Full-aza** and PCT approach may be more efficient than PET. For example, with amide group in **Full-aza** replaced by alkyne group, **Full-alkyne-aza** with strong charge-transfer characteristic and lower binding affinity to metal ions is going to be explored for cation release.



Scheme 1. Molecular structure of **Full-alkyne-aza**.

Treatment of solvatochromic effect of **Bet-aza** with $E_T(30)$ and Kamlet-Taft correlation demonstrated that in the ground state solvatochromism of **Bet-aza** was mainly dominated by solvent polarity, even though the specific hydrogen bonding interaction was not negligible; while in the excited state solvatochromism was almost independent on solvent polarity but affected by hydrogen bonding interaction, indicating that dipole moment of **Bet-aza** in the excited state is 0 D. Based on the literatures, we identically attributed a dipole inversion in the excited state. Study of complexation properties by spectral titrations demonstrated that benzimidazole was the binding site of **Bet-aza** to metal ions, as verified by ${}^1\text{H}$ NMR titration in CD_3CN and model compound **Bet-DiMe** and **SBPa**. Mesomerism induced positive charge on the nitrogen atom of azacrown was proposed to explain the loss of the binding ability of azacrown moiety. Kinetic study base on 1:1 complex further confirmed the strong binding affinity of **Bet-aza** to Ca^{2+} . Growing a complex crystal is ongoing in our lab to obtain direct evidence of their binding mode. It's hypothesized that photoexcited dipole moment inversion would change the charge distribution on **Bet-aza** by decreasing the density on benzimidazole moiety and increase for nitrogen of azacrown, which consequently causes cation translocation from benzimidazole moiety to azacrown moiety in the excited state. Femtosecond transient absorption will be used to monitor the photochemical processes.

Chapter 6. Experimental Section

6.1. General procedures

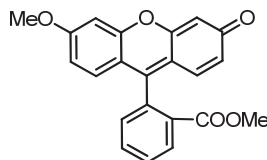
All chemicals were purchased from Sigma-Aldrich and used as received. Solvents for synthesis were synthetic or spectroscopic grade and purchased from Carlo-Erba or SDS. Anhydrous solvents (toluene, tetrahydrofuran, acetonitrile, dichloromethane, dimethylformamide) were purchased from Sigma-Aldrich. The deuterated solvents were purchased from SDS. Column chromatography was performed on silica gel 60 (40-63 μm). Analytical thin layer chromatography (TLC) was performed on silica gel F250 plates (SDS), detected by UV light (254 and 365 nm).

^1H and ^{13}C NMR were performed at room temperature on a JEOL JNM ECS 400MHz spectrometer using tetramethylsilane or solvent peak (^1H NMR: CHCl_3 in CDCl_3 , 7.26 ppm; $\text{CHD}_2\text{SOCD}_3$ in $\text{DMSO-}d_6$, 2.49 ppm; CHD_2CN in CD_3CN , 1.94 ppm; ^{13}C NMR: $^{13}\text{CDCl}_3$ in CDCl_3 , 77.14 ppm; $^{13}\text{CD}_3\text{SOCD}_3$ in $\text{DMSO-}d_6$, 39.6 ppm) as a reference; chemical shift were given in ppm, coupling constants in Hz.

Mass spectra were recorded on an ESI/TOF mass spectrometer at ICSN institute (Gif sur Yvette, France).

6.2. Synthesis and characterization

6.2.1. 9-[1-(2-Methoxycarbonyl)phenyl]-6-methoxy-3*H*-xanthen-3-one: **Flu-1**



C₂₂H₁₆O₅ (360.36 g/mol)

To a suspension solution of fluorescein (0.2 g, 0.6 mmol) in MeOH (15 mL) was added 6 drops of concentrated H₂SO₄. The resulting mixture was refluxed for 15 h. After the reaction mixture was cooled down to room temperature, it was poured onto ice and then extracted with CH₂Cl₂ three times. The organic layer was evaporated to obtain a red solid which was used directly for the next step. The above solid was dispersed in acetone followed by addition of Cs₂CO₃ (0.39g) and CH₃I (75 μL, 1.2mmol), and then the mixture was stirred at room temperature for 28 h. After concentration, H₂O was added and the mixture extracted by CH₂Cl₂. The organic layer was dried over MgSO₄ and evaporated. The crude product was purified by column chromatograph with elute CH₂Cl₂/CH₃OH (97:3) to give the titled compound in 55% yield.¹

¹H NMR (400 MHz, CDCl₃): δ(ppm) 3.64 (s, 3H,), 3.92 (s, 3H), 6.46 (d, 1H, *J* = 1.8Hz), 6.54 (dd, 1H, *J* = 9.6, 1.8Hz), 6.74 (dd, 1H, *J* = 8.7, 2.3Hz), 6.85 (d, 1H, *J* = 9.6Hz), 6.88 (d, 1H, *J* = 9.2Hz), 6.96 (d, 1H, *J* = 2.3Hz), 7.31(dd, 1H, *J* = 7.3, 1.3Hz), 7.67 (td, 1H, *J* = 7.8, 1.3Hz), 7.74 (td, 1H, *J* = 7.8, 1.4Hz), 8.25 (dd, 1H, *J* = 7.8, 1.3Hz);

¹³C NMR (100 MHz, CDCl₃): δ (ppm) 52.6, 56.1, 100.4, 105.9, 113.5, 114.9, 117.7, 130.0, 130.3, 130.9, 131.3, 132.8, 150.2, 154.4, 159.1, 164.1, 165.8, 185.9.

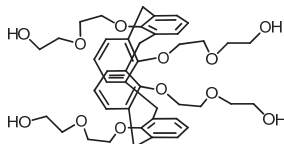
6.2.2. Toluene-4-sulfonic acid 2-(2-hydroxyethoxy)ethyl ether: 72

$C_{11}H_{16}O_5S$ (260.30 g/mol)

Diethyleneglycol (10 mL, 11.2 g, 0.105 mol, 4 equiv) and triethylamine (7.1 mL, 0.053 mol, 2 equiv) were dissolved in dry DCM (80 mL) followed by the addition of tosyl chloride (5.03 g, 0.027 mol, 1equiv) at one portion. The mixture was stirred overnight at room temperature. After washing twice with 1N HCl and 5% NaHCO₃, the organic layer was dried over MgSO₄ and evaporated to obtain crude product which was purified by column chromatography over silica gel (eluent: DCM was firstly used to remove the di-tosylated product followed by DCM/MeOH (95:5)). The pure mono-tosylated product was obtained as a colorless oil (4.0 g, 58%).²

¹H NMR (400 MHz, CDCl₃): δ 7.80 (d, *J* = 8.2 Hz, 2H), 7.35 (d, *J* = 8.2 Hz, 2H), 4.19 (t, *J* = 4.6 Hz, 2H), 3.68 (m, 4H), 3.53 (t, *J* = 4.6 Hz, 2H), 2.45 (s, 3H), 2.14 (s, 1H);

¹³C NMR (100 MHz, CDCl₃): δ 145.1, 133.1, 130.0, 128.1, 72.6, 69.3, 68.7, 61.7, 21.8 ppm.

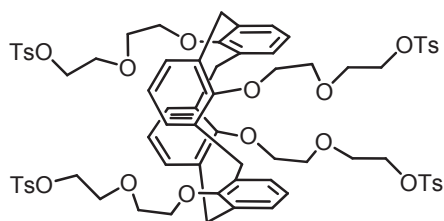
6.2.3. 25,26,27,28-Tetra(2-(2-hydroxyethoxy)ethoxy)calix[4]arene: 73

$C_{44}H_{56}O_{12}$ (776.90 g/mol)

Calix[4]arene (0.37 g, 0.89 mmol) and K₂CO₃ (0.92 g, 6.6 mmol) in dry MeCN (10 mL) was stirred at room temperature for 30 min. Then compound **72** (1.38 g, 5.3 mmol) in MeCN (5 mL) was added and the resulting mixture was refluxed for 45 h under Ar. The solvent was then removed by evaporation and the crude product was dissolved in DCM and washed with 1N HCl twice and H₂O. The organic layer was dried over MgSO₄ and evaporated to obtain crude product. The pure product (0.3 g, 50%) was obtained by column chromatography over silica (elute: DCM was firstly used to remove calix[4]arene followed by DCM/MeOH (95:5)).³

¹H NMR (400 MHz, CDCl₃): δ 7.10 (d, *J* = 7.3 Hz, 8H), 6.78 (t, *J* = 7.4 Hz, 4H), 3.80 (m, 16H), 3.67 (s, 8H), 3.62 (m, 16H);

¹³C NMR (100 MHz, CDCl₃): δ 156.0, 133.8, 130.6, 122.9, 72.8, 71.2, 70.2, 61.8, 36.6 ppm.

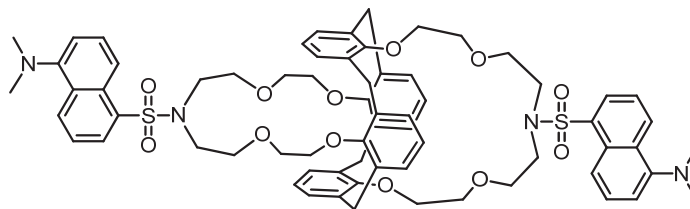
6.2.4. 25,26,27,28-Tetra(2-(2-tosylethoxy)ethoxy)calix[4]arene: 74**C₇₂H₈₀O₂₀S₄ (1393.65g/mol)**

To a solution of compound **73** (0.2 g, 0.25 mmol), tosyl chloride (0.27 g, 1.3 mmol) in dry THF (15 mL) in an iced bath, was added NaOH (0.1 g, 2.5 mmol in 0.7 mL H₂O) dropwise under Ar. The resulting mixture was stirred for 5 days at room temperature. The solvent was removed by evaporation and the residual was dissolved in DCM and washed with H₂O twice. The organic layer was dried over MgSO₄ and the crude product was purified by column chromatography over silica (elute: first with CHCl₃ followed by CHCl₃/MeOH (99.5:0.5)) to obtain pure product (0.06g, 16%).³

¹H NMR (400 MHz, CDCl₃): δ 7.80 (d, *J* = 8.2 Hz, 8H), 7.32 (d, *J* = 8.2 Hz, 8H), 6.97 (d, *J* = 7.3 Hz, 8H), 6.64 (t, *J* = 7.3 Hz, 4H), 4.18 (t, *J* = 4.6 Hz, 8H), 3.65 (m, 16H), 3.58 (s, 8H), 3.47 (t, *J* = 5.0 Hz, 8H);

¹³C NMR (100 MHz, CDCl₃): δ 155.8, 144.8, 133.6, 132.9, 129.9, 129.8, 127.9, 122.0, 70.4, 70.2, 69.3, 68.7, 36.0, 21.6 ppm.

6.2.5. 25,27:26,28-Bis(5'-*N,N*-dimethylaminonaphthalene-1'-sulfonyl bis(2-(2-aminoethoxy)ethoxy))calix[4]arene: Calix-Dansyl



C₆₈H₇₈N₄O₁₂S₂ (1207.49g/mol)

Dansylamide (0.114 g, 0.46 mmol) and K₂CO₃ (0.16 g, 1.15 mmol) in dry MeCN (20 mL) was stirred at room temperature for 30 min followed by the addition of compound **74** (0.32 g, 0.23 mmol in MeCN (10 mL) at one pot. The resulting mixture was refluxed overnight. Then solvent was evaporated and the residual was dissolved in CHCl₃, washed with H₂O twice. The organic layer was dried over MgSO₄ and evaporated to obtain crude product. It was purified by column chromatography over silica (elute: DCM/MeOH (99:1)) to obtain pure product (0.25 g, 47%).⁴

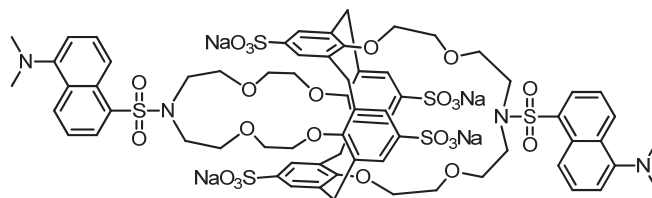
¹H NMR (400 MHz, CDCl₃): δ 8.54 (d, *J* = 8.2 Hz, 2H), 8.33 (d, *J* = 8.7 Hz, 2H), 8.18 (dd, *J* = 7.3, 1.4 Hz, 2H), 7.59 (t, *J* = 7.8 Hz, 2H), 7.53 (t, *J* = 7.4 Hz, 2H), 7.20 (d, *J* = 7.8 Hz, 2H), 7.04 (d, *J* = 7.3 Hz, 8H), 6.79 (t, *J* = 7.4 Hz, 4H), 3.82 (s, 8H), 3.47 (m, 16H), 3.40 (t, *J* = 5.0 Hz, 8H), 3.04 (t, *J* = 5.0 Hz, 8H), 2.89 (s, 12H);

¹³C NMR (100 MHz, CDCl₃): δ 157.3, 151.8, 135.3, 133.6, 130.3, 130.2, 130.1, 129.7, 129.3, 128.1, 123.2, 122.5, 119.7, 115.3, 70.8, 70.3, 69.5, 47.5, 45.5, 38.2 ppm;

HRMS (ESI) *m/z* calcd for C₆₈H₇₆N₄NaO₁₂S₂ [M + Na⁺] 1227.4799, found 1227.4822.

6.2.6.

5,11,17,23-Tetrasulfonated

25,27:26,28-Bis(5'-*N,N*-dimethylaminonaphtalene-1'-sulfonylbis(2-(2-aminoethoxy)ethoxy))calix[4]arene sodium salt: **SulfCalix-Dansyl**
 $C_{68}H_{74}N_4Na_4O_{24}S_6$ (1615.67g/mol)

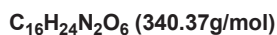
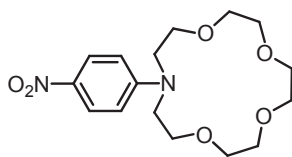
To a solution of compound **Calix-Dansyl** (110 mg, 0.091 mmol) in dry DCM (3 mL) was added HSO_3Cl (120 μ L in 3 mL DCM) dropwise at $-20^\circ C$. After stirring at room temperature for 3h, the solution was poured into ice-water solution and adjusted pH to 7 with $NaHCO_3$. The aqueous solution was evaporated to dry and redissolved in pyridine (6 mL) and water (2 mL). After stirring at room temperature for 2 h, the solution was concentrated (about 1.0 mL). Large precipitate was obtained by the addition of addition of acetone. The precipitate was again dispersed in 0.5 mL H_2O at $30^\circ C$. The insoluble residual was filtered off and washed with acetone to obtain the pure product (80 mg, 54%).⁵

1H NMR (400 MHz, D_2O): δ 8.34 (d, $J = 8.7$ Hz, 2H), 8.10 (d, $J = 7.4$ Hz, 2H), 8.06 (d, $J = 8.7$ Hz, 2H), 7.63 (t, $J = 8.2$ Hz, 2H), 7.58 (t, $J = 7.8$ Hz, 2H), 7.43 (s, 8H), 7.28 (d, $J = 7.8$ Hz, 2H), 3.90 (s, 8H), 3.39 (m, 16H), 3.14 (t, $J = 5.0$ Hz, 8H), 2.81 (t, $J = 5.0$ Hz, 8H), 2.73 (s, 12H);

^{13}C NMR (100 MHz, $CDCl_3$): δ 159.2, 150.4, 137.5, 133.8, 130.0, 129.4, 129.1, 128.9, 126.6, 124.2, 123.2, 119.8, 116.1, 70.0, 68.6, 46.4, 45.0, 36.9 ppm;

HRMS (ESI) m/z calcd for $C_{68}H_{72}N_4Na_3O_{24}S_6$ [$M + Na^+$] 1589.2554, found 1589.2628.

6.2.7. *N*-(4-Nitrophenyl)aza-15-crown-5: **95**

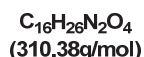
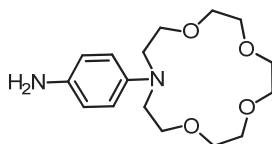


A Schlenk tube was charged with 1-bromo-4-nitrobenzene (80mg, 0.4mmol), NaO^tBu (50mg, 0.52 mmol), Pd(OAc)₂ (5mg, 0.055eq), PPh₃ (13mg, 0.05mmol) and toluene (3 mL) under argon. Then 1-aza-15-crown-5 (100mg, 0.48mmol) in anhydrous toluene (2 mL) was injected with syringe. After that the reaction mixture was heated to 100°C for 3 days. The reaction mixture was cooled down to room temperature and absorbed onto silica gel and purified by column chromatograph (elutes: ethyl acetate/hexane (1:1) followed by ethyl acetate) to obtain the titled compound as a yellow solid (105 mg, 78%).⁶

¹H NMR (400 MHz, CDCl₃): δ 8.10 (d, *J* = 9.6 Hz, 2H), 6.62 (d, *J* = 9.6 Hz, 2H), 3.79 (t, *J* = 6.0 Hz, 4H), 3.69 (m, 12H), 3.63 ppm (s, 4H);

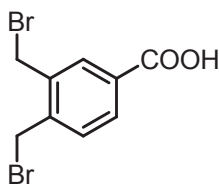
¹³C NMR (100 MHz, CDCl₃): δ 152.9, 126.4, 110.6, 71.5, 70.2, 70.5, 68.2, 53.3 ppm.

6.2.8. *N*-(4-Aminophenyl)aza-15-crown-5: **96**



A schlenk tube was charged with compound **95** (50mg, 0.15mmol), Pd/C (10%, 10mg), 0.6 mL CH₃OH and 2.4 mL EtOAc. Then the mixture was stirred under a H₂ atmosphere (via balloon) for 2 hour until the solution color disappeared. The mixture was filtered through a plug of Celiteo and the solvent was removed under reduced pressure to give an oil (40 mg, 90%).⁷

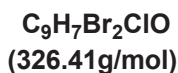
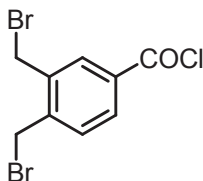
¹H NMR (400 MHz, CDCl₃): δ 6.65 (m, 2H), 6.58 (m, 2H), 3.61-3.80 (m, 16H), 3.53 (m, 4H);

6.2.9. 3,4-Bis(bromomethyl)benzoic acid: 97

3,4-Dimethylbenzoic acid (0.45g, 3 mmol) was dispersed in CCl₄ (25 mL). NBS (1.10g, 6.2 mmol) and BPO (0.05g) was added batch by batch during 2h at 80°C. The reaction mixture was stirred at 80°C for another 2h. The formed succinIamide was removed by filtration and the filtrate was evaporated. The crude product was allowed to crystallize in MeOH at -20°C. The obtained white solid was subjected to column chromatography (elute: CH₂Cl₂ and 0.5%-1% AcOH) to obtain pure compound (0.35 g, 38%).⁸

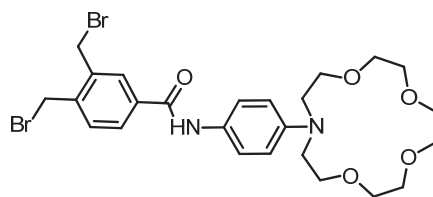
¹H NMR (400 MHz, CDCl₃): δ 8.11 (d, *J* = 1.4 Hz, 1H), 8.04 (dd, *J* = 7.8 Hz, *J* = 1.8 Hz, 1H), 7.50 (d, *J* = 7.8 Hz, 1H), 4.69 (s, 2H), 4.68 ppm (s, 2H);

¹³C NMR (100 MHz, CDCl₃): δ 166.4, 141.2, 137.0, 132.0, 131.6, 131.4, 129.9, 30.3, 29.8 ppm.

6.2.10. 3,4-Bis(bromomethyl)benzoyl chloride: 98

Compound **97** (0.1 g, 0.32 mmol) and oxalyl chloride (0.16 mL, 1.86 mmol) were dissolved in dry toluene (4 mL). The resulting mixture was stirred at 80°C for 4h. Then it was cooled down to room temperature and evaporated to obtain a yellow liquid.⁹

¹H NMR (400 MHz, CDCl₃): δ 8.13 (s, 1H), 8.05 (m, 1H), 7.54 (m, 1H), 4.67 (m, 4H).

6.2.11. *N*-(4-(Aza-15-crown-5)phenyl)-3,4-bis(bromomethyl)benzamide: 99

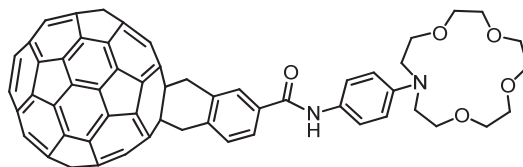
C₂₅H₃₂Br₂N₂O₅
(600.34g/mol)

Compound **96** (0.09 g, 0.3 mmol) was dissolved in dry THF (4 mL) under Ar followed by the addition of Et₃N (0.15 mL, 1.1 mmol). Compound **98** (0.13 g, 0.4 mmol) in THF (3 mL) was added dropwise at 0°C. The reaction mixture was stirred at 0°C for another hour then at room temperature for 24 h. The solvent was removed by evaporation and absorbed to silica, which was then purified by column chromatography over silica (elute: EtOAc/Cyclohexane(1:1)) to obtain a pale yellow solid (0.12 g, 67%).¹⁰

¹H NMR (400 MHz, CDCl₃): δ 7.7–8.0 (br d, 3H), 7.46 (m, 3H), 6.67 (br s, 2H), 4.69 (s, 2H), 4.67 (s, 2H), 3.4–3.8 (m, 20H);

¹³C NMR (100 MHz, CDCl₃): δ 164.3, 145.2, 140.0, 137.2, 136.1, 131.6, 130.0, 127.9, 126.5, 122.8, 111.8, 71.4, 70.4, 70.2, 68.6, 52.7, 29.4, 29.0 ppm;

HRMS (ESI) *m/z* calcd for C₂₅H₃₃Br₂N₂O₅ [M + H⁺] 601.0736, found 601.0759.

6.2.12. *N*-(4-(Aza-15-crown-5)phenyl)-[1,9](C₆₀-I_h)[5,6]fullerene-3',4'-bismethylbenzamide:**Flu-aza**

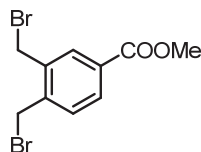
C₈₅H₃₂N₂O₅ (1160.23g/mol)

To a schlenk tube charged with compound **99** (29.6 mg, 0.05 mmol), KI (58 mg, 0.35 mmol), 18-crown-6 (53 mg, 0.2 mmol) and C₆₀ (37 mg, 0.05 mmol) was added dry toluene (20 mL). The resulting mixture was refluxed at 110 °C for 22h under Ar. The product was absorbed onto silica and purified by column chromatography over silica (elute: toluene first to collect unreacted C₆₀ followed by CHCl₃/MeOH(99.5:0.5)) (6 mg, 10%).¹⁰

¹H NMR (400 MHz, CDCl₃): δ ; 8.21 (s, 1H), 8.04 (d, *J* = 7.8 Hz, 1H), 7.87 (s, 1H), 7.78 (d, *J* = 7.8 Hz, 1H), 7.51 (d, *J* = 8.7 Hz, 2H), 6.69 (d, *J* = 7.8 Hz, 2H), 4.86 (d, *J* = 12.8 Hz, 2H), 4.52 (d, *J* = 14.6 Hz, 2H), 3.78 (d, *J* = 6.0 Hz, 4H), 3.58-3.72 (m, 16H);

¹³C NMR (100 MHz, CDCl₃): δ 165.5, 156.7, 156.3, 147.9, 146.7, 146.4, 145.7, 145.3, 145.2, 144.9, 143.2, 142.7, 142.3, 142.2, 142.0, 141.9, 141.7, 140.5, 140.3, 138.9, 136.2, 136.1, 135.5, 135.2, 128.5, 126.9, 126.8, 126.6, 122.8, 111.8, 71.5, 70.4, 70.3, 68.7, 65.8, 52.8, 45.2, 45.1, 31.1, ppm;

HRMS (ESI) *m/z* calcd for C₈₅H₃₃N₂O₅ [M + H⁺] 1161.2389, found 1161.2360.

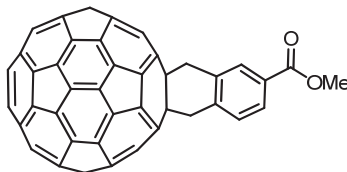
6.2.13. Methyl 3,4-bis(bromomethyl)benzoate: 100

C₁₀H₁₀Br₂O₂ (321.99g/mol)

To a solution of compound **3** (0.1 g, 0.32 mmol) in MeOH (6 mL) was added SOCl₂ (0.069 mL, 0.96 mmol). The resulting mixture was refluxed for 2 h. After removal of the solvent, the residual was dissolved in EtOAc and washed with H₂O. The organic layer was dried over MgSO₄ and evaporated to obtain the product (0.09 g, 86%).

¹H NMR (400 MHz, CDCl₃): δ 8.04 (d, *J* = 1.4 Hz, 1H), 7.97 (dd, *J* = 7.8, 1.8 Hz, 1H), 7.46 (d, *J* = 8.2 Hz, 1H), 4.74 (br s, 4H), 3.89 (s, 3H);

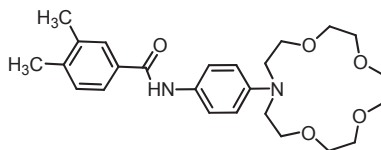
¹³C NMR (100 MHz, CDCl₃): δ 166.1, 140.9, 136.5, 131.9, 131.0, 130.9, 130.5, 52.5, 42.8, 42.5 ppm.

6.2.14. Methyl [1,9](C₆₀-I_h)[5,6]fullerene-3',4'-dimethylbenzoate: Full-Ben

C₇₀H₁₀O₂ (882.82g/mol)

C₆₀ (100 mg, 0.14 mmol), compound **100** (45 mg, 0.14 mmol), KI (166 mg, 1.0 mmol) and 18-crown-6 (80 mg, 0.3 mmol) were dissolved in dry toluene (100 mL). The resulting mixture was refluxed for 22 h under Ar. After removal of the solvent, the crude product was purified by column chromatograph over silica (elute: toluene/hexane (2:1)) to obtain black solid (50 mg, 41%).⁸

¹H NMR (400 MHz, CDCl₃): δ 8.37 (s, 1H), 8.25 (d, *J* = 7.8 Hz, 1H), 7.77 (d, *J* = 7.8 Hz, 1H), 4.84 (br s, 2H), 4.53 (br s, 2H), 4.01 (s, 3H);

6.2.15. *N*-(4-(Aza-15-crown-5)phenyl)-3,4-dimethylbenzamide: Ben-aza $C_{25}H_{34}N_2O_5$ (442.54g/mol)

To a solution of 3,4-dimethylbenzoic acid (60 mg, 0.4 mmol) in toluene (4 mL) was added oxalyl chloride (0.19 mL, 2.2 mmol). The reaction mixture was refluxed at 100°C for 4 h. The solvent was evaporated to obtain acyl chloride.

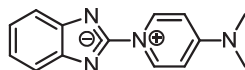
To a solution of compound **96** (0.09 g, 0.3 mmol) and Et₃N (0.23 mL, 1.7 mmol) in dry THF (4 mL) was added acyl chloride (67 mg, 0.4 mmol in 5 mL THF) under Ar at 0°C. The reaction mixture was stirred at room temperature overnight. The solvent was removed by evaporation and absorbed to silica, which was then purified by column chromatography over silica (elute: DCM/MeOH(98:2)) to obtain a viscous yellow solid (0.05 g, 38%).⁷

¹H NMR (400 MHz, CDCl₃): δ 7.67 (s, 1H), 7.64 (s, 1H), 7.56 (d, *J* = 7.8 Hz, 1H), 7.43 (d, *J* = 8.7 Hz, 2H), 7.20 (d, *J* = 7.8 Hz, 1H), 6.64 (d, *J* = 8.7 Hz, 2H), 3.75 (t, *J* = 7.4 Hz, 4H), 3.64-3.68 (m, 12H), 3.59 (t, *J* = 7.4 Hz, 4H), 2.32 (s, 6H);

¹³C NMR (100 MHz, CDCl₃): δ 165.9, 145.1, 140.7, 137.2, 132.9, 129.9, 128.4, 127.1, 124.4, 122.6, 111.8, 71.4, 70.3, 68.7, 52.7, 20.0 ppm;

HRMS (ESI) *m/z* calcd for C₂₅H₃₅N₂O₅ [M + H⁺] 443.2546, found 443.2546.

6.2.16. 1-*N*-Benzimidazolyl-4-dimethylaminopyridinium: **Bet-DiMe**



$C_{14}H_{14}N_4$ (238.28g/mol)

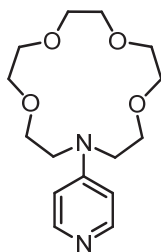
To a schlenk tube were added 2-chlorobenzimidazole (0.2 g, 1.32 mmol) and dimethylpyridine (1.6 g, 13.2 mmol). After the reaction mixture was stirred at 150°C for 3 h under Ar, it was cooled down to room temperature followed by the addition of 30 mL H₂O. The precipitate was filtered off and washed with water, ethanol twice to obtain a pure product. (0.27 g, 75%).¹¹

¹H NMR (400 MHz, CD₃OD): δ 8.89 (d, *J* = 8.2 Hz, 2H), 7.48 (dd, *J* = 6.4, 3.2 Hz, 2H), 7.07 (d, *J* = 7.8 Hz, 2H), 7.02 (dd, *J* = 6.4, 3.2 Hz, 2H), 3.27 (s, 6H);

¹³C NMR (100 MHz, CD₃OD): δ 158.3, 154.9, 146.1, 138.9, 121.3, 117.4, 108.6, 48.4 ppm;

HRMS (ESI) *m/z* calcd for C₁₄H₁₅N₄ [M + H⁺] 239.1297, found 239.1289.

6.2.17. *N*-Pyridine-aza-15-crown-5: **104**

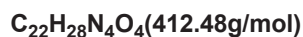
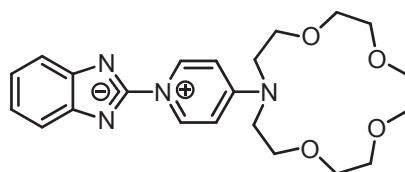


$C_{15}H_{24}N_2O_4$ (296.36g/mol)

To a schlenk tube added 4-bromopyridine hydrochloride (0.2 g, 1.0 mmol) aza-15-crown-5 (0.1 g, 0.46 mmol), *t*-BuONa (0.19 g, 2.0 mmol), Pd(*dba*)₂ (21 mg, 0.04 mmol) and 2-dicyclohexylphosphino-2'-(*N,N*-dimethylamino)biphenyl (20 mg, 0.05 mmol). The reaction mixture was stirred at 100°C for 41 h under Ar. Crude product containing some Et₃N and aza-15-crown-5 was obtained by column chromatography on silica gel (elute: MeOH/DCM/Et₃N = 5:95:0.5) (40 mg, 30%).¹²

¹H NMR (400 MHz, CDCl₃): δ 8.18 (d, *J* = 5.5 Hz, 2H), 6.48 (d, *J* = 5.0, 2H), 3.6–3.8 (m, 20H);

6.2.18. 1-(1-*N*-Benzimidazolylpyridinium)-aza-15-crown-5: **Bet-aza**



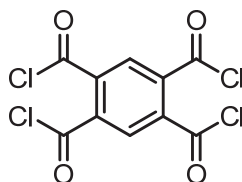
Compound **104** (0.17 g, 0.57 mmol) and 2-chlorobenzimidazole (0.13 g, 0.86 mmol) dissolved in dry *n*-BuOH (3 mL) were stirred at 110°C for 50 h under Ar. The solvent was evaporated and the residual was redissolved in MeOH (2 mL) followed by the addition of concentrated aqueous NH₃ (33%, 1 mL) and stirred at room temperature for 30 min. The solvent was evaporated and the crude product was separated by column chromatography (elute: MeOH/DCM/Et₃N = 2:95:1) to obtain a viscous solid which was dissolved in diluted aqueous NH₃ (10%) and extracted with CHCl₃. The organic layer was dried over MgSO₄ and evaporated to obtain a yellow solid (100 mg, 40%).¹³

¹H NMR (400 MHz, CDCl₃): δ 9.26 (d, *J* = 7.8 Hz, 2H), 7.63 (dd, *J* = 6.0, 3.2 Hz, 2H), 7.09 (dd, *J* = 6.0, 3.2 Hz, 2H), 6.76 (d, *J* = 7.8 Hz, 2H), 3.80 (t, *J* = 5.5 Hz, 4H), 3.65 (m, 12H), 3.58 (s, 4H);

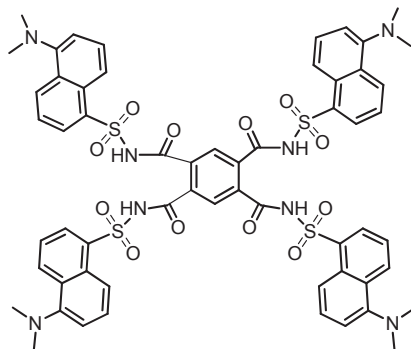
¹³C NMR (100 MHz, CDCl₃): 156.2, 154.1, 146.0, 137.8, 120.0, 117.0, 107.4, 72.3, 70.6, 70.0, 68.1, 53.8 ppm;

HRMS (ESI) *m/z* calcd for C₂₂H₂₉N₄O₄ [M + H⁺] 413.2189, found 413.2179.

6.2.19. Benzene-1,2,4,5-tetracarboxyl tetrachloride: **105**



1,2,4,5-Benzenetetracarboxylic acid (0.8g, 3.1 mmol) was digested with PCl₅ (2.63g, 12.8mmol) at 150°C for 24 hours. After that the reaction was cooled down to room temperature and POCl₃ was evaporated under reduced pressure. The obtained solid was used directly for the next step.¹⁴

6.2.20. Benzene-1,2,4,5-tetra(5'-*N,N*-dimethylaminonaphthalene-1'-sulfonyl carboxamide):**106****C₅₈H₅₄N₈O₁₂S₄ (1183.35g/mol)**

Dansyl amide (0.34g, 0.3 mmol), DAMP (0.18g, 1.47), Et₃N (0.4mL, 2.75 mmol) were dispersed in 15 mL DCM and 1 mL DMF followed by the dropwise addition of **105** (0.1g, 0.3 mmol in 5 mL DCM) at 0°C. After that the reaction mixture was stirred at 0°C for another hour and then at room temperature for 3 days. After the reaction completed, there is a large amount of white precipitate in the solution, which was then filtered and washed with DCM 3 times, and dispersed in 0.5M HCl to remove the Et₃N. Finally the precipitate was again filtered and washed with H₂O until the pH 6~7. The obtained yellow solid was dry under high vacuum condition.

¹H NMR (400 MHz, DMSO-*d*₆): δ 8.26 (br, s, 4H), 8.23 (br, s, 8H), 7.60 (br, d, 10H), 7.30 (br, s, 4H), 2.86 ppm (s, 24H);

¹³C NMR (100 MHz, DMSO-*d*₆): δ 164.3, 150.7, 135.3, 134.4, 130.5, 130.3, 128.9, 128.6, 128.3, 123.7, 118.7, 115.6, 40.1 ppm.

ESI-HRMS (m/z): for C₅₈H₅₅N₈O₁₂S₄ Calcd. 1183.2822 (M + H⁺), found: 1183.2811 and for C₅₈H₅₄N₈NaO₁₂S₄ (M + Na⁺) Calcd. 1205.2642, found: 1205.2709.

6.3. Spectroscopic measurement

6.3.1. Instrumentation

UV-visible absorption spectroscopy

Hellma quartz cells with an inner path length of 10 mm were used for absorption spectroscopy measurement. The UV-visible absorption spectra were recorded on double beam Uvikon 943, Cary-5E, or Cary-5000 spectrophotometers.

Steady state fluorescence spectroscopy

Hellma quartz cells with an inner path length of 10 mm were used for fluorescence spectroscopy measurement. The fluorescence was recorded on FluoroMax-3, FluoroMax-4, and Fluorolog spectrophotometers.

FluoroMax-3: A Xenon arc lamp (150W) was used as the light source. The spectral range went through 200 to 900 nm. The band pass of the monochromator of excitation and emission were automatically adjusted via the software (0.5 to 10 nm).

FluoroMax-4: A Xenon arc lamp (150W) was used as the light source. The spectral range went through 200 to 950 nm. The band pass of the monochromator of excitation and emission were automatically adjusted via the software (0 to 30 nm).

Fluorolog FL3-221: A Xenon arc lamp (450W) was used as the light source. The spectral range covers from 200 to 1300 nm. The band pass of the monochromator of excitation and emission were automatically adjusted via the software (0 to 30 nm). The excitation and emission beam can be polarized independently.

6.3.2. Time-resolved spectroscopy

Instrument of time-resolved spectroscopy

The fluorescence decay was obtained with a time-correlated single-photon-counting (TCSPC) technique. The technique is based on the repetitive precisely timed registration of single photons of a fluorescence signal, the probability of detecting a photon at a time t after the excitation pulse is proportional to the fluorescence signal. Each photon detected is stored in different channels. The fluorescence decay is finally reconstructed by summing the photon of each channel.

The excitation source is a tunable Titanium Sapphire laser pumped by a argon ion laser. It delivers pulse with 300 fs in width at half maximum at a rate of 80 MHz (12 ns between two

pulses) within a wavelength range between 690 and 1000 nm. The pulse rate is reduced to 4 MHz to guarantee that long lifetime components can relax completely before the next pulse. The frequency of the excitation beam can be doubled with excitation wavelength between 280 and 330 nm or tripled with excitation wavelength between 420 and 500 nm.

After excitation by pulse, the fluorescence is collected at 90° through a monochromator, with width of the slit adjusted manually. The fluorescence photons are then detected by Photomultiplier (PM) microchannel plate. A constant fraction discriminator is placed after the PM to pass the signal with a suitable amplitude and remove a portion of noise and interference pulse. The signal is sent to the channel and start time-to-amplitude converter. A portion of the excitation beam is sent to a photodiode with a discriminator. The detected signal delayed by a delay box stop time-to-amplitude converter.

The fluorescence decay was recorded on 4096 channels. For each measurement, at least 10^4 photons were counted at the channel with the maximum intensity and excitation function $E(t)$ was measured from the Ludox scattering at the excitation wavelength of the laser.

Analysis of fluorescence time decay

When the excitation pulse is infinitely short, multiple-exponential fluorescence with n components can be expressed as eq. 6-1:

$$I_F(t) = \sum_{i=1}^n \alpha_i \exp(-t / \tau_i) \quad (\text{eq. 6-1})$$

where $I_F(t)$ represents the decay of fluorescence intensity, τ_i is the decay time of each component, α_i is the pre-exponential factor.

However, when the duration of the pulse is not short enough compared with the decay time, the recorded $I(t)$ is convolution of the excitation function $E(t)$, as shown in eq. 6-2:

$$I(t) = E(t) \otimes I_F(t) = E(t) \otimes \sum_{i=1}^n \alpha_i \exp(-t / \tau_i) \quad (\text{eq. 6-2})$$

The collected data were analyzed by a nonlinear least-square method with the aid of Globals software (Globals Unlimited, University of Illinois at Urbana-Champaign, Laboratory of Fluorescence Dynamics). Pulse deconvolution was carried out by using the decay profile of the exciting pulse recorded by using Ludox solution under the identical condition. To evaluate the quantity of the collected data, χ^2 defined as the weighted sum of the squares of the deviations of experimental response from the calculated ones is used as an indicator. A good

fit require χ^2 should be close to the unity, with the acceptable value range from 0.8 to 1.2.

6.3.3. Transient absorption spectroscopy

Nanosecond transient absorption spectra were obtained from **LP 920** using a pump-probe setup, as shown in Figure 6-1. It composes of four parts: Xe lamp as the probe, the sample compartment, monochromator and PMT detector. Neodymium-YAG laser with pulse at 10 Hz was equipped with two nonlinear crystals to obtain the third harmonic generation at 355 nm with a maximum energy at 160 mJ/pulse. The energy can be reduced by increasing Q-switch delay or adjusting the attenuator. Using optical parametric oscillator (OPO) we could transfer 355 nm into 432 nm at *ca.* 5 mJ/pulse, which was directed to the sample to produce the transient species. Xe lamp of 450 W producing a wide range of spectrum from 160 to 2600 nm was used as the probe. The intensity of the probe beam after absorbed by sample was detected by photomultiplier which received the photons passing through the monochromator and converted them into electric voltage.

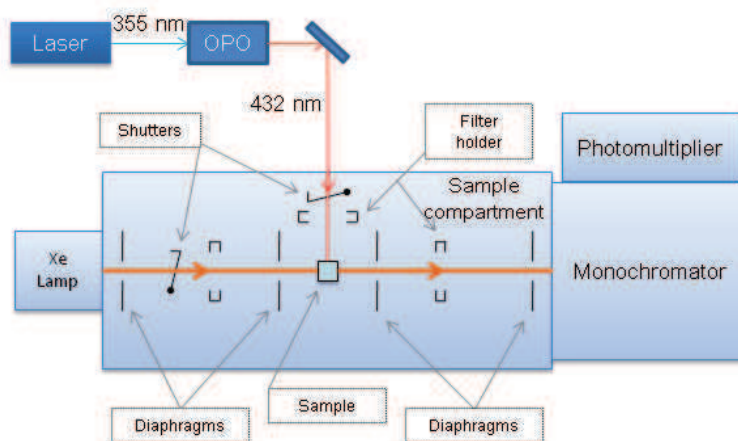


Figure 6-1. Experimental setup of transient absorption spectroscopy.

6.4. Reagents and solvents

The solvent used for spectral investigation were spectroscopic grade and commercially available from Aldrich or SDS. Perchloric acid (70% in water) was purchased from Aldrich and its purity was 99.999%. 2,6-Lutidine, HEPES were used as buffer systems as received from Aldrich or Fluka. The tested metal salts were $\text{Cu}(\text{ClO}_4)_2$, AgNO_3 , $\text{Ba}(\text{ClO}_4)_2$, $\text{Mn}(\text{ClO}_4)_2$, $\text{Co}(\text{ClO}_4)_2$, $\text{Cd}(\text{ClO}_4)_2$, $\text{Zn}(\text{ClO}_4)_2$, $\text{Ni}(\text{ClO}_4)_2$, $\text{Fe}(\text{ClO}_4)_2$, $\text{Pb}(\text{ClO}_4)_2$, $\text{Mg}(\text{ClO}_4)_2$, $\text{Ca}(\text{ClO}_4)_2$, $\text{Hg}(\text{ClO}_4)_2$, KSCN , NaSCN , LiClO_4 , $\text{Al}(\text{NO}_3)_3$, $\text{Eu}(\text{NO}_3)_3$, $\text{La}(\text{NO}_3)_3$, FeCl_3 and they were all commercially available.

6.5. Experimental protocols

6.5.1. Determination of fluorescence quantum yield

The fluorescence quantum yield Φ_F is the ratio of the number of the emitted photons to the number of absorbed photons. Fluorescence quantum yield was determined using a standard reference. It's preferable to choose a reference which is capable to be excited at the same wavelength and whose emission spectrum overlaps with that of the tested compound. The quantum yield is calculated using eq. 6-3:

$$\Phi_{unk} = \Phi_{std} \frac{(I_{unk} / A_{unk})}{(I_{std} / A_{std})} \left(\frac{n_{unk}}{n_{std}} \right)^2 \quad (\text{eq. 6-3})$$

Where Φ_{unk} and Φ_{std} are the quantum yield of the sample and standard, I_{unk} and I_{std} are the integrated emission intensity of the corrected spectra of the sample and standard, A_{unk} and A_{std} are the absorbance of the sample and standard at the excitation wavelength (lower than 0.05), and n is the refractive index of the solvent used for the two solutions.

The standard reference compounds used for the determination of the fluorescence quantum yield were quinine sulfate in 0.5 N H_2SO_4 ($\Phi_{std} = 0.546$),¹⁵ coumarine 153 in EtOH ($\Phi_{std} = 0.53$).¹⁶

6.5.2. Measurement of stability constants

The stability constants were obtained from the absorption or fluorescence titrations. By using Specfit Global Analysis system V3.0 for 32-bit windows system, the complexation stability constants, and binding stoichiometry were easily obtained. Furthermore, this software provides the access to have the spectra of different species and the proportion of different species as a function of cation concentrations.

For the 1:1 complexation, eq. 6-4 was also used to get the stability constant:¹⁷

$$Y = Y_0 + \frac{Y_{lim} - Y_0}{2} \left\{ 1 + \frac{c_M}{c_L} + \frac{1}{K_s c_L} - \left[\left(1 + \frac{c_M}{c_L} + \frac{1}{K_s c_L} \right)^2 - 4 \frac{c_M}{c_L} \right]^{1/2} \right\} \quad (\text{eq. 6-4})$$

where Y donates the fluorescence intensity or absorbance; c_M and c_L are the concentrations of metal ions and ligand; K_s is the association constant of 1:1 complex. Y_0 and Y_{lim} are the fluorescence intensity or absorbance value when $C_M = 0$ and for full complexation.

Reference

- [1] Miura, T.; Urano, Y.; Tanaka, K.; Nagano, T.; Ohkubo, K.; Fukuzumi, S. "Rational design principle for modulating fluorescence properties of fluorescein-based probes by photoinduced electron transfer." Journal of the American Chemical Society **2003**, *125*, 8666-8671.
- [2] van Ameijde, J.; Liskamp, R. M. J. "Synthesis of novel trivalent amino acid glycoconjugates based on the cyclotrimeratrylene ('CTV') scaffold." Organic & Biomolecular Chemistry **2003**, *1*, 2661-2669.
- [3] Kim, S. K.; Sim, W.; Vicens, J.; Kim, J. S. "Modular chemistry. Double- and multi-1,3-alternate-calixcrowns." Tetrahedron Letters **2003**, *44*, 805-809.
- [4] Kim, J. S.; Lee, W. K.; No, K.; Asfari, Z.; Vicens, J. "Two novel 1,3-calix[4]azacrowns." Tetrahedron Letters **2000**, *41*, 3345-3348.
- [5] Souchon, V.; Leray, I.; Valeur, B. "Selective detection of cesium by a water-soluble fluorescent molecular sensor based on a calix[4]arene-bis(crown-6-ether)." Chemical Communications **2006**, 4224-4226.
- [6] Witulski, B. "Palladium-catalyzed synthesis of N-aryl- and N-heteroaryl-aza-crown ethers via cross-coupling reactions of aryl- and heteroaryl bromides with aza-crown ethers." Synlett **1999**, 1223-1226.
- [7] Kelly, D. P.; Bateman, S. A.; Martin, R. F.; Reum, M. E.; Rose, M.; Whittaker, A. R. D. "DNA-Binding Compounds .5. Synthesis and Characterization of Boron-Containing Bibenzimidazoles Related to the DNA Minor-Groove Binder, Hoechst-33258." Australian Journal of Chemistry **1994**, *47*, 247-262.
- [8] Belik, P.; Gugel, A.; Kraus, A.; Walter, M.; Mullen, K. "Diels-Alder Adduct of C-60 and 4-Carboxy-O-Quinodimethane - Synthesis and Chemical-Transformations." Journal of Organic Chemistry **1995**, *60*, 3307-3310.
- [9] Ishi-i, T.; Shinkai, S. "Synthesis of chiral [60]fullerene-steroid bisadducts using steroid templates." Tetrahedron **1999**, *55*, 12515-12530.
- [10] Rajkumar, G. A.; Sandanayaka, A. S. D.; Ikeshita, K.; Itou, M.; Araki, Y.; Furusho, Y.; Kihara, N.; Ito, O.; Takata, T. "Photoinduced intramolecular electron-transfer processes in [60]fullerene-(spacer)-N,N-bis(biphenyl)aniline dyad in solutions." Journal of Physical Chemistry A **2005**, *109*, 2428-2435.
- [11] Alcalde, E.; Perezgarcia, L.; Dinares, I.; Coombs, G. H.; Frigola, J. "Synthesis and Antitrichomonal Activity of Azinium (Azolium) 4-Nitrobenzimidazolate Betaines and Their Derivatives." European Journal of Medicinal Chemistry **1992**, *27*, 171-176.
- [12] Chi, K. W.; Addicott, C.; Stang, P. J. "Incorporation of a flexible, pyridine-functionalized diaza-crown ether into discrete supramolecules via coordination-driven self-assembly." Journal of Organic Chemistry **2004**, *69*, 2910-2912.
- [13] Nemoto, N.; Abe, J.; Miyata, F.; Shirai, Y.; Nagase, Y. "New class of second-order non-linear optical material: stilbazolium benzimidazolate derived from alkylsulfonyl substituted stilbazole." Journal of Materials Chemistry **1998**, *8*, 1193-1197.
- [14] Ranganathan, S.; Muraleedharan, K. M.; Rao, C. H. C.; Vairamani, M.; Karle, I. L.;

Gilardi, R. D. "Stacking of a benzenehexacarboxylic acid core in the crystal structure of benzenehexacarboxylic acid alpha-aminomethyl isobutyrate amide (MA-Aib(6))-sodium nitrate complex." Chemical Communications **2001**, 2544-2545.

[15] Demas, J. N.; Crosby, G. A. "Measurement of Photoluminescence Quantum Yields - Review." Journal of Physical Chemistry **1971**, 75, 991-&.

[16] Grabolle, M.; Spieles, M.; Lesnyak, V.; Gaponik, N.; Eychmuller, A.; Resch-Genger, U. "Determination of the Fluorescence Quantum Yield of Quantum Dots: Suitable Procedures and Achievable Uncertainties." Analytical Chemistry **2009**, 81, 6285-6294.

[17] Valeur, B. "Molecular Fluorescence: Principles and Applications" Wiley-VCH Verlag GmbH, **2001**.

Publications

Publications

- [1] Ruan, Y. B.; Li, C.; Tang, J.; Xie, J. "Highly sensitive naked-eye and fluorescence 'turn-on' detection of Cu^{2+} using Fenton reaction assisted signal amplification." Chemical Communications **2010**, 46, 9220-9222.
- [2] Ruan, Y. B.; Maisonneuve, S.; Xie, J. A. "Highly selective fluorescent and colorimetric sensor for Hg^{2+} based on triazole-linked NBD." Dyes and Pigments **2011**, 90, 239-244.
- [3] Ruan, Y. B.; Xie, J. "Unexpected highly selective fluorescence 'turn-on' and ratiometric detection of Hg^{2+} based on fluorescein platform." Tetrahedron **2011**, 67, 8717-8723.
- [4] Ruan, Y. B.; Maisonneuve, S.; Li, C.; Tang, J.; Xie, J. "Cooperative recognition of Cu^{2+} based on amino acids tethered benzothiadiazoyl-bistriazoles." Frontiers of Chemistry in China **2010**, 5, 208-213.

Conference

- [1] Ruan, Y. B.; Li, C.; Tang, J.; Leray, I.; Xie, J. "Synthesis of fluorescent amino esters and their applications in recognition of copper ions" XXV International Conference on Photochemistry, Beijing, August, **2011**.

